Molecular-level Insights into Reversed-phase Liquid Chromatographic Systems via Monte Carlo Simulation

A THESIS
SUBMITTED TO THE FACULTY OF THE GRADUATE SCHOOL
OF THE UNIVERSITY OF MINNESOTA
BY

Jake Leland Rafferty

IN PARTIAL FULFILLMENT OF THE REQUIREMENTS
FOR THE DEGREE OF
Doctor Of Philosophy

August, 2009

Acknowledgements

This work would not have been possible without the assistance of my advisor, Prof. J. Ilja Siepmann. His level of knowledge, continuous support, and understanding have been invaluable to the successful completion of my degree. Prof. Siepmann's positive influence will continue with me for the remainder of my professional career.

I would also like to thank the other members of the Siepmann group, past and present. It has taken many years to develop the tools necessary to properly simulate RPLC and without these people this would not have been possible. In addition, Dr. Mark R. Schure has been a long time collaborator of the group. Dr. Schure's expertise in the fields of chromatography and simulation has been a great asset.

I have been fortunate to receive financial support from the University of Minnesota in the form Graduate School, Owens, Frieda Martha Kunze, and Doctoral Dissertation Fellowships. The research projects in which I was involved were also financially supported by grants from the National Science Foundation and the Rohm and Haas Company. The Minnesota Supercomputing institute is also acknowledged for generous allocations of computer time. The amount of work I was able to complete as a graduate student would not have been possible without these financial and computational resources.

Molecular-level Insights into Reversed-phase Liquid Chromatographic Systems via Monte Carlo Simulation

by Jake Leland Rafferty

ABSTRACT

Separations are of utmost importance in the feild of chemistry and reversed-phase liquid chromatography (RPLC) is among the most popular techniques for this purpose. Despite this popularity, and decades of research efforts, a fundamental understanding of RPLC at the molecular-level is lacking. To gain this detailed understanding, molecular simulations using advanced Monte Carlo algorithms and accurate force fields are applied to examine structure and retention in various realistic model RPLC systems. The simulations are able to afford quantitative agreement with experimental retention data and offer many new insights on stationary phase structure and the molecular mechanism of solute retention in RPLC.

Contents

Acknowledgements i

Abstract ii

List of Tables vii

List of Figures ix

Overview 1

1 Reversed-phase Liquid Chromatography 3

1.1 Introduction to the RPLC Technique 3

1.2 The Elusive Retention Mechanism 6

2 Statistical Mechanics and Molecular Simulation 8

3 Accuracy and Precision in a Simulation 12

3.1 Advanced Monte Carlo Methods 12

3.1.1 Gibbs Ensemble Monte Carlo 13

3.1.2 Configurational-bias Monte Carlo 17

3.2 The Transferable Potentials for Phase Equilibria Force Field 20

4 The Driving Forces for Retention in RPLC 26

4.1 Background 26

4.2 Simulation Details 29

4.3 Results and Discussion 31

4.3.1 Mobile to Vapor Phase Transfer . . . 34
4.3.2 Vapor to Stationary Phase Transfer . . . 44
4.4 Conclusions . . . 47

5 Simulating Realistic Models of RPLC 50
5.1 Simulation Setup . . . 50
5.2 Force Field . . . 54
5.3 Data Analysis . . . 55
5.3.1 Chain Conformation . . . 56
5.3.2 Heterogeneity in System Composition . . . 58
5.3.3 Solute Distribution Coefficients and Transfer Free Energies . . . 59
5.3.4 Solute/Solvent Orientation . . . 59
5.3.5 Hydrogen Bonding . . . 60

6 Mobile Phase Effects. I. Stationary Phase Solvation and Structure 61
6.1 Background . . . 61
6.2 Simulation Details . . . 63
6.3 Results and Discussion . . . 66
6.3.1 Solvation of the Stationary Phase . . . 66
6.3.2 Structure of the Stationary Phase . . . 71
6.4 Conclusions . . . 75

7 Mobile Phase Effects. II. The Solute Retention Mechanism 77
7.1 Background . . . 77
7.2 Results and Discussion . . . 79
7.3 Conclusions . . . 89

8 Influence of Surface Coverage. I. Effects on Chain Conformation and Interfacial Properties 91
8.1 Background . . . 91
8.1.1 Experimental Studies of Bonding Density . . . 92
8.1.2 Previous Simulations of the Effects of Bonding density . . . 94
8.2 Simulation Details . . . 94

8.3 Results and Discussion 98
8.3.1 Alkylsilane Chain Conformation 99
8.3.2 Solvation of the Alkylsilane Phase 102
8.3.3 Interfacial and Alkyl Surface Properties 105
8.4 Conclusions 108

9 Influence of Surface Coverage. II. Effects on solute retention. 110
9.1 Background 110
9.2 Results and Discussion 114
9.3 Conclusions 126

10 Effects of Polar Embedded Groups 127
10.1 Background 127
10.2 Simulation Details 129
10.3 Results and Discussion 130
10.3.1 Solvent Penetration and Wetting 130
10.3.2 Interactions of Polar-embedded Groups with Silanols 134
10.3.3 Bonded Phase Conformation 135
10.3.4 Solute Retention 140
10.3.5 Peak Tailing 145
10.4 Conclusions 146

11 The Effects of Chain Length, Pressure, and Pore Shape on Structure and Retention 147
11.1 Simulation Details 148
11.2 Analysis Details 150
11.3 Results and Discussion 151
11.3.1 Chain length effects 151
11.3.2 Pressure Effects 158
11.3.3 Surface curvature 161
11.4 Conclusions 165

12 Molecular Origins of Shape Selectivity **167**

12.1 Background 167

12.2 Simulation Details 171

12.3 Results and Discussion 173

12.4 Conclusions 188

13 Effects of Solute Chain Length **189**

13.1 Background 189

13.2 Simulation Details 190

13.3 Results and Discussion 191

13.4 Conclusions 195

References **196**

List of Tables

4.1 Total number of molecules in each of the simulated systems. 29
4.2 Average number of solvent molecules in each simulation box. 30
4.3 Free energies of solute transfer between the stationary, mobile and vapor phases. 32
4.4 Incremental free energies of transfer between stationary, mobile, and vapor phases for methylene and hydroxyl groups. 33
4.5 Number of hydrogen bonds for mobile phase molecules outside and inside the solvation shell of alkane CH_2 groups. 40
4.6 Number of hydrogen bonds per propanol solute molecule in the mobile, stationary, and vapor phases 44
6.1 Average number of solvent molecules in each simulation box. 64
6.2 Percentage of surface silanols with zero, one, two, or three hydrogen bonds with solvent molecules. 68
6.3 Structural properties of alkylsilane chains in contact with different mobile phase solvents 71
7.1 Number of hydrogen bonds per alcohol solute molecule in the ODS, mobile, and bulk *n*-hexadecane phases. 88
8.1 Average number of solvent and solute molecules in each simulation box at the five surface coverages examined 95
8.2 Summary of the average structural properties of alkylsilane chains at five different surface coverages. 99
8.3 Average solvent density and methanol molfraction enhancement within the stationary phase. 102

8.4 Number of hydrogen bonds per solvent molecule residing within the interfacial region of stationary phases with different surface coverages and in the bulk mobile phase 105
8.5 Average interfacial and alkyl surface properties for the five different surface coverages 107
9.1 Net distribution coefficients, retention factors, selectivities, and incremental free energies of retention. 116
9.2 Number of hydrogen bonds per alcohol solute molecule in retentive and mobile phases 125
10.1 Number of hydrogen bonds with solvent per stationary phase chain. . . 134
10.2 Averages of some conformational properties for stationary phases with and without polar embedded groups. 136
10.3 Number of hydrogen-bonded tethers per polar-embedded stationary phase chain 139
10.4 Number of hydrogen bonds per alcohol solute molecule in stationary phases with and without polar-embedded group. 143
10.5 Incremental free energies of retention for methylene and hydroxyl groups. 144
11.1 Summary of the chromatographic parameters and average values of stationary phase and interfacial properties. 151
11.2 Number of hydrogen bonds per surface silanol. 153
11.3 Net distribution coefficients and incremental free energies of retention. . 156
11.4 Hydrogen bond numbers for alcohol solute molecules in retentive and mobile phases. 158
12.1 Comparison of incremental free energies of retention for the phenyl group computed from simulation and obtained from experiment. 174
12.2 Simulated selectivities of $C_{18}H_{12}$ PAH isomers relative to TrP compared to experiment at different surface coverages. 175
12.3 Structural properties of C_{18} stationary phase chains nearby a four-ring PAH molecule and in the absence of any analyte molecules. 184

List of Figures

1.1 Schematic diagram of a typical RPLC system. 4
3.1 Diagram of the move types in the NpT Gibbs ensemble. 14
3.2 Diagram of a CBMC regrowth or insertion. 18
3.3 Diagram of the TraPPE intramolecular potential. 22
3.4 Diagram of the TraPPE parameterization philosophy. 23
3.5 Validation of the TraPPE parameterization philosophy. 24
4.1 Thermodynamic cycle used to decompose the free energy of retention into mobile and stationary phase contributions. 27
4.2 Snapshots of the mobile phase for the binary solvent systems. 35
4.3 Local mole fraction enhancements around solvent molecules in the mobile phase. 36
4.4 Local mole fraction enhancements around solute methyl and hydroxyl groups in the mobile phase. 37
4.5 Radial distribution functions between solute methylene groups and solvent atoms/groups in the mobile phase. 39
4.6 Radial distribution functions between propanol's oxygen atom and solvent atoms/groups in the mobile phase. 43
4.7 Snapshots of the stationary phase for systems ACN and MET. 46
4.8 Probability distribution for hydrogen-bonding molecules (solvent or solute) in the hexadecane phase to be in hydrogen-bonded aggregates composed of N_{agg} molecules. 47
5.1 Simulation boxes used in the Gibbs ensemble simulation of RPLC. . . . 51
5.2 Definition of the 1–3 and end-to-end (ete) angles and the z-location of the terminal methyl group. 57

6.1 Simulation snapshots for RPLC systems with varying mobile phase composition. . . . 65
6.2 Solvent and stationary phase density profiles for systems with varying mobile phase composition. . . . 67
6.3 Orientation of the end-to-end vector of the organic modifier and the dipole vector of water as function of z for water-acetonitrile and water-methanol mixtures. . . . 70
6.4 Fraction of gauche defects along the chain backbone. . . . 72
6.5 Probability distribution for the angle between the C_{18} end-to-end vectors and the silica surface normal and the order parameter along the chain backbone. . . . 73
7.1 Distribution coefficient profiles for butane and propanol in systems with different mobile phase compositions. . . . 80
7.2 Order parameter profiles for butane and end-to-end vector orientation profiles for propanol in systems with different mobile phase compositions. 83
7.3 Incremental retention free energy profiles for the methylene and hydroxyl groups in systems with different mobile phase compositions. . . . 85
7.4 Incremental free energy level diagrams for the methylene and hydroxyl groups. . . . 86
8.1 Evolution of the height of the terminal methyl group above the silica surface for 4 independent simulations at the 5 different surface coverages. 96
8.2 Average height of the terminal methyl group on each side of the silica slab for the five different surface coverages. . . . 97
8.3 Snapshots from simulations at five different grafting densities. . . . 98
8.4 Probability distribution of the angle between the chain end-to-end vector and the normal to the silica surface at five different grafting densities. . 100
8.5 Order parameter along chain backbone for the angle between 1–3 backbone vectors and the normal to the silica surface at five different grafting densities. . . . 101
8.6 Density profiles at five different grafting densities. . . . 103
8.7 Local methanol molfraction enhancement profiles at five different grafting densities. . . . 104

8.8 End-to-end vector orientation of methanol at five different grafting densities. . . . 106
8.9 Solvent-accessible surface area density (SASAD) as function of z at the five different grafting densities . . . 108
9.1 Distribution coefficients and retention factors for *n*-butane and 1-propanol and free energies of retention for the methylene and the hydroxyl group at different surface coverages. . . . 115
9.2 Distribution coefficient profiles for *n*-butane and 1-propanol at different surface coverages. . . . 117
9.3 Solute orientational profiles at different surface coverages. . . . 119
9.4 Distribution of *n*-butane in the plane parallel to the silica surface at different surface coverages. . . . 120
9.5 Simulation snapshots of retained *n*-butane molecules at a coverage of 4.2 μmol/m^2. . . . 121
9.6 Distribution of 1-propanol in the plane parallel to the silica surface at different surface coverages. . . . 123
9.7 Simulation snapshots of retained 1-propanol molecules at a coverage of 2.9 μmol/m^2. . . . 124
9.8 Incremental free energy profiles at different surface coverages. . . . 126
10.1 Bonded phase chemical structures. . . . 129
10.2 Simulation snapshots and density profiles for stationary phases with and without polar-embedded group. . . . 131
10.3 Local methanol molfraction enhancement profiles for systems 33M and 67M. . . . 132
10.4 Bonded phase–solvent radial distribution functions for the amide and ether phases in solvent 33M. . . . 133
10.5 Polar-embedded group–silanol radial distribution functions in solvent system 33M. . . . 135
10.6 Probability distribution for the cosine of the angle between the chain end-to-end vector and the normal to the silica substrate. . . . 137
10.7 Order parameter and fraction of gauche defects along the chain backbone in solvent 33M. . . . 138

10.8 Definitions of the different types of hydrogen bonded tethers for polar embedded groups (PEG) and snapshot of a solvent mediated tether. . . 139
10.9 Distribution coefficient profiles for n-butane and 1-propanol on stationary phases with and without polar-embedded group. 140
10.10Incremental free energy profiles for methylene and hydroxyl groups on stationary phases with and without polar embedded groups. 142
11.1 Simulation snapshot of the slitpore used for the examination of surface curvature effects. 149
11.2 Simulation snapshots and density profiles for stationary phases with different alkyl chain lengths. 152
11.3 Methanol molfraction enhancement profiles and end-to-end vector orientational distributions for stationary phases with different alkyl chain lengths. 154
11.4 Solute distribution coefficient and incremental free energy profiles for stationary phases with different alkyl chain lengths. 155
11.5 Simulation snapshots and density profiles for stationary phases at different pressuress. 159
11.6 Methanol molfraction enhancement profiles and end-to-end vector orientational distributions for stationary phases at different pressures. 160
11.7 Solute distribution coefficient and incremental free energy profiles for stationary phases at different pressures. 161
11.8 Simulation snapshots and density profiles for stationary phases with different pore shapes. 162
11.9 Methanol molfraction enhancement profiles and end-to-end vector orientational distributions for stationary phases with different pore shapes. . 163
11.10Solute distribution coefficient and incremental free energy profiles for stationary phases with pore shapes. 164
12.1 PAH solutes present in the simulations. The double headed arrows indicate the pairs involved in molecular identity interchange moves. 171
12.2 Distribution coefficient profiles for PAHs of increasing size. 176
12.3 Order parameter profiles for PAHs of different size. 178

12.4 Lateral distribution of PAH solutes of different size in the x-y plane at a surface coverage of 4.15 μmol/m^2. 179
12.5 Distribution coefficient and order parameter profiles for the NAP and BcP PAH isomers. 180
12.6 Lateral distribution of retained NAP and BcP analytes in the x-y plane at the three different surface coverages. 181
12.7 Snapshots of the stationary chain structure in the presence and absence of a solute. Both snapshots were taken from the same perspective, but at different periods during the simulation. 183
12.8 Order parameter along the chain backbone indicating chain alignment. . 185
12.9 Stationary phase carbon density in the x-y plane. 187
13.1 Free energy of retention versus solute carbon number for the homologous series of alkanes. 191
13.2 Distribution coefficient profiles for alkane solutes of different length. . . 192
13.3 Order parameter profiles for linear alkane solutes of different length. . . 194
13.4 Snapshot of a C_{14} alkane solute retained on a C_8 stationary phase. . . . 195

Overview

With the ever increasing speed and availability of computational resources the "computer experiment" (i.e., molecular simulation) has become a extremely powerful tool for conducting scientific research. A molecular simulation is carried out by simply specifying the system of interest, for example, the number of molecules of each type, temperature and pressure. Then, statistical mechanics allows one to follow the trajectory of the system through phase space. From the data contained in this trajectory, one can compute various mechanical and thermal properties for the system.

There are numerous advantages for the use of molecular simulation in the study of chemical systems. First, simulations may be used as a predictive tool for thermodynamic and other properties when experiments are not feasible (for example, due to cost or safety concerns). Second, simulations allow for the unperturbed study of chemical systems under precisely defined and controlled conditions. Finally, the particle based nature of simulation allows one to gain a microscopic-level insight into the physical world that is often not realizable experimentally. This insight can be used to shed light on experimental results that have eluded a detailed molecular explanation. In the present work, molecular simulation is applied to study of reversed-phase liquid chromatography (RPLC).

In the chemical industry, separation processes, in general, represent 40–70% of both capital and operating costs [1] and are large sources of energy consumption and chemical waste production. Furthermore, separations are of utmost importance in chemical research where sample purification and analysis is often a daily task. Liquid chromatography (LC) is the method of choice for an extremely wide range of chemical separations and, among the various modes of LC, RPLC is by far the most popular [2]. In fact, it has been estimated that approximately 90% of all analytical separations involving small

organic molecules are carried out using RPLC [3].

Clearly, optimizing various separation processes, such as RPLC, can significantly reduce costs and benefit the environment. The first step towards improving an existing separation process, and the goal of this study in the context of RPLC, is a better understanding of that process at the molecular level. Furthermore, this detailed understanding will facilitate development of new, and greener, separation technologies. In this thesis it will be shown that efficient Monte Carlo simulations using accurate and transferable force fields are a very effective tools for attaining this molecular-level understanding.

This thesis begins with an overview of the RPLC technique and some of the current issues that need to be resolved. Next, the basic principles of molecular simulation are introduced and some of the advanced simulation techniques used in this work are described. Following this, a systematic molecular simulation study aimed at yielding numerous microscopic insights into RPLC is discussed.

Chapter 1

Reversed-phase Liquid Chromatography

1.1 Introduction to the RPLC Technique

The heart of the any RPLC system is the column (see Figure 1.1). Inside this column is the stationary phase, which most often consists of a packing of micrometer-sized beads of porous silica whose surfaces have been chemically modified by the grafting of C_{18} chains, although other functionalities are commonly used. Through this column the mobile phase, usually an aqueous-organic solvent, is pumped. The mixture that is to be separated is injected at the front of the column and is carried through by the mobile phase solvent. The components of this chemical mixture will travel through the column at different rates governed by their relative affinities for the nonpolar stationary phase and polar mobile phase. For example, a more nonpolar molecule will have a higher affinity for the stationary phase and will be retained in the column longer than a more polar molecule that has a higher affinity for the mobile phase. The time it takes the various analyte molecules to traverse the column, or retention time, is quantified by an appropriate detection system at the end of the column. This retention time is intimately related to the thermodynamics of the retention process, which will be discussed in the following paragraphs.

In the description of retention in RPLC it is often assumed that a distribution equilibria is established between the mobile and stationary phases [3, 4]. In this case,

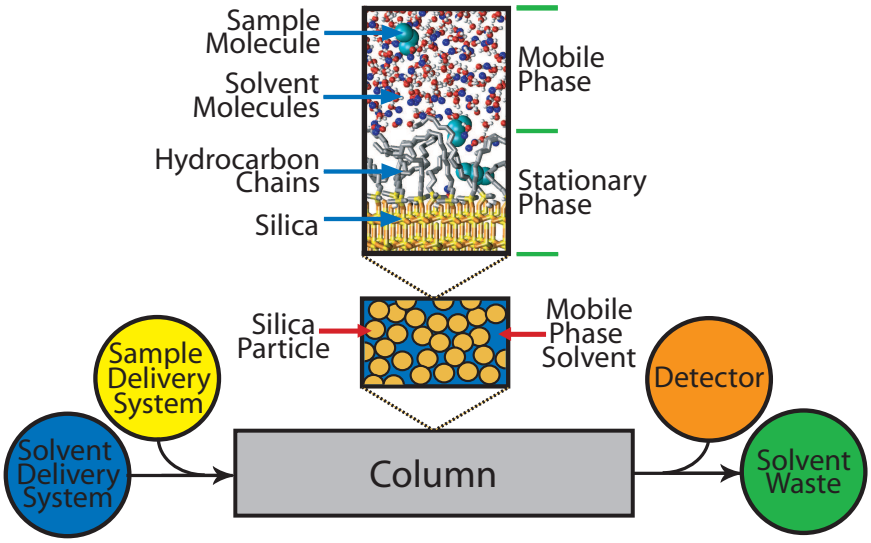

Figure 1.1: Schematic diagram of a typical RPLC system.

for an analyte molecule A, one may write

$$\mathrm{A}_{\mathrm{mobile}} \rightleftharpoons \mathrm{A}_{\mathrm{stationary}} \tag{1.1}$$

and this implies an equilibrium constant, K, or distribution coefficient as it will be referred to hereafter, for the analyte molecule

$$K = \frac{[A]_{\mathrm{s}}}{[A]_{\mathrm{m}}} \tag{1.2}$$

where $[A]_{\mathrm{s}}$ and $[A]_{\mathrm{m}}$ are the concentrations of A in the stationary and mobile phases, respectively. From this distribution coefficient one can define a free energy of transfer from the mobile phase to the stationary phase, or free energy of retention ΔG_{retn}, for the molecule A

$$\Delta G_{\mathrm{retn}} = -RT \ln K \tag{1.3}$$

Thus, a more retained solute will have a larger K and a more negative (favorable) ΔG_{retn}. Instead of distribution coefficients and free energies it is often more convenient to describe the degree solute retention through the retention time (t_{R}) since this is a more easily measurable quantity. It is trivial to show that this retention time can be

related to the distribution coefficient by

$$K/\phi = k' = \frac{t_{\mathrm{R}}}{t_{\mathrm{M}}} - 1 \tag{1.4}$$

where ϕ is the ratio of volume of mobile phase to the volume of stationary phase in the column, or phase ratio, and t_{M} is the time is take the unretained species to traverse the column [3, 4]. The capacity factor (k') above is often used in chromatography, rather than K, since the it does not depend on the phase ratio, a difficult quantity to measure.

In chromatography one is interested in the separation of two (or more) analytes, call them A and B. For this to occur the affinities of A and B for the mobile and stationary phases must be different. One can quantify this difference in affinity through the selectivity factor [3, 4]

$$\alpha = \frac{K_{\mathrm{B}}}{K_{\mathrm{A}}} = \frac{k'_{\mathrm{B}}}{k'_{\mathrm{A}}} \tag{1.5}$$

where the more retained solute (larger K) appears in the numerator so that $\alpha > 1$. Inserting equation 1.4, this selectivity factor may be related to the retention times of A and B through

$$\alpha = \frac{t_{\mathrm{R,B}} - t_{\mathrm{M}}}{t_{\mathrm{R,A}} - t_{\mathrm{M}}} \tag{1.6}$$

In order for two peaks on a chromatogram to be resolved (i.e., for an effective separation) one typically desires a selectivity factor greater than 1.1–1.2 [3, 4]. Using equations 1.3 and 1.5, one can express this selectivity in terms of a difference in free energy of retention.

$$\Delta G_{\mathrm{retn,A}} - \Delta G_{\mathrm{retn,B}} = RT \ln K_{\mathrm{B}} - RT \ln K_{\mathrm{A}} = RT \ln \alpha \tag{1.7}$$

Inserting the minimum selectivity factor of 1.1 into the above equation one sees that the difference free energy is small, only about 0.2 kJ/mol.

From the discussion above, one can see that RPLC is extremely sensitive to small differences in a molecule's interactions with the mobile and stationary phases. Thus, in order to understand the RPLC technique it is extremely important to understand these interactions, or the retention mechanism, at the molecular-level. However, attaining this detailed understanding has been quite difficult.

1.2 The Elusive Retention Mechanism

Due to importance and popularity of RPLC, discerning the mechanism of solute retention has been the subject of intense research for the past three decades [5, 6, 7, 8, 9, 10, 11, 12, 13, 14, 15, 16, 17, 18, 19, 20, 21, 22, 23, 24, 25, 26, 27, 28, 29, 30, 31, 32, 33, 34, 35, 36, 37, 38, 39, 40, 41, 42, 43, 44]. Indeed these studies have yielded a wealth of information about retention in RPLC, but despite these efforts many of the key details behind the retention process are still not settled. For example, many of these studies have reached conflicting conclusions regarding whether adsorption at the stationary phase/mobile phase interface or full partitioning into the stationary phase is more important for solute retention and to what extent various chromatographic parameters, such as mobile phase composition and grafting density, affect this. Even if partitioning is taken to be the dominant mechanism of retention, it is not clear if the process can be modeled accurately by bulk liquid–liquid (oil–water) partitioning [11, 15] or if partitioning into the more ordered RPLC stationary phase involves a different molecular mechanism [19, 20]. Furthermore, it has been debated whether the thermodynamic driving forces for solute retention (transfer from mobile to stationary phase) are primarily from solvophobic interactions with the mobile phase [16, 17, 18] or lipophilic interactions with the stationary phase [11, 15]

The difficulty in arriving at a clear molecular picture of retention stems from difficulty in attaining molecular-level information from experiment. The majority of studies on the retention mechanism are based upon the analysis of retention data for different analytes under various chromatographic conditions [5, 6, 7, 8, 9, 10, 11, 12, 13, 14, 15, 16, 17, 18, 19, 20, 21, 22, 23, 24]. However, retention data, or any thermodynamic quantity, can only be shown to be consistent with a particular molecular mechanism and cannot offer conclusive proof. Another experimental means of studying retention mechanisms is via spectroscopic measurements [26, 27, 28, 29, 30, 31, 32, 33, 34]. While these measurements can indeed yield more direct molecular information than a thermodynamic analysis, spectroscopy is hampered by the inability to observe precise configurations of a single solute molecule in the RPLC system. Instead one is left with the daunting task of analyzing a complex distribution of solute configurations. A third line of investigation involves the use of theory [35, 36, 37, 38, 39, 40, 41, 42, 43, 44]. Most of these

theoretical investigations employ some sort of simplified lattice model to describe the RPLC system since more sophisticated models would be far too complex to allow for an analytical treatment. Although many insights have been gained from these models, they have failed to offer true atomistic details and quantitative agreement with experiment.

The problem of pinpointing the retention mechanism in RPLC is further exacerbated by an incomplete picture of the structure of the tethered alkyl chains in the stationary phase. Most would agree that the chains cannot simply be described as a disordered liquid or an ordered solid [26], but to what extent they are ordered is not fully characterized. Furthermore, it is not understood how these chains interact with the mobile phase solvent. While it is generally held that organic component of the aqueous-organic preferentially solvates the stationary phase, it is not fully resolved if this excess solvation occurs solely through the formation of an organic layer atop the stationary phase [45, 46] or if penetration of the organic modifier into the stationary phase is also important [47, 48]. In the former case, retention could be affected by partitioning of the solutes into this organic layer, and in the latter case, solutes may compete with solvent molecules for space inside the stationary phase. Furthermore, changes in the extent of solvation of the stationary phase with changing mobile phase composition may effect the conformation of the alkyl chains.

The need for a detailed molecular picture of retention and the difficulty in attaining this view experimentally has led many groups to explore the use of molecular simulation for the study of RPLC [49, 50, 51, 52, 53, 54, 55, 56, 57, 58, 59, 60, 61, 62, 63, 64, 65, 66, 67], including our own [68, 69, 70, 71, 72, 73, 74, 75, 76, 77, 78]. The clear advantage of simulation is that the one can model the RPLC system at the individual atom level of detail and a true molecular picture of structure and retention can be achieved. However, the validity of this molecular picture hinges on the accuracy and precision of the simulation. All of the previous simulations of RPLC carried out by other groups have utilized the molecular dynamics technique, while the work described in this thesis employs the Monte Carlo technique. In the following chapters these two simulation techniques will be introduced and the merits of using the Monte Carlo method to study RPLC will be discussed.

Chapter 2

Statistical Mechanics and Molecular Simulation

Molecules are small. For example, a 12 oz. glass of water contains over 10^{25} molecules. At room temperature, the water in this glass has a density of 0.9971 g/mL, a vapor pressure of 3166 Pa, and a heat capacity of 4.184 J/g°C. These are a few of the macroscopic properties of water. One does not need to know anything about molecules, or if they even exist, to know the macroscopic properties of a system. They can simply be measured or observed. However, each of these macroscopic properties is intimately tied to the microscopic behavior of the molecules that make up the system. In fact, if one can accurately describe the intra and intermolecular interactions in a system, then one can predict the macroscopic properties for that system without ever physically measuring them. The prescription for this conversion from the microscopic world in which molecules live to the macroscopic world is rooted in the theoretical framework of statistical mechanics and molecular simulation is an important tool by which this transformation can be carried out. In the following some important concepts in statistical mechanics will be discussed and the technique of molecular simulation will be introduced.

In a liquid system, a wide range of molecular states, or configurations, can be accessed. Classically, each possible state in the system is characterized by a set of coordinates $\mathbf{r}$ and $\mathbf{p}$ that describe the position and momenta of every atom in the system. The

entire collection of all possible states is called phase space, while a given set of **r** and **p** is called a point in phase space. According to statistical mechanics [79], for a system under the macroscopic constraints of constant temperature, pressure, and number of molecules (i.e., a canonical, or NVT, ensemble), the probability of the system visiting any one of the these states i is

$$\rho_i = \frac{\exp(-\beta E_i)}{Q} \tag{2.1}$$

where E_i is the energy of the system, $\beta = 1/kT$, k is Boltzmann's constant and T is temperature. In the denominator is Q, the canonical ensemble partition function

$$Q = \sum_j \exp(-\beta E_j) \tag{2.2}$$

and the above sum runs over all possible states of the system. The average of any mechanical property, $\langle M \rangle$, in the system can be expressed as

$$\langle M \rangle = \frac{\sum_j M_j \exp(-\beta E_j)}{Q} \tag{2.3}$$

where M_j is the value of the property for state j. In addition to averages, knowledge of the partition function allows for the calculation of thermal properties. For example, in the canonical ensemble the Helmholtz free energy is related to the logarithm of the partition function by

$$A(N, V, T) = -k_{\mathrm{B}} T \ln Q(N, V, T) \tag{2.4}$$

Note that both A and Q are functions of the same natural variables (N, V, T).

There are other common ensembles, each characterized by some set of macroscopic constraints. For example, the isobaric-isothermal has constant N, p (pressure), and T and the grand-canonical ensemble has constant μ (chemical potential), V, and T. Each of these ensembles will have a unique partition function that allows for the calculation of probabilities and averages and each is tied to a particular thermodynamic state function that shares the same natural variables. For a given problem, one chooses a particular ensemble purely as a matter of convenience and in the limit of infinitely large system size all ensembles will give equivalent results [79, 80].

At this point it appears that there are some seemingly simple equations that allow one to compute average properties of a system as long as one knows how to compute the energy (an issue that will be addressed in Chapter 3). However, in practice things are

not that simple. The number of terms in the summation in equation 2.3 is enormous, it is of magnitude 10^N, where N is the number of molecules in the system [79]. Consider a fairly small system of 1000 molecules. That's 10^{1000} terms! Clearly, even with today's vast computational resources, one cannot visit all of these states and directly compute the average. Instead, one must reduce the number of terms and estimate the average in equation 2.3 by sampling some small subset of the states. An imprecise estimate of the average might be attained by sampling 1 in every 10^{100} states. This leaves 10^{900} terms that need to be evaluated, and the problem is still intractable. The key idea that allows for an accurate calculation of the average while generating a manageable number of states is that most of the states of a system are of significantly high energy that they contribute very little to the average (E_i is large, so $\exp(-\beta E_i)$ is small). Thus, if one can find a way to sample only those states that contribute significantly to the average, then the problem is truncated greatly. To accomplish this, some means of generating these higher probability configurations of the system is needed. This is where molecular simulation comes in.

Molecular simulations are carried out via two principle methods, molecular dynamics (MD) and Monte Carlo (MC). The former is a deterministic method with an explicit dependence on time while the latter is stochastic method with no dependence on time. However, both methods depend on a well-defined way to describe the energy of the system, i.e., a potential energy function, and both methods generate configurations of the system based on their statistical mechanical probabilities described above. For this reason, MD and MC simulations will yield equivalent results for a given system, so long as the simulations are performed correctly.

In a MD simulation one starts with the system in some initial state described by the position and momenta of all particles. Forces between the particles (the derivative of the potential energy) are computed in predetermined increments of time. With these forces and the current particle positions and momenta, the position and momenta of each particle at the next time increment can be computed via Newton's equations of motion [80]. The process is repeated for some number of steps and, thus, the system evolves with time. The average properties for the system can then be computed by averaging the properties at each individual time step.

The application of the MC simulation method is most easily demonstrated in the

canonical ensemble. For simplicity, the process will be described for an atomic system (only translational degrees of freedom) but an analogous procedure can be demonstrated for molecular systems with rotational and conformational degrees of freedom. In a MC simulation, one starts with the system in some initial state described by the position of all of the particles. With these coordinates, the initial potential energy of the system, U_{old}, can be computed. Next, a trial move is attempted by randomly picking a particle in the system. This particle is then moved in a random direction by a distance between zero an arbitrary maximum displacement. The new potential energy, U_{new}, of the system is then computed. If the energy of this system is lowered, the move is immediately accepted. Otherwise, the move is accepted with a probability of

$$P_{\text{accept}} = \exp[-\beta(U_{\text{new}} - U_{\text{old}})] \tag{2.5}$$

When a move is accepted, the new configuration is kept and its properties are counted towards the averages for the system. When a move is rejected, the old coordinates of the system are restored and the properties of this old configuration are counted again towards the averages of the system. It can be shown that this technique samples configurations with exact probability prescribed by equation 2.1 above. This basic MC technique was originally described by Metropolis and coworkers in 1953 [81] and many more sophisticated algorithms have been developed since then.

In the above examples, it appears that the MD method is much more intuitive (envision computing the position of the balls after a player shoots in a billiards game) while the MC method is much more abstract. However, there are some distinct advantages to the MC method. First, the MC method has no dependence on time. Most modern MD simulations are limited to fractions of a microsecond at most. If a physical process requires more time than this, its simulation is out of the reach of the time scale accessible with MD. Second, MC methods allow for simulations to be carried out in open ensembles where the number of particles is allowed to fluctuate. This allows one to carefully control the chemical potentials of the species involved in the simulation. Third, MC simulations allow one to carry out unphysical moves that greatly enhance the sampling of phase space. These last two advantages will be expanded upon the following sections.

Chapter 3

Accuracy and Precision in a Simulation

Just as with experimental measurements, the are two principal challenges that must be overcome in a simulation. The first is to attain results that are precise and the second is to attain results that are accurate. In a simulation, precision depends solely on the efficient sampling of the important configurations of the system (the relevant regions of phase space) and accuracy depends solely on the model used to describe the inter- and intramolecular interactions (the force field). It has taken more than ten years to develop the capability to simulate RPLC systems with the level of precision and accuracy needed to reproduce experimental retention data and to provide molecular insights on the retention mechanism. This includes the development of accurate and transferable force fields and advanced Monte Carlo algorithms that dramatically enhance sampling efficiency. Because of their importance to the current work, this chapter will be devoted to a discussion of these algorithms and force fields.

3.1 Advanced Monte Carlo Methods

As discussed in Chapter 2, only a few small regions of phase space possess favorable enough energies to make significant contributions to the average properties of a system. Sampling problems can arise when these important regions of phase space are separated from each other by large free energy barriers. In these cases, the system can get "stuck"

in one of these important regions and never sample the others. In order to get around this problem, advanced Monte Carlo algorithms that allow the system to hop over these free energy barriers are used. The following sections will deal with a couple of the advanced Monte Carlo methods that are employed in this work for the simulation of RPLC.

3.1.1 Gibbs Ensemble Monte Carlo

Simulations of phase equilibria in standard ensembles, such as the canonical ensemble, can be problematic. If one starts the system as a homogeneous mixture it is highly unlikely that this mixture will phase separate during the simulation since there is an enormous free energy barrier for interface formation. Even if one starts with a two phase system, precisely calculating quantities like solute partition constants is rather difficult. For a precise value of the partition constant, the solute would need to move between the two phases numerous times during the simulation. However, particle diffusion is rather slow and this would require a prohibitively long simulation.

A rather ingenious solution this problem was put forth by Panagiotopoulos who developed a completely new ensemble, called the Gibbs ensemble, for the simulation of phase equilibria [82, 83]. In this ensemble multiple subsystems (i.e., simulation boxes), which represent the different phases, are in thermodynamic contact but do not share a direct physical interface. The temperature and total number of particles in the entire system is fixed, but the particles are allowed to transfer between the different subsystems. This movement of particles between subsystems allows the system to hop over the free energy barriers associated with particle diffusion and the absence of a physical interface between the phases removes the barrier for interface formation. There are two versions of the Gibbs ensemble, NVT and NpT. In the NVT version, the total volume of the system is fixed, but the subsystems may exchange volume while, in the NpT version, the pressure is fixed and subsystems' volumes fluctuate independently of one another. The following discussion will be limited to the NpT version as it the technique used in the this work.

There are four principle types of moves in a Gibbs ensemble Monte Carlo simulation as applied in this work (see Figure 3.1). The first three of these moves were described in the original work [82, 83] while the fourth was developed slightly later [84]. The

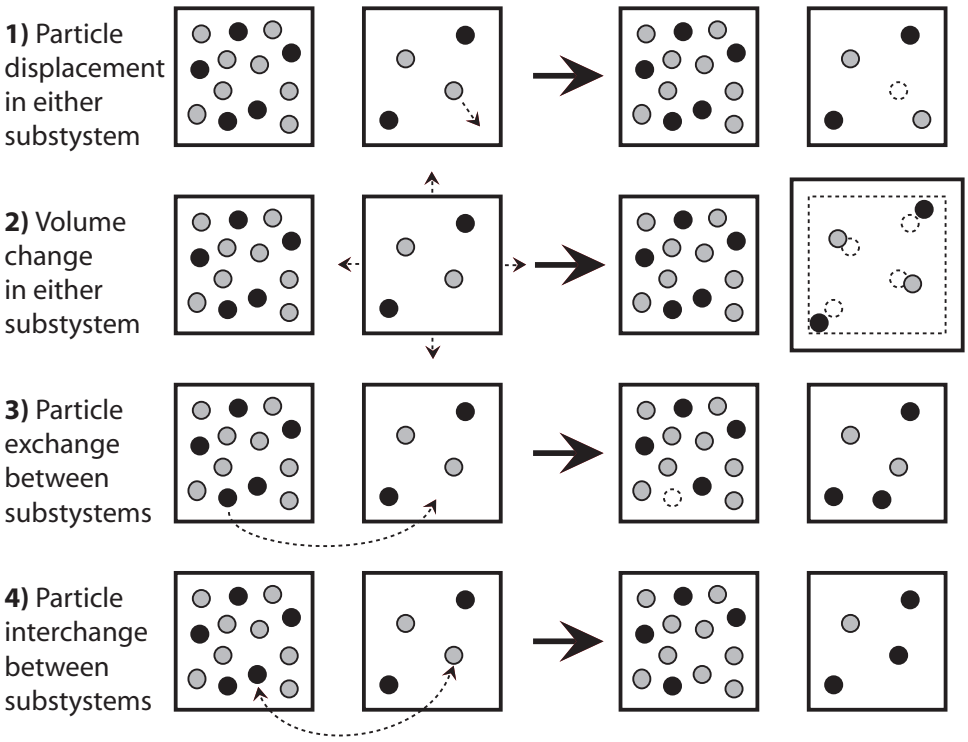

Figure 3.1: Diagram of the move types in the NpT Gibbs ensemble.

description of these moves will be limited to the atomic system for simplicity and the extension to molecular systems will be made in the next section. To demonstrate these moves a system with two components, X and Y, and with two subsystems, A and B, will be considered.

The first type of move involves particle displacement within a given subsystem. In this move a particle type (X or Y) is chosen at random and a particle of that type is randomly selected without regard to which subsystem the particle is currently in. After a particle is selected, it is translated a distance chosen randomly between zero and some predetermined, but arbitrary maximum. This move is equivalent to the Metropolis scheme discussed in Chapter 2. Thus, the probability of accepting the move P_{accept} can be expressed as

$$P_{\text{accept}} = \min[1, \exp(-\beta \Delta U)] \tag{3.1}$$

where ΔU is the change in potential energy for the entire system. This means the move is accepted if the energy is lowered and accepted with a probability of $\exp(-\beta\Delta U)$ if the energy goes up. These particle displacement moves ensure that the system reaches thermal equilibrium at the specified temperature.

The second type of move involves a volume change for one of the subsystems. In this move, one of the subsystems is chosen at random and given some random volume change ΔV between 0 and some predetermined maximum. During the volume change, the particle positions are scaled uniformly. The energy is computed for the initial volume V and the new volume V' and the move is accepted with a probability of

$$P_{\text{accept}} = \min\left[1, \exp\left\{-\beta\left(\Delta U + p\Delta V + \beta^{-1}N^{\text{T}}\ln\frac{V}{V'}\right)\right\}\right] \tag{3.2}$$

where p is the external pressure chosen for the simulation and N^{T} is the total number of particles in that subsystem. These volume moves ensure that the system reaches mechanical equilibrium at the specified external pressure.

The third type of move involves particle transfer between the subsystems. In this move, a particle type and direction for the transfer are chosen at random. Next, a particle from the proper subsystem is selected randomly. The particle is then moved from its current subsystem to a random location in the other subsystem and ΔU for the move is computed. Suppose that particle type X was chosen and moved from subsystem A to subsystem B. In this case the acceptance probability would be

$$P_{\text{accept}} = \min\left[1, \exp\left\{-\beta\left(\Delta U + \beta^{-1}\ln\frac{V_{\text{A}}(N_{\text{B}}^{\text{X}}+1)}{V_{\text{B}}N_{\text{A}}^{\text{X}}}\right)\right\}\right] \tag{3.3}$$

where V_{A} and V_{B} are the volumes of subsystem A and B, and N_{A}^{X} and N_{B}^{X} are the numbers of particles of type X in subsystems A and B before the move was executed. These particle exchange moves ensure that the chemical potential of each species is the same in all subsystems. This is absolutely critical for simulating processes involving phase equilibria because when a species is distributed between two phases, it is only an equilibrium distribution when its chemical potential is the same in both phases.

The fourth type of moves involves interchanging the identities of particles in two different subsystems. In this move, the direction of the interchange is first chosen at random. Next, particles of the appropriate types are selected randomly from subsystems

A and B and their locations are exchanged. Suppose that it was chosen to interchange a particle of type X in subsystem A with a particle of type Y in subsystem B. In this case, the acceptance probability would be

$$P_{\text{accept}} = \min\left[1, \exp\left\{-\beta\left(\Delta U + \beta^{-1}\ln\frac{(N_{\text{B}}^{\text{X}}+1)(N_{\text{A}}^{\text{Y}}+1)}{N_{\text{A}}^{\text{X}}N_{\text{B}}^{\text{Y}}}\right)\right\}\right] \tag{3.4}$$

where N_i^j refers to the number of particles of type j in system i before the move was executed. This move ensures the difference in chemical potentials between the different particle types is equilibrated. The move is not strictly necessary in the Gibbs ensemble since particle transfers should also ensure this. However, this move can can greatly enhance sampling efficiency. For example, consider the case where type X is a small particle and type Y is large. Finding a cavity of sufficient size for particle Y during a standard particle transfer may be highly improbable due to its size, but when X and Y are exchanged a cavity already exists and the move should be accepted at a much higher rate.

One of the distinct advantages of the Gibbs ensemble is that, in addition to yielding the properties of coexisting phases at given state point, it allows for the calculation of solute partition coefficients and free energies of transfer from a single simulation. Furthermore, these quantities are computed from mechanical properties, namely the number densities, via

$$K_{\alpha\to\beta} = \frac{\rho_\beta}{\rho_\alpha} \tag{3.5}$$

$$\Delta G_{\alpha\to\beta} = -RT\ln K_{\alpha\to\beta} \tag{3.6}$$

where $K_{\alpha\to\beta}$ and $\Delta G_{\alpha\to\beta}$ are the partition constant and free energy for transfer from phase α to phase β and ρ_i is the ensemble averaged number density in phase i [85, 86]. The determination of mechanical properties from simulation can typically be done with very high precision, whereas computing thermal properties, such as free energies, by traditional means (e.g. thermodynamic integration and free energy perturbation) is usually more challenging [87]. This is very important in the simulation of RPLC since very precise data is needed on solute partitioning.

3.1.2 Configurational-bias Monte Carlo

In the atomic system, simple translational moves are often sufficient to adequately sample the important regions of phase space. For molecular systems, one can envision a similar type of move. Consider a system composed of C_{18} chains. To sample the conformational degrees of freedom in the chains, one could randomly choose a chain, then randomly choose a dihedral angle. This angle could be displaced by some random amount and the initial and final energies of the system could be computed. This energy change could then be used to decide if the move should be accepted in exactly the same manner as a translational displacement. The problem with this strategy is that even for a small change of a dihedral angle in the center of the chain, there could be a large displacement of the chain ends. This large displacement would lead to a very high probability of overlap with a neighboring chain molecule, especially in a system with a typical liquid density. Thus, the vast majority of these types of moves would be rejected and very little phase space could be sampled. A similar problem arises when carrying out particle transfer moves in the Gibbs ensemble. It is extremely unlikely to find a favorable position by simply inserting an entire molecule in a single step.

To overcome this problem, the configurational-bias Monte Carlo (CBMC) technique was developed [88, 89]. In the CBMC technique, the chain molecule is regrown one segment at a time, which greatly enhances the acceptance probability of a conformational change. There are various descriptions of the CBMC algorithm, but for the present discussion the procedure given in reference [90] will be described.

It is often useful, when using CBMC, to split the potential energy into bonded (u^{int}) and nonbonded (u^{ext}) parts. The bonded part of the potential, which may include torsional, bending, and stretching potentials, is used to generate trial sites for the segments of the chain. The nonbonded potential is then used to bias the selection of a trial site from the rest of the trial sites. The separation of the potential into these two parts is completely arbitrary and may be adjusted to increase efficiency for specific applications.

Consider the regrowth of a whole chain of s segments (see Figure 3.2). For segment 1 of the chain, k trial sites are placed at random positions in the simulation box and one of them, call it i, is selected with a probability

$$P_{1i}^{\text{selecting}}(\mathbf{b}_i) = \frac{\exp(-\beta u_{1i}^{\text{ext}})}{w_1(\text{n})} \tag{3.7}$$

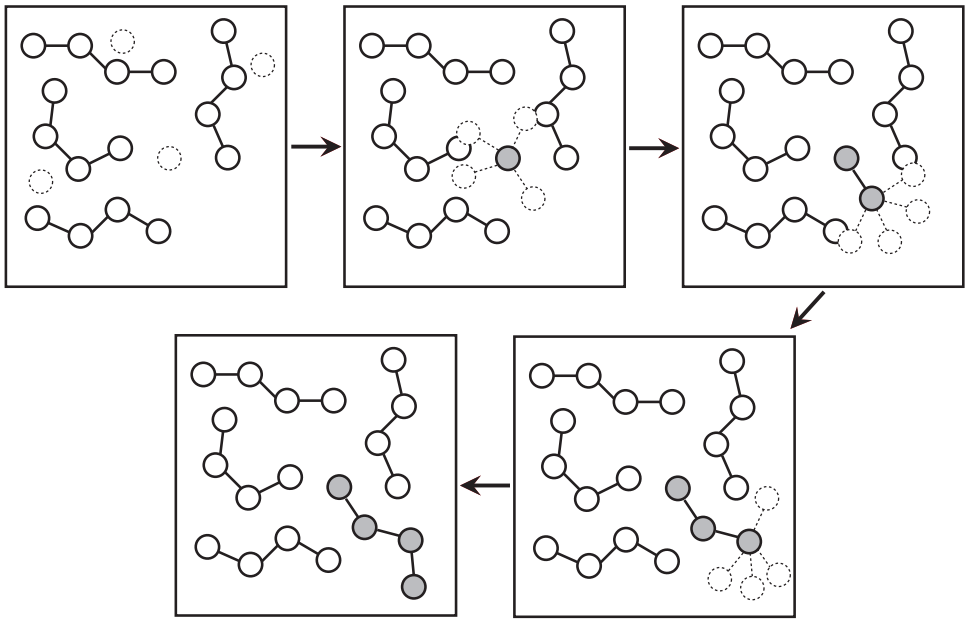

Figure 3.2: Diagram of a CBMC regrowth or insertion. In the each step, random locations for the next segment are generated (circles with dashed lines). One of these sites is then selected according to its Boltzmann weight (shaded circles). Trial sites resulting in unfavorable interactions with neighboring molecules or intramolecular strain are unlikely to be selected.

where

$$w_1(\mathrm{n}) = \sum_{j=1}^{k} \exp(-\beta u_{1j}^{\mathrm{ext}}) \tag{3.8}$$

and is termed the Rosenbluth weight of the first segment. Consecutive trial segments l of the chain are then grown until the chain is complete by first generating k trial orientations $\mathbf{b}_i$ according to the Boltzmann weight of the internal potential of the segment

$$P_{li}^{\mathrm{generating}}(\mathbf{b}_i)\mathrm{d}\mathbf{b} = \frac{\exp(-\beta u_{li}^{\mathrm{int}})\mathrm{d}\mathbf{b}}{\int \exp(-\beta u_{l}^{\mathrm{int}})\mathrm{d}\mathbf{b}} \tag{3.9}$$

One of the k trials is then selected with a probability, like the first segment, according to the Boltzmann weight of its external potential

$$P_{li}^{\mathrm{selecting}}(\mathbf{b}_i) = \frac{\exp(-\beta u_{li}^{\mathrm{ext}})}{w_l(\mathrm{n})} \tag{3.10}$$

where

$$w_l(\mathrm{n}) = \sum_{j=1}^{k} \exp(-\beta u_{lj}^{\mathrm{ext}}) \tag{3.11}$$

Once complete, the probability $P(\mathrm{n})$ of growing the new chain may be computed from the products of the probabilities of generating and selecting each segment

$$P(\mathrm{n}) = \prod_{l=1}^{s} P_{li}^{\mathrm{selecting}} P_{li}^{\mathrm{generating}} \tag{3.12}$$

where the index i denotes the trial segment that was selected. Additionally, the Rosenbluth weight $W(\mathrm{n})$ for the whole chain may be computed by

$$W(\mathrm{n}) = \prod_{l=1}^{s} w_l(\mathrm{n}) \tag{3.13}$$

In order to compute the acceptance probability for the newly grown chain, the Rosenbluth weight $W(\mathrm{o})$ for the old configuration of the chain must also be computed. To do so $k-1$ random positions for segment 1 are generated to compute the old Rosenbluth weight for the first segment

$$w_1(\mathrm{o}) = \exp(-\beta u_{1k}^{\mathrm{ext}}) + \sum_{j=1}^{k-1} \exp(-\beta u_{1j}^{\mathrm{ext}}) \tag{3.14}$$

where $\exp(-\beta u_{1k}^{\mathrm{ext}})$ is the actual external potential for the first segment in the old configuration. The probability that this segment would have been selected is then

$$P_{1k}^{\mathrm{selecting}}(\mathbf{b}_k) = \frac{\exp(-\beta u_{1f}^{\mathrm{ext}})}{w_1(\mathrm{o})} \tag{3.15}$$

Similarly, $k-1$ trial orientations are generated for each of the subsequent segments by the probability given in equation 3.9. The Rosenbluth weight for each of these segments is given by

$$w_l(\mathrm{o}) = \exp(-\beta u_{lk}^{\mathrm{ext}}) + \sum_{j=1}^{k-1} \exp(-\beta u_{lj}^{\mathrm{ext}}) \tag{3.16}$$

and, again, $\exp(-\beta u_{lk}^{\mathrm{ext}})$ is the actual external potential for the l^{th} segment in the old configuration. The probability that each of the k^{th} segments would have been generated and selected is, respectively

$$P_{lk}^{\mathrm{generating}}(\mathbf{b}_k)\mathrm{d}\mathbf{b} = \frac{\exp(-\beta u_{lk}^{\mathrm{int}})\mathrm{d}\mathbf{b}}{\int \exp(-\beta u_{l}^{\mathrm{int}})\mathrm{d}\mathbf{b}} \tag{3.17}$$

and

$$P_{lk}^{\text{selecting}}(\mathbf{b}_k) = \frac{\exp(-\beta u_{lk}^{\text{ext}})}{w_l(0)} \tag{3.18}$$

and the overall probability $P(\text{o})$ of growing the old chain is

$$P(\text{o}) = \prod_{l=1}^{s} P_{lk}^{\text{selecting}} P_{lk}^{\text{generating}} \tag{3.19}$$

From the Rosenbluth weights of the each of old segments, the Rosenbluth weight for the old configuration may be computed by

$$W(\text{o}) = \prod_{l=1}^{s} w_l(\text{o}) \tag{3.20}$$

One can then express the ratio of probability densities of the new and old configurations in terms of the probabilities of growing the chains and their Rosenbluth weights

$$\frac{\rho_{\text{new}}}{\rho_{\text{old}}} = \frac{W(\text{n})}{W(\text{o})} \frac{P(\text{n})}{P(\text{o})} \tag{3.21}$$

From this ratio, it can be shown that, in order to satisfy the proper statistical mechanical probabilities, the move should be accepted with a probability of

$$P_{\text{acc}} = \min\left(1, \frac{W(\text{n})}{W(\text{o})}\right) \tag{3.22}$$

In a similar manner, the CBMC technique may be applied not only to the regrowth of a molecule but also to particle exchange [91, 92] and indentity interchange [93, 94] moves in the Gibbs ensemble. This allows for the simulation of the phase equilibria of large molecules, which would otherwise be impossible. It should also be noted that this work makes use of the SAFE-CBMC algorithm [95] to regrow the interior portions of longer chains, although this algorithm will not be discussed here.

3.2 The Transferable Potentials for Phase Equilibria Force Field

In a Monte Carlo simulation the potential energy is of utmost importance because it determines whether a move is accepted or rejected. Therefore, it is absolutely critical

to have a potential energy function, or force field, that accurately represents the interactions between the molecules in the system under study. If a force field does not accurately describe these molecular interactions it will not accurately reproduce the thermophysical properties observed in experiment. If these thermophysical properties are not reproduced one cannot be confident in the molecular-level data gathered in the simulation. Beyond accuracy, another highly desirable trait of a force field is transferability. Here, transferability has many different definitions. The force field parameters for a given interaction site (say, the methyl group in butane) should be transferable to different molecules (butanol). The force field should be transferable to different state points (different pressures, temperatures, and compositions). The force field should be transferable to different properties (thermodynamic, structural, and transport). The Siepmann research group has devoted significant effort to the development of a force field with these qualities. This force field is called called the Transferable Potentials for Phase Equilibria (TraPPE) force field [96].

The present work extensively uses this force field, specifically TraPPE-UA, the united-atom version [97, 98, 99, 100, 101, 102, 103], so some discussion should be devoted to a description of this force field and its development. The united-atom term is used to denote that all CH_x segments are represented as one interaction site rather than, for example, using four interactions sites to describe a methyl (CH_3) group. This drastically reduces the time spent computing molecular interactions and sacrifices little in the way of accuracy. All hydrogen atoms in other types of functional groups (for example, OH and NH_2) are accounted for explicitly.

There are two components to the TraPPE force field, an intermolecular (nonbonded) and an intramolecular (bonded) part. The nonbonded interactions are described by a combination of Lennard-Jones and Coulombic potentials. The former describes dispersive, or van der Waals, interactions and the latter describes first-order electrostatic interactions between sites bearing partial charges. The general intermolecular potential energy function is as follows:

$$U(\mathbf{r}) = \sum_{i=1}^{N-1} \sum_{j=i+1}^{N} 4\epsilon_{ij} \left(\frac{\sigma_{ij}}{r_{ij}^{12}} - \frac{\sigma_{ij}}{r_{ij}^{6}} \right) + \frac{q_i q_j}{4\pi\epsilon_o r_{ij}} \tag{3.23}$$

where $\mathbf{r}$ is the set of coordinates for all interaction sites in the system, N is the number of interactions sites, r_{ij} is the distance between sites i and j, and ϵ_o is the permittivity

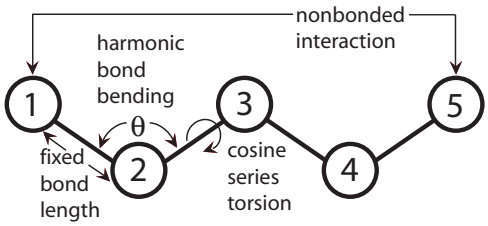

Figure 3.3: Diagram of the TraPPE intramolecular potential.

of free space. The remaining variables parameters are fit to each type of interaction site. In the Lennard-Jones portion of the potential, each interaction site is described by a well-depth, ϵ_i, and diameter σ_i. For interactions between two sites i and j, the Lorentz-Berthelot combining rules are applied $\epsilon_{ij} = \sqrt{\epsilon_i \epsilon_j}$ and $\sigma_{ij} = (\sigma_i \sigma_j)/2$. For the Coulombic portion of the potential, each interaction site is describe by a partial charge q_i.

The functional form for the intramolecular portion of the potential is

$$U(\mathbf{r}) = \sum_{\text{dihedrals}} u_{\text{tor}}(\phi) + \sum_{\text{angles}} \frac{k_\theta}{2}(\theta - \theta_{\text{eq}})^2 \tag{3.24}$$

where the first sum runs over all possible dihedral (torsional) angles ϕ and the second sum runs over all possible bond angles θ with force constants k_θ and equilibrium angles θ_{eq}. The functional form of the torsional potential u_{tors} varies, but it is usually a cosine series. In the TraPPE force field, bond lengths are held fixed at their equilibrium values. These bond lengths and the torsional and bond bending potentials are usually fit to potential energy surfaces generated using high-level quantum mechanical calculations. In addition, sites separated by four or more bonds in a molecule interact via the nonbonded potential described by equation 3.23. A diagram depicting this intramolecular potential is shown in Figure 3.3.

The parameters in the nonbonded portion of the potential (ϵ, σ, and q) are fit to reproduce experimental vapor-liquid coexistence curves (VLCC's, a plot of temperature versus the vapor and liquid phase densities) for single component systems. This data is used in the fitting process as it (1) covers a wide range of temperatures and pressures, (2) is extremely sensitive to small differences in the parameters, and (3) since this force

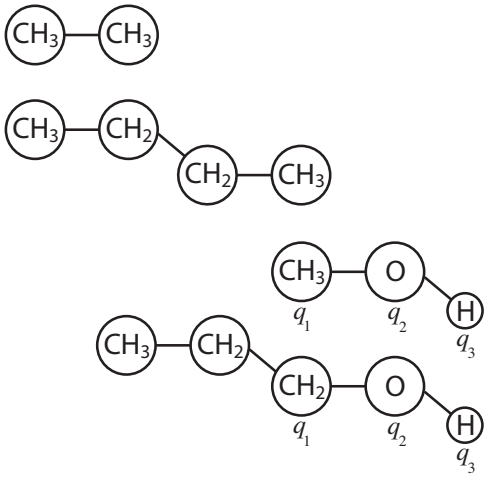

Figure 3.4: Diagram of the TraPPE parameterization philosophy.

field is intended for simulating processes that involve phase equilibria.

To fit the force field parameters for different molecules, a building up strategy is employed (see Figure 3.4). This process ensures that parameters from functional groups in one molecule are transferable to another and that very few new parameters need to be fit when new molecules with different functional groups are to be described. This process will be demonstrated for *n*-alkanes and *n*-alkanols. The process starts with ethane, which is modeled as two CH_3 groups. Since ethane is a nonpolar molecule, there are no partial charges and only two parameters need to be fit, σ_{CH_3} and ϵ_{CH_3}. Vapor–Liquid equilibrium (VLE) simulations of the molecule, using the Gibbs ensemble technique, with multiple parameter sets allow one to locate the best parameter set to reproduce the experimental data. Next, larger linear alkanes, for example butane are examined. The parameters for the methyl group, σ_{CH_3} and ϵ_{CH_3}, can be transferred from ethane and now only two new parameters need to be fit for the methylene group, σ_{CH_2} and ϵ_{CH_2}, and again VLE simulations are employed for this purpose.

At this point the force field contains a parameter set that can describe *any* linear alkane. However, one needs to simulate more than just alkanes, so this technique is extended to include different functional groups. To describe methanol, the σ_{CH_3} and ϵ_{CH_3} parameters are taken from ethane. Now, an optimum σ_O and ϵ_O are needed for the

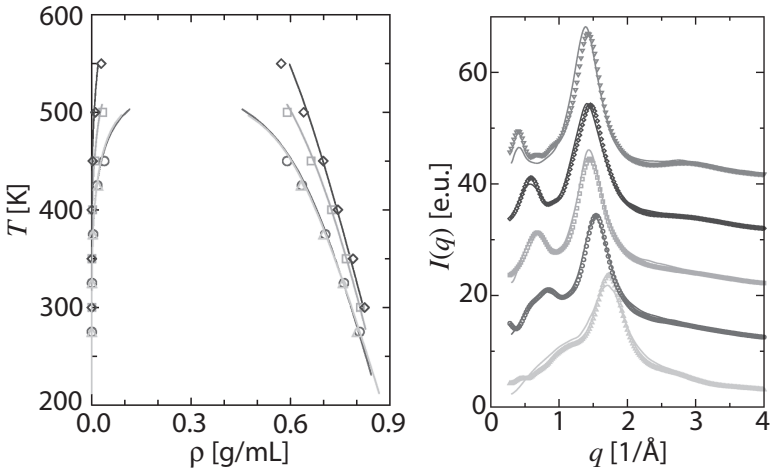

Figure 3.5: Validation of the TraPPE parameterization philosophy. Left, vapor–liquid coexistence curves from experiment and simulation. The simulation data is shown as symbols with methanol depicted as triangles, ethanol as circles, 1-pentanol as squares, and 1-octanol as diamonds. Right, X-ray scattering intensities for the liquid phase (at 293 K and 1 atm). Simulation data is shown with symbols; methanol (triangles-up), ethanol (circles), 1-propanol (squares), 1-butanol (diamonds), and 1-octanol (triangles-down). In both plots the experimental data [104, 105] is shown as lines.

hydroxyl oxygen (no σ and ϵ are needed for hydrogen due to its small size). Additionally, a set of partial charges needs to be optimized since methanol is a polar molecule. These partial charges are located on the methyl, oxygen, and hydrogen sites and are denoted as q_1, q_2, and q_3, respectively. After these parameters are optimized to fit the experimental VLE data, any linear alkanol can be described. For example, to describe propanol, one would take the needed Lennard-Jones parameters from butane and methanol and the three partial charges from methanol (see Figure 3.4). At this point, it is easy to envision the extension of this technique to additional functional groups. This extension has already been made and the TraPPE-UA forcefield is capable of describing the vast majority of functional groups important for organic molecules [97, 98, 99, 100, 101, 102, 103].

To demonstrate the robustness of this fitting process two plots are shown (see Figure 3.5). The first shows the VLCC's for a series of alcohols in comparison to experiment,

and the agreement is excellent. In this plot, the only molecule to which parameters were fit is methanol. The parameters for the other alcohols were transferred from methanol and the alkanes as described above. The second plot in this figure shows the force field is capable of reproducing the experimentally observed X-ray scattering intensities for the liquid phase of these alcohols. In addition, this force field has been shown to accurately reproduce the viscosities of various alcohols over a range of pressures [106]. At no point was any structural or transport data used in the fitting process, therefore this is a great testament to the transferability of the force field.

In addition to property prediction for single component systems, the TraPPE force field has been successfully applied to numerous multicomponent systems. As will be described later in this thesis, it can accurately predict free energies of retention (retention times) in RPLC and has done the same for previous work with gas chromatography [107, 108, 109, 110, 111, 112, 113]. Additionally, and among other things, it has been applied to accurately predict solute partitioning in a variety of other systems [114, 115, 116], phase diagrams in binary and ternary systems [117, 118, 119, 120], Hildebrand solubility parameters [121], and phenomena involving nucleation and aggregation [117, 122, 123, 124]. The ability of this force field to reproduce these various experimentally measured quantities gives one great confidence as to the validity of the molecular-level phenomena observed in the simulations.

Chapter 4

The Driving Forces for Retention in RPLC

4.1 Background

Retention in RPLC is based upon the transfer of the solute from the mobile phase to the stationary phase. Associated with this process is a free energy of transfer, or free energy of retention, as it is called in this specific case. As discussed in Chapter 1, there is some debate over what contributes more to this free energy, interactions with the mobile phase or interactions with the stationary phase. Stated otherwise, what are the thermodynamic driving force for retention? On one side of this issue is the "solvophobic" view of Horváth and coworkers [16, 17, 18] and on the other side is the "revisionist" or "lipophilic" view of Carr and coworkers [11, 12, 15]. This chapter describes simulations aimed at assessing the validity of these two viewpoints and understanding the origin of these driving forces at the molecular-level. Before discussing the simulation results is pertinent to give a little background on the solvophobic and lipophilic views.

The solvophobic theory [16, 17, 18] is a detailed thermodynamic treatment and has been successful in predicting retention times in RPLC. The theory suggests that the overall free energy of retention in RPLC is driven by unfavorable interactions of the

[†] This chapter describes the outcome of a collaborative research project carried out by Jake L. Rafferty and Li Sun and advised by J. Ilja Siepmann and Mark. R. Schure. A report on this research project has been submitted [76].

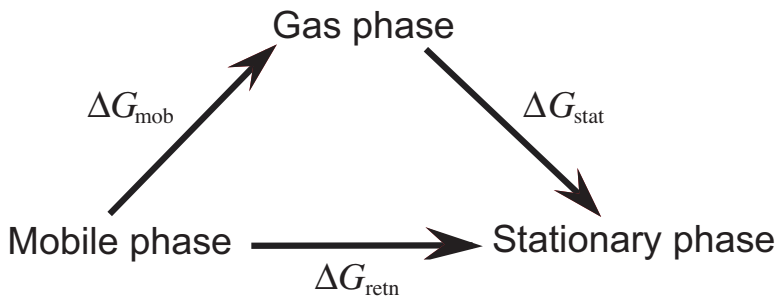

Figure 4.1: Thermodynamic cycle used to decompose the free energy of retention into mobile and stationary phase contributions.

solute with the mobile phase. These unfavorable interactions arise from the free energy penalty for cavity creation in the hydrogen bonding network of the aqueous-organic mobile phase. Retention, or transfer of a solute from mobile to stationary phase, is driven by the mobile phase because this free energy penalty is ameliorated when the solute leaves the mobile phase and enters the stationary phase. In the solvophobic theory, the stationary phase plays a relatively passive and minor role in the retention process.

The revisionist view [11, 12, 15] suggests that favorable interactions between the solute and the stationary phase drive the transfer from mobile to stationary phase. To arrive at this conclusion, the net free energy of retention was decomposed into the thermodynamic cycle shown in Figure 4.1. By introducing an ideal gas reference state as an intermediate step in the transfer between mobile and stationary phases, one can separate the free energy contributions of the mobile and stationary phases by separately measuring the free energy change in the mobile to vapor phase transfer (ΔG_{mobile}) and the vapor to stationary phase transfer (ΔG_{stat}). The sum of these two quantities then gives the free energy of retention.

$$\Delta G_{\text{retn}} = \Delta G_{\text{mob}} + \Delta G_{\text{stat}} \tag{4.1}$$

Using liquid n-hexadecane as a model stationary phase, aqueous-organic solvents as the mobile phase, and an ideal gas reference phase, Carr and coworkers have measured the mobile and stationary-phase contributions to the free energy of retention for both nonpolar and polar solutes [11, 12, 15]. In contrast to the solvophobic theory, it was found that the net free energy of retention for the nonpolar methylene group is

dominated by stationary-phase contributions, that is $|\Delta G_{\mathrm{ret}}| \simeq |\Delta G_{\mathrm{stat}}| > |\Delta G_{\mathrm{mob}}|$ over a wide range of methanol/water and acetonitrile/water mobile-phase compositions [11, 15]. Additionally, the mobile to gas phase transfer is unfavorable ($\Delta G_{\mathrm{mob}} > 0$), rather than favorable as predicted by the solvophobic theory, for mobile phases with more than 40% volume fraction of organic solvent [15]. For polar groups, it was shown that the net contribution of the stationary phase is less than the mobile phase. However, ΔG_{mob} was always positive and, therefore, not due to solvophobic interactions [12]. Thus, for both nonpolar and polar solutes it is not solvophobism that drives solutes from the mobile phase, rather these solutes prefer the mobile phase to the ideal gas state.

Guided by Carr's work, the present study makes use of molecular simulation to examine the partitioning of small alkane and alcohol solutes between liquid *n*-hexadecane, various aqueous-organic solvents, and an ideal vapor phase. Liquid hexadecane is chosen as the model RPLC stationary phase as it is more convenient to simulate than the explicit RPLC stationary phase, which consists of alkyl chains chemically grafted to a silica surface. This choice is rationalized by the fact that there is an excellent correlation between free energies of retention in RPLC and free energies of transfer between typical mobile phases and hexadecane, at least for nonpolar solutes [11, 15]. Thus, for the assessment of thermodynamic driving forces, liquid hexadecane should serve as a good model. In subsequent chapters simulations of the explicit RPLC system, which probe other important aspects of the retention mechanism, will be discussed.

Seven different solvents with varying concentrations of water/acetonitrile or water/methanol were studied. Multiple solvent systems were studied for a couple of reasons. First, selectivity in RPLC is most often optimized by adjusting the mobile-phase composition so it is important to understand these effects. Second, it has been reported that the thermodynamics for the retention process are different depending on whether water/acetonitrile or water/methanol are used [15, 125, 126, 127]. This difference has been attributed to the tendency of the organic component in the water-acetonitrile mixture to preferentially solvate the solute, perhaps through the formation of acetonitrile clusters. In addition to allowing for the precise calculations of free energies of transfer between the various phases, the molecular-level data generated from the simulations can be used to analyze solvation environments of the solutes to examine effects such as clustering and preferential solvation.

Table 4.1: Total number of molecules in each of the simulated systems.

	WAT	33A/33M	67A/67M	ACN/MET
water	864	576	288	0
organic modifier[a]	0	288	576	864
n-hexadecane	216	216	216	216
helium	10	10	10	10
other solute types[b]	2	2	2	2

[a]For systems 33A, 67A,and ACN the organic modifier is acetonitrile, while it is methanol in systems 33M, 67M, and MET

[b]Includes methanol, ethanol, 1-propanol, methane, ethane, propane, and *n*-butane

4.2 Simulation Details

To examine the partitioning of solutes between liquid *n*-hexadecane, various aqueous-organic solvents, and a vapor phase, coupled-decoupled configurational-bias Monte Carlo (CBMC) simulations [89, 90, 98] were carried out in the isobaric-isothermal (NpT) version of the Gibbs ensemble [83]. All simulations utilized a temperature of 323.15 K, and a pressure of 1 atm. Seven different solvent-phase compositions were used for this study: pure water (denoted as system WAT), 33% molfraction acetonitrile (33A), 67% acetonitrile (67A), pure acetonitrile (ACN), 33% methanol (33M), 67% methanol (67M), and pure methanol (MET). For reference, systems 33A and 67A correspond to roughly 59% and 86% volume fraction acetonitrile and systems 33M and 67M correspond to roughly 53% and 82% volume fraction methanol, respectively. Also present in each simulation were a set of 14 solutes consisting of small normal alkanes and alcohols. The total number of each molecule type used in the seven systems is listed in Table 4.1.

The present Gibbs ensemble simulations made use of three separate simulation boxes that are in thermodynamic contact but do not share an explicit interface. The first box contains the hexadecane phase, the second box the aqueous-organic solvent phase, and the third box an ideal helium gas phase. The volume of each of the three boxes was allowed to fluctuate in response to the external pressure so that each box would achieve mechanical equilibrium at the specified pressure. Thermal equilibrium was achieved by allowing the particles within a given box to translate, rotate, and undergo CBMC regrowths. Phase equilibrium was attained by allowing particle exchange between the various boxes with CBMC particle exchange [91, 92] and identity interchange [93, 94]

Table 4.2: Average number of solvent molecules in each simulation box.[a]

	mobile		stationary		vapor	
System	N_{H_2O}	$N_{organic}$	N_{H_2O}	$N_{organic}$	N_{H_2O}	$N_{organic}$
WAT	860.2_1	–	0.19_3	–	3.6_1	–
33A	572.1_1	281.5_3	0.20_1	3.8_2	3.7_1	4.6_1
67A	287.1_2	563.5_2	0.15_1	5.8_1	2.7_1	6.6_1
ACN	–	844.8_5	–	10.7_4	–	8.44_2
33M	572.4_2	283.5_4	0.13_3	1.5_2	3.4_1	4.9_3
67M	286.8_2	559_1	0.29_6	6.3_8	2.9_1	10.4_5
MET	–	824_2	–	22_2	–	18.5_4

[a]Subscripts indicate the statistical uncertainty in the final digit.

moves. While water, acetonitrile, methanol, helium, and the solute molecules were allowed to transfer between all three phases, the *n*-hexadecane molecules were confined to the first box because their solubility in the aqueous-organic phase and saturated vapor pressure are extremely low. The principal advantage of the Gibbs ensemble in this work is that the properties of coexisting phases at a given state point, such as the solubility of the aqueous-organic solvent in hexadecane and free energies of solute transfer, can be computed in a single simulation directly from a mechanical property, namely the number densities of each species in the different phases [85, 86]

$$\Delta G_{a\to b} = -RT \ln K = -RT \ln \frac{\rho_b}{\rho_a} \tag{4.2}$$

where ρ_i is the number density of the species in phase i. Thus, based upon the distribution of each solute between the three phases, one can compute the free energy of retention and its mobile and stationary-phase components as defined in Figure 4.1.

Due to the relatively large number of solutes present in the simulation it was necessary to control the average number of solute molecules in the hexadecane and solvent phases in order to prevent overloading of these phases and to enhance sampling for species that had low solubility in a given phase (e.g., butane in the aqueous phase). This was accomplished by applying a uniform bias potential to each solute type in each box. The bias potential was adjusted such that each solute, on average, was distributed about evenly between the three boxes. The free energies of transfer calculated from the simulations via equation 4.2 above were adjusted to account for these bias potentials. No bias potentials were applied to the solvent species. The resulting average numbers

of solvent molecules present in each box are given in Table 4.2.

To describe the intra and intermolecular interactions in these systems, the TIP4P model [128] was used for water while alkanes, alcohols, acetonitrile, and helium were represented by the united-atom version of the transferable potentials for phase equilibria (TraPPE) force field [97, 100, 102, 129]. A spherical truncation of 14 Å and analytical tail corrections [80] were used for Lennard-Jones interactions while Coulombic interactions were evaluated with the Ewald summation technique [80] using a direct space cutoff of 14 Å and a convergence parameter of $\kappa = 0.2$.

Ten independent simulations were carried out for each of the seven solvent compositions. Each simulation was equilibrated for at least 10^5 Monte Carlo (MC) cycles (one MC cycle equals N moves, where N is the total number of particles in the system) and, thereafter, 2×10^5 MC cycles of production were carried out. Therefore, a total of 2×10^6 MC cycles were available to calculate averages for each solvent composition. To estimate uncertainties in the simulation results, standard errors of the mean were determined from the 10 independent simulations.

4.3 Results and Discussion

As mentioned in section 4.2, simulations in the Gibbs ensemble allow one to directly compute free energies of transfer between separate phases. These free energies of transfer between the three phases simulated are presented in Table 4.3 for each of the different solutes examined. From these individual solute transfer free energies the methylene and hydroxyl incremental free energies were computed (see Table 4.4). The methylene increment, $\Delta G^{\mathrm{CH_2}}$, is defined as the change in the free energy of transfer upon increasing solute size by one CH_2 group. As described by the Martin equation [130], this quantity can be found from the slope of a plot of the free energy of transfer versus number of carbons for the n-alkanes. The methylene increment will be one of the focal points in subsequent discussion since it serves as a prototypical non-polar group present in many compounds and because it allows the data from the current work on small solutes to be extended to larger species. To compare the behavior of non-polar and polar groups, the hydroxyl increment, ΔG^{OH}, was also computed. This quantity is defined as the difference in transfer free energy between an n-alkanol and an n-alkane with the same

Table 4.3: Free energies of solute transfer between the stationary, mobile and vapor phases.[a]

	$\Delta G_{\mathrm{mob}\rightarrow\mathrm{stat}}$ (ΔG_{ret})						
	WAT	33A	67A	ACN	33M	67M	MET
methane	-8.49_8	-3.97_5	-2.09_2	-1.11_3	-4.54_8	-2.35_4	-0.61_4
ethane	-12.2_1	-5.65_6	-3.07_4	-1.77_4	-6.6_1	-3.63_5	-1.39_5
propane	-15.9_1	-7.29_9	-4.11_4	-2.46_5	-8.5_1	-4.82_7	-2.03_7
butane	-19.7_2	-9.0_1	-5.12_7	-3.10_7	-10.3_1	-5.99_9	-2.63_9
methanol	16.0_2	15.8_2	14.8_1	11.8_1	17.0_4	14.4_4	11.6_4
ethanol	11.6_2	13.4_2	13.1_1	10.8_1	12.0_3	12.7_4	10.7_4
propanol	7.9_2	11.3_2	11.7_1	9.9_2	10.0_4	11.1_3	9.9_3
	$\Delta G_{\mathrm{mob}\rightarrow\mathrm{vap}}$ (ΔG_{mob})						
	WAT	33A	67A	ACN	33M	67M	MET
methane	-10.1_1	-5.53_5	-3.67_2	-2.65_3	-6.14_8	-3.94_3	-2.18_3
ethane	-9.71_9	-3.17_5	-0.59_3	0.74_4	-4.14_9	-1.16_4	1.08_5
propane	-10.7_1	-2.15_7	1.05_3	2.74_4	-3.37_9	0.33_6	3.12_6
butane	-11.8_2	-1.12_9	2.78_4	4.80_6	-2.5_1	1.85_9	5.21_7
methanol	19.0_1	19.3_1	18.3_1	16.2_1	19.9_1	19.4_1	18.9_1
ethanol	17.2_1	19.3_1	19.0_1	17.5_1	19.6_1	20.0_1	20.2_1
propanol	16.0_2	19.8_1	20.3_1	19.3_1	19.9_1	21.0_1	21.8_1
	$\Delta G_{\mathrm{vap}\rightarrow\mathrm{stat}}$ (ΔG_{stat})						
	WAT	33A	67A	ACN	33M	67M	MET
methane	1.57_2	1.56_1	1.57_1	1.55_1	1.60_2	1.58_1	1.57_1
ethane	-2.51_2	-2.48_2	-2.48_2	-2.51_2	-2.48_2	-2.47_2	-2.49_1
propane	-5.18_3	-5.15_3	-5.16_3	-5.19_2	-5.15_3	-5.15_2	-5.16_2
butane	-7.93_3	-7.86_5	-7.89_4	-7.90_3	-7.85_4	-7.84_2	-7.85_3
methanol	-3.0_2	-3.4_1	-3.5_1	-4.4_1	-2.9_3	-5.1_4	-7.3_4
ethanol	-5.6_2	-5.9_1	-5.9_1	-6.8_1	-5.3_3	-7.3_4	-9.5_4
propanol	-8.1_2	-8.5_1	-8.5_1	-9.3_1	-8.0_3	-9.9_3	-11.9_4

[a]Subscripts indicate the statistical uncertainty in the final digit.

number of carbons.

As can be seen in Table 4.4 the free energy of transfer from mobile to stationary phase (the free energy of retention, ΔG_{retn}) is negative and favorable at all mobile-phase compositions for the methylene group, although it becomes less favorable as the concentration of the organic component in the mobile phase increases. When comparing water/acetonitrile and water/methanol mobile phases with the same fraction of organic

Table 4.4: Incremental free energies of transfer between stationary, mobile, and vapor phases for methylene and hydroxyl groups.[a,b]

	WAT	33A	67A	ACN	33M	67M	MET
$\Delta G^{CH_2}_{mob\rightarrow stat}$ ($\Delta G^{CH_2}_{retn}$)	-3.76_8	-1.62_8	-1.02_2	-0.66_2	-1.86_3	-1.18_3	-0.61_2
	−3.62	*−1.77*	*−1.10*	*−0.74*	*−1.94*	*−1.16*	*−0.75*
$\Delta G^{CH_2}_{mob\rightarrow vap}$ ($\Delta G^{CH_2}_{mob}$)	-1.05_8	1.06_7	1.68_2	2.03_2	0.82_3	1.51_3	2.06_2
	−1.05	*1.13*	*1.60*	*1.87*	*0.67*	*1.39*	*1.84*
$\Delta G^{CH_2}_{vap\rightarrow ret}$ ($\Delta G^{CH_2}_{stat}$)	-2.71_1	-2.68_2	-2.71_1	-2.69_1	-2.68_1	-2.68_1	-2.68_1
	−2.57[c]						
$\Delta G^{OH}_{mob\rightarrow stat}$ (ΔG^{OH}_{retn})	23.8_2	18.8_2	16.0_1	12.5_2	20.7_3	16.1_4	12.0_3
$\Delta G^{OH}_{mob\rightarrow vap}$ (ΔG^{OH}_{mob})	26.8_1	22.2_2	19.4_1	16.7_1	23.5_1	20.9_3	18.9_1
$\Delta G^{OH}_{vap\rightarrow stat}$ (ΔG^{OH}_{stat})	-3.0_2	-3.4_2	-3.4_1	-4.2_1	-2.9_3	-4.8_4	-6.9_4

[a]Subscripts indicate the statistical uncertainty in the final digit.
[b]Experimental values [15] in italic.
[c]Experimental value available only for the vapor to neat hexadecane transfer, whereas simulation results are for solvent-saturated hexadecane.

modifier, the methanol containing systems show more favorable free energies of retention for the methylene group, but the difference is rather small (about 0.2 kJ/mol). For validation of these simulation results, the experimental values for the methylene increment are also presented in Table 4.4 [15]. The simulated values are in excellent agreement with experiment with a mean unsigned error of 0.11 kJ/mol.

In contrast to the methylene increment, the free energy of retention for hydroxyl group is much larger and positive (unfavorable) for all solvent compositions. For example, in system WAT the free energy of retention is 28 kJ/mol greater for the hydroxyl increment than it is for the methylene increment. Unlike the methylene group, the free energy of retention becomes more favorable as the concentration of organic component is increased. The change in free energy with changing mobile-phase composition is also much more dramatic for the hydroxyl increment than for the methylene increment. The hydroxyl increment decreases by about 11 kJ/mol when going from system WAT to systems ACN or MET, while it increases by about 4 kJ/mol for the methylene group.

Furthermore, the differences in the transfer free energies for systems with the same organic modifier concentration are significantly larger for the hydroxyl group increment than for the methylene group.

To gain a better understanding of driving forces for solute transfer from mobile to stationary phase, the free energy of retention is broken into two components, namely the mobile and stationary-phase contributions, as outlined in Section 4.1. The following two sections will discuss these two contributions for both nonpolar and polar groups and offer a molecular level analysis of the solvation environment of the solutes in the mobile and stationary phases.

4.3.1 Mobile to Vapor Phase Transfer

The Nonpolar Methylene Group

In the thermodynamic cycle shown in Figure 4.1, the free energy of transfer from mobile to vapor phase represents the mobile phase contribution to the free energy of retention, or ΔG_{mob}. For the methylene group, ΔG_{mob} is favorable (negative) only for system WAT. For systems 33A and 33M, ΔG_{mob} is unfavorable and becomes increasingly positive as the molfraction of organic modifier is increased (Table 4.4). Thus, in most cases the methylene group prefers the solvent phase to the ideal gas phase and solvophobic forces only contribute to the retention process when the mobile phase is rich in water. Another interesting observation is that the acetonitrile containing systems 33A and 67A have slightly more positive ΔG_{mob} than their 33M and 67M counterparts. That is, more free energy is required to remove the methylene group from a water/acetonitrile phase than from a water/methanol mobile phase of the same composition. This is in agreement with the experimental data [15]. In addition to free energy, Carr and coworkers have reported that the enthalpy and entropy of transfer for the methylene group is generally more positive in water/acetonitrile mixtures than in water/methanol mixtures [15]. To better understand these differences in thermodynamics for the mobile to vapor phase transfer a molecular-level analysis of the solvent structure around the methylene group was carried out.

It is often argued that these differing thermodynamics are caused by aggregation of the organic component in water/acetonitrile mixtures. These acetonitrile enriched

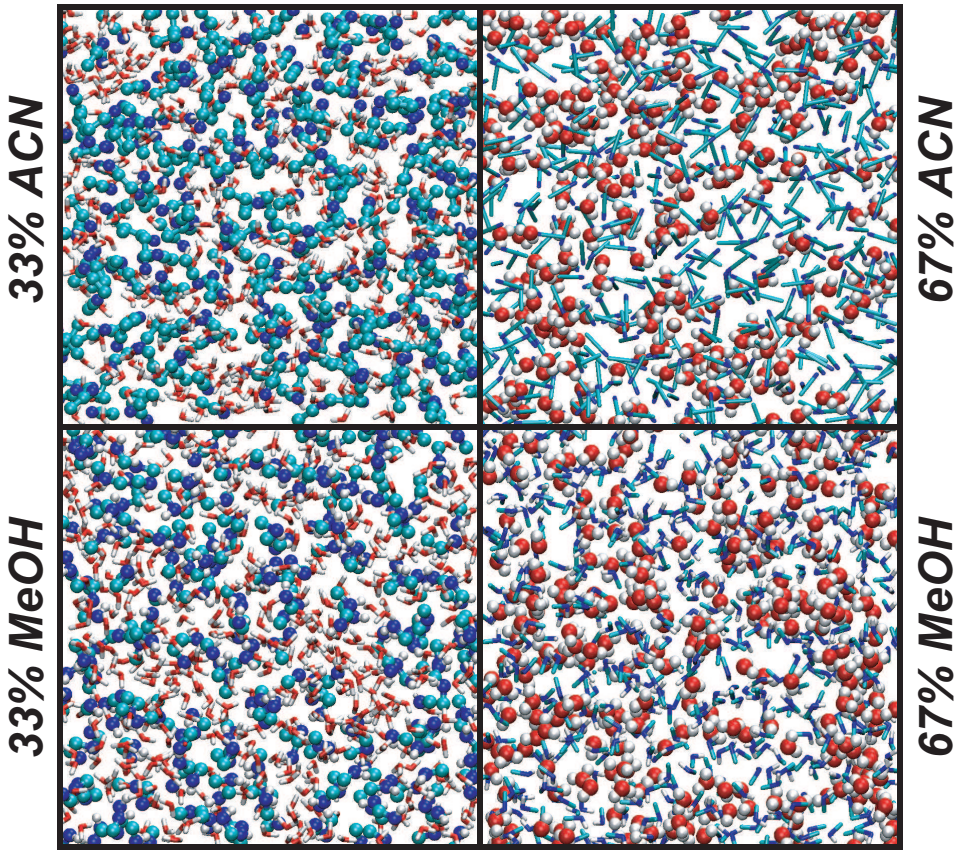

Figure 4.2: Snapshots of the mobile phase for the binary solvent systems. For water, oxygen is shown in red and hydrogen in white. For the organic component, nitrogen/oxygen is shown in blue, carbon in cyan, and hydrogen in white. The component with the lower molfraction is depicted as spheres while the higher molfraction component is depicted as tubes.

regions can more favorably solvate the solute than a mixture of water/methanol, which is thought to be more uniform (homogeneous) with respect to the local composition [125, 126, 127, 131]. To visualize if these clusters are present in our simulations, snapshots of the mobile phase for systems 33A, 67A, 33M, and 67M are shown in Figure 4.2. Upon examination of these snapshots, significant clustering of acetonitrile in systems 33A and 67A does not appear to be present. If anything, it appears that the water molecules in system 67A show a tendency to aggregate. Similar conclusions can be drawn from the snapshots of systems 33M and 67M. Thus, in all of the binary systems

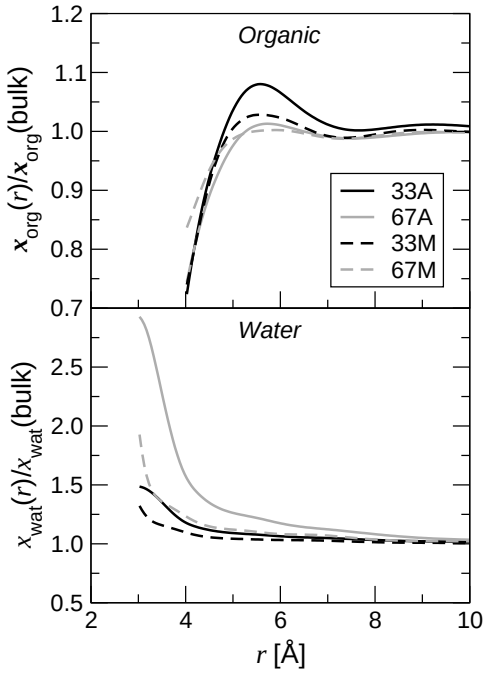

Figure 4.3: Local mole fraction enhancements around solvent molecules in the mobile phase. The upper panel shows the enhancement of the organic component of the solvent around itself and the lower panel shows the enhancement of water around itself.

studied here, there does not appear to be significant clustering of the organic component of the solvent. However, it should be noted that each of these snapshots represent a single configuration of the millions generated during the simulation. To quantify these observations, ensemble-averaged properties measuring the extent of clustering were computed for each of the solvent systems.

Figure 4.3 presents radial profiles for the local molfraction enhancement around organic and water molecules in the solvent phase of systems 33A, 67A, 33M, and 67M. For the organic modifier, the plots show the molfraction of organic component relative to the bulk mole fraction as a function of distance from the organic molecule. Values greater than one for the profile indicate that there is an enrichment organic molecules around themselves, i.e., a tendency to cluster. The larger the distance r from the molecule that this enhancement exists indicates how far the cluster extends. For water molecules, the same quantity is presented but for the enrichment of water around itself.

The largest local molfraction enhancement for the organic modifier is seen in system

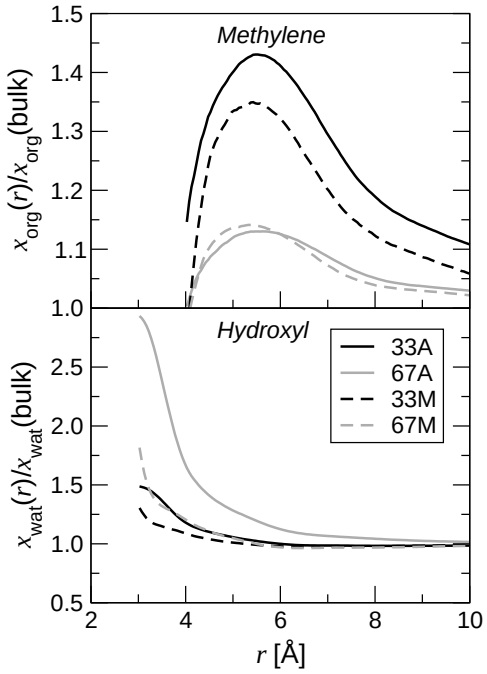

Figure 4.4: Local mole fraction enhancements around solute methyl and hydroxyl groups in the mobile phase. Enhancement of the organic component of the solvent around methyl groups is shown in the upper panel while the enhancement of water around hydroxyl groups is shown below.

33A. However, this enhancement is relatively weak, peaking just short of 1.1 at $r \approx 6$ Å. There is an even smaller enhancement in system 33M and no appreciable enhancement in systems 67A and 67M. Upon examining the local molfraction enhancement of water around itself, a more distinct solvent structure is observed. In system 67A, an enhancement of nearly 3 is observed at $r \approx 3$ Å. This enhancement drops quickly as r is increased to 4 Å but decays slowly after that. Thus, there is a very strong enrichment of the water molfraction in the first solvation shell of a water molecule and a weaker, but persistent, enrichment after that. Similar, but less dramatic, trends are observed for system 67M and these trends become even less noticeable for systems 33A and 33M. From these local molfraction enhancements, it appears that acetonitrile clusters are not an important species, rather water tends to aggregate in the organic-rich solvents.

The local molfraction enhancements in Figure 4.3 describe the solvation environment around solvent molecules, however it is also important to examine the solvation

environment around solutes. For this reason, Figure 4.4 shows the local molfraction enhancement of the organic modifier around solute methylene groups and the enhancement of water around solute hydroxyl groups in systems 33A, 67A, 33M, and 67M. There is a significant enhancement of the organic modifier around methylene groups in systems 33A and 33M. This enhancement peaks near $r \approx 6$ Å and is stronger in system 33A with a peak value of just over 1.4 as compared 1.3 in system 33M. The enhancement decays rather slowly and is still present, albeit slight, at $r = 10$ Å. For systems 67A and 67M the enhancement of the organic modifier around methylene groups is much weaker, reaching a maximum of around 1.1. Thus, for mobile phases with lower organic composition, there is a significant preferential solvation of methylene groups by the organic component of the solvent and the preference is stronger for acetonitrile mixtures.

Additional information on the solvation environment of methylene groups in each of the systems studied can be gleaned by $g(r)$, or the radial distribution functions (RDFs), shown in Figure 4.5. The RDFs shown are between solute methylene groups and various groups/atoms present in the different solvent molecules. Complimentary to the local molfraction enhancement around methylene groups shown in Figure 4.4, the RDFs also indicate that there is an enhancement of the organic component of the solvent around the methylene group. For systems 33A, 67A, 33M, and 67M the RDFs between methylene groups and acetonitrile or methanol atoms have larger values than the corresponding RDFs between methylene groups and water oxygens at distances up to $r \approx 7$ Å. In this region water is depleted ($g(r) < 1$) and the organic component is enriched ($g(r) > 1$).

Another interesting effect can be seen by comparing the RDFs involving acetonitrile nitrogen atoms and methyl groups with the RDFs involving methanol oxygen atoms and methyl groups. For acetonitrile, the first peak in $g(r)$ is at roughly the same position for the nitrogen and the methyl group. For methanol, the peak due to the methyl group occurs about 1 Å closer to the solute methylene group than does the peak for the oxygen. Therefore, acetonitrile shows no preferred orientation when solvating a methylene group whereas methanol prefers to align its methyl group towards the solute methylene group and its oxygen atom away.

The data shown in the local molfraction enhancement profiles and RDFs indicate that there is preferential solvation of the methylene group by the organic component of

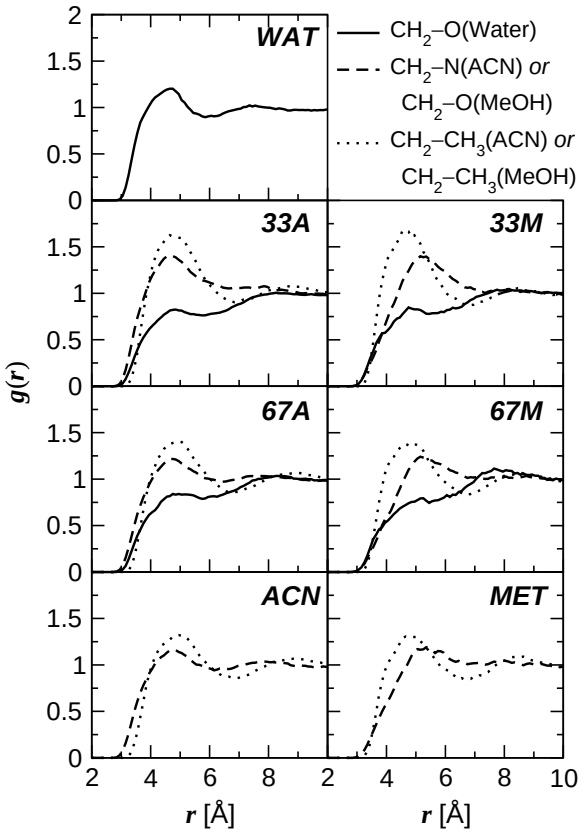

Figure 4.5: Radial distribution functions between solute methylene groups and solvent atoms/groups in the mobile phase.

the solvent and that this enhancement is not due to the preexisting clusters of organic modifier. Thus, it appears that the solvent can rearrange itself to accommodate the solute. To discern if this rearrangement of the solvent structure disrupts the hydrogen bonding network within the solvent, the number of hydrogen bonds per solvent molecule was computed for free solvent molecules and for solvent molecules within the first solvation shell of any methylene group (see Table 4.5). A hydrogen bond is defined by the following geometric criteria: An oxygen–oxygen or nitrogen–oxygen distance less than 3.3 Å, an oxygen–hydrogen or nitrogen–hydrogen distance less than 2.5 Å, and a hydrogen bond angle with a cosine less than -0.1 [132].

In the Lum-Chandler-Weeks theory of hydrophobic solvation, it was predicted that the hydrogen-bonded network of the solvent is not disrupted by small nonpolar solutes,

Table 4.5: Number of hydrogen bonds for mobile phase molecules outside and inside the solvation shell of alkane CH_2 groups.[a,b]

		$N_{\text{H-bonds}}^{\text{in}}$ [b]	$N_{\text{H-bonds}}^{\text{out}}$ [c]	$N_{\text{H-bonds}}^{\text{lost}}$ [d]
WAT	water	3.676_1	3.603_2	0.8_1
33A	water	3.104_1	2.926_2	0.19_3
	acetonitrile	1.038_1	0.900_3	0.23_3
			Total:	0.42_4
67A	water	2.567_1	2.435_2	0.05_1
	acetonitrile	0.514_1	0.447_3	0.17_2
			Total:	0.22_3
33M	water	3.339_1	3.211_2	0.20_4
	methanol	2.167_1	2.139_2	0.02_2
			Total:	0.22_5
67M	water	3.125_1	2.990_3	0.09_2
	methanol	2.010_1	1.983_1	0.15_3
			Total:	0.23_3
MET	methanol	1.870_1	1.838_2	0.14_5

[a]Subscripts indicate the statistical uncertainty in the final digit.
[b]Average number of hydrogen bonds for solvent molecules outside the solvation shell of any alkane CH_2 group.
[c]Average number of hydrogen bonds for solvent molecules inside the solvation shell of any alkane CH_2 group.
[d]Average number of hydrogen bonds lost by the solvent phase when solvating an incremental CH_2 group.

such as the ones examined here [133]. The present data indicates that there is a slight disruption in the hydrogen bonding for all solvents (except in system ACN, since acetonitrile cannot hydrogen bond with itself). For example, in system WAT, each water molecule solvating a methylene group loses only 0.073, or 2.0%, of its hydrogen bonds. For the mixtures, the water molecules in the first solvation shell lose a somewhat larger number of their hydrogen bonds. While the decrease in hydrogen bonds for acetonitrile molecules in the first solvation shell is similar to that for water molecules, methanol molecules lose a significantly smaller number of hydrogen bonds, presumably because

the methanol molecules orient themselves with the hydroxyl group pointing away from the non-polar methylene group.

Another metric of the disturbance of the hydrogen-bonded network in the first solvation shell is the total number of hydrogen bonds, $N^{\text{lost}}_{\text{H}-\text{bonds}}$ lost upon increasing the solute size by one methylene group, i.e., the difference in loss for n-butane versus propane. As is evident from the numbers summarized in Table 4.5, the loss is largest in WAT with a value of 0.8, this is followed by 33A (0.42), then systems 67A, 33M, and 67M (0.22), and the loss (0.14) is smallest in neat methanol.

As mentioned at the beginning of this section, the calculated free energies of transfer from mobile to vapor phase are slightly more positive for the acetonitrile mixtures and experimental measurements have shown that the enthalpy and entropy of transfer are also more positive for acetonitrile mixtures [15]. Because the acetonitrile and methanol mixtures show similar changes in hydrogen bonding upon solvating the methylene group, it appears that the differences in the thermodynamics between these mixtures may be the result of acetonitrile's greater preferential solvation of the methylene group as compared to methanol (see Figure 4.4). It was shown that no significant clustering of acetonitrile occurs in the absence of solute. Thus, when solvating the methylene group, the acetonitrile mixture must undergo significant changes in solvent structure to accomplish this preferential solvation. When the solute transfers from mobile to vapor phase it loses this favorable solvation environment (explaining the more positive enthalpy) and the solvent rearranges to a more disordered state (explaining the more positive entropy).

The Polar Hydroxyl Group

The free energies of transfer for the hydroxyl group from the various mobile-phase solvents to the ideal gas phase (or ΔG_{mob}, the mobile-phase contribution to the free energy of retention) are listed in Table 4.4. Regardless of mobile-phase composition, ΔG_{mob} for the hydroxyl group is always positive and is much more unfavorable than for the methylene group. Also in contrast to the methylene group, the transfer becomes less unfavorable as the concentration of the organic modifier is increased. For the methylene group, ΔG_{mob} increases from -1.73 kJ/mol in pure water to 2.04 kJ/mol in methanol, while it decreases from 26.6 to 19.0 kJ/mol for the hydroxyl group. These trends in

free energy of transfer with changing mobile-phase composition can be explained by examining the solvation environment of the hydroxyl group.

The local molfraction enhancements of water molecules around the hydroxyl groups are shown in Figure 4.4. The plots indicate that there is a preferential solvation of the hydroxyl group by water, in contrast to the methylene group, which is preferentially solvated by the organic modifier. The enhancement around hydroxyl groups is also more pronounced than the enhancement around methylene groups. However, it is a shorter ranged enhancement mainly tailing off by about 4 Å. This preferential solvation of hydroxyl groups by water is strongest in the acetonitrile mixtures and at the lower water molfractions. It should be noted here that the local molfraction enhancements of water around the hydroxyl group is very similar to that of water around water, whereas a stronger enhancement of the organic modifier was found around the solute methylene group than around another organic modifier molecule (compare Figure 4.4 to Figure 4.3). The preference of the hydroxyl group to be solvated by water is at least one reason for the decrease in the mobile to vapor phase transfer free energy with decreasing water concentration.

Figure 4.6 shows solute–solvent RDFs involving the hydroxyl oxygen atom of propanol, the largest of the alcohol solutes investigated here. As already inferred from the molfraction enhancements, there is an enhancement of hydrogen bond peak ($r = 2.8$ Å) between propanol and water for all mixtures. The O(Pr)–O(Water) peak height increases with decreasing concentration of water and is higher for the mixtures with acetonitrile than methanol at the same molfraction of organic modifier. In addition, the peak height for hydrogen-bonding to either the nitrogen atom of acetonitrile or the oxygen atom of methanol also increases with increasing modifier concentration, presumably because of the reduced competition with water due to the decreasing water concentration. Furthermore, the peak height for O(Pr)–O(MeOH) exceeds that for O(Pr)–N(ACN) at the same concentration because the methanol molecule can both accept or donate a hydrogen bond to the hydroxyl group of propanol, whereas the acetonitrile molecule can only act as hydrogen bond acceptor. From the positions of the first peak in the RDFs with the organic modifier's polar and methyl ends, one can conclude that the organic modifiers are preferentially oriented with their polar side pointing toward the hydroxyl group of the solute.

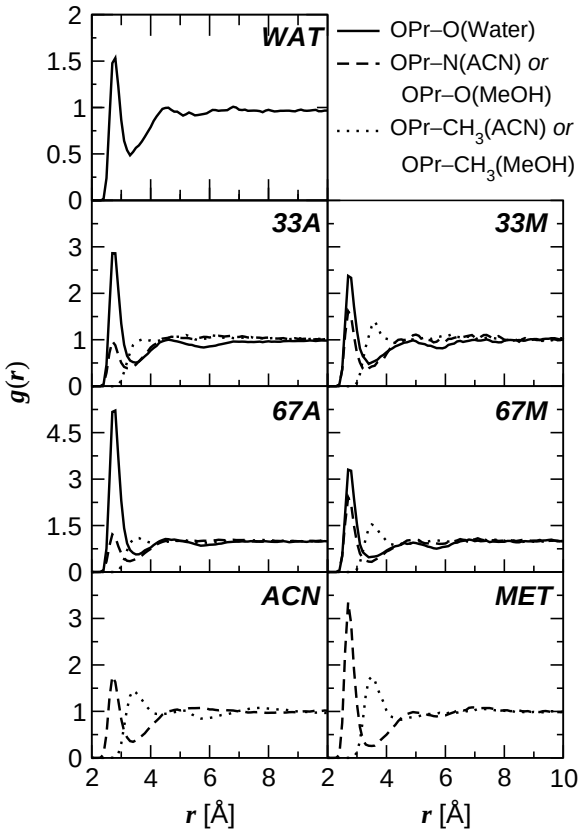

Figure 4.6: Radial distribution functions between propanol's oxygen atom and solvent atoms/groups in the mobile phase.

Further information about the solvation environment of the hydroxyl group can be found in Table 4.6, which shows the number of hydrogen bonds per solute hydroxyl group in the mobile, stationary, and vapor phases. Upon comparing the number of hydrogen bonds in the different mobile phases, one sees the number of hydrogen bonds per solute decreases in the order WAT>33M>67M≈33A>M>67A>A. That is, the number hydrogen bonds decreases as the concentration of water decreases. This correlates well with the decrease in ΔG_{mob} with decreasing water concentration. Furthermore, there is more hydrogen bonding for the solute in the methanol containing mobile phases than in the acetonitrile phases (methanol can both donate and accept hydrogen bonds while acetonitrile can only accept). This explains why there is a larger free energy penalty to go from mobile to vapor phase in methanol mixtures as compared to acetonitrile

Table 4.6: Number of hydrogen bonds per propanol solute molecule in the mobile, stationary, and vapor phases.[a,b]

	Mobile			Stationary			Vapor		
	N_{don}	N_{acc}	N_{tot}	N_{don}	N_{acc}	N_{tot}	N_{don}	N_{acc}	N_{tot}
WAT	1.47_2	0.91_1	2.38_2	0.20_3	0.21_3	0.41_4	0.013_2	0.025_4	0.038_4
33A	0.91_1	1.05_1	1.96_1	0.32_2	0.13_2	0.45_2	0.029_3	0.018_2	0.047_3
67A	0.91_1	0.67_1	1.58_1	0.32_1	0.06_1	0.38_1	0.033_4	0.015_5	0.048_5
ACN	0.89_1	0.01_1	0.90_1	0.47_1	0.08_1	0.53_1	0.040_3	0.005_1	0.045_3
33M	0.89_1	1.25_1	2.14_1	0.28_5	0.29_6	0.57_6	0.034_8	0.038_4	0.072_8
67M	0.91_1	1.08_1	1.99_1	0.62_4	0.63_3	1.25_5	0.12_2	0.13_2	0.25_3
MET	0.94_1	0.92_1	1.85_1	0.82_1	0.78_2	1.61_2	0.072_2	0.093_2	0.165_3

[a]Subscripts indicate statistical uncertainty in the final digit.
[b]N_{tot}, N_{acc}, and N_{don} refer to the average total number of hydrogen bonds and the average number accepted and donated (per propanol solute molecule).

mixtures of the same compositions.

In summary, the mobile-phase contribution to retention (transfer from mobile to vapor phase) is highly unfavorable for the hydroxyl group. In aqueous-organic mixtures, water shows preferential solvation of the hydroxyl group and the main factor leading to this unfavorable transfer is a loss of hydrogen bonding for the solute hydroxyl group.

4.3.2 Vapor to Stationary Phase Transfer

The second leg of the thermodynamic cycle shown in Figure 4.1 is the transfer from ideal gas to stationary phase. This leg represents ΔG_{stat}, the stationary-phase contribution to the free energy of retention. The following two subsections will examine this contribution for the nonpolar methylene and polar hydroxyl groups. Before this discussion, it is pertinent to note that there are important differences in the hexadecane stationary phase for the different solvent systems. Because the stationary phase is in thermodynamic contact with the mobile phase, solvent molecules will partition into the stationary phase to an extent based on their solubility. Table 4.2 shows the average number of solvent molecules in the stationary phase. Water is not very soluble in the nonpolar stationary phase, so very few solvent molecules are found in the stationary phase in system WAT. However, as the fraction of organic modifier is increased, a significant number of solvent molecules partition into the stationary phase. In systems ACN and MET, there are

10.7 and 21.5 solvent molecules in the hexadecane stationary phase corresponding to molfraction of 0.047 and 0.091, respectively. In comparison to experimental data [134, 135], these simulated solubilities are slightly underestimated.

The Nonpolar Methylene Group

For the methylene group, ΔG_{stat} is close to -2.7 kJ/mol irrespective of the mobile-phase composition (see Table 4.4). Thus, the increase in solvent partitioning into the stationary phase at higher organic molfractions has no effect on the partitioning of the nonpolar solute. This is not of great surprise as the molfraction of organic modifier is always less than 0.1 (and the volume fraction is even smaller) and since the nonpolar methylene group will have the same type of molecular interactions with hexadecane and the solvent, i.e., mainly dispersive.

Significant in the context of the driving forces for retention is that the free energy of transfer from vapor to stationary phase, or ΔG_{stat}, is negative and favorable for the methylene group, unlike ΔG_{mob}, which was generally positive and unfavorable. Therefore, the stationary phase contributes much more to the overall negative free energy of retention for the methylene group. It should also be noted that, unlike ΔG_{stat}, ΔG_{mob} changes when the organic modifier concentration is increased. Thus, the selectivity for nonpolar solutes is controlled to a much greater extent by the mobile phase than it is by the stationary phase.

The Polar Hydroxyl Group

The free energies of transfer from vapor to stationary phase for the hydroxyl group are given Table 4.4. Like the methylene group ΔG_{stat} is favorable for the hydroxyl group in all systems studied. This is in contrast to ΔG_{mob} for the polar hydroxyl group, which is unfavorable. Unlike for the methylene group, the mobile-phase composition has a significant effect on the transfer of the hydroxyl group from vapor to stationary phase. As the concentration of the organic modifier is increased the transfer from vapor to stationary phase becomes more favorable. Additionally, when comparing organic-rich acetonitrile to methanol (systems 67A, 67M, ACN, and MET), the methanol containing stationary phases at the same mobile-phase composition have a more negative and favorable ΔG_{stat}.

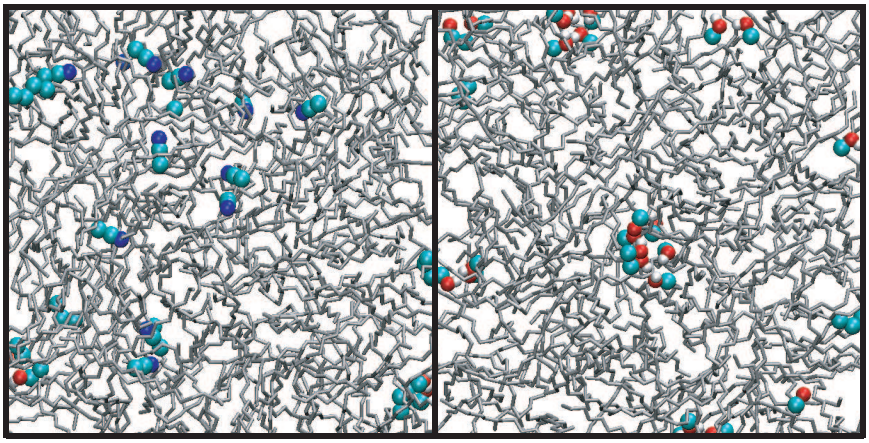

Figure 4.7: Snapshots of the stationary phase for systems ACN (left) and MET (right). Hexadecane molecules are depicted as gray tubes while solvent and solute molecules are shown as spheres with carbon in cyan, oxygen in red, nitrogen in blue, and hydrogen in white.

The change in ΔG_{stat} with changing mobile-phase composition stems from the solubility of acetonitrile and methanol in the stationary phase. The presence of acetonitrile and methanol gives rise to hydrogen bonding sites for the hydroxyl group within the stationary phase. Note that the numbers of water molecules present in the stationary phase is smaller (by factors of 10 to 40) than the numbers of organic modifier molecules (see Table 4.2). As shown in Table 4.6, the solute hydroxyl group is able to form a significant number of hydrogen bonds while in the stationary phase, ranging from 0.41 in system WAT to 1.61 in system MET. The number of hydrogen bonds correlates well with ΔG_{stat} for the different solvent compositions, that is, more hydrogen bonding in the stationary phase leads to a more favorable transfer from vapor to stationary phase.

The presence of hydrogen bonding species in the nonpolar stationary phase gives rise to the possibility of hydrogen bonded aggregates in this phase [136]. Figure 4.7 shows snapshots of the stationary phase for systems ACN and MET, the two systems with the most solvent present in the stationary phase. For system ACN, it appears the acetonitrile molecules exist primarily as free species, while in system MET the snapshot indicates a strong presence of hydrogen bonded aggregates. A more in-depth analysis of these aggregates is presented in Figure 4.8, which shows the distribution of hydrogen bonded aggregates of different sizes within the stationary phase for the

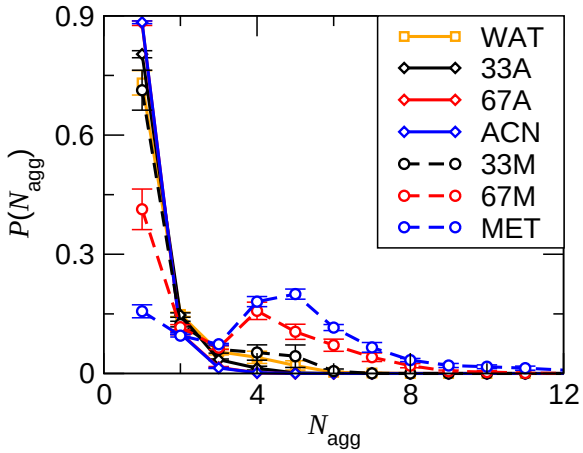

Figure 4.8: Probability distribution for hydrogen-bonding molecules (solvent or solute) in the hexadecane phase to be in hydrogen-bonded aggregates composed of N_{agg} molecules.

seven systems studied. The distributions show that there is little aggregate formation in systems WAT, 33A, 67A, and ACN. In these systems, solvent partitioned into the stationary phase exists primarily as monomers. In the water-methanol mixtures there is a much larger probability of aggregation and this probability increases as the methanol concentration is increased. For system MET, there is a significant probability of clusters containing four to six molecules in agreement with previous simulation studies [136].

4.4 Conclusions

In an effort to better understand the mechanism of retention in RPLC, particularly the driving forces for retention, configurational-bias Monte Carlo simulations in the Gibbs ensemble were carried out to examine the partitioning of solutes between common mobile-phase solvents used in RPLC and a liquid hexadecane as a model stationary phase. In addition to mobile and model stationary phases, an ideal gas reference state was present in the simulation to allow for the separation of the mobile and stationary-phase contributions to the free energy of retention. Analysis of the simulation trajectory reveals some important molecular-level details on the solvation environment of nonpolar and polar solutes in the mobile and stationary phases.

For the nonpolar methylene group the mobile-phase contribution to the free energy

of retention is unfavorable for all mobile-phase compositions studied, except for pure water. Thus, in most cases the methylene group is solvophilic rather than solvophobic. The stationary-phase contribution to the free energy of retention is favorable and shows no dependence on mobile-phase composition. Since ΔG_{stat} is negative like the net free energy of retention and the magnitude of ΔG_{stat} is greater than ΔG_{mob}, interactions with the stationary phase are the more important driving force for retention. Despite that interactions with the mobile phase contribute less to retention, the composition of mobile phase has a much greater influence on selectivity for nonpolar groups.

Analysis of the solvation environment around methylene groups indicates differences between water-methanol and water-acetonitrile mobile phases. In both mobile phases there is a preferential solvation of the methylene group by the organic component of the solvent. This preferential solvation is greater for acetonitrile mixtures than for methanol mixtures. Significant clustering of methanol or acetonitrile does not occur in these mixtures when the solute is not present. Thus, the presence of a non-polar solute causes significant rearrangement in the solvent structure.

The mobile-phase contribution to the free energy of retention for the polar hydroxyl group is highly unfavorable in all mobile-phase compositions. However, it becomes less unfavorable as organic concentration is increased. This trend is understood in terms of the hydroxyl groups preferential solvation by water and the smaller number of hydrogen bonds in organic-rich mixtures. The large and positive ΔG_{mob} indicates the hydroxyl group is very solvophilic.

As with the methylene group, the stationary-phase contribution to the free energy of retention for the hydroxyl group is favorable. However, this contribution is significantly affected by the mobile-phase composition. As the concentration of organic modifier is increased, there is a greater extent of solvent partitioning into the stationary phase. The leads to a larger number of hydrogen bonding sites in the stationary phase and hydrogen bonded aggregate formation. These factors create a much more favorable solvation environment for polar solutes in the stationary phase.

For the hydroxyl group, the stationary-phase and mobile-phase contributions to the free energy of retention are of opposite sign. However, the magnitude of ΔG_{mob} is much larger than ΔG_{stat}. Furthermore, ΔG_{stat} is largely dependent on the amount of solvent in the stationary phase. Thus, interactions with the mobile phase, especially

hydrogen bonding, are the most important factor for retention of the hydroxyl group. For this reason, retention of hydroxyl group is driven neither by solvophobic or lipophilic interactions, but by solvophilic interactions.

At this point it is evident that neither the solvophobic or lipophilic models are completely adequate descriptions of the driving forces for retention. Both nonpolar and polar solutes show prefer interacting with the mobile and stationary phase (except for neat water) over being unsolvated in the ideal gas phase. Since the interactions with the mobile phase are favorable (ΔG_{mob} is positive), the solvophobic theory is discounted. The lipophilic view is correct in that interactions with the stationary phase are favorable in all cases. However, interactions with the mobile phase are of importance, especially for solutes with polar groups.

Chapter 5

Simulating Realistic Models of RPLC

The previous chapter in this thesis dealt with simulations using liquid n-hexadecane as a simplified model of the RPLC stationary phase. However, the remainder of this thesis deals with simulations using a much more realistic model of the RPLC system. Details on this model system and the techniques used to simulate retention in RPLC will be discussed in this chapter. The merits of using these simulation techniques will also be highlighted. In addition, details on the analysis of simulation trajectory will be described here. The goal of this chapter is a general description of the simulation setup and methodology used throughout most of this work. It will be necessary at later points in this thesis give some further details on specific simulations.

5.1 Simulation Setup

To examine structure and retention in RPLC coupled-decoupled configurational-bias Monte Carlo (CBMC) simulations [89, 90, 95, 98] were carried out in the isobaric-isothermal (NpT) version of the Gibbs ensemble [83] (see Chapter 3). The simulations make use of three periodic simulation boxes that are in thermodynamic contact but do not share an explicit physical interface. The first box contains the stationary phase in contact with the mobile phase solvent, the second box contains a bulk solvent reservoir, and the third an ideal gas phase (see Figure 5.1). To mimic the size of actual systems,

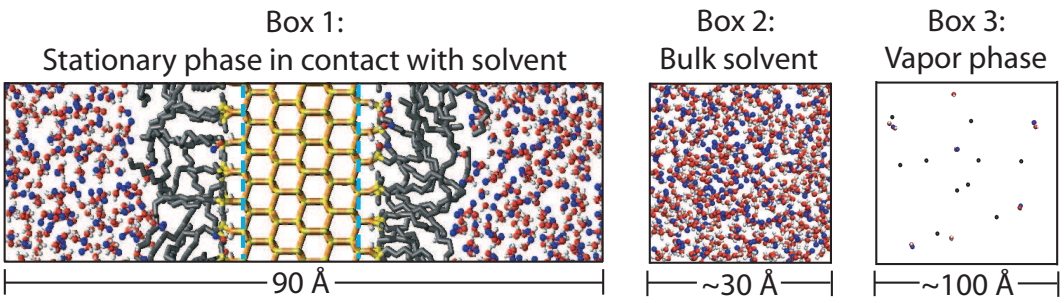

Figure 5.1: Simulation boxes used in the Gibbs ensemble simulation of RPLC.

all of the boxes are surrounded by periodic replicas of themselves in all directions.

To box containing the stationary phase is of fixed volume and is elongated in the z-direction with $L_x = 20$ Å, $L_y = 26$ Å, $L_z = 90$ Å. In the center of this box is a five layer slab of the β-cristobalite polymorph of silica with its two (1 1 1) surfaces exposed. The slab is ≈20 Å thick and initially has 24 vicinal silanols one each side (silanol surface density of 7.7 μmol/m^2). This surface was chosen as it is representative of the silanol surface density in a typical chromatographic system [137]. To this surface, dimethyl octadecyl siloxane chains (or other ligands) are bonded by randomly replacing some of the surface silanols, but avoiding chain overlap, until the desired surface coverage is achieved. Once the chains have been placed, the remainder of the box is filled with the desired solvent. It should be noted that this setup corresponds to a slit pore with a planar surface. Simulations utilizing a curved silica surface are described in Chapter 11.

The mobile and ideal gas phase boxes are both cubic and their volumes are allowed to fluctuate in response to the external pressure. The mobile phase box is filled with enough of the desired solvent to maintain box length of around 30 Å while the vapor box is filled with enough helium molecules to maintain a box length of around 100 Å. In addition to the stationary phase, solvent, and helium, various solutes molecules are also present in the simulations to allow for an exploration of the retention mechanism. These solutes and the solvent molecules are allowed to transfer between the three boxes via CBMC particle exchange [91, 92] and identity interchange [93, 94] moves (see Chapter 3).

The solvent box in the simulations is held at constant temperature and pressure and, therefore, the solvent molecules contained in this box will have a chemical potential equal to that of a bulk solvent at the temperature and pressure specified for the simulation.

Since solvent molecules are allowed to exchange between all three boxes (a move unique to the Gibbs ensemble), it is ensured that the chemical potential of the solvent is the same in all three boxes. Therefore, the chemical potential of the solvent in contact with the stationary phase is the same as that of a bulk solvent, i.e., has the desired temperature and pressure. This is exactly what occurs in a real RPLC system, but this feature has not been replicated in any molecular dynamics simulations to date. When carrying out an molecular dynamics simulation, the number of solvent molecules has to be chosen, somewhat arbitrarily, at the beginning of the simulation. There is no way to tell how the solvent will interact with the chains ahead of time. The solvent may penetrate into the chains and there may be enrichment/depletion of particular solvent components at the interface. With a single box of fixed size and number of particles, molecular dynamics simulations have no control over the chemical potential of the solvent. However, in Gibbs ensemble simulations, the system can respond to the interactions between the mobile and stationary phases. For example, if solvent molecules penetrate into the stationary phase at the start of the simulation, more solvent molecules will leave the solvent reservoir to replace them. Not replacing these solvent molecules can lead to an overall solvent density that is too low and/or the appearance of voids in the solvent structure during molecular dynamics simulations [62, 63].

Another advantage of Gibbs ensemble simulation method also relates to these particle transfer moves, but in this case for the solutes being examined. Like the solvent, solute molecules in the simulations are also allowed to transfer between the three boxes. In the Gibbs ensemble one can directly compute partition coefficients and Gibbs free energies of transfer (free energies of retention) from the average number densities of the solute molecules in each box or given subregions of the box (equation 3.6). This direct method is analogous to what is actually measured in experiment and is inherently more precise than the umbrella sampling and thermodynamic integration methods that must be used in molecular dynamics. Perhaps this is why few have attempted to compute these quantities in a molecular dynamics simulation of RPLC.

In the context of particle transfers, the purpose of the vapor box in the simulation should be discussed at this point. First, the vapor box acts as a thermodynamic reference state, so that the retention process may be decomposed into stationary and mobile phase components (as discussed in Chapter 4) and, second, it serves to facilitate the

particle exchange moves, particularly for hydrogen bonding species. For example, when a molecule is removed from the solvent phase hydrogen bonds may be broken. This contributes unfavorably to the acceptance rule in equation 3.3. Then, if the molecule is transferred to the stationary phase, there is a good chance that it will initially have an unfavorable interaction due to close contacts. On the other hand, if the molecule is transferred from the solvent phase to the vapor phase and then, sometime later in the simulation after the system is relaxed, transferred from the vapor phase to the stationary phase, these two energetic penalties are separated. This greatly increases the chance of accepting the (net) move of bringing the solute from the mobile to the stationary phase, or vice versa.

In addition to allowing for the precise calculation of free energies of retention, these particle exchange moves greatly enhance spatial sampling of the solvent and solute molecules. For example, when a solute is transferred from the solvent box to the box containing the stationary phase, it can be inserted in one of many possible regions. During a simulation, solutes are moved in and out of the box literally tens of thousands of times. Therefore, they are able to visit (sample) the different regions of the box numerous times. Each time they visit a region, it may have a different local arrangement and the solute will have a different probability of residing there. In an molecular dynamics simulation, one must wait for the solute to diffuse to the different regions of the box, which is an inherently long process. Spatial sampling is very important for simulating RPLC. To determine the retention mechanism (for example, adsorption versus partition) one needs to now exactly where the solutes prefer to reside within the stationary phase with great precision.

The preceding paragraphs demonstrated the importance of the particle transfer moves for the precise sampling of the distribution of solvent and solute molecules in the RPLC system. Another important aspect of the simulation is that the structure of the stationary phase chains is adequately sampled. The CBMC moves applied to the bonded stationary phase chains are absolutely critical for this. In Chapter 8, it will be demonstrated that the current simulation method is able to converge structural properties of the chains to the same values (within statistical uncertainties) regardless of the starting configuration of the system. In one set of simulations, the chains are placed in an all-trans conformation directed away from the surface. Before the chains

are allowed to relax, solvent is added to this system with solvent penetration in between the chains. In another set of simulations the chains are pre-equilibrated in vacuum via CBMC regrowths. Since vacuum is a poor solvent, the C_{18} chains in this case tend to interact with each other and form a somewhat compressed layer. The solvent is then added to this starting structure. Thereafter, the simulations are allowed to reach equilibrium with the bulk mobile phase through various types of Monte Carlo moves. The excellent agreement of the simulation data for systems started with these contrasting initial configurations verifies that the simulation protocol is capable of yielding results that are independent of the starting structure after an initial equilibration period. This ability has not been demonstrated, or even attempted, by workers carrying out molecular dynamics simulations and could be the reason for some of the conflicting results. For example, molecular dynamics simulations starting with the chains in the all-trans conformation suggest that the chains are oriented perpendicular to the substrate surface [53, 58] while molecular dynamics simulations starting the chains in collapsed states suggest that the chains have many gauche defects and large tilt angles [51, 52].

A final point to be made, and one that was mentioned earlier, is that molecular dynamics simulations have an explicit dependence on time. In RPLC, it has been shown that it can take tens of minutes to reequilibrate a column after switching solvents [138, 139]. This is a severe problem because the time scale accessible for a molecular dynamics simulation is microseconds at best. Thus, processes occurring in RPLC may be completely out of reach for a molecular dynamics simulation. However, Monte Carlo simulations, which do not depend on time, will work even for processes occurring on long physical time scales.

5.2 Force Field

To describe molecular interactions the TraPPE-UA force field [97, 98, 100, 102, 129] is used for all species in the simulated RPLC systems with the exception of water molecules and silica substrate. Water is described by the popular TIP4P model [128] and silica by a rigid zeolite potential [140, 141, 142]. Surface silanols were given bending and torsional degrees of freedom and had charges assigned based on the TraPPE alcohol model ($-0.739e$ for oxygen, $+0.435e$ for hydrogen) [100]. Lennard-Jones interactions

were truncated at a distance of 10 Å and Coloumbic interactions were treated with the Ewald summation technique [80] using a direct space cutoff of 10 Å and a convergence parameter of $\kappa = 0.28$. The the number of reciprocal space vectors in a particular direction is set equal to the next integer greater than $\kappa \times L_\alpha$, where L_α is the box length in that direction. In this manner, the box containing the stationary phase has a larger number of reciprocal space vectors in its elongated z-direction than in the x- and y-directions.

5.3 Data Analysis

The Monte Carlo simulation of RPLC produces millions of configurations for each of the systems studied. Each of these configurations are generated according to their statistical mechanical probabilities. At specified intervals during the simulation, the exact coordinates of each of the atoms in these configurations are written to a file. Once a simulation is complete, this file contains a highly detailed record of the system's trajectory through configuration space. One can then analyze this trajectory to compute various properties related to the structure of the system at the molecular-level. In addition, this molecular-level data can be translated into bulk thermodynamic properties that may be compared directly to those properties measured in experiment. In the following sections it is defined how the various properties used in this thesis to describe structure and retention in RPLC are computed from the simulation trajectory. The first of these sections describe properties related to chain conformation, the next sections deal with system composition and solute distribution, and the final ones with solvent/solute orientation and hydrogen bonding.

Before discussing these properties definitions for the orientational and positional reference points in the system, i.e., the silica surface normal and the coordinate z, need to be given. In the slit pore setup, the silica surface is planar and lies in the x-y plane of the simulation box, thus there is no ambiguity in defining the surface normal. The position of this planar surface along the z-axis of the simulation box is defined by the location of the outermost silicon atoms in the silica surface, which are all coplanar (dashed lines in Figure 5.1). The location of this surface is defined to be at $z = 0$, and z increases with increasing distance from the surface.

5.3.1 Chain Conformation

Gauche Defect Statistics

One of the easier metrics to study experimentally (i.e., through Raman spectroscopy) is the fraction gauche defects (f_{gauche}) along the stationary phase chains. This metric can be computed unambiguously in a simulation. A gauche defect is defined as a dihedral angle deviating by more than 60° from the angle of the trans conformer. The minimum energy conformer for an alkane would have no gauche defects, thus larger fractions of gauche defects are related to greater disorder. From the trajectory file described above, all of the dihedral angles for each bond in the chain can be measured and it can be determined if gauche defects are present. The number of gauche defects can then be averaged for a particular location in the chain or for the chain as a whole.

End-to-end Distance

Another property that gives an indication of the conformation of the chains is the end-to-end (ete) distance, or r_{ete}. This distance is measured from the first methylene group on the grafted end of the chain to the terminal methyl group. Larger values of r_{ete} correspond to more extended chains and smaller values to more folded or coiled chains.

End-to-end Orientation

The first and terminal groups also define the end-to-end vector. Chain alignment can be quantified by the angle this vector makes with the silica surface, through $\cos\theta_{\text{ete}}$ (see Figure 5.2). Values of $\cos\theta_{\text{ete}}$ approaching unity indicate chains perpendicular to the surface while values approaching zero indicate chains parallel to the surface, i.e., lying flat.

Terminal Methyl Group Position

To judge how far the chains are extended away from the silica surface the quantity z_{CH_3} is used (see Figure 5.2). This quantity is computed by simply averaging the z-position of each stationary phase chain's terminal methyl group over the course of the simulation. Larger values of z_{CH_3} indicate chains more extended away from the silica surface, smaller value indicate chains closer to the surface (more collapsed or back folded).

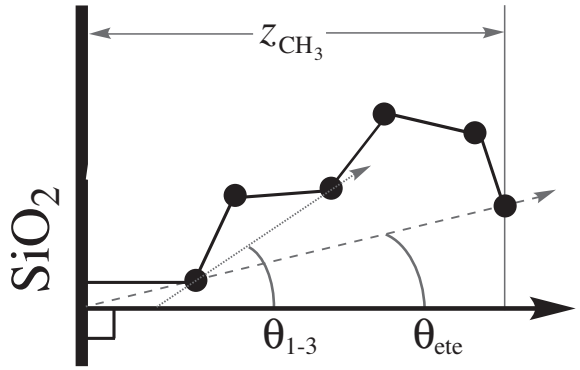

Figure 5.2: Definition of the 1–3 and end-to-end (ete) angles and the z-location of the terminal methyl group.

Order Parameter

A property which gives further indication of the chain alignment with respect to the silica surface is the order parameter S defined as

$$S_i = \frac{1}{2}\langle 3\cos^2\theta_{1-3,i} - 1\rangle \tag{5.1}$$

where $\theta_{1-3,i}$ is the angle between the i^{th} 1–3 backbone vector in the alkyl chain (between carbons separated by two bonds) and the normal to the silica surface (see Figure 5.2). The brackets indicate that an average through the entire simulation has been taken. This order parameter approaches unity for vectors preferentially aligned perpendicular to the silica surface, -0.5 for parallel vectors, and vanishes if there is no preferential orientation (or for a very narrow distribution around the magic angle). For more local information one can examine this order parameter as a function of position within the chain i.e., S_1 is for the first 1–3 vector in a C_{18} chain (between carbons 1 and 3) and S_{16} is for last (between carbons 16 and 18) or one can average the order parameter over all 1–3 vectors in the chain

$$S_n = \frac{1}{n}\sum_{i=1}^{n} S_i \tag{5.2}$$

where n is the number of 1–3 vectors in the chain. The experimental equivalent to this order parameter is the NMR order parameter for deuterated alkyl chains [143, 144].

5.3.2 Heterogeneity in System Composition

The RPLC system is a very heterogeneous one. This means that the various components of the system are not distributed evenly and one needs a way to quantify this. The main tool used in this respect is the (specific) density profile, $\rho(z)$, which allows one to the describe the composition of the system relative to the silica substrate. These profiles are computed by dividing the simulation box into slices of width 0.45 Å along the z-coordinate. The number of solvent molecules and stationary phase (united) atoms in each of these slices is then averaged over the course of the simulation. Thus, the magnitude of $\rho(z)$ allows one to discern how much of a particular component resides, on average, at a particular location.

To compare different systems, it is useful to define a boundary between the retentive and stationary phases. The density profiles described above allow for the location of a Gibbs dividing surface (GDS), a plane that defines this boundary [145, 146]. The GDS is fit to the total solvent density (water and organic co-solvent) using a hyperbolic tangent fitting method [147]

$$\rho(z) = \frac{1}{2}(\rho_{\text{mob}} + \rho_{\text{stat}}) + \frac{1}{2}(\rho_{\text{mob}} - \rho_{\text{stat}}) \tanh[2.197(z - z_{\text{GDS}})/\delta_{\text{int}}] \tag{5.3}$$

where ρ_{mob}, ρ_{stat}, z_{GDS}, δ_{int} are parameters in the fit corresponding to the solvent density in the bulk mobile phase, solvent density in the stationary phase, z-location of the GDS, and the interfacial width (reflecting the 10%–90% range of the total solvent density between the two phases).

Another quantity related to the heterogeneity of the RPLC system is the molfraction enhancement profile for the organic component of the mobile phase, $x_{\text{org}}(z)/x_{\text{org}}(\text{bulk})$. With the density profiles for water and the organic co-solvent, the molfraction of the organic component can be computed as a function of z

$$x_{\text{org}}(z) = \frac{\rho_{\text{org}}(z)}{\rho_{\text{org}}(z) + \rho_{\text{water}}(z)} \tag{5.4}$$

This quantity is then divided by the bulk molfraction (the molfraction in the solvent box). Thus, values of $x_{\text{org}}(z)/x_{\text{org}}(\text{bulk})$ larger than unity at a given value of z indicate an enrichment of the concentration of the organic component at that location and values below unity indicate a depletion.

5.3.3 Solute Distribution Coefficients and Transfer Free Energies

As indicated in section 3.1.1, distribution coefficients and free energies of transfer can be computed directly from the number densities of a particular species in each phase (i.e., in each simulation box) during a Gibbs ensemble simulation. This information can be further localized. The partition coefficient or free energy of transfer can be computed in the same way for a given sub-region of a simulation box. This allows one to compute the z-dependent distribution coefficient profiles, $K(z)$ and incremental free energy profiles, $\Delta G(z)$. The exact procedure for this is outlined in the following.

Just as is done for the solvent molecules, the density profiles for the solute molecules are computed. Dividing this density profile by the density of the solute in the bulk solvent box gives $K(z)$, the distribution coefficient for transfer of the solute from the solvent phase to a specific z-location in the box containing the stationary phase. This partition coefficient profile can then be converted to a free energy profile by the standard relationship $\Delta G(z) = -RT \ln K(z)$. The overall free energy of transfer for a given solute (the free energy of retention) can also be computed by using the GDS described above as a border between the two phases. The excess concentration of the solute in the interfacial region is also taken into account in this process.

In many of the simulations described in this thesis, two sets of solutes are used. The first set is a homologous series of n-alkanes, from methane to butane. The second set is a series of 1-alkanols, from methanol to butanol. Once $\Delta G(z)$ is computed for each member in the homologous series of alkanes, the incremental free energy profile for the methylene group $\Delta G_{\mathrm{CH_2}}(z)$ can also be computed. For each value of z, the slope of a linear fit to the free energy versus number of carbons is computed. This slope corresponds to $\Delta G_{\mathrm{CH_2}}(z)$. The incremental free energy profile for the hydroxyl group is computed by taking $\Delta G(z)$ for a 1-alkanol and subtracting $\Delta G(z)$ for an alkane with the same number of carbons

5.3.4 Solute/Solvent Orientation

In addition to knowledge about the preferred location of the solvent and solutes through $\rho(z)$, $K(z)$, and $G(z)$, it is useful to have information about the preferred orientation of the various species as a function of z when discussing structure and retention. For

alcohols and acetonitrile, profiles of $\cos\theta_{\text{ete}}$ are used for this purpose, where θ_{ete} is the angle between the molecule's end-to-end vector and the normal to the silica surface. Here, the end-to-end vector originates at the methyl group and terminates at the hydroxyl hydrogen (in the case of alcohols) or nitrogen (in the case of acetonitrile). Thus, positive values of $\cos\theta_{\text{ete}}$ indicate methyl groups pointing away from the silica surface, negative values towards, and values near zero indicate no preferential orientation or a preference for the end-to-end vector to be parallel to the silica. For water, $\cos\theta_p$ profiles are used, where θ_p is the angle between a water molecule's dipole vector and the surface normal. For linear alkanes solutes, it would not be informative to use $\cos\theta_{\text{ete}}$ since, because of symmetry, this quantity will average to zero. Instead, the z-profiles of S_n are used, where S_n is defined in the same way as for the stationary phase chains, but in this case computed as a function of z.

5.3.5 Hydrogen Bonding

Hydrogen bond interactions can be very important in RPLC. Solvent molecules, various solutes, and surface silanols are all capable of participating in these interactions. Therefore, the extent of this hydrogen bonding needs to be characterized. For this purpose the following geometric criteria for hydrogen bonding is used through this work: an X(acceptor)–X(donor) distance less than 3.3 Å, an X(acceptor)–hydrogen(donor) distance less than 2.5 Å, and a hydrogen bond angle with a cosine less than -0.1, where X may be either an oxygen or a nitrogen atom. [132]

Chapter 6

Mobile Phase Effects. I. Stationary Phase Solvation and Structure

6.1 Background

The most common stationary phases in RPLC consist of porous silica particles upon which alkyl silane chains (typically 18 carbons in length) are grafted through single bond linkages with surface silanols. Because they are immobilized on a surface, the stationary phase chains have unique properties that differ from both the liquid and solid states of matter. The molecular conformation of these chains and their interaction with the mobile phase solvent has been the subject of research for around three decades and an excellent review of this topic has been given by Sander and coworkers [26]. Despite these intense research efforts, a clear molecular picture of the structure of these tethered chains remains lacking. This molecular picture is a necessary piece in completely describing the solute retention mechanism, the principle goal of this work.

Investigations into the structure of the stationary phase chains and their contacting solvent has occurred mainly along three lines of inquiry. The first of these is to examine

[†] This chapter describes the outcome of a collaborative research project carried out by Jake L. Rafferty, Ling Zhang and Li Sun and advised by J. Ilja Siepmann and Mark. R. Schure. Reports on portions of this research project have been published [69] and/or submitted [78].

thermodynamic data, typically generated through retention measurements, and then try to infer details about the molecular structure [11, 12, 15, 16, 17, 18, 45, 46]. However, it is impossible to extract conformational details on the chains from thermodynamic-based data [54]. Thermodynamics is an energy bookkeeping system based on macroscopic measurement and cannot give molecular-level insights, but can only be used to infer such details [148].

The second line of investigation uses spectroscopic techniques which directly probe the chains or some molecule that interacts with the chains. Experiments using a host of techniques including nuclear magnetic resonance [28, 149, 150, 151, 152], infrared [153, 154], Raman [48, 155, 156, 157, 158], sum-frequency generation [159, 160], and fluorescence [29, 30, 34, 161, 162, 163] spectroscopies, and small angle neutron scattering [164] have generated a great deal of information on structure and dynamics of alkyl stationary phases. However, none of these techniques are able to observe the conformation of individual chains and one must analyze data relating to a complex distribution of chain conformations. Despite this difficulty, a couple of trends are supported by the experimental data. First, conformational order increases with increasing surface coverage, increasing chain length, and decreasing temperature. Second, conformational order is affected to only a small extent by changes in typical RPLC solvents (but nonpolar solvents, such as hexane, can have a large effect).

A third line of investigation involves theory [36, 40, 43]. This method involves the construction of some model system and then application of statistical mechanics to exactly solve for the properties of this model. In one well-known case [36], empirical parameters such as chain stiffness were used to construct a lattice model. However, a detailed model of chain conformation should yield chain stiffness as a result rather than use it as an input parameter. The ultimate goal of any investigation into bonded chain structure is to give atomistic-level detail, but the models needed to do this through a strict theoretical treatment are far too complex to be solved analytically. However, the use of molecular simulation does allow one to utilize these complex models and the system can be represented at the individual atom level of detail.

In this chapter, simulations of a dimethyl octadecylsilane (C_{18}) stationary phase at an intermediate surface coverage of 2.9 μmol/m^2 in contact with water/acetonitrile and water/methanol mobile phases of varying organic modifier concentration are described.

These simulations allow for a direct analysis of the molecular conformation of the chains and the structure of the contacting solvent. One of the motivations for examining the effects of solvent composition is the anomalous behavior of alkyl silane based RPLC columns when highly aqueous mobile phases are used [138, 165]. When the fraction of organic modifier falls below a certain threshold a dramatic loss of retention is observed (the precise threshold can depend on many parameters such as pressure and pore size). On explanation for this behavior is that the alkyl chains collapse in the presence of highly aqueous solvents [165, 166, 167]. A more recent, competing explanation for this retention loss is pore dewetting where the highly aqueous mobile phase does not enter a substantial fraction of the smaller pores and hence is not able to bring the solutes in contact with the stationary phase chains [138]. This dewetting is a consequence of the principle of capillarity and results from the higher surface tension of water as compared to the organic modifier (i.e., it is not driven by changes in chain conformation). Another motivation for studying influence of solvent composition is to examine preferential sorption of the organic component of the mobile phase into/onto the stationary phase. This effect is well known, but it is not fully resolved if this preferential solvation occurs solely through the formation of an organic layer atop the stationary phase [45, 46] or if penetration of the organic modifier into the stationary phase is also important [47, 48].

6.2 Simulation Details

To examine the effects of mobile phase composition on stationary phase solvation and structure, configurational-bias Monte Carlo simulations in the NpT version of the Gibbs ensemble using a three-box slit pore setup (see Figure 5.1) were carried out. The main details on the simulation method and setup were given in the preceding chapter. The simulations made use of dimethyl octadecylsilane (C_{18}) chains grafted at density of 2.9 μmol/m^2 (9 chains on each of the two silica surfaces) resulting in a residual silanol density of 4.8 μmol/m^2 (15 silanols on each surface). Seven different mobile phase compositions were considered: pure water (denoted as system WAT), 33% molfraction acetonitrile (33A), 67% acetonitrile (67A), pure acetonitrile (ACN), 33% methanol (33M), 67% methanol (67M), and pure methanol (MET). For reference, systems 33A and 67A correspond to roughly 59% and 86% volume fraction acetonitrile and systems

Table 6.1: Average number of solvent molecules in each simulation box.[a]

	N_{water}			N_{organic}[b]		
System	Box 1	Box 2	Box 3	Box 1	Box 2	Box 3
WAT	764_5	396_5	3.0_2	–	–	–
33A	288_9	504_9	7.7_2	160_3	229_5	10.2_3
67A	101_2	294_2	4.4_1	227_1	561_1	11.4_1
ACN	–	–	–	261_1	921_1	18.5_4
33M	335_6	458_6	5.7_1	193_1	199_1	7.7_1
67M	131_2	265_2	2.6_3	290_2	499_3	10_1
MET	–	–	–	338_2	420_1	9.4_5

[a]Subscripts indicate the statistical uncertainty in the final digit.

33M and 67M correspond to roughly 53% and 82% volume fraction methanol, respectively. The average number of solvent molecules in each of three simulation boxes is given in Table 6.1. Also present in each simulation were a set of 16 solutes molecules (two each for methane to *n*-butane and methanol to 1-butanol) that allowed for an exploration of the retention mechanism (to be discussed in Chapter 7) and 20 helium atoms to maintain a vapor box of adequate size. Solvent and solute molecules were allowed to transfer between the three boxes while helium atoms were constrained to the vapor phase. To keep from overloading the stationary phase with too many of these solutes and possibly alter its structure, additional bias potentials were applied in each box for the different solutes. The bias potentials were adjusted during the equilibration period such the each solute was distributed about evenly between the three boxes. All simulations were performed at a temperature of 323 K and a pressure of 1 atm.

For each solvent composition studied, four independent simulations were carried out. Each simulation was equilibrated for 2×10^5 Monte Carlo (MC) cycles (one MC cycle corresponds to N MC moves, where N is the total number of molecules in the system). Thereafter, the simulations proceeded with an additional 2×10^5 MC cycles during which averages were collected. Statistical uncertainties in all reported quantities were estimated from the standard error of the mean for the averages from the four independent simulations.

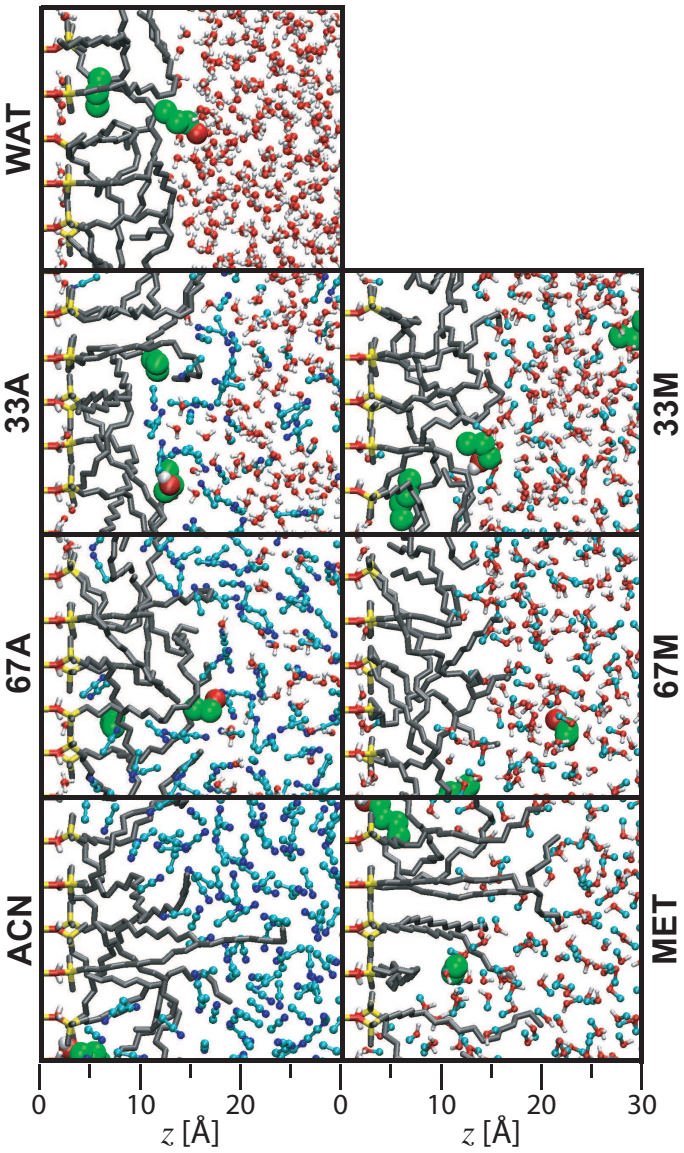

Figure 6.1: Simulation snapshots for RPLC systems with varying mobile phase composition. The stationary phase is shown as tubes with carbon in grey, silicon in yellow, and oxygen in red. The mobile phase is shown in the ball and stick representation with carbon in cyan, oxygen in red, nitrogen in blue, and hydrogen in white. Solutes are depicted as large spheres with carbon in green, oxygen in red, and hydrogen in white.

6.3 Results and Discussion

Snapshots from simulations at each solvent composition are shown in Figure 6.1. Although each of these snapshots represents only a single configuration of the millions generated during the simulation, they already demonstrate some distinct differences between the systems with different solvent compositions. As the fraction of organic modifier is increased, there is significantly more penetration of solvent into the stationary phase. Near the silica surface, most of the solvent is water. However, throughout the remainder of the stationary phase the majority this sorbed solvent appears to be the organic modifier. More solvent penetration is observable for the acetonitrile containing systems. Also appearing enriched in organic component of the solvent is the interfacial region. This is most apparent when viewing the snapshot for system 33A where the region just above the alkyl chains appears to be highly concentrated in acetonitrile. The snapshots also indicate that the chains are more extended and aligned away from the silica surface in the organic rich phases. The solutes present in the snapshots suggest that retention can occur at the surface of the alkyl chains (adsorption) or deep within the bonded phase (partitioning), but this will be discussed in more detail in the following chapter. A full analysis of the simulation trajectory offers more precise details on the preliminary observations from these snapshots and this is the topic of the following subsections on stationary phase solvation and chain structure.

It should also be noted that at the bottom of the snaphots shown in Figure 6.1 is a scale defining the z-coordinate, which is zero at the silica surface and increases as one moves away from the surface. Throughout this thesis many system properties are reported as a function of this z-coordinate.

6.3.1 Solvation of the Stationary Phase

To describe the system composition as a function of z, the distance from the silica surface, density profiles for water, acetonitrile, and the stationary phase alkyl chains are presented in Figure 6.2. Also shown in this figure is the location of the Gibbs dividing surface (GDS) between mobile and stationary phase and the width of this interfacial region. In examining the density profiles, one definitely sees an increase in solvent penetration into chain region as the molfraction of organic modifier is increased. For

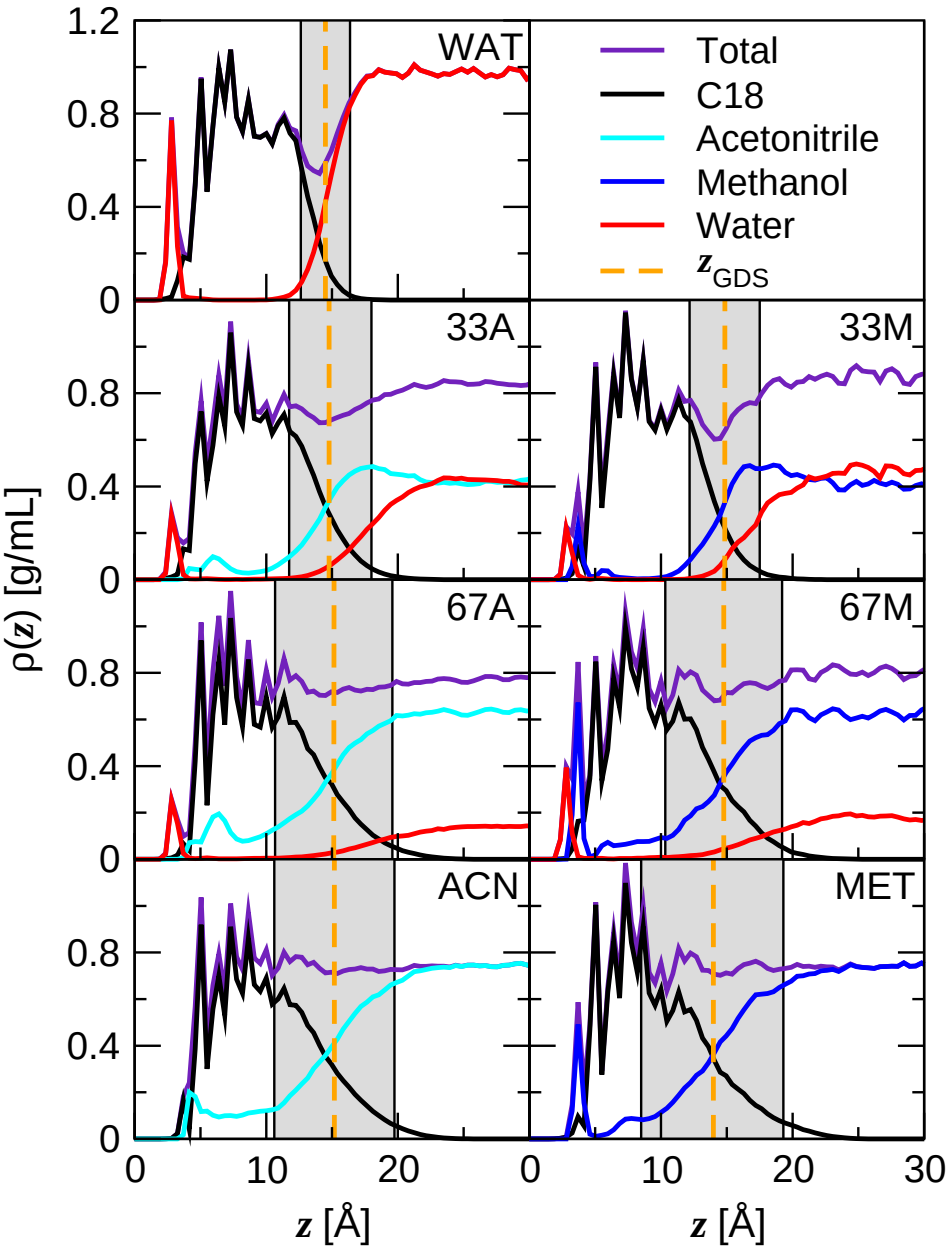

Figure 6.2: Solvent and stationary phase density profiles for systems with varying mobile phase composition. The shaded gray area represents the interfacial region.

Table 6.2: Percentage of surface silanols with zero, one, two, or three hydrogen bonds with solvent molecules.[a]

System	0	1	2	3
WAT	21	39	35	4
33A	53	39	9	<1
67A	54	38	7	<1
ACN	85	15	0	0
33M	19	41	36	4
67M	23	43	31	3
MET	33	38	28	1

[a]Uncertainties in all data are less than 1%

system WAT, the center of the bonded phase is nearly void of solvent while in systems ACN and MET there is a substantial amount of solvent in the bonded phase. For the mixed solvent systems, the solvent penetrated into the stationary phase is primarily the organic modifier. Despite the increase in solvent penetration with increasing organic molfraction, the GDS (which is fit to the total solvent density) does not change significantly and is located at around 15 Å in all systems. However, an increase in the interfacial width is observed with increasing organic molfraction. In system WAT this width is about 4 Å while it is closer to 10 Å in systems ACN and MET.

In comparing water/acetonitrile and water/methanol mixtures with the same organic molfraction, there is a larger extent of solvent penetration for the acetonitrile containing solvents except very near the silica substrate ($z < 4$ Å) where methanol exhibits sharp peaks. These sharp peaks, which are also present in the density profiles of water, result from direct hydrogen bonds between solvent molecules and surface silanols. The number of hydrogen bonds between silanols and solvent is quantified in Table 6.2. In system WAT, only 21% of silanols are not involved in any hydrogen bonds with solvent molecules and the majority of silanols have either one or two hydrogen bonds with solvent. The number of silanols with no hydrogen bonds increases markedly as acetonitrile concentration is increased. In systems 33A and 67A, the percentage of silanols with no hydrogen bonds is over 50% and in system ACN this number jumps to 85%. For those silanols that are hydrogen bonded to solvent in the acetonitrile containing systems, very few have more the one hydrogen bond. The methanol containing systems are in stark contrast to this. For systems 33M and 67M, the number of silanols

with no hydrogen bonds is similar to system WAT and this number increases to only 33% in system MET. In these systems there is also a significant fraction of silanols with two hydrogen bonds. These trends stem from the fact that acetonitrile can only be involved in one hydrogen bond (as an acceptor) while methanol can participate in three (donating one and accepting two) and water can participate in four (donating two and accepting two). This lack of hydrogen bonding between surface silanols and solvent molecules in the acetonitrile rich systems has important consequences for the retention of hydrogen bonding solutes, a topic that will be addressed in Chapter 7.

Other interesting phenomenon in the density profiles can also be seen in the interfacial region. For system WAT, there is a depletion in the total system density, or dewetting near the GDS. This depletion becomes less apparent as the molfraction of organic modifier is increased and disappears in systems ACN and MET. For the mixed solvents, the depletion is stronger for the methanol containing mixtures. This dewetting effect for water near extended hydrophobic surfaces has been predicted by Lum, Chandler, and Weeks and is attributed to a disruption of the solvent's hydrogen bonding network [133]. It appears that this effect is less important in the more weakly hydrogen bonding acetonitrile mixtures as compared to the methanol mixtures. Also present in the interfacial region is an enrichment in the organic modifier concentration for the binary solvent systems. This effect is most dramatic for systems 33A and 33M where the organic solvent density reaches a maximum in the interfacial region, which actually exceeds its bulk mobile phase density, despite the minimum in total system density. The enrichment in the interfacial region appears to be only slightly stronger for the acetonitrile containing systems.

Kazakevich and coworkers have measured the excess adsorption isotherms of acetonitrile and methanol from their mixtures with water onto RPLC stationary phases [45, 46]. In agreement with this experimental work, it is found that there is an excess adsorption of the organic component of the solvent and that this excess is greater for acetonitrile mixtures than for methanol mixtures. From the adsorption isotherm data, Kazakevich and coworkers inferred that methanol forms one monolayer at the C_{18}/mobile phase interface and acetonitrile forms 5 molecular layers [46]. Indeed, the present work shows an enhancement of the organic modifier in the interfacial region. However, the solvent composition in the interfacial region is never 100% organic modifier and, therefore, no

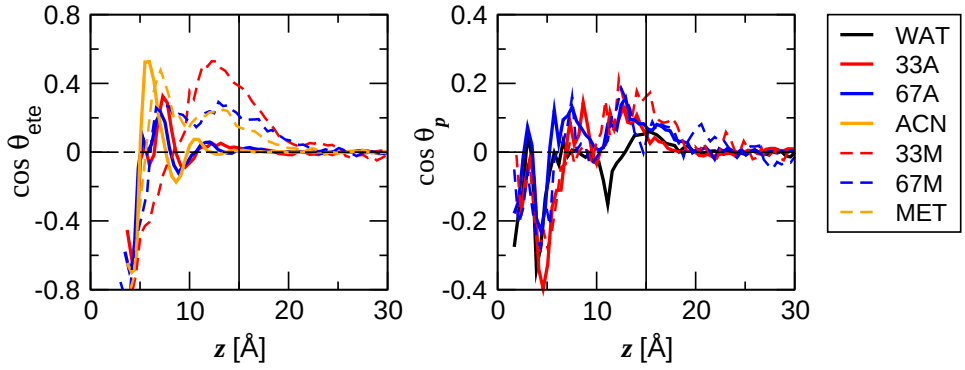

Figure 6.3: Orientation of the end-to-end vector of the organic modifier (left) and the dipole vector of water (right) as a function of z for water-acetonitrile and water-methanol mixtures. The horizontal line at $z = 15$ Å serves as a rough guide for the position of the GDS in each system.

layers of organic modifier exist. Additionally, since the enhancement of organic modifier in the interfacial region is only slightly greater for the water-acetonitrile mixtures, the increased amount of adsorption of organic modifier for water/acetonitrile as compared to water/methanol is not solely due to enhancement at the C_{18} surface. Rather, it is also the result of increased partitioning of acetonitrile inside of the C_{18} phase relative to methanol.

The orientation of solvent molecules within the stationary phase and interfacial region is also important for characterizing stationary phase solvation. For this reason, the orientation of end-to-end vectors for acetonitrile and methanol and dipole vectors for water are examined through z-profiles of $\cos\theta_{\text{ete}}$ and $\cos\theta_p$, respectively (see Figure 6.3). As defined in Chapter 5, positive values of $\cos\theta_{\text{ete}}$ indicate solvent methyl groups pointing towards the silica substrate and negative values indicate methyl groups pointing away. Positive values of $\cos\theta_p$ indicate dipole vectors directed away from the substrate and negative values towards.

For acetonitrile there is a distinct preference for the methyl group to point away from, and the nitrogen towards, the silica surface in the region for $z < 5$ Å. In this orientation, acetonitrile may interact via hydrogen bonding with the surface silanols. In the region from $z = 5$–8 Å, acetonitrile orients its methyl group towards the silica surface, i.e., with

Table 6.3: Structural properties of alkylsilane chains in contact with different mobile phase solvents.[a,b]

	System						
Property	WAT	33A	67A	ACN	33M	67M	MET
f_{gauche}	0.25_1	0.27_1	0.26_1	0.27_1	0.27_1	0.26_1	0.26_1
$\cos\theta_{\text{ete}}$	0.25_1	0.46_3	0.52_2	0.56_2	0.43_3	0.51_2	0.53_4
r_{ete} (Å)	16.2_3	15.9_3	16.2_4	16.2_2	15.7_3	16.1_3	16.2_3
z_{CH_3} (Å)	9.1_1	11.2_3	12.4_1	12.9_3	10.9_1	12.3_1	12.5_4
S_n	-0.14_2	-0.02_1	0.02_2	0.05_1	-0.05_2	0.01_2	0.02_1

[a]Subscripts indicate the statistical uncertainty in the final digit.
[b]These structural properties are defined in Chapter 5.

its dipole moment directed away the silica surface. Moving outward beyond $z = 8$ Å, the alignment of acetonitrile oscillates but decays to zero in the interfacial region. There is no orientational preference for acetonitrile outside of the GDS. Methanol has an orientational preference similar to acetonitrile when near the silica surface, i.e., it points it methyl group away from the surface and its hydroxyl group towards so that it can hydrogen bond with the surface silanols. In the interfacial region, methanol has a much stronger orientational preference than acetonitrile. Methanol aligns it methyl groups towards the stationary phase and its hydroxyl group towards the solvent. In this manner, the hydroxyl group can participate in hydrogen bonding with the mobile phase solvent while the nonpolar methyl group interacts with the alkyl stationary phase. The stronger orientational preference for methanol in the interfacial region, as compared to acetonitrile, is in disagreement with interpretations of spectroscopic data [160] but in agreement with previous molecular dynamics simulations [58]. Water has a somewhat weaker and more rapidly varying orientational preference than acetonitrile or methanol. In general, its dipole vector point towards the silica surface for $z < 5$ Å and towards the mobile phase when in the interfacial region.

6.3.2 Structure of the Stationary Phase

From the solvent density profiles shown in Figure 6.2, it is clear that the alkyl chains in the stationary phase are solvated to a larger extent when the concentration of organic modifier in the mobile phase is increased. Coinciding with the increase in solvation

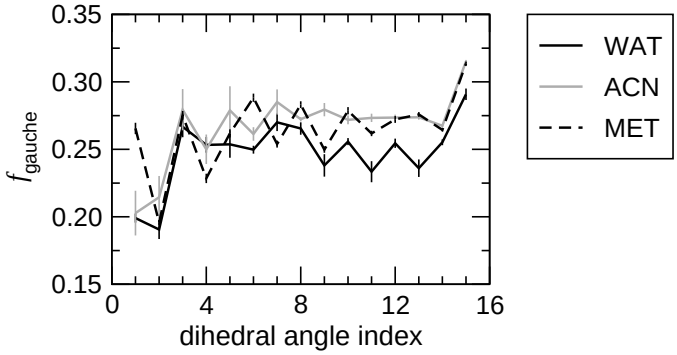

Figure 6.4: Fraction of gauche defects along the chain backbone.

is an extension of the C_{18} chain density into the solvent region. To ascertain what effect this has on the structure of the stationary phase, various structural properties for the alkyl chains were calculated (Table 6.3 and Figures 6.4 and 6.5). The first property to be discussed is f_{gauche}, the fraction of gauche defects. Figure 6.4 shows the fraction of gauche defects at each dihedral angle along the chain backbone for the single component solvent systems (WAT, ACN, and MET) and Table 6.3 shows the shows the fraction of gauche defects averaged over all 15 backbone dihedral angles in all solvent systems. These data indicate there is little dependence of the dihedral angle on solvent composition, with system WAT having only slightly fewer gauche defects. A slightly fewer number of gauche defects for pure water as compared to pure acetonitrile or methanol was also observed by Pemberton and coworkers via Raman spectroscopic measurements [47, 48].

The conformation of the stationary phase chains can also be quantified by the orientation of the chain end-to-end vector through $\cos\theta_{\text{ete}}$. The cosine of this angle would be unity for chains perpendicular to the silica surface (aligned with the normal) and zero for chains parallel to the surface. The average value for $\cos\theta_{\text{ete}}$ in each solvent system is shown in Table 6.3. Unlike the fraction of gauche defects, the orientation of the end-to-end vector changes significantly with changes in solvent composition. In system WAT, the value of $\cos\theta_{\text{ete}}$ is 0.25 ($\theta_{\text{ete}} = 75°$) and it increases to 0.56 (56°) in system ACN and 0.53 (58°) in system MET. Thus, in going from a pure water to a pure

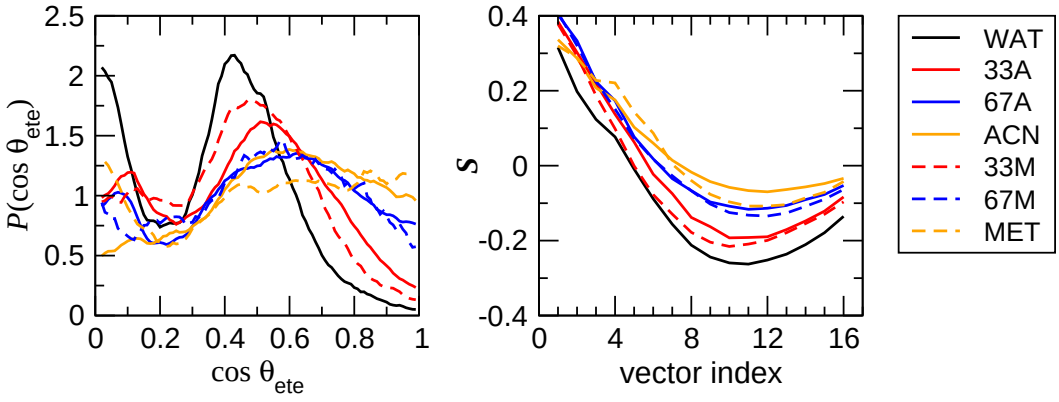

Figure 6.5: Probability distribution for the angle between the C_{18} end-to-end vectors and the silica surface normal (left) and the order parameter along the chain backbone (right).

organic mobile phase the end-to-end vector becomes aligned about 20° closer to the surface normal, indicating that the chains are aligned more away from the silica surface as organic concentration increases. This preference for chain alignment is slightly greater in the acetonitrile mixtures, perhaps the result of greater solvent partitioning into the stationary phase as compared to methanol mixtures with the same concentration.

In addition to the average value of $\cos\theta_{\text{ete}}$, it is important to examine the distribution of this angle (shown in Figure 6.5). For system WAT, the distribution is clearly bimodal with peaks in $\cos\theta_{\text{ete}}$ near values 0 and 0.4, corresponding to chains nearly parallel to the surface and chains with $\theta_{\text{ete}} = 66°$, respectively. This bimodal behavior also appears in the other solvent systems, but as the concentration of organic modifier is increased the height of the peak corresponding to nearly parallel chains decreases significantly. Furthermore, the peak corresponding to more extended chains becomes broadened and shifts to around $\cos\theta_{\text{ete}} = 0.6$ in the organic rich systems (67X and 100X). In these systems there is also a significant probability for chains nearly perpendicular to the silica surface ($\cos\theta_{\text{ete}}$ close to 1). It is interesting to note that, despite these differences in end-to-end orientation in the different solvents, there remains a somewhat broad distribution of chain alignments in all systems. There is no single conformation that dominates in any system and there remains a probability for both parallel and perpendicular

chains. These distributions only shift to a more perpendicular alignment as organic concentration is increased.

Information complimentary to the end-to-end orientation is the average end-to-end length of the alkyl chains (r_{ete}) and the height of the terminal methyl group above the silica surface ($z_{\mathrm{CH_3}}$), which are shown in Table 6.3. Like the fraction of gauche defects, the length of the alkyl chains changes very little when the mobile phase composition is changed. However, in correlation with $\cos\theta_{\mathrm{ete}}$, the height of the terminal methyl group steadily increases when the concentration of organic modifier is increased. It appears that the conformation of the individual chains (as measured through gauche defects and length) does not change to a significant extent when the solvent is changes, however, the alignment of the chains is greatly affected. With molecular simulation, Sun and coworkers have examined the conformation of an isolated C_{18} chain (not grafted to a surface) using the same set of solvents and force field as employed in this work [168]. Interestingly, for the isolated chain, the fraction of gauche defects decreased and end-to-end length increased, albeit to a fairly small extent, with increases in organic modifier concentration. Thus, chain solvation in the RPLC system elicits rather different effects on chain conformation.

Another property reported here, which gives additional and more local information on chain alignment, is the order parameter S for the 1–3 backbone vectors. As described in Chapter 5, this order parameter approaches unity for vectors preferentially aligned perpendicular to the surface, -0.5 for parallel vectors, and vanishes if there is no preferred orientation. Figure 6.5 shows the order parameter for each 1–3 vector along the chain backbone and Table 6.3 gives S_n, the value of the order parameter averaged over all 16 1–3 backbone vectors.

Like $\cos\theta_{\mathrm{ete}}$, S_n indicates the chains become aligned more perpendicular to the silica surface as the organic modifier concentration is increased. For system WAT, the value of S_n is -0.14, indicating parallel 1–3 vectors. The order parameter increases to values slightly greater than zero for systems ACN and MET, indicating 1–3 vectors with a slight perpendicular preference. Looking at the more local information for the order parameter along the chain backbone (Figure 6.5), one sees a similar trend for all seven solvent systems. The order parameter is large and positive for the first few backbone vectors and reaches a minimum somewhere near vector number 10. However, the curves are

shifted upward as acetonitrile or methanol concentration is increased. Comparing water/acetonitrile and water/methanol mixtures with the same organic concentration, one sees that curves for water/acetonitrile mixtures are shifted upward by a small amount indicating a slightly greater perpendicular alignment in these systems.

Beyond the conformation of the individual chains, another parameter used to described the stationary phase is the bonded phase thickness. One could characterize the bonded phase thickness in multiple ways, for example through the position of the GDS or the height of the terminal methyl group. The current data indicate that the position of the GDS changes very little upon changing solvent composition and is fairly constant at around $z = 15$ Å. In contrast, the height of the terminal methyl group increases from 9.1 Å in system WAT to 12.9 and 12.5 Å in systems ACN and MET, respectively. Different experimental studies have also sought to characterize this thickness, but these show diverging results. Kazakevich and coworkers interpreted a C_{18} bonded phase thickness of around 9 Å from low-temperature nitrogen adsorption measurements [45] while Sander and coworkers measured a thickness of 17±3 Å from neutron scattering experiments with chains in contact with a pure methanol solvent [164]. Assuming low-temperature nitrogen is a poor solvent for the chains, like water, the value of z_{CH_3} seems to agree with the data from Kazakevich and coworkers. However, the value of z_{GDS} is in agreement value reported by Sander and coworkers.

6.4 Conclusions

Simulations of a C_{18} stationary phase in contact with water/acetonitrile and water/methanol mixtures of varying organic modifier concentration indicate that changes in the solvation environment and structure of the stationary phase chains occur with changes in mobile phase composition. As the molfraction of organic modifier is increased, there is a marked increase in the degree of solvent penetration into the bonded phase. Water/acetonitrile mixtures show greater solvent penetration relative to water/methanol mixtures with the same organic molfraction. However, in either case, the primary species partitioned into the bonded phase is the organic modifier. In addition to partitioning into the bonded phase, the solvent is observed to adsorb at the silica surface. This is

most important for water and methanol, which interact strongly with the residual surface silanols, saturating nearly all of them. In contrast, acetonitrile has a much weaker interaction with the surface. In a pure acetonitrile solvent a very large fraction of the surface silanols would be available for interaction with solute molecules.

Interesting phenomena are also observed at the interface between the C_{18} chains and the solvent. In this interfacial region, there is a density depletion, or drying effect, especially for solvents with a high molfraction of water. For binary aqueous-organic solvents, there is an enhancement in the concentration of the organic component of the solvent at the interface. This enhancement is only slightly stronger for water/acetonitrile mixtures as compared to water/methanol mixtures.

Ordering of the C_{18} chains in the stationary phase is increased as the concentration of organic modifier is increased. The increased order is seen in parameters that relate to chain alignment ($\cos\theta_{\mathrm{ete}}$ and S_n), but parameters that relate to chain conformation (f_{gauche} and r_{ete}) are affected only to a small extent. Interestingly, spectroscopic techniques, such as Raman spectroscopy, typically measure conformational properties like gauche defect fractions. This study shows that parameters related to chain alignment are better indicators of chain ordering.

As far as mobile phase effects are concerned, solvent penetration into the stationary phase appears to be the largest factor contributing to increased chain order. With pure water, there is very little penetration of the solvent and the least amount chain alignment is observed. In the pure organic solvents, there is a much greater extent of solvent penetration and enhanced chain alignment is seen. In comparing to water/acetonitrile and water/methanol mixtures, slightly more penetration of the solvent is observed for the acetonitrile mixtures and this results in a mild increase in chain ordering. However, the differences between water/acetonitrile and water/methanol mixtures with the same organic modifier concentration are much smaller than differences incurred by changing organic modifier concentration. From these results, one can conclude that less polar solvents will penetrate further into the chain structure and produce more chain order. This conclusion is similar to the one reached by Pemberton and coworkers who carried out Raman spectroscopic measurements for a monomeric C_{18} stationary phase at a coverage of 3.09 $\mu\mathrm{mol}^2$ in contact with a wide range of solvents [47, 48].

Chapter 7

Mobile Phase Effects. II. The Solute Retention Mechanism

7.1 Background

As discussed in Chapter 1, a detailed, molecular-level, understanding of the retention mechanism in RPLC has eluded chemists for decades. It is, at present, unclear whether retention is better described by a partitioning process in which the solutes fully embed themselves into the bonded phase or if adsorption at the bonded phase/solvent interface is more important [11, 18, 22, 25, 40]. Furthermore, it is debated whether the thermodynamic driving forces for retention lie primarily in the hydrophobic interactions with the aqueous mobile phase [16, 17, 18] or in the lipophilic interactions with the stationary phase [11, 15]. The driving forces for retention were addressed in Chapter 4, using liquid hexadecane as a model stationary phase. This topic will be revisited here, with a more sophisticated and realistic model. The model will also allow additional aspects of the retention mechanism, such as adsorption versus partition, to be examined.

The problem of pinpointing the retention mechanism is further complicated by an incomplete understanding of the structure of the stationary phase chains and the interactions of these chains with the mobile phase solvent. Ordering in these grafted alkyl

† This chapter describes the outcome of a collaborative research project carried out by Jake L. Rafferty, Ling Zhang and Li Sun and advised by J. Ilja Siepmann and Mark. R. Schure. Reports on portions of this research project have been published [71] and/or submitted [78].

chains may have important implications for retention because, even if one assumes that partitioning is the dominant retention mechanism, it is questioned, as with partitioning into lipid bilayers, whether the process can be modeled faithfully by bulk oil–water partitioning [11, 15] or if partitioning into the at least partially ordered chains in the stationary phase involves a distinctly different mechanism [19, 20]. In addition, it is well known that the stationary phase is preferentially solvated by the organic component of the mobile phase, but it is not completely clear whether this solvation occurs primarily by the formation of an organic layer atop the stationary phase chains [45, 46] or through penetration of the organic modifier into the stationary phase [47, 48]. In the former case, retention could be affected by partitioning of the solutes into this organic layer, and in the latter case, solutes may compete with solvent molecules for space inside the stationary phase. Furthermore, changes in the extent of solvation of the stationary phase with changing mobile phase composition may effect the conformation of the alkyl chains. These effects where characterized through the use of molecular simulation in the previous chapter. Specifically, it was demonstrated that preferential solvation by the organic modifier occurs both atop and within the stationary phase and is slightly greater for water/acetonitrile as compared to water/methanol mixtures. Additionally, the stationary phase was shown to be more ordered in less polar solvents due to the increased solvent penetration in these systems. Here, it will be examined if these solvent effects have any influence on the solute retention mechanism.

To fully understand the retention process more detailed, molecular-level information with chemical specificity is needed. However, there is great difficulty associated with obtaining this molecular-level information from experimental observations. For example, retention data, which by nature are thermodynamic measurements, cannot yield a molecular picture of retention, but may only be used to infer such details. Furthermore, spectroscopic studies [26, 30, 34, 48], which can indeed give more detailed insight than thermodynamic measurements, are hampered by the inability to observe the precise configuration of a single solute molecule in the RPLC system and require the analysis of a complex distribution of solute configurations. For these reasons, this work has chosen to employ an efficient Monte Carlo simulation approach to study the retention mechanism in a typical RPLC system. Specifically, the distribution of small alkane and alcohol solutes in a system containing a realistic C_{18} stationary phase in

contact with aqueous-organic solvents (water/acetonitrile and water/methanol) ranging in composition from pure water to pure organic modifier.

The effects of organic modifier type and concentration on the retention mechanism in RPLC is an important topic because selectivity in RPLC is most often optimized by adjusting the composition of the mobile phase. It has been suggested that the mechanism of retention changes when different organic modifiers are used, adsorption for water/acetonitrile and possibly partitioning for water/methanol mixtures [22]. Furthermore, the thermodynamics of the retention process are different depending on whether water/methanol or water/acetonitrile is used [15, 125, 126, 127, 169]. It is thought that this may result from acetonitrile's greater affinity to aggregate around the solutes as compared to methanol [125, 126, 127] or from acetonitrile penetrating into the stationary phase to a larger extent than methanol [169]. The solvation environment of alkane and alcohol solutes in water/acetonitrile and water/methanol mobile phases was analyzed in Chapter 4. It was shown that acetonitrile preferentially solvates the nonpolar methylene group to a larger extent than methanol and suggested that this may contribute to the smaller methylene increment when acetonitrile mixtures are used in RPLC. Here, it will be examined if penetration of acetonitrile into stationary phase also has an effect on the methylene increment. Details on these simulations were given in the previous chapter, so the present chapter will immediately proceed with a discussion of the simulation results.

7.2 Results and Discussion

To access the mechanism of solute retention one needs to know, with high resolution, the preferred locations of the solute within the stationary phase. The simulations described here are able to directly yield this type of data. Figure 7.1 shows the z-dependent distribution coefficient profiles, or $K(z)$, for n-butane and 1-propanol in the seven different mobile phase systems. The technique for computing these profiles was described in Chapter 5, but it should be noted here that these profiles are analogous to the (experimentally measurable) distribution coefficient for transfer from mobile to stationary phase (equation 1.2), but offer much more detailed information on where retention occurs within the stationary phase. I.e., larger values of $K(z)$ correspond to more favorable

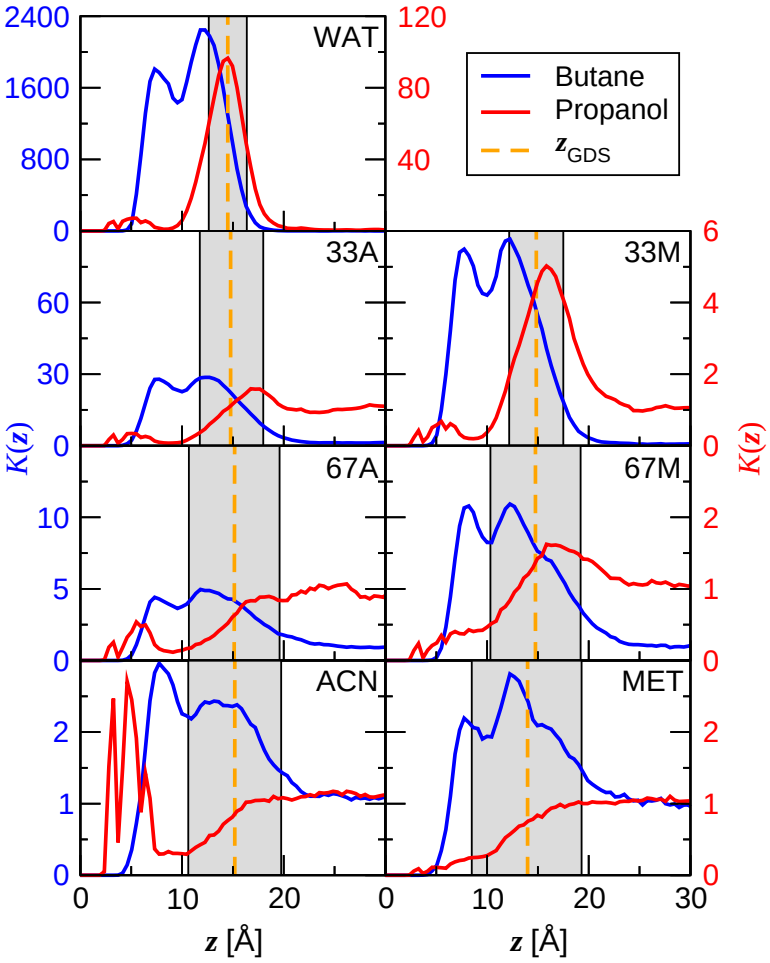

Figure 7.1: Distribution coefficient profiles for butane and propanol in systems with different mobile phase compositions.

(lower free energy) locations of the solute within the stationary phase. One of the most striking results concerning solute retention is the large dependence of the solute distribution coefficient on z. With the spatial resolution afforded by the simulations, it is clearly evident that the stationary phase is not a homogeneous medium into which solutes partition, but a heterogeneous medium with multiple preferred regions.

For butane, the $K(z)$ profiles show a bimodal distribution in all seven solvent compositions. There is one peak in the center of the bonded phase ($z \approx 8$ Å) and another in

the interfacial region, but inside the GDS (located at around $z = 15$ Å in all systems). The peak in the center of the bonded phase remains rather sharp regardless of solvent composition. However, the shape of the peak in the interfacial region is influenced by solvent composition, broadening as the fraction of organic modifier is increased. The broadening of this interfacial peak coincides with increasing width of the interfacial region. From this it is apparent that even a simple nonpolar solute has multiple modes of sorption. It can either partition deep into the bonded phase or adsorb at the surface of the hydrocarbon/solvent interface.

The preference of *n*-butane to reside in the interfacial region is not entirely surprising since a density depletion is observed in this region (see Figure 6.2) and this would lead to a lower entropic cost of cavity formation. However, the peak deeper in the bonded phase is in a region where the overall system density is significantly higher. Analysis of the bonded-phase structure shows that it is much more ordered in this region, so there may be more free volume of appropriate size and shape for the solute here (Figure 6.5). Sander and co-workers have recently reviewed the important role that partial ordering of the alkyl stationary phase may play for retention [26]. Free energy minima at the location where the C_{18} density reaches a bulk-like value ($z \approx 13$ Å) and another deeper in the bonded phase were also observed for a methane analyte in molecular dynamics simulations by Klatte and Beck [51], but not by Slusher and Mountain for a C_8 bonded phase [58].

When comparing the water/acetonitrile and water/methanol mixtures with the same organic molfraction, the general shape of the $K(z)$ profiles for butane are very similar, although the magnitude of $K(z)$ is larger for the water/methanol mixtures. The free energy of transfer from mobile phase to vapor phase is more favorable for butane with water/methanol mixtures than with water/acetonitrile mixtures (see Table 4.4). Thus, the difference in the magnitude of $K(z)$ stems mainly from a mobile phase contribution and not from changes in the stationary phase. From this it can be concluded that the retention mechanism of this nonpolar solute does not change for any of the solvent mixtures examined here and remains a mixed partition/adsorption mechanism.

A retention mechanism differing from that of butane is observed for the polar solute, propanol, and this retention mechanism appears to be somewhat dependent on the mobile phase composition. In system WAT, propanol exhibits a distinct preference

to reside in the interfacial region with a peak centered directly on the GDS (but the peak height is much lower than for *n*-butane). This preference clearly diminishes as the organic molfraction is increased and propanol becomes more soluble in the solvent. Interestingly, and this is most apparent when going from system WAT to 33M or 33A, the center of the peak in $K(z)$ shifts to larger z, from directly under the GDS to the solvent side of the interfacial region. This is likely caused by the interfacial enrichment of the organic component of the solvent.

Additional, but much smaller peaks in the $K(z)$ profile of propanol are observed in the $z = 3$–7 Å region of system WAT. These are due to hydrogen bonding of propanol molecules directly to residual surface silanols and to solvent molecules which are bound to the substrate (this is discussed further below). Interestingly these peaks become much stronger as acetonitrile concentration is increased, but not as methanol concentration is increased. This is related to the availability of the surface silanols for hydrogen bonding. These silanols are nearly saturated in water/methanol mixtures, but almost freely available in a pure acetonitrile mobile phase (see Table 6.2). Note that it is very improbable for the alkane solute to be found at a position less than $z = 5$ Å, or about where the dimethyl side chains of the -$Si(CH_3)_2C_{18}H_{37}$ alkylsilane groups are located, since this region is very crowded. However, the polar alcohol can partially compensate for the entropic cost of cavity formation in this region by hydrogen bonding to the substrate or substrate bound solvent molecules.

In addition to describing where the solutes are retained through the $K(z)$ profiles, it is important for a detailed understanding of the retention process, to examine the orientational preferences of the solutes within the stationary phase and interfacial region. For this reason, the z-dependent S profiles for butane and $\cos\theta_{\mathrm{ete}}$ profiles for propanol are shown in Figure 7.2. As defined in Chapter 5, S will approach unity for butane molecules aligned perpendicular to the silica surface, -0.5 for alignment parallel to the surface, and vanish if there is no preferred alignment. The end-to-end vector of propanol originates at the methyl group and terminates at the hydroxyl hydrogen. Thus, $\cos\theta_{\mathrm{ete}}$ will be positive for hydroxyl groups pointing away from the silica surface, negative for hydroxyl groups directed towards the surface and vanish if there is no preferred direction for the hydroxyl group.

The $S(z)$ profiles for butane show that this solute has some definite orientational

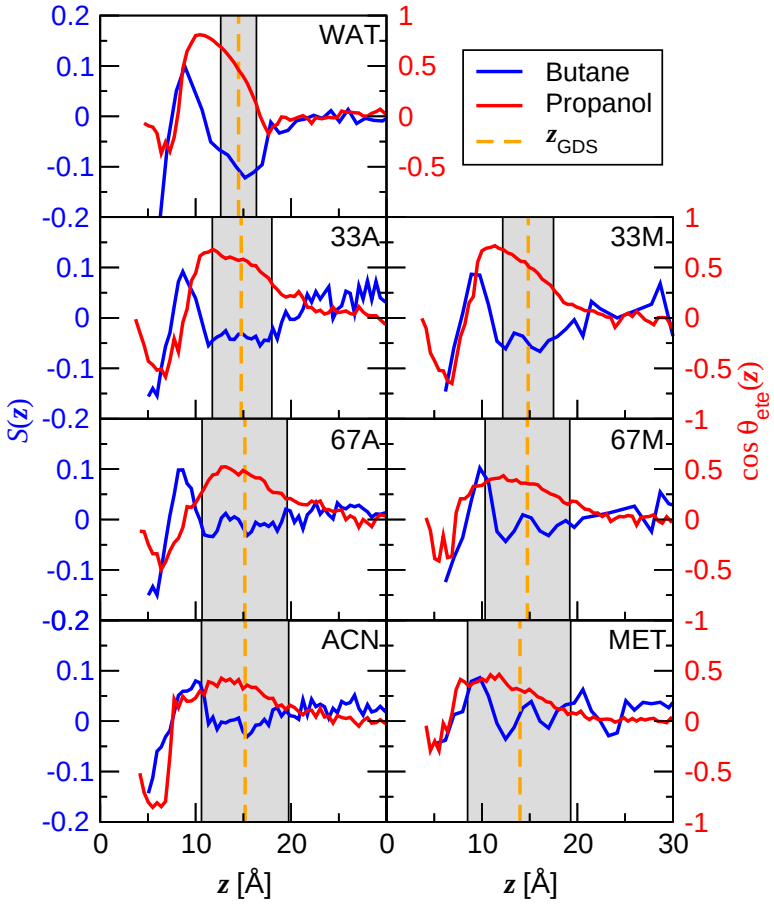

Figure 7.2: Order parameter profiles for butane and end-to-end vector orientation profiles for propanol in systems with different mobile phase compositions.

preferences in stationary phase and interfacial region, although these preferences are not extremely strong. In the interfacial region the butane molecule prefers to lie parallel to the interface, seeming consistent with interfacial adsorption. However, this preference appears to diminish as the organic molfraction is increased. In the purely aqueous mobile phase, the solute may be driven against the interface due to hydrophobic interactions, but as the organic concentration increases these hydrophobic interactions vanish. In the center of the bonded phase, butane changes it orientational preference to perpendicular with a peak in $S(z)$ at around $z = 8$ Å. This peak occurs at the same position as the peak

in the $K(z)$ profile that was attributed to partitioning. Clearly, given the perpendicular orientational preference of butane, this partitioning does not resemble bulk liquid–liquid partitioning where one would see no orientational preference. Moving further into the bonded phase, $S(z)$ values become negative at around $z = 6$ Å, indicating a parallel preference. It appears that the butane solute lies flat as it encounters that "wall" created by the dimethyl side chains. The $S(z)$ profiles for butane look very similar regardless of whether a water/acetonitrile or water/methanol mixture is used, again suggesting that the retention mechanism is the same in these solvent systems.

Propanol exhibits stronger orientational preferences than butane. In the interfacial region, the $\cos\theta_{\mathrm{ete}}(z)$ profiles indicate that this solute has a preference to direct its hydroxyl group towards mobile phase and its alkyl tail towards the stationary phase. In this manner the solute can hydrogen bond with the solvent while its nonpolar tail is solvated by the hydrocarbon stationary phase. The magnitude of the interfacial peak in $\cos\theta_{\mathrm{ete}}(z)$ decreases as the molfraction of the organic modifier is increased but does not appear to be influenced by whether the organic modifier is acetonitrile or methanol. Moving through the bonded phase to near the silica surface, $\cos\theta_{\mathrm{ete}}(z)$ shifts from positive to negative values, thus indicating that the polar hydroxyl group is directed towards the silica surface. In this manner, the propanol solute can form hydrogen bonds with the surface silanols. This preference is weakest in system WAT, where the silanols are mostly saturated, but very strong in system ACN, where the silanols are mostly unsaturated.

Important insight on the contribution of polar and non-polar groups to the thermodynamics of retention and validation of the simulation results can be gleaned from the incremental free energies of transfer for methylene and hydroxyl groups, $\Delta G_{\mathrm{CH_2}}$ and ΔG_{OH}. These two quantities, which were described in Chapter 5, are plotted as a function of z in Figure 7.3. As can be seen from the profiles, the incremental free energies show a strong dependence on z in the model RPLC system. $\Delta G_{\mathrm{CH_2}}$ is most favorable at $z \approx 9$ Å, i.e., in the interior of the stationary phase, and its magnitude decreases as the organic molfraction is increased. The general shape of the profile does not depend on whether acetonitrile or methanol is present. However, the profiles for systems 33M and 67M lie slightly below the ones for systems 33A and 67A, while the profile for system MET is just above the one for system ACN. These differences are mainly due to the

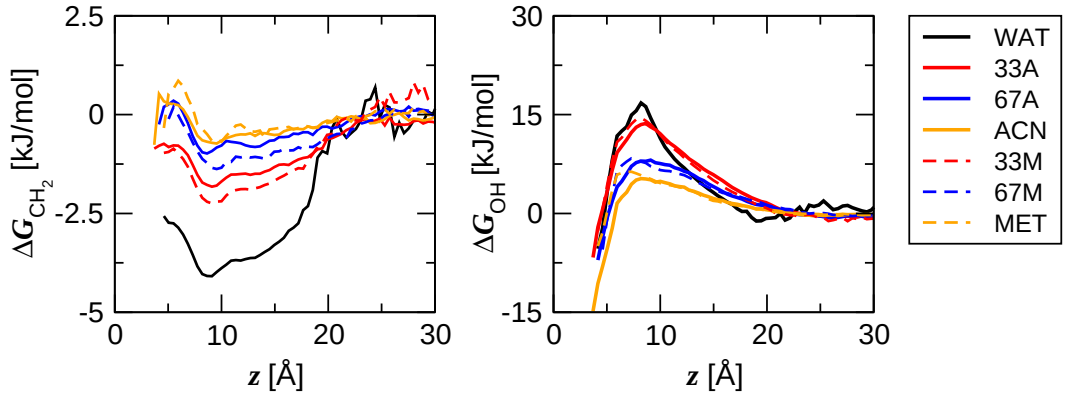

Figure 7.3: Incremental retention free energy profiles for the methylene (left) and hydroxyl (right) groups in systems with different mobile phase compositions.

mobile phase contribution to the free energy of retention (see Table 4.4). In contrast, ΔG_{OH} shows a maximum at $z \approx 9$ Å that is large in magnitude compared to $\Delta G_{\mathrm{CH_2}}$. ΔG_{OH} is favorable at $z \approx 5$ Å, where the OH group can hydrogen bond to residual silanols or substrate-bound solvent molecules. ΔG_{OH} is most favorable in system ACN, due the most favorable mobile phase contribution (Table 4.4) and silanol accessibility.

In addition to calculating the incremental free energies of retention as a function of z, they may also be calculated as a net free energy of retention for the entire stationary phase (as described in Chapter 5). This is useful because these net free energies of retention may be directly compared to experimental retention data. This comparison is made in the free energy level diagram shown in Figure 7.4. By assigning the vapor phase as the zero on the free energy scale, this diagram also depicts the mobile and stationary phase contributions to the free energy of retention (see Figure 4.1) for the realistic model RPLC system described in this chapter (labeled ODS) and for the model hexadecane system described in Chapter 4 (labeled C16). The experimental retention data in this figure comes from careful studies by Alvarez-Zepeda (for water/acetonitrile mixtures) [170] and Barman (for water/methanol mixtures) [171] and is for stationary phases very similar to the one modeled here. The experimental data for hexadecane partitioning is from the work of Ranatunga and Carr [15].

First it is noted that the calculated values of $\Delta G_{\mathrm{CH_2}}$ are in excellent agreement with

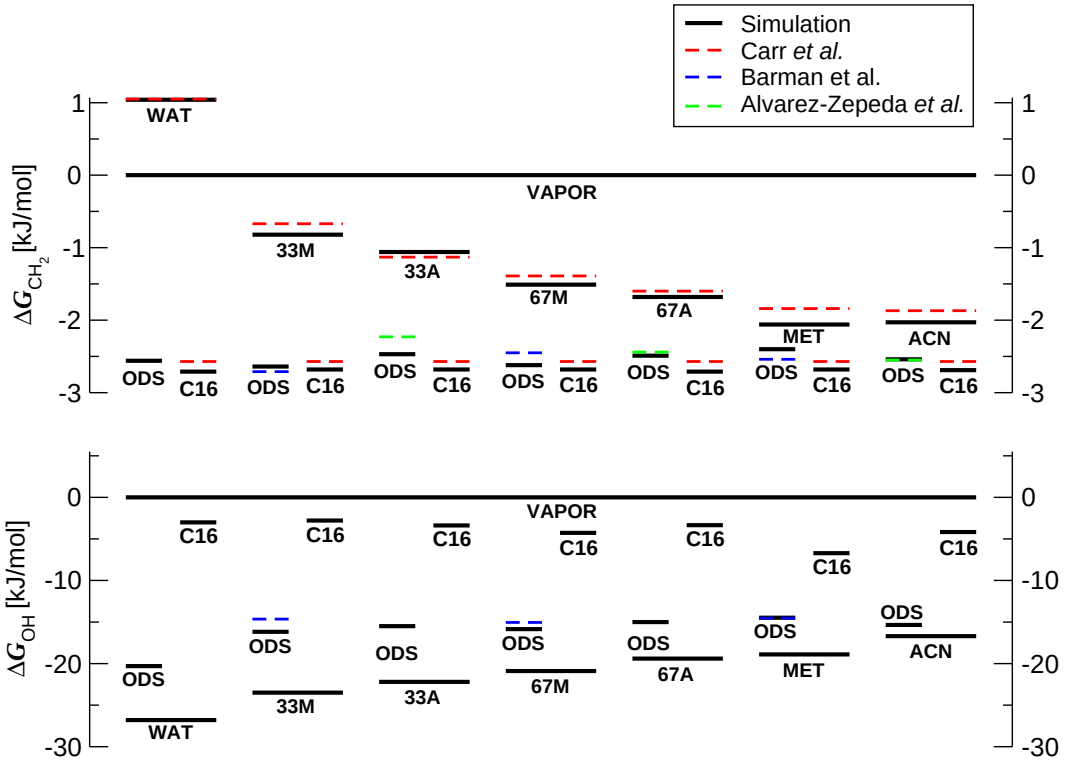

Figure 7.4: Incremental free energy level diagrams for the methylene (top) and hydroxyl (bottom) groups. Solid lines indicate values calculated from simulation while dashed lines correspond to experimental values [15, 170, 171]

experiment (compare the solid and dashed lines above the ODS label in Figure 7.4). The largest deviation observed is around 0.2 kJ/mol, an very small value in terms of free energy, and in many cases the deviation is even smaller. Simulation data for the methylene increment in the hexadecane model system also agree very well with experiment, as discussed in Chapter 4. Reliable retention data for the hydroxyl increment were only available for water/methanol mixtures, but agreement with this data is also very good. The fact that the simulations are able to reproduce the thermodynamics of the retention process, as measured experimentally, provides good confidence that the molecular details observed in simulations are indeed correct.

The free energy diagram also allows for a revisiting of the discussion about the

driving forces for retention and for a comparison of retention in RPLC to bulk liquid–liquid partitioning (i.e., hexadecane partitioning). As noted in Chapter 4, the mobile to vapor phase transfer (or mobile phase contribution to retention) for the methylene group is favorable only in system WAT. Thus, solvophobic forces [16, 17, 18] are not important for retention unless highly aqueous mobile phases are used. The free energy of transfer from the vapor phase to the ODS stationary phase (or stationary phase contribution to retention) is always favorable and greater in magnitude than the mobile contribution in all solvent systems examined. This is in agreement with the lipophilic view of Carr and coworkers [11, 12, 15]. The free energy level of the ODS phase changes little with changing solvent composition suggesting that solvent penetration into the stationary phase has little effect for nonpolar groups.

Comparing the ODS phase to the hexadecane phase, one sees that they are very similar in terms of free energy. This similarity has been used to suggest that the retention mechanism in RPLC resembles bulk liquid–liquid partitioning [12, 40]. The current work shows this conclusion is not valid and this comparison should not be made when accessing the molecular mechanism of retention. The profiles in Figures 7.1 and 7.3 clearly indicate that nonpolar solutes can either partition into the stationary phase or adsorb at the surface. Additionally, the free energy of retention for the methylene group in the interfacial region (where adsorption occurs) is slightly smaller, but very similar to the free energy in the center of the bonded phase (where partitioning occurs). Thus, thermodynamics cannot easily distinguish these two processes. This is an excellent example of why great caution should be used when inferring molecular details from thermodynamic data.

The polar hydroxyl group shows a very unfavorable transfer from mobile to vapor phase (or mobile phase contribution), but this free energy penalty decreases as the fraction of organic modifier is increased. Like the methylene group, the transfer from the vapor phase to the ODS phase (stationary phase contribution) is favorable for the hydroxyl group. However, the stationary phase contribution becomes less favorable as the fraction of organic modifier is increased. Comparing the ODS phase to the hexadecane phase, one observes that the ODS phase lies significantly lower in free energy than the hexadecane phase. This was observed experimentally by Carr and coworkers for other polar groups [12]. The authors of this work attribute these differences to

Table 7.1: Number of hydrogen bonds per alcohol solute molecule in the ODS, mobile, and bulk n-hexadecane phases.[a,b]

System	N^{c}_{SiOH}	N^{d}_{in}	N^{e}_{out}	N^{f}_{total}	N^{g}_{mob}	$N^{h}_{C_{16}}$
WAT	0.12_4	0.43_6	1.62_7	2.17_5	2.42_1	0.06_2
33A	0.16_2	0.81_2	0.84_3	1.81_5	1.46_2	0.12_1
67A	0.28_3	0.62_1	0.68_2	1.58_1	1.35_1	0.13_1
ACN	0.82_7	0.28_1	0.27_2	1.37_4	0.66_2	0.18_1
33M	0.08_2	0.41_3	1.48_2	1.97_2	2.17_2	0.30_8
67M	0.09_2	0.57_5	1.24_5	1.90_3	2.01_1	0.9_1
MET	0.07_1	0.41_1	1.34_2	1.82_1	1.83_1	1.33_7

[a]A solute is defined to be in the ODS phase when it is inside the first solvation shell (6 Å) of any stationary phase CH_x segment.
[b]Subscripts indicate the statistical uncertainty in the final digit.
[c]Average number (per alcohol solute molecule) of hydrogen bonds with silanol groups.
[d]Average number of hydrogen bonds with solvent molecules inside the GDS.
[e]Average number of hydrogen bonds with solvent molecules outside the GDS.
[f]Total number of hydrogen bonds in the ODS stationary phase.
[g]Total number of hydrogen bonds in the bulk mobile phase.
[i]Total number of hydrogen bonds in a bulk n-hexadecane phase that is in contact with the mobile phase (from simulations described in Chapter 4).

three possible reasons: (1) hydrogen bonding of polar solutes with the silanols, (2) polar solutes residing at the ODS–mobile phase interface, and (3) polar solutes being preferentially solvated by solvent which is sorbed into the bonded phase [12]. It is also interesting to note that an increase in the organic modifier concentration makes the ODS phase less favorable for hydroxyl groups, whereas it makes a bulk n-hexadecane phase in contact with the same mobile phase more favorable for hydroxyl groups. These trends can be explained by a hydrogen-bond analysis for the alcohol solutes (see Table 7.1).

The number of hydrogen bonds per alcohol solute is found to decrease with increasing organic modifier concentration in the ODS phase, while it increases in the n-hexadecane phase because of swelling by methanol or acetonitrile. Furthermore, the number of hydrogen bonds in the ODS phase exceeds that for the corresponding n-hexadecane phase by factors of anywhere from 36.2 in system WAT to 1.5 in system MET, thereby explaining the differences in free energies between the two retentive phases. For the ODS phase, the total number of hydrogen bonds for the alcohol solute is slightly smaller in

the acetonitrile containing systems as compared to the methanol containing systems, thus explaining why the ODS phase in these systems lies slightly higher in free energy. Additionally, the distribution of hydrogen bonds is quite different between the different solvent systems. The simulation data demonstrate that for pure water, pure methanol, or water/methanol mixtures hydrogen-bonding to solvent molecules outside the GDS (i.e., solvent molecules that are located at the interface) is most important, followed by hydrogen bonding to sorbed solvent, and that the formation of direct hydrogen bonds to residual silanols is least important. The situation is quite different for water/acetonitrile mixtures where hydrogen bonding to the surface silanols becomes more important, but only outweighing hydrogen bonds with solvent in pure acetonitrile. In all acetonitrile containing systems the number of hydrogen bonds with sorbed solvent is comparable to the number of hydrogen bonds with solvent outside the GDS. These differences between water/acetonitrile and water/methanol mixtures are the result of greater solvent partitioning and silanol availability in the acetonitrile containing systems.

7.3 Conclusions

The most important observation from this simulation study is that the bonded phase does not participate in the retention process as a homogeneous phase. For the alkane solute there clearly exists multiple sorption sites, including the center of the bonded phase and the interfacial region. The existence of sorption site(s) near the interface and the observation that the solute prefers to lie flat in this region suggests that adsorption plays an important role in the retention of this solute. This is in contrast to generally accepted view that the retention of small non-polar solutes is dominated by partitioning [7, 11, 36, 40, 43]. The second sorption site for *n*-butane is in the center of the bonded phase, but this region differs from an isotropic alkane phase. Although the molecular-level details are distinctly different, the overall thermodynamics of the RPLC retention process for small nonpolar molecules, as indicated by $\Delta G_{\mathrm{CH_2}}$, are similar to bulk oil–water partitioning. The thermodynamic driving force for the retention of the non-polar methylene segment is its *lipophilic* interaction with the bonded phase that is nearly three times larger in magnitude than the unfavorable interaction with a neat

water mobile phase. Furthermore, the thermodynamic interaction of the methylene segment with water/acetonitrile and water/methanol mobile phases containing more than 33% molfraction organic modifier is favorable, i.e., *solvophilic*. The mechanism of retention for the nonpolar solutes examined here did not show significant dependence on whether acetonitrile or methanol were used as the organic modifier. Free energies of retention are slightly more favorable in water/methanol mixtures, but this is a mobile phase property and not due to modification of the stationary phase or interfacial region by the mobile phase solvent.

In contrast to *n*-butane, 1-propanol shows a much more distinct preference to reside in the interfacial region and does not partition into the center of the bonded phase. This implies that adsorption in the interfacial region is the most important factor in the retention of this small polar solute. This is in agreement with Martire and Boehm who assert that interfacial adsorption may be of importance for small, polar solutes [36]. In addition to this large contribution from interfacial adsorption, the retention of this alcohol is influenced by its interactions with sorbed solvent molecules and surface silanols. The interaction with surface silanols becomes very important in acetonitrile rich mixtures where the surface silanols are largely unsaturated. Furthermore, it is observed that the stationary phase in the model RPLC system is drastically different from bulk *n*-hexadecane for the polar solute. The fact that the thermodynamics of RPLC retention for polar solutes may not be well-modeled by *n*-hexadecane partitioning has been suggested by Carr and coworkers [11]. Overall, the most important contribution to the distribution of the polar hydroxyl group is its *solvophilic* interaction with the mobile phase that is larger in magnitude than its favorable interaction with the bonded phase.

The data gathered from these simulations provides a new level of insight into the retention process in RPLC. Indeed, some of the commonly held notions about retention have been challenged but it is hoped that the results presented here lead to a more complete understanding of the retention process and improve the field of analytical separation science. Having established the quantitative nature of the methods employed here (as demonstrated by the agreement with experimental retention data), this study was extended to address additional issues in RPLC. The following chapters in this thesis will examine the influence of stationary phase properties (surface coverage, chain length, and chemistry), pressure, pore shape, and analyte size on structure and retention.

Chapter 8

Influence of Surface Coverage. I. Effects on Chain Conformation and Interfacial Properties

8.1 Background

The surface coverage, or bonding density, of alkylsilane chains on the silica surface is one important chromatographic parameter that can be adjusted in order to achieve the desired efficiency in a chromatographic separation. The density of bonding sites (surface silanols) on silica surfaces typically used in RPLC is taken to be around 8.1 μmol/m^2, but, in general, the practical limit of chain bonding density is around half of this for monomeric stationary phases [137, 172] and coverages below this limit are often used. This chapter describes a molecular simulation study that probes the effects of surface coverage by examining stationary phases with bonding densities ranging from 1.6 to 4.2 μmol/m^2. A detailed discussion on the structure of these stationary phases, their interfaces with the mobile phase solvent, and solute retention will be given. However, before commencing with this discussion, a brief overview of previous studies relevant to the current work will be given.

[†] This chapter describes the outcome of a collaborative research project carried out by Jake L. Rafferty and advised by J. Ilja Siepmann and Mark. R. Schure. A report on this research project has been published [72].

8.1.1 Experimental Studies of Bonding Density

There are two principal means of studying the effects of bonding density via experiment. The first is to measure differences in the retentive behavior among a series of solutes on stationary phases with different bonding densities. From this data, which is thermodynamically based, one may infer molecular details that are consistent. The second method is to utilize spectroscopic techniques that more directly probe the stationary phase or a molecule that interacts with the stationary phase.

Retention Measurements

Many experimental studies have shown that the retention of a variety of solutes increases as bonding density is increased [7, 9, 14, 25, 173, 174, 175, 176, 177], however, at a certain bonding density retention may begin to level off or even decrease [7, 25, 174, 177]. In terms of stationary phase and interfacial structure, this retentive behavior has been interpreted in a variety of ways. To rationalize the initial increase in retention, Kikta and Grushka speculated that more of the organic component of the mobile phase, into which the solutes can partition, is adsorbed onto the alkyl surface as the density is increased [173]. In contrast, Tan and Carr explain the increase by assuming that, at lower densities, the chains are collapsed upon the silica surface forming a film too thin for solutes to partition into [14]. At higher densities the phase is thick enough to resemble a more liquid-like medium that solutes can partition into. To explain the drop in retention at high densities, Sentell and Dorsey have suggested that the solutes are entropically expelled due to packing constraints in the stationary phase chains [7]. In addition to just general increases/decreases in retention, various studies have shown that increases in grafting density lead to an increase in shape selectivity [8, 178, 179]. Many overviews on the topic of shape selectivity have been given [26, 179, 180] and these suggest that any parameter that increases alkyl conformational order will also increase shape selectivity.

In addition to making retention measurements on solutes, they can be made on components of the mobile phase itself. Gritti, Kazakevich, and Guiochon have taken advantage of this in order to generate the excess adsorption isotherms of several organic modifiers from water on stationary phases with various grafting densities [46]. This study showed that under most conditions there is a positive excess of the organic

component adsorbed onto the stationary phase and that the excess is larger for more nonpolar solvents. Assuming that all of this excess adsorbate resides at the surface of the alkyl phase and forms a single component phase they found that the width of the adsorbed organic layer increases as grafting density is increased. It should be mentioned that present work indicates these assumptions are not entirely correct (see Chapter 6).

Spectroscopic Techniques

A number of spectroscopic studies have set out to examine the effects of bonding density in RPLC systems. In this respect, a wide variety of techniques including, electron pair resonance (EPR) [181], fluorescence [30, 149], NMR [149], and Raman [48, 155, 157, 158] spectrometry have been applied.

The EPR technique allowed Wright and coworkers to monitor probe solutes within stationary phases with grafting densities from 1.74 to 3.48 μmol/m^2 [181]. Here, they found that the probe molecules see a less polar environment as the grafting density is increased. This was attributed to a decrease in the amount of methanol penetrated into the bonded phase. It was also observed that the rotational anisotropy of the probe molecules increased with increasing surface coverage. It was suggested this resulted from an increase in alkyl chain ordering.

Pursch and coworkers analyzed polymeric C_{22} stationary phases with grafting densities from 3.6 to 7.0 μmol/m^2 with NMR and fluorescence spectroscopies [149]. The NMR data showed that the number of gauche defects decreases with increasing density and that above 4.0 μmol/m^2 the chains are predominantly in the trans conformation. Using fluorescence spectroscopy they were able to track the probe molecule 1,6-diphenylhexatriene. They found a maximum in solute partitioning into the bonded phase at 4.9 μmol/m^2 and that the mobility of the probe solute was minimized at this coverage.

Raman spectroscopy has been used by Doyle and coworkers to examine monomeric C_{18} stationary phases with coverages of 2.34 and 3.52 μmol/m^2 [157, 158] and also by Ducey and coworkers to probe both monomeric and polymeric phases with coverages ranging from 3.09 to 6.45 μmol/m^2 [48, 155]. The spectral data from Doyle and coworkers suggests that there are only small structural differences between the 2.34 and 3.52 μmol/m^2 coverages, with the higher density phase being slightly more ordered.

Ducey and coworkers found an increase in alkyl chain ordering with increasing chain density. This increase in order is most dramatic at the lowest temperature studied, 258 K. There are much smaller differences in alkyl chain order at 333 K, a temperature close to the one used in this study.

8.1.2 Previous Simulations of the Effects of Bonding density

As mentioned in Chapter 1, numerous molecular dynamics simulations of model RPLC systems have been carried out. However, only a handful of these have examined the effects of the octadecyl phase's bonding density [50, 56, 59, 61], and none of these studied the chains under RPLC conditions, rather the chains were simulated without the presence of solvent (i.e., in vacuum). In general, these studies indicate an increase in the order of the alkyl phase as the density is increased.

Upon increasing surface coverage from 1.64 to 3.69 μmol/m^2 in MD simulations, Yarovsky and Hearn reported a dramatic increase in thickness of the alkyl phase, an extension of the chains, a small decrease in gauche defects, and a decrease in the accessible area of the silica surface [56]. Using MD simulations for a different force field, Klatte and Beck also found an increase in chain alignment perpendicular to the surface upon increasing the surface coverage [50]. Lippa, Sander, and Mountain, who examined monomeric C_{18} phases from 1.71 to 4.97 μmol/m^2, noted a similar change in stationary phase thickness but a much larger decrease in gauche defects and chains standing nearly perpendicular to the surface at the highest coverage [59]. Unfortunately, since these previous simulation studies investigating coverage effects were carried out in the absence of solvent, the results cannot be compared directly to the current work.

8.2 Simulation Details

To examine the effects of surface coverage, configurational-bias Monte Carlo simulations in the NpT version of the Gibbs ensemble were carried out using the three-box slit pore setup and force field described in Chapter 5. This was accomplished by carrying out simulations for five different surface coverages, namely 1.60, 2.24, 2.88, 3.52, and 4.15 μmol/m^2. In contact with the stationary phase was a methanol/water solvent at a methanol molfraction of 0.5 (about 0.65 volume fraction). The simulations were

Table 8.1: Average number of solvent and solute molecules in each simulation box at the five surface coverages examined.[a,b]

		N_{water}			N_{methanol}	
Coverage	Box 1	Box 2	Box 3	Box 1	Box 2	Box 3
1.6 μmol/m^2	282_5	215_5	3.9_2	292_1	200_1	8.4_5
2.3 μmol/m^2	247_2	249_2	4.2_4	268_1	223_1	8.6_9
2.9 μmol/m^2	227_2	270_2	3.1_1	241_1	252_1	7.0_3
3.5 μmol/m^2	202_3	295_4	3.7_2	222_1	270_2	7.7_5
4.2 μmol/m^2	179_4	318_4	3.8_2	201_2	291_3	8.2_6
		N_{alkane}			N_{alcohol}	
Coverage	Box 1	Box 2	Box 3	Box 1	Box 2	Box 3
1.6 μmol/m^2	2.40_3	1.95_3	3.64_4	2.29_3	1.17_1	2.53_4
2.3 μmol/m^2	2.72_4	1.54_2	3.74_5	2.32_4	1.24_2	2.44_6
2.9 μmol/m^2	3.92_3	2.14_1	1.93_2	2.28_2	1.56_1	2.16_3
3.5 μmol/m^2	2.54_3	1.87_2	3.58_3	2.10_2	1.58_2	2.32_4
4.2 μmol/m^2	2.64_2	1.78_2	3.57_3	1.91_2	1.68_3	2.40_5

[a]Subscripts indicate the statistical uncertainty in the final digit.
[b]Box 1, 2, and 3 refer to the box containing the stationary phase, the bulk mobile phase box, and the ideal vapor box, respectively.

performed at a temperature of 323 K and a pressure of 1 atm.

A total of 500 water and 500 methanol molecules were used in all simulations. The average numbers of solvent molecules found in each box during the production period of the simulation are summarized in Table 1. As one can see, the actual composition of the mobile phase (box 2) is close to 48% methanol for all five coverages. Also present in each system, but constrained to the vapor phase because of their low solubility, are 10 helium atoms that help to maintain a vapor box of an adequate size. In addition, these systems contain 14 solute molecules (two each for methane to *n*-butane and ethanol to 1-butanol) that allow for an exploration of the retention mechanism (to be discussed in Chapter 9). To keep from overloading the stationary phase with too many of these solutes and possibly altering its structure, additional bias potentials were applied in each box for the different solutes. The resulting average numbers of solute molecules found in each box during the production period of the simulation are also shown in Table 8.1.

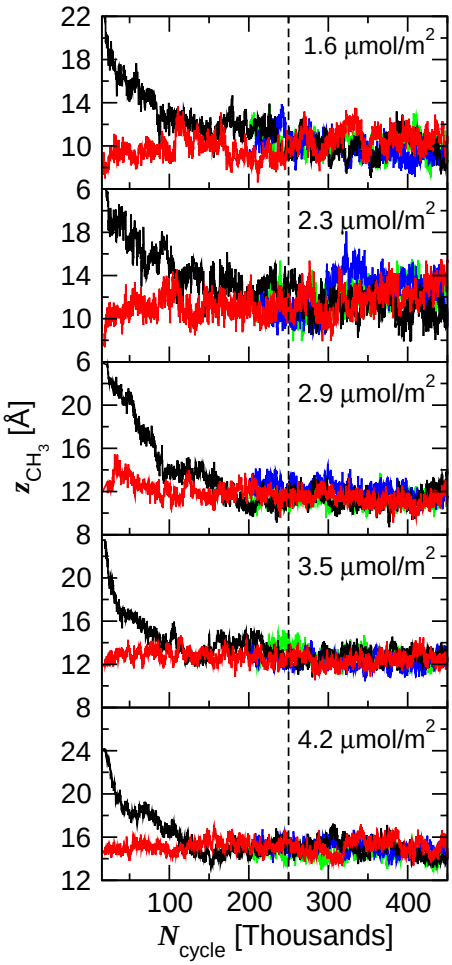

Figure 8.1: Evolution of the height of the terminal methyl group above the silica surface for 4 independent simulations at the 5 different surface coverages. The dashed line indicates when the production period began.

To establish the ability of the simulation technique to generate equilibrated stationary phases at each grafting density regardless of starting configuration, a rigorous setup protocol was followed. First, the arrangement of stationary phase chains on the silica surface was generated by randomly selecting silanol sites, but avoiding close contacts of the chains, until the desired coverage was achieved. At this point the chains were in the all-trans configuration. Then, two replicas of the simulation box at each grafting density

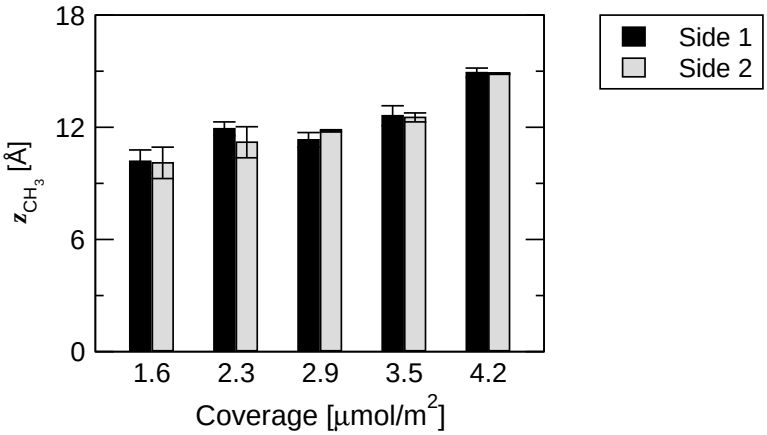

Figure 8.2: Average height of the terminal methyl group on each side of the silica slab for the five different surface coverages.

were made and each followed a separate simulation path. One of the simulations was pre-equilibrated in vacuum before the addition of solvent while, in the other simulation, solvent was added before any movement of the chains was allowed.

Once these two trajectories were nearing equilibrated structures, i.e., after 2×10^5 Monte Carlo (MC) cycles (one MC cycle corresponds to N MC moves, where N is the total number of molecules in the system), a second set of two simulations was begun using a different random number seed, and all four simulations were equilibrated for another 5×10^4 MC cycles. This was followed by a production period of 2×10^5 MC cycles during which averages were computed. Statistical uncertainties in all reported quantities were estimated from the standard error of the mean of the averages from the four independent simulations for each coverage.

Equilibration was monitored via the evolution of the number of solvent molecules in each box and the height of the terminal methyl group relative to the silica substrate. Before production began, it was ensured that these quantities had converged to the same average value for each independent simulation. The slowest of these two values to converge was the position of the terminal methyl group ($z_{\mathrm{CH_3}}$). Its evolution as function of the number of MC cycles is shown in Figure 8.1 and, from this, it is evident that the simulations were well-equilibrated before the start of the production period.

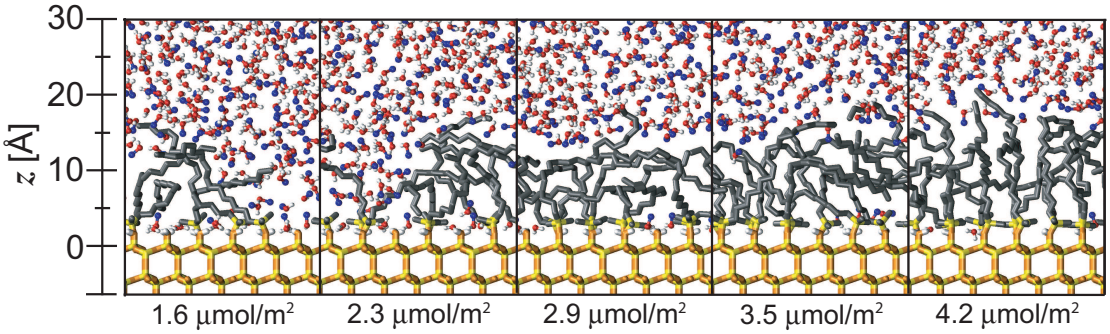

Figure 8.3: Snapshots from simulations at five different grafting densities.

As a further check on the validity of the simulations the average height of the terminal methyl group was computed separately for each of the two sides of the silica slab during the production period of the simulation (Figure 8.2). Since each of these two surfaces has different (random) arrangements of the alkyl chains, this will give some indication of the dependence of the results on chain arrangement. This analysis shows that, in most cases, the difference in z_{CH_3} between two surfaces at the same coverage is smaller than the difference between surfaces with different coverages. The exception to this is the system with a coverage of 2.3 μmol/m^2. However, even in this case the averages for the two different surfaces agree within their statistical uncertainties. This suggests that, for randomly arranged chains, the results should show little dependence on chain arrangement.

8.3 Results and Discussion

Snapshots taken from simulations at each surface coverage are shown in Figure 8.3. Although each of these snapshots represent only a single configuration of the millions generated during the simulation, they already convey a wealth of information about the influence of grafting density on structure. Perhaps most apparent, but also as one may expect, the alkyl chains appear to have the greatest amount of order in the system with the highest density. However, even in this system one can see a distribution of chain structures, i.e., the chains are not in the all trans conformation with uniform tilt angles.

Table 8.2: Summary of the average structural properties of alkylsilane chains at five different surface coverages.[a,b]

	Coverage (μmol/m^2)				
Property	1.6	2.3	2.9	3.5	4.2
f_{gauche}	0.257_{16}	0.275_{7}	0.273_{4}	0.265_{5}	0.268_{4}
r_{ete} (Å)	16.4_{6}	15.9_{3}	15.8_{2}	16.1_{2}	16.1_{2}
$\cos\theta_{\text{ete}}$	0.39_{2}	0.44_{5}	0.48_{2}	0.53_{3}	0.66_{2}
z_{CH_3} (Å)	10.2_{2}	11.6_{7}	11.6_{2}	12.6_{1}	14.9_{1}
S_{16}	-0.10_{1}	-0.03_{2}	-0.02_{2}	0.04_{1}	0.14_{2}

[a]These properties are described in Chapter 5.
[b]Subscripts indicate the statistical uncertainty in the final digit.

The alkyl chains at the higher grafting densities appear to form a somewhat uniform layer while the chains at the lower grafting densities are unable to accomplish this and exist in a somewhat clustered state with significant amounts of solvent penetrating all the way down to the silica surface. Many more qualitative observations could be made from these snapshots, however, the remainder of this section will focus on a more quantitative analysis of these structural aspects using the full simulation trajectory.

8.3.1 Alkylsilane Chain Conformation

As discussed in Chapter 5, a variety of descriptors can be used to quantify the order/disorder of the alkyl chains in the stationary phase. A summary of these descriptors is given in Table 8.2. The first two rows of this table show the fraction of gauche defects and end-to-end length of the chains. These two properties show little dependence on surface coverage. Thus, when not factoring in chain orientation, the average chain conformation is similar at all grafting densities. Interestingly, these gauche defect fractions and end-to-end distances indicate that RPLC chains are more extended than isolated C_{18} chains in a water/methanol solvent but, rather, they are more similar to chains in a bulk C_{18} liquid phase [182]. The small dependence of the gauche defect fraction is in contrast to previous simulation [59] and NMR studies [149]. However, this is not of great concern as both the simulation and NMR studies were performed in the gas phase where chain self-solvation will be much more important. Conformational relaxation in high-density alkyl systems is also relatively slow and one may question whether

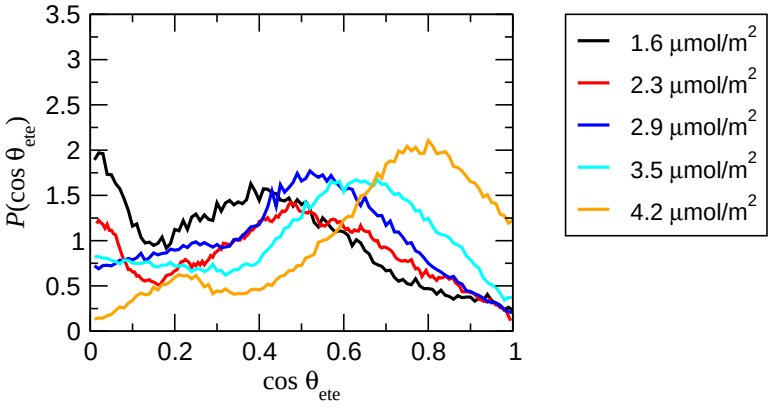

Figure 8.4: Probability distribution of the angle between the chain end-to-end vector and the normal to the silica surface at five different grafting densities.

previous MD simulations were able to assess the relevant timescales. Furthermore, the NMR work examined polymeric C_{22} phases primarily at higher densities than those studied in this work. Here, a comparison to well-characterized alkyl thiol self-assembled monolayers is instructive. It is well known that long-chain thiols exist in well-ordered structures with very few gauche defects and uniform tilt angle near 30° [183, 184], but the chain coverage for these alkyl thiol monolayers is 7.7 μmol/m^2, i.e. a much higher chain coverage than found in monomeric RPLC phases such as studied here.

The next three descriptors in Table 8.2 tell a much different story about the influence of bonding density on chain order. The first of these descriptors is $\cos\theta_{\mathrm{ete}}$. Despite that the end-to-end length changes very little, $\cos\theta_{\mathrm{ete}}$ steadily increases from 0.39 for the lowest to 0.66 for the highest density studied here. Thus, at lower grafting densities the average chain tilt is oriented more towards, but not parallel to, the silica substrate's surface and at higher densities the average tilt is oriented more away from, but not perpendicular to, the substrate. Clearly, from the snapshots in Figure 8.3, the alkyl chains do not possess uniform tilt angles even at the highest bonding density. To assess the extent of tilt uniformity, information in addition to the average tilt angle is needed and, therefore, distributions of $\cos\theta_{\mathrm{ete}}$ for the different bonding densities are shown in Figure 8.4. These distributions show that, at all densities, the chains exhibit finite probabilities of having tilt angles both nearly parallel and nearly perpendicular to

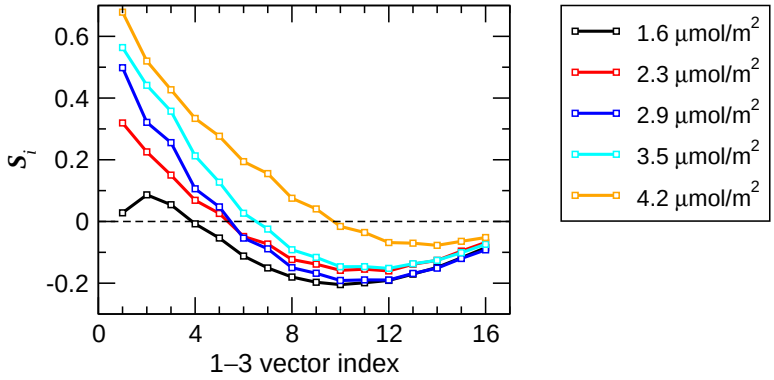

Figure 8.5: Order parameter along chain backbone for the angle between 1–3 backbone vectors and the normal to the silica surface at five different grafting densities.

the silica surface. All of the distributions appear to be bimodal with one peak at larger $\cos\theta_{\mathrm{ete}}$ values and another at smaller $\cos\theta_{\mathrm{ete}}$ values. For the highest grafting these peaks occur at around 35° and 75°, corresponding to chains pointing nearly perpendicular and parallel to the surface, respectively. Both of these peaks shift to smaller $\cos\theta_{\mathrm{ete}}$ values at lower densities. For the lowest grafting density, these peaks are at about 65° and close to 90°. Thus, at low densities there is a significant probability of finding a chain collapsed on the surface, although this is not the most probable conformation.

Although the end-to-end vector provides a picture of the overall alignment of the chains, more local information on individual chain segments can be seen in Figure 8.5, which shows the order parameter S_i along the chain backbone. Starting with the first 1–3 segment one sees that, at all grafting densities, the value of S_1 is positive and, at all but the lowest grafting density, larger than any other S_i value. The value of S_1 ranges from 0.68 for the highest grafting density to 0.02 for the lowest. Moving along the chain backbone, S_i decreases in value and reaches a minimum before the chain terminus. This minimum is shallower and shifts further towards the chain end as the density is increased. Thus, in all systems, the initial portion of the alkyl chain has the largest preference for alignment perpendicular to the silica surface, this preference diminishes as one moves along the chain backbone, and the upper part of the alkyl chains shows at least a slight preference for alignment parallel to the silica surface. Despite some

Table 8.3: Average solvent density and methanol molfraction enhancement within the stationary phase (as defined by the GDS).[a]

Coverage (μmol/m^2)	Solvent Density (g/mL)	Molfraction Enhancement
1.6	0.270_9	1.23_2
2.2	0.219_7	1.32_3
2.9	0.098_2	1.37_1
3.5	0.073_3	1.53_2
4.2	0.057_3	1.53_3
Bulk solvent	0.844_1	–

[a]Subscripts indicate the statistical uncertainty in the final digit.

of these general similarities there are stark contrasts. The backbone vectors of chains at the lowest density show the highest preference for alignment parallel to the surface, since only the first few vectors of the 1.6 μmol/m^2 system have S_i values greater than zero, while all but the final 7 vectors at a coverage of 4.2 μmol/m^2 are positive. The minimum in S_i shifts from vector 10 at the lowest density to vector 14 at the highest density. Upon averaging the order parameter over all 16 1–3 vectors, values range from -0.10, a parallel preference, for the lowest density, to 0.14, a perpendicular preference, for the highest (see Table 8.2).

8.3.2 Solvation of the Alkylsilane Phase

As indicated in the brief discussion of the simulation snapshots, there is a great deal more penetration of solvent into stationary phases with lower surface coverages. The amount of solvent penetration as a function of surface coverage can be quantified by examining the density profiles for each system (Figure 8.6) and the average solvent densities within the stationary phase (Table 8.3). At the highest surface coverages, the profiles show that the only regions within the stationary phase containing significant amounts of solvent are just inside the GDS and near the silica surface ($z \approx 3$ Å for water and $z \approx 4$ Å for methanol). These peaks near the silica surface are due to direct hydrogen bonds between the solvent and the surface silanols. There is also a very small peak at $z \approx 6$ Å resulting from solvent hydrogen bonded to those surface bound solvent molecules. For the lower surface coverages, one finds significant amounts

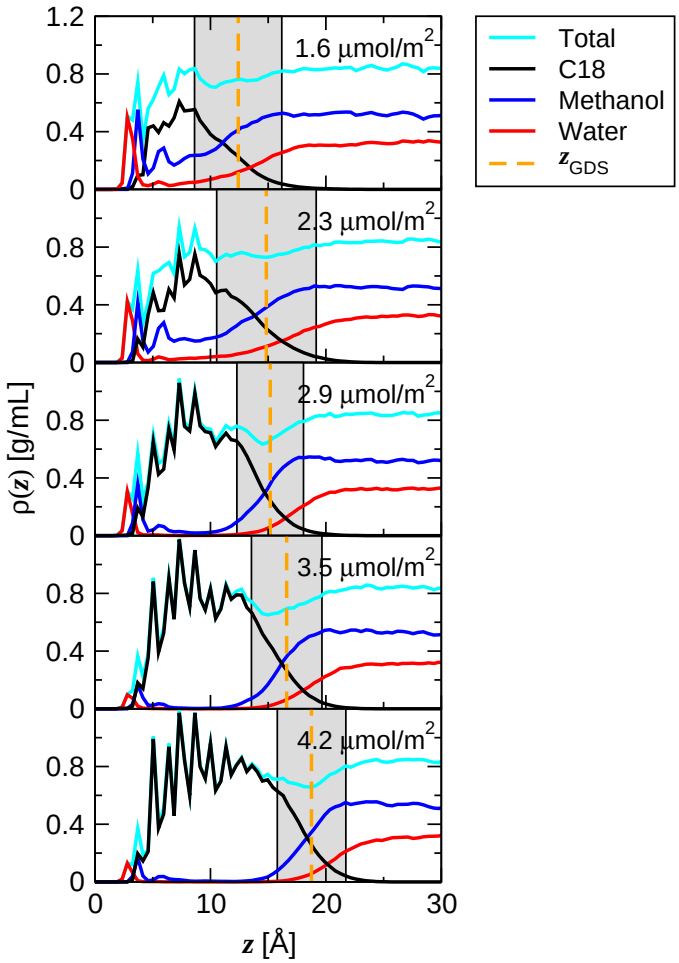

Figure 8.6: Total, stationary phase, methanol and water density profiles. The shaded gray area represents the interfacial region.

of solvent throughout the stationary phase and it is present continuously from the GDS to the silica substrate. The average solvent density contained within the GDS for the 1.6 μmol/m^2 system is 0.27 g/mL, nearly one-third of the bulk solvent density. At the highest surface coverage, this penetrated solvent density decreases by a factor of five. This decrease in the solvent density agrees with the experimental work of Wright and coworkers [181]. Interestingly, at a coverage of 1.6 μmol/m^2, the solvent density at the silica surface is close to that of the bulk solvent density. This is a result of the large

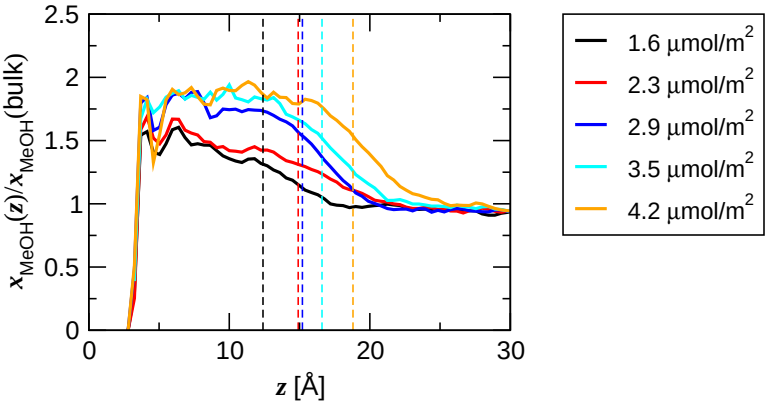

Figure 8.7: Local methanol molfraction enhancement as function of distance from the substrate. Dashed vertical lines indicate the position of the GDS.

number of residual silanols available in this system. Thus, the increased wettability of the hydrophobic alkyl chains at lower coverages is likely the result of the increased number of silanols and availability of the hydrophilic silica surface (see section 8.3.3 for discussion of surface properties).

Additionally, the density profiles indicate that there is a significant enhancement of the methanol concentration in the interfacial region and within the stationary phase. To quantitatively assess this, Figure 8.7 shows this enhancement as a function of z. From this one sees that, at all grafting densities, the methanol enrichment starts outside the GDS and persists throughout the stationary phase until reaching locations where steric reasons prevent the center-of-mass of methanol to approach the surface as closely as water even though both can hydrogen-bond directly to residual silanols. In agreement with the adsorption studies by Gritti and coworkers [46], the enrichment increases with grafting density. This increase occurs both in the stationary phase and interfacial regions, but reaches a maximum of near double that of the bulk in the center of the bonded phase at 4.2 μmol/m^2. Table 8.3 quantifies the average enhancement inside the GDS, which ranges from about 1.2 to 1.5 for the systems studied here.

Table 8.4: Number of hydrogen bonds per solvent molecule residing within the interfacial region of stationary phases with different surface coverages and in the bulk mobile phase.[a]

Coverage	Water			MeOH		
(μmol/m^2)	N_{donor}	N_{accep}	Total	N_{donor}	N_{accep}	Total
1.6	1.76_1	1.21_1	2.97_2	0.91_1	1.46_1	2.37_2
2.2	1.76_1	1.19_1	2.95_1	0.91_1	1.48_1	2.39_1
2.9	1.72_2	1.03_1	2.75_3	0.91_1	1.59_2	2.50_2
3.5	1.73_2	1.08_2	2.80_2	0.91_1	1.56_1	2.46_2
4.2	1.72_3	1.05_2	2.78_4	0.91_2	1.58_2	2.48_3
Bulk solvent	1.80_2	1.54_2	3.34_2	0.92_2	1.18_2	2.09_2

[a]Subscripts indicate the statistical uncertainty in the final digit.

8.3.3 Interfacial and Alkyl Surface Properties

An interesting phenomenon, observable in the interfacial region of the density profiles, is a depletion in the overall system density, i.e., a dewetting at the alkyl surface. This dewetting effect is more apparent in the systems with higher alkyl grafting densities. Lum, Chandler, and Weeks predicted this effect for extended hydrophobic surfaces, like the ones studied here, but not for small hydrophobic solutes [133]. They argue that this is the result of a disruption of the solvent's hydrogen bonding network near larger surfaces, but not around small solutes.

To check if this disruption exists near RPLC stationary phase surfaces, the number of hydrogen bonds per solvent molecule in the interfacial region and in the bulk solvent were computed (see Table 8.4). It was found that water molecules in the interfacial region form fewer hydrogen bonds than water in the bulk solvent. This comes mostly from a decrease in the number of hydrogen bond acceptors as donors show only a small decrease. In complete contrast to water, methanol molecules have more hydrogen bonds in the interfacial region than in the bulk and this is mainly due to an increase in acceptors. These effects are slightly more pronounced as grafting density is increased. Indeed, the interfacial region has an increased methanol content, but this does not fully explain this peculiar hydrogen bonding since increasing the methanol content would decrease the number of hydrogen bond acceptors for both methanol and water [182] while it is observed here only for water.

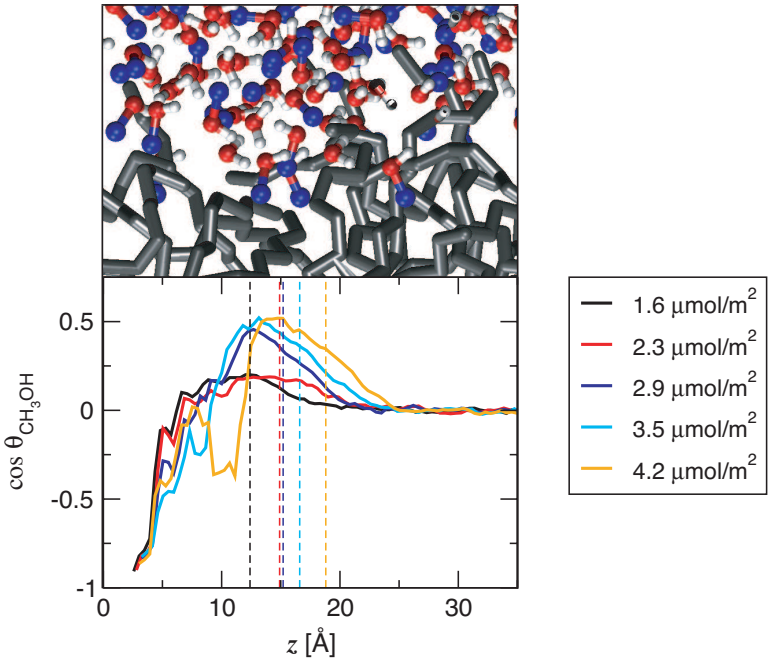

Figure 8.8: Snapshot of the interface taken from a 4.2 μmol/m^2 simulation and plot of the end-to-end vector orientation of methanol as function of z (positive values indicate methyl groups pointing towards the silica surface, negative values away). Dashed vertical lines indicate the position of the GDS.

In order to better understand this hydrogen bonding pattern, the orientation of methanol and water molecules as function of z was examined (Figure 8.8). This analysis showed that methanol molecules in the interfacial region possess a relatively strong preference to align their methyl groups toward the alkyl surface and point their polar hydroxyl groups away from it. Methanol molecules with this orientation are visible in the snapshot shown in the top part of Figure 8.8. Water molecules near the GDS show a weaker preference for their dipole vector to point away from the substrate, i.e., the hydrogens are oriented toward the mobile phase. This orientation of methanol molecules leaves its oxygen available to accept more hydrogen bonds from solvent molecules in the mobile phase. Since both interfacial methanol and water are donating near their maximum number of hydrogen bonds, if methanol is accepting more, then water must accept fewer.

Table 8.5: Average interfacial and alkyl surface properties for the five different surface coverages.[a]

	Coverage (μmol/m^2)				
	1.6	2.3	2.9	3.5	4.2
z_{Gibbs}[b] (Å)	12.4_1	14.9_4	15.2_1	16.6_1	18.8_1
$\delta_{\text{interface}}$[b] (Å)	7.6_8	8.6_4	5.7_3	6.1_2	5.9_3
$\text{SASA}_{\text{total}}$[c]	2.35_1	2.48_7	2.08_4	2.02_1	2.04_2
$\text{SASA}_{\text{alkyl}}$	2.00_1	2.24_4	2.05_3	2.01_1	2.04_2
$\text{SASA}_{\text{SiOH}}$	0.35_1	0.23_3	0.03_1	< 0.01	< 0.01
SASA per chain (Å^2)	103.7_3	83.3_{16}	59.3_9	47.6_3	40.8_3

[a]Subscripts indicate the statistical uncertainty in the final digit.
[b]Defined in Chapter 5.
[c]Solvent-accessible surface area relative to a flat interface.

A summary of various other interfacial and surface properties is given in Table 8.5. The first two entries in this table are the position of the Gibbs dividing surface and interfacial width, both of which are fit to the total solvent density. As the grafting density is increased, the position of the Gibbs dividing surface shifts outward from 12.4 Å to 18.8 Å, indicating an increase in thickness of the alkyl phase. The interfacial width shows a less systematic trend, but tends towards a larger value of 8 Å for the lower two grafting densities and a smaller value of 6 Å for the three higher densities. The increase in interfacial width likely occurs as a result of better solvation of the stationary phase at lower coverages.

Another property relevant for explaining stationary phase properties is the amount of stationary phase surface that is accessible to the mobile phase solvent. The total amount of solvent accessible surface area (SASA) at the interface of stationary and mobile phases, the portions of this surface area that are alkyl and siliceous, and the alkyl surface area per chain are presented in Table 8.5. It should be mentioned that since the silica surfaces studied here are planar and not curved, the change in surface area that comes from simply increasing the alkyl layer width will not be observed. Thus, these alkyl surface areas are more a measure of surface roughness.

The two phases with the lowest grafting densities are the only ones for which any significant amount of silica surface is directly accessible to the solvent and this is likely the reason why these two phases are so wettable. The low density phases are also the

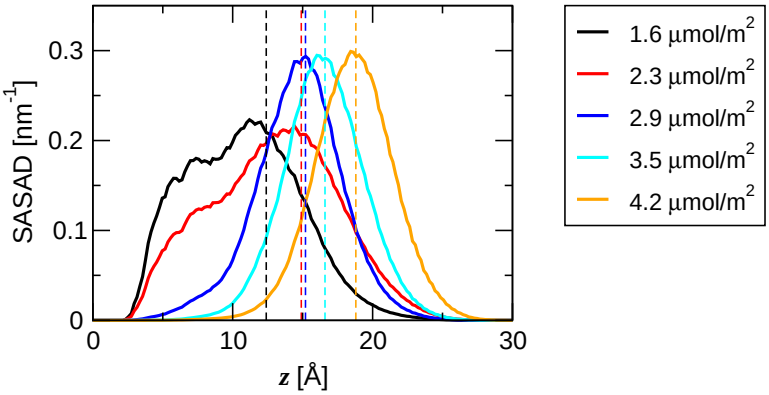

Figure 8.9: Solvent-accessible surface area density (SASAD) as function of z at the five different grafting densities. Dashed vertical lines indicate the position of the GDS.

ones with the most total accessible area. In terms of just nonpolar alkyl surface area, the 2.3 μmol/m^2 coverage has the largest alkyl surface area while the other four phases are very similar to each other. However, if the alkyl surface area is divided by the number of ODS chains in the system one finds that there is a definite trend. As grafting density is increased, the SASA per chain decreases. Thus, at low grafting densities the chains are solvated more by the mobile phase while at higher densities they are more self-solvated. Finally, the distribution of alkyl surface area as function of distance from the substrate is shown in Figure 8.9. These surface area distributions indicate that the two lower grafting densities have a more diffuse, or rough, surface while the higher grafting densities have a more sharply defined surface. For all five grafting densities, the main peak is located at the GDS, but the distributions for the two lower grafting densities show a shoulder at $z \approx 7$ Å, a value close to what one would expect for alkyl chains laying flat on the silica substrate.

8.4 Conclusions

Realistic model RPLC systems with different alkyl surface coverages were studied with configurational-bias Monte Carlo simulations in the constant pressure version of the Gibbs ensemble. The simulations afford a wealth of molecular-level information on the

effects of surface coverage on the stationary phase order, solvation of the alkyl chains by the mobile phase, and the properties of the nonpolar stationary phase/polar mobile phase interface.

As grafting density is increased, the alkyl chains in the stationary phase have a larger preference to align themselves more perpendicular to the silica surface and form a more uniform alkyl layer. However, even at the highest density, there is still a wide distribution of chain conformations and the chains are not found to even nearly resemble the all-trans/uniform tilt conformation.

At lower grafting densities, the chains are more easily wetted by the mobile phase. Presumably, this results from a direct accessibility of the silica surface which cannot be completely covered at low grafting densities. With the exception of a persistance at the residual silanol sites, the mobile phase solvent is nearly excluded from the stationary phase at the highest grafting density.

The interface between the hydrophilic mobile phase and hydrophobic stationary phase is enriched in the organic component of the solvent and shows changes in the hydrogen-bond network of interfacial solvent (due to preferential orientations) compared to that of a bulk solvent. These effects become more dramatic as grafting density is increased and the stationary phase becomes more hydrophobic.

Chapter 9

Influence of Surface Coverage. II. Effects on solute retention.

9.1 Background

Selectivity and efficiency in RPLC can be optimized by adjusting the conditions under which a separation is carried out, for example, by changing the mobile phase composition, temperature, pressure, or the nature of the stationary phase (chain length, bonding density, or chain chemistry). In this chapter attention is given to the effects of alkylsilane bonding density on the retention mechanism. In the preceding chapter, the effects of bonding density on stationary phase chain structure and solvation were characterized using molecular simulation. Here, a molecular-level analysis of the retention of both polar and nonpolar solutes in the same set of systems is presented. This chapter will start with a brief overview of some relevant experimental studies.

A handful of theoretical treatments aimed at yielding molecular-level information regarding the effects of bonding density on solute retention have appeared in the literature [39, 40, 43]. However, the primary means of attempting to gather this molecular information has been to use retention data itself. In this respect, the retention of a series of solutes is measured on stationary phases of different grafting densities. The differing

[†] This chapter describes the outcome of a collaborative research project carried out by Jake L. Rafferty and advised by J. Ilja Siepmann and Mark. R. Schure. A report on this research project has been published [73].

retentive properties are then used to infer details about the retention mechanism. The following paragraphs will review some of this work. This review serves two purposes in the context of the current paper: (1) to demonstrate the current level of knowledge in the field, and (2) to introduce the experimental data that will later be compared to the simulation results as a means of validation. This validation is important if the molecular-level information from the simulation is to be trusted.

First, it should be mentioned that various studies have shown increases in grafting density lead to an increase in shape selectivity. The term shape selectivity is used to describe the ability of a stationary phase to separate a class of solutes based on their molecular shape rather than their molecular weight or functional groups, for example the separation of the geometric isomers of a polycyclic aromatic hydrocarbon. This shape selectivity will be examined in Chapter 12. In contrast, the focus of the present chapter is on the separation of compounds based on their functional groups so only work related to this topic will be discussed here.

Kikta and Grushka examined the retention of a homologous series of alkylphenones on C_9 phases with bonding densities ranging from 0.3 to 1.5 μmol/m^2 [173]. They found that the retention factor of each member of homologous series increased with increasing grafting density. Computing the methylene increment from their data with a 50/50 (v/v) water/methanol mobile phase at 313 K, one finds a range of -1.2 to -1.8 kJ/mol from the lowest to the highest bonding densities. These authors speculate that one possible reason for the increase in retention is that more methanol, into which the solutes can partition, is adsorbed onto the alkyl surface as the density is increased.

Hennion, Picard, and Caude synthesized octadecyl silane (ODS) stationary phases with surface coverages ranging from 0.36 to 4.2 μmol/m^2 and examined the retention of a series of alkylbenzenes and phenol derivatives using water/methanol as the mobile phase [174]. Their data show that with increases in bonding density, the retention factor of the nonpolar alkybenzenes increased continuously while the retention factor for some of the more polar phenol derivatives reached a maximum at a density around 2 μmol/m^2. They also report data on the selectivity between various solute pairs as density is increased. For example, both the toluene-benzene and cresol-phenol selectivities increased, which indicates that the hydrophobicity of the stationary phase increases with increased grafting density.

Retention factors of various benzene derivatives on C_{18} phases ranging in grafting density from 2.4 to 3.4 μmol/m^2 were measured by Tanaka, Goodell, and Karger [175] and a similar class of solutes was studied by Miller and coworkers [176], but for lower grafting densities ranging from 0.33 to 1.4 μmol/m^2. Both studies directly compare polar and nonpolar solutes on the same columns and find that the relative increase in retention with increased density is much larger for the nonpolar solutes. In some cases the retention of the more polar solutes actually decreased with increased bonding density. This behavior was attributed to the decreased availability of residual silanols at higher bonding densities. As a quantitative measure of the hydrophobicity of these phases the methylene and hydroxyl increments were computed from Tanaka's retention data at 303 K with a 50/50 (v/v) water/methanol mobile phase. Methylene increments (from ethylbenzene and toluene retention factors) were -1.4 kJ/mol and -1.7 kJ/mol for the lowest and highest density phases, respectively. Hydroxyl increments (from 2-phenyl-ethanol and ethylbenzene) were found to be $+4.4$ kJ/mol at 2.4 μmol/m^2 and $+5.4$ kJ/mol at 3.4 μmol/m^2.

Sentell and Dorsey found that upon increasing C_{18} bonding density from 1.6 to 4.1 μmol/m^2 the partition coefficient for napthalene shows a linear increase until it reaches a maximum at 3.1 μmol/m^2 [7]. They suggested that this maximum results from an entropic expulsion of the solute due to packing constraints in the stationary phase chains and that the dominant retention mechanism must be partitioning since adsorption would not be affected by chain density. They also show that while the partition coefficient had a maximum, the retention factor steadily increased since this quantity is not multiplied by the decreasing phase ratio. The same authors have also measured the retention of a series of alkylbenzenes and showed that methylene selectivity increased only slightly as bonding density increased [8].

ODS stationary phases ranging in coverage from 0.0 (bare silica) to 4.24 μmol/m^2 were examined by Buszewski and coworkers [9]. Like previous studies, they found that retention factors increased with increasing surface coverage. The authors state that this supports a partition-like retention mechanism at high coverages since adsorption should not depend on coverage. They also found that selectivity increased for nonpolar molecules (judged by toluene/benzene test mixtures), decreased for polar molecules (nitrobenzene/phenol), and increased for nonpolar/polar mixtures (benzene/phenol)

with increases surface coverage. Since there are fewer accessible silanols at higher chain coverages, the decrease in nitrobenzene/phenol selectivity was thought to support a retention mechanism in which adsorption to the silica surface is important. They also cite that this is the reason for the increase in benzene/phenol selectivity.

Tan and Carr [14] examined the retention of nonpolar solutes on stationary phases with grafting densities from 0.6 to 2.3 μmol/m^2. They determined the free energies of transfer from water/methanol mobile phases to these stationary phases and to a hexadecane liquid phase. According to Dill's lattice theory, the ratio of free energies for the hexadecane transfer to the RPLC transfer, the F factor, should be unity if partitioning is the dominant retention mechanism and approach six if adsorption is dominant [39, 40]. It was found that F values decreased from near two for the lowest grafting density to near one for the highest density. This was used to suggest that the retention mechanism is more adsorption-like for lower density phases and more partition-like for higher density phases. This was rationalized by assuming that, at lower densities, the chains are collapsed upon the silica surface forming a film too thin for solutes to partition into. At higher densities the phase becomes thick enough for it to become a more liquid-like medium that the solutes can partition into.

For C_{18} phases with grafting densities ranging from 0.59 to 3.2 μmol/m^2 Miyabe and Guiochon [185] found that partition coefficients increase linearly with increasing grafting density up to 2.3 μmol/m^2 after which they begin to level off. These researchers state that if the solutes interacted with more than one stationary phase chain at a time, then one should not see this leveling off, but rather a concave upward behavior. It appears that the authors concluded that each chain is a single adsorption site.

In another study on grafting density, Gritti and Guiochon measured the excess adsorption isotherms of a few solutes from water/methanol mixtures onto C_{18} stationary phases with grafting densities of 0.42, 1.01, 2.03 and 3.15 μmol/m^2 [25]. Under linear chromatography conditions, they find a maximum in the partition coefficient at 2.03 μmol/m^2, but find that the saturation capacity is highest at 0.42 μmol/m^2. The type of isotherm model that best fit the adsorption isotherm data for a given solute did not change upon changing the grafting density and all solutes showed a best fit to a multi-site Langmuir model. Furthermore, the adsorption energies from these models also showed little dependence on grafting density. This suggests that there are similar

types of adsorption sites in stationary phases with different grafting densities. The authors suggest that these sites may be between chains in the bonded phase and at the mobile/stationary phase interface. As grafting density is increased, the chains become more tightly packed and the interchain sites become less available and, therefore, the partition coefficient and saturation capacity decrease.

Indeed, the retention measurements discussed above have given much information and insight, however, retention is a thermodynamic measurement and therefore cannot directly prove the molecular details of a process. In contrast, the use of simulation allows one to monitor precisely where the solutes reside within the RPLC system and with what probability. This information is exactly what one needs to draw any firm conclusions about the retention mechanism. In this chapter simulations aimed at discerning the effects of alkyl surface coverage on the molecular mechanism retention are described. Details on these simulations were given in Chapter 8 and will not discussed here.

9.2 Results and Discussion

This section shall begin by a presentation of simulation results that can be compared directly to experimental retention data. This is done to establish that the simulations yield accurate thermodynamics when compared to experiment. Agreement of thermodynamic quantities validates the simulations and gives more weight to the validity of molecular-level details that will be presented later in this chapter.

Plots of the net distribution coefficients and retention factors for two probe solutes, *n*-butane and 1-propanol, along with the methylene and hydroxyl increments are presented in Figure 9.1 and numerical results for these quantities are given in Table 9.1. Results are presented for *n*-butane and 1-propanol since the former was the largest alkane studied and since the latter has the same number of heavy atoms (i.e., similar strength of dispersive interactions).

In general, the data in Table 9.1 and Figure 9.1 agree very well with experiment. With increases in surface coverage, a steadily increasing retention factor is observed for the nonpolar probe solute, *n*-butane, and this is in accord with the retention data for other nonpolar solutes discussed in the introduction [7, 9, 173, 174, 175, 176]. Furthermore, the maximum in the distribution coefficient for the nonpolar solute also agrees

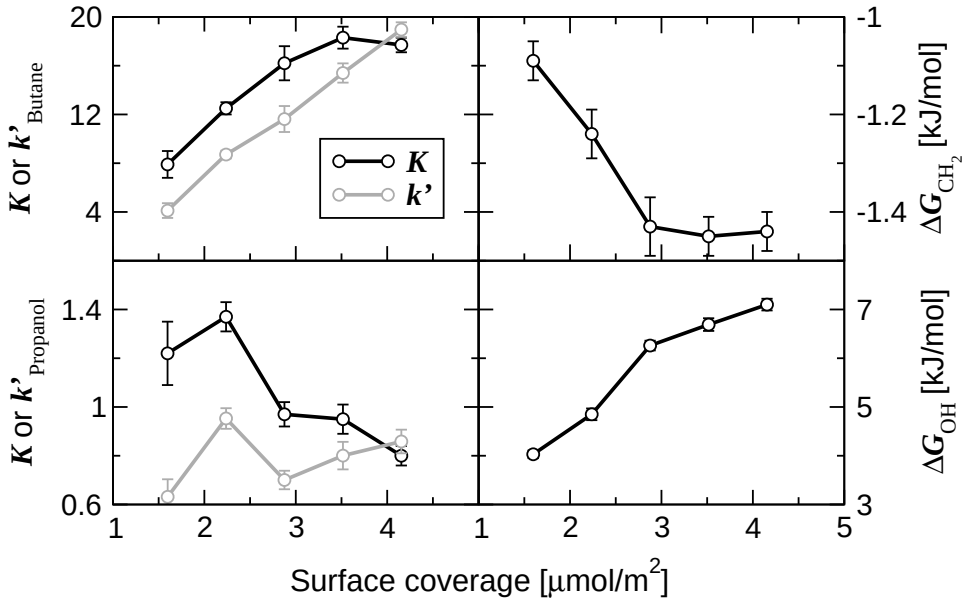

Figure 9.1: Distribution coefficients and retention factors for *n*-butane and 1-propanol (top and bottom left, respectively) and free energies of retention for the methylene and the hydroxyl group (top and bottom right, respectively).

with previous experimental work [7, 25, 185]. When examining the polar solute 1-propanol, it is evident that it behaves quite differently and actually shows a partition coefficient that reaches its maximum more quickly than *n*-butane when bonding density is increased. Additionally, the selectivity between the nonpolar and polar probe solutes increased continuously with increases in surface coverage. These two observations also match the experimental retention data [9, 174, 175, 176].

In Chapter 7, it was shown that the values of $\Delta G_{\mathrm{CH_2}}$ and ΔG_{OH} for the simulated 2.9 μmol/m^2 stationary phase agree very well with the experimental work of Barman, which was carried out under very similar conditions, over a wide range of water/methanol ratios [171]. Although it was not possible to make as direct a comparison to experiment here, the proper trends in these incremental free energies are observed. From the simulations, the methylene increment decreases slightly from -1.1 to -1.4 kJ/mol when increasing the grafting density from 1.6 to 2.9 μmol/m^2. The methylene increment then remains constant with further increases in density. For the

Table 9.1: Net distribution coefficients, retention factors, selectivities, and incremental free energies of retention.[a,b]

Coverage	K_{butane}	k'_{butane}	K_{propanol}	k'_{propanol}	$\frac{k'_{\text{butane}}}{k'_{\text{propanol}}}$	ΔG_{CH_2}	ΔG_{OH}
1.6 μmol/m^2	7.9_{11}	4.1_6	1.22_{13}	0.63_7	6.6_8	-1.09_4	4.03_8
2.3 μmol/m^2	12.5_4	8.7_3	1.37_6	0.95_4	9.2_2	-1.24_5	4.85_{12}
2.9 μmol/m^2	16.2_{14}	11.6_{11}	0.97_5	0.70_3	16.6_3	-1.43_6	6.26_{10}
3.5 μmol/m^2	18.3_9	15.4_8	0.95_6	0.80_6	19.3_{10}	-1.45_4	6.69_{13}
4.2 μmol/m^2	17.7_6	19.0_6	0.80_4	0.86_4	22.1_5	-1.44_4	7.10_{12}

[a]Subscripts indicate the statistical uncertainty in the final digit(s).
[b]Free energies in units of kJ/mol.

hydroxyl increment, the opposite trend is observed. This increment steadily increases with increasing grafting density.

Data from Tanaka and coworkers show that the methylene increment decreased by about 0.2 kJ/mol and the hydroxyl increment increased by about 1.0 kJ/mol when going from 2.4 to 3.4 μmol/m^2 [175]. The same decrease in methylene increment and a slightly larger increase in hydroxyl increment when with a similar increase in density (2.3 to 3.5 μmol/m^2) is observed from the simulations. However, this experimental study used a slightly lower methanol volume fraction and temperature than the current simulation study. Thus, an exact match in free energies is not expected, rather just similar trends. The increase in methylene selectivity also agrees with other work discussed in the introduction [8, 9, 14, 173, 174, 176].

An important point that should be mentioned is that not only do the simulations yield accurate free energies (which is dependent solely on the force field), many of these free energies can be computed with greater precision than the corresponding experimental numbers. This is a testament to the efficiency of the advanced Monte Carlo techniques employed in this study.

Now that it has been validated that the method yields the correct thermodynamics at the macroscopic level, the microscopic information that is also provided by the simulations will be discussed. Figure 9.2 shows the distribution coefficient K of *n*-butane and 1-propanol as function of z, or distance from the silica surface, for the five different grafting densities studied. Larger values of $K(z)$ indicate the regions where the solutes

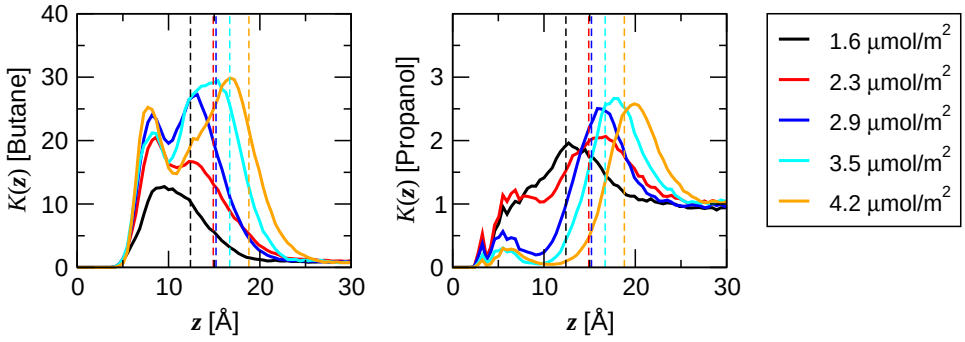

Figure 9.2: Distribution coefficient profiles for *n*-butane (left) and 1-propanol (right). For reference, the position of the Gibbs dividing surfaces are indicated by the dashed vertical lines.

have a larger probability of residing (regions of lower free energy). The features in these plots indicate that for both solutes the stationary phase behaves as a heterogeneous medium with multiple preferred regions.

For *n*-butane, it was shown in Chapter 7 that there is a bimodal behavior in the $K(z)$ profiles for a 2.9 μmol/m^2 stationary phase over a wide range of water/methanol and water/acetonitrile concentrations. There was one peak in the center of the bonded phase ($z \approx 8$ Å) and one in the interfacial region just inside the GDS ($z \approx 14$ Å). In general, this behavior seems to preserved when the grafting density is changed. Two peaks, one at $z \approx 8$ Å and one just inside the GDS, are evident at all coverages except 1.6 μmol/m^2. However, at the lowest coverage these two peaks likely overlap since the GDS has shifted to z values much closer to 8 Å.

The heights of both of these $K(z)$ peaks increase with increases in grafting density, although it appears that the peak in the interfacial region increases more rapidly. This suggests that interfacial adsorption becomes increasingly important relative to full penetration into the bonded phase as the bonded phase becomes more dense. This is in contrast to previous assumptions that an adsorption mechanism would not be affected by grafting density, and casts doubts on the conclusions that partitioning is the primary retention mechanism at higher coverages [7, 9, 14]. Nonetheless, it is interesting to note that the height of the peak in center of the bonded phase, the one that could definitely

be called partitioning, continues to increase with increasing grafting density despite that the total amount of free volume within the bonded phase decreases. It was suggested in Chapter 7 that retention in this region of the bonded phase may be related to ordering of the alkylsilane chains and, therefore, differs from bulk partitioning. This ordering clearly increases with grafting density (see Chapter 8).

For 1-propanol, the $K(z)$ profiles also indicate some degree of heterogeneity in the stationary phase. At all grafting densities there is a large peak in the interfacial region nearly centered on the GDS. This indicates that interfacial adsorption is the most important factor for retention of this polar, hydrogen bonding solute regardless of the stationary phase coverage. However, as the surface coverage decreases, there is a great deal more penetration of 1-propanol into the stationary phase. This is likely the direct result of the increased amount of mobile phase solvent within the stationary phase (see Chapter 8). These solvent molecules within the stationary phase can serve as hydrogen bonding sites for the solute. Additionally, all systems show $K(z)$ peaks for 1-propanol in the 3–7 Å region. These are the result of hydrogen bonding of the solute to the residual silanol groups and surface bound solvent as discussed in Chapter 7. Clearly, this phenomenon is more important at lower surface coverages where there are more residual silanols and surface bound solvent. This confirms previous conclusions that the reduction in the number accessible silanols is the reason for the decrease in retention of polar solutes with increased grafting density [9, 175]. However, this effect may be more indirect. The increased number of silanol groups at lower coverages leads to more mobile phase solvent throughout the bonded phase. This results in a stationary phase with an increased number of hydrogen bonding sites for polar solutes at regions other than just near the silica surface. This hydrogen bonding will be quantified and discussed in more detail later.

The positional distribution of solutes within the stationary phase already gives much information about the retention process, but additional insight can be achieved by examining the orientation of solutes as a function of position. To do this, the order parameter S_n is plotted as a function of z for *n*-butane in Figure 9.3. Additionally, since 1-propanol has a polar head and a nonpolar tail, the orientation of its end-to-end vector ($\cos\theta_{\text{ete}}$) is also presented in the figure.

The $S(z)$ profiles for *n*-butane indicate that near the silica substrate there is a

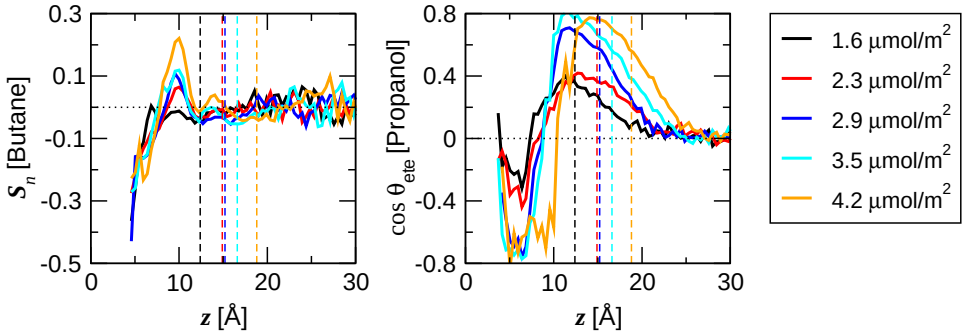

Figure 9.3: Solute orientational profiles at different surface coverages. Dashed vertical lines indicate the location of the GDS.

preference to be parallel to the surface (negative S values), in the center of the bonded phase the preference changes to a perpendicular alignment (positive S values), and in the interfacial region there is a very slight preference for parallel alignment. The magnitude of the $S(z)$ values, and thus the preferential orientation of *n*-butane, near the substrate and in the interfacial region are similar among the five grafting densities. However, the preferred orientation in the center of the bonded phase becomes more pronounced as grafting density is increased. At the lowest coverage their is essentially no preference near z =10 Å, but the value of $S(z)$ steadily increases to a maximum of about 0.22 at the highest coverage. This increase in rotational anisotropy with increased bonding density is in agreement with conclusions drawn by Wright and coworkers from their EPR data [181].

For 1-propanol, unlike *n*-butane, there is a huge preference to be perpendicular to silica surface when near it. Combined with this is a preference to have its polar hydroxyl group pointing towards the surface when it is in lower part of the bonded phase. In this manner it can best interact with the surface silanols and surface bound solvent. Additionally, 1-propanol molecules in the interfacial region prefer to direct their polar hydroxyl groups towards the mobile phase where they can hydrogen bond with the solvent. The preferred orientations of 1-propanol become much stronger as the grafting density is increased. This is the result of the drastic decrease in the amount of solvent molecules within the stationary phase. At the highest grafting densities there are very

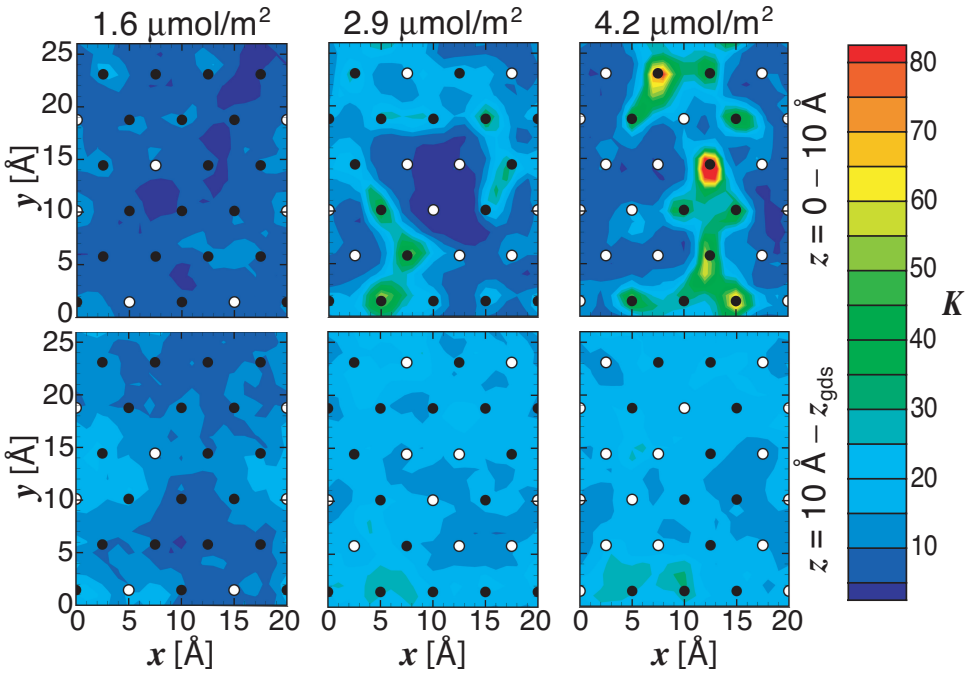

Figure 9.4: Distribution of *n*-butane in the *x*–*y* plane (the plane parallel to the silica surface) for molecules within 10 Å of silica surface (top row) and for molecules more than 10 Å from silica surface, but inside the GDS (bottom row). Black circles represent the location of the residual silanol groups and white circles indicate where the dimethyl octadecylsilane chains are tethered to the substrate.

few solvent molecules within the stationary phase for 1-propanol to interact with, so it must find hydrogen bonding sites near the silica surface and at the stationary/mobile phase interface if it would like to keep its nonpolar tail in the stationary phase.

The distribution of solute molecules as a function of z is clearly heterogeneous. It is also of interest whether the stationary phase shows heterogeneity in the x–y plane, i.e., the plane parallel to the silica surface. Figure 9.4 shows contour plots that depict the distribution of *n*-butane in this plane. Plots are shown for molecules in the more ordered region of the stationary phase (within 10 Å of the silica surface) and in the more disordered/interfacial region of the stationary phase (from $z = 10$ Å to the GDS). In each simulation, there are two silica surfaces, but for brevity the plots are shown for one of these surfaces and for three of the five surface coverages. The same general

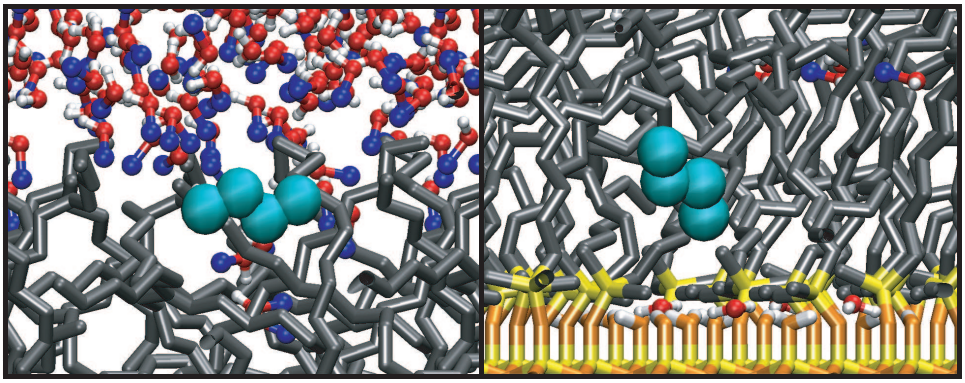

Figure 9.5: Simulation snapshots of retained *n*-butane molecules at a coverage of 4.2 μmol/m^2.

conclusions can be drawn are regardless of which of two surfaces are chosen and the same trends are observed if only three of the five coverages are examined.

At the lowest surface coverage, the distribution of *n*-butane shows the least amount of heterogeneity in the x–y plane for both of the regions. Upon increasing the surface coverage, the distribution in the upper region (z = 10 Å to the GDS) does not change significantly. However, the lower region begins to show a great deal of heterogeneity. The *n*-butane molecules begin to localize at positions where the C_{18} chains are not anchored, i.e., right above the residual silanol groups (the grafting locations of the C_{18} chains and residual silanol groups are indicated in the figure by white and black circles, respectively). At the highest grafting densities, the stationary phase becomes highly crowded and these sites above the silanols are the only favorable locations *n*-butane molecules can find without significant overlap with the chains and their dimethyl side groups.

In summary, the simulations demonstrate that *n*-butane molecules show two main preferred locations within the stationary phase. The first location is in the center of the bonded phase. Here, *n*-butane prefers to align itself perpendicular to the substrate and to reside at locations where the alkylsilane chains are absent. The second location is in the interfacial region. In this location, *n*-butane has a slight preference for an alignment parallel to the surface and a more homogeneous distribution in the plane parallel to

the substrate. Representative snapshots of retained *n*-butane molecules in these two locations are shown in Figure 9.5.

The *x*–*y* distribution of 1-propanol is shown in Figure 9.6. Like *n*-butane, 1-propanol prefers some specific regions within the *x*–*y* plane when in the lower portion of the bonded phase ($z < 10$ Å). However, unlike *n*-butane, the presence of these regions is not strongly dependent on the grafting density. Looking at the locations of these regions relative to the locations of the residual silanol groups a pattern is seen. 1-propanol molecules have the highest preference to reside at positions where they can interact with three residual silanol groups. In this manner, 1-propanol is able to form its maximum of three hydrogen bonds by accepting hydrogen bonds from two of the silanols and donating to the third. It is very interesting to note that *n*-butane shows a much stronger preference to localize in specific regions of the lower portion of stationary phase (K values up to 80), despite that for 1-propanol there are locations where it can maximize hydrogen bonding. This may be connected to the fact that 1-propanol forms more hydrogen bonds with solvent molecules than with the silanols when in the bonded phase (see discussion below).

The distribution of 1-propanol in the upper portion of the stationary phase ($z = 10$ Å to GDS) is much less heterogeneous than in the lower portion, however there is still some detectable heterogeneity. This heterogeneity also seems to have little dependence on the grafting density. Some of these more favorable regions in the upper portion of the stationary phase are directly above favorable regions in the lower portion of stationary phase. It has been shown that solvent molecules can form bridges from the mobile phase to the silanol groups on the silica surface [69]. Thus, it appears that these bridges create favorable regions for polar solutes in the otherwise hydrophobic stationary phase.

The detailed analysis of 1-propanol's distribution reveals that there are two important factors for retention, adsorption at the stationary–mobile phase interface and interaction with silanols and/or sorbed solvent. Representative snapshots of retained 1-propanol molecules in these two locations are shown in Fig. 9.7. The snapshot on the left shows a 1-propanol molecule in the interfacial region. Here, it inserts its hydrophobic tail into the stationary phase and leaves its hydroxyl group available to hydrogen bond with the mobile phase solvent. In the other snapshot, 1-propanol is hydrogen bonding with three silanol groups.

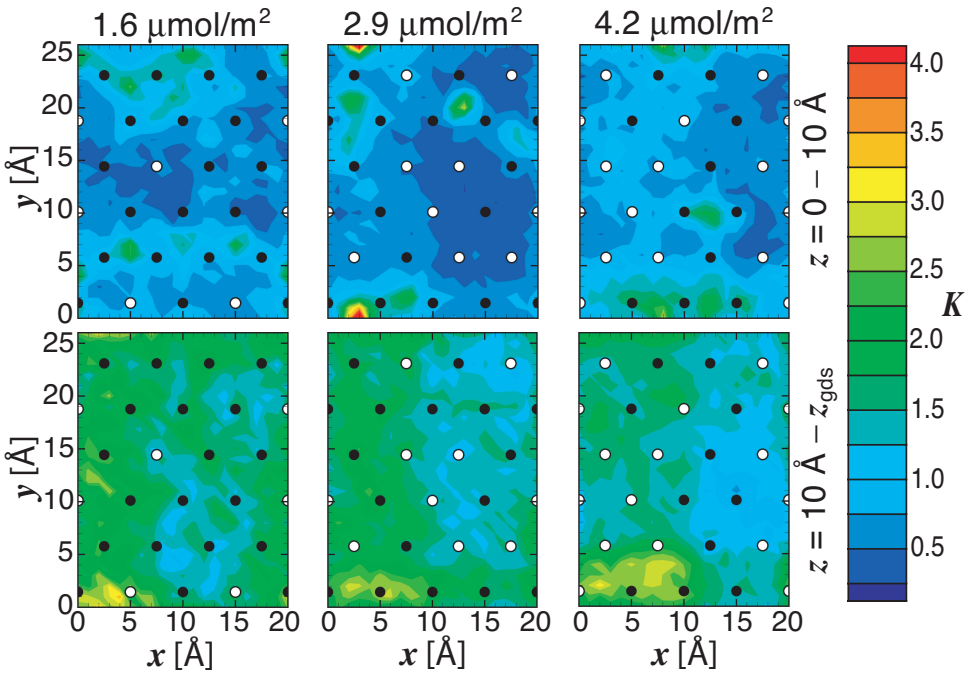

Figure 9.6: Distribution of 1-propanol in the x–y plane. Panel arrangement and symbol style as in Fig. 9.4.

The retentive behavior of the alcohol molecule can be at least partially explained by an analysis of its hydrogen bonding. Therefore, Table 9.2 shows the number of hydrogen bonds with the residual silanols, sorbed solvent (inside the GDS), and non-sorbed solvent (outside the GDS) per alcohol solute retained in the stationary phase. This data indicates that at all grafting densities the number of hydrogen bonds with silanol groups is significantly smaller than the number with sorbed solvent. The number is smallest for the highest grafting densities, as there are fewer residual silanols present. However, the alcohol solutes at the lowest grafting density show similar amounts of hydrogen bonding with the surface silanols as at the intermediate densities. This reflects a balance between the number of available silanol sites and competition with the solvent molecules for these sites. At the lowest grafting density there are more silanol sites, but also more mobile phase solvent within the stationary phase (see Chapter 8). The

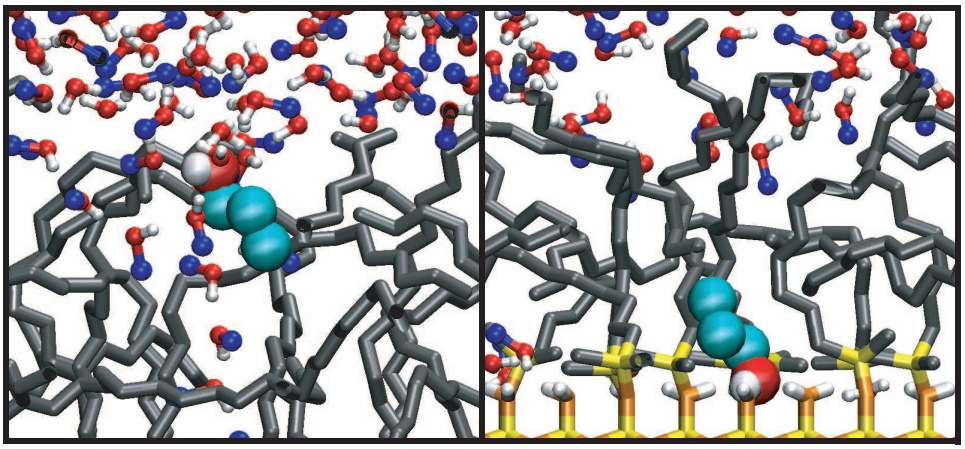

Figure 9.7: Simulation snapshots of retained 1-propanol molecules at a coverage of 2.9 μmol/m^2.

number of hydrogen bonds with solvent inside the stationary phase is higher for the lower grafting densities and this is why more alcohol solutes penetrate into the center of the bonded phase. However, this is not a continuous trend, but rather there is a maximum at 2.3 μmol/m^2. This is probably a result of the fact that, as the grafting is increased, the volume of the stationary phase increases while the density of the solvent within it decreases.

Interestingly, the number of hydrogen bonds with sorbed solvent at the three highest coverages is similar to a *n*-hexadecane phase saturated with a 50/50 water/methanol solvent (simulation details as in Chapter 4), although this may not be the case if other solvent mixtures are used (see Chapter 7). In contrast to the number of hydrogen bonds with sorbed solvent, the number of hydrogen bonds with molecules outside the GDS is larger for the higher grafting densities and this is why the interfacial region is more favorable at these densities. The total number of hydrogen bonds per alcohol molecule in the stationary phase shows little dependence on coverage and is always smaller than the number of hydrogen bonds for solutes in the mobile phase. This decrease in hydrogen bonding in the stationary phase as compared to the mobile phase is what drives the partition coefficients for 1-propanol to much smaller values than for *n*-butane at all grafting densities.

Table 9.2: Number of hydrogen bonds per alcohol solute molecule in retentive and mobile phases.[a,b,c]

Phase	N_{SiOH}	N_{in}	N_{out}	Total
1.6 μmol/m^2	0.13_2	0.76_3	1.08_1	1.98_1
2.3 μmol/m^2	0.14_3	0.84_2	0.99_1	1.96_1
2.9 μmol/m^2	0.12_1	0.40_1	1.41_2	1.93_1
3.5 μmol/m^2	0.06_2	0.42_2	1.47_1	1.92_1
4.2 μmol/m^2	0.05_1	0.44_1	1.44_1	1.94_1
50/50 water/methanol				2.08_1
n-hexadecane[d]				0.42_1

[a]A solute is defined to be in the retentive phase when it is in the first solvation shell (6.0 Å) of any stationary phase segment.
[b]Subscripts indicate the statistical uncertainty in the final digit.
[c]N_{SiOH}, N_{in}, N_{out} indicate the average number of hydrogen bonds (per alcohol solute) with silanol groups, solvent molecules inside the GDS and solute molecules outside the GDS, respectively.
[d]Saturated with 50/50 water/methanol

In the beginning of this Results and Discussion Section, the overall incremental free energies of retention for the methylene and the hydroxyl groups were discussed. Just like the plots of $K(z)$ these incremental free energies can be plotted as function of distance from the substrate (see Figure 9.8). For the methylene increment, the general shape of the free energy profile looks similar at all grafting densities. The free energy begins to become negative as the solute moves from the mobile phase into the interfacial region, reaches a minimum at around $z = 10$ Å, and then increases rapidly as the dimethyl side chains and the silica substrate are encountered. The minimum at 10 Å decreases from about -1.2 kJ/mol at 1.6 μmol/m^2 to -1.7 kJ/mol at 2.9 μmol/m^2 and then shows no further decrease as the density is increased.

The interfacial region also becomes more favorable for the methylene group as grafting density is increased. This is in contrast to suggestions that an adsorption mechanism should not be affected by grafting density [7, 9]. Additionally, the F factor, or ratio of free energies for the hexadecane transfer to the RPLC transfer, appears to be somewhat meaningless in interpreting the retention mechanism. The methylene increment is only slightly smaller in the interfacial region (adsorption) than in the center of the bonded phase (partition), not a factor of six smaller as predicted by Dill's lattice theory [39, 40].

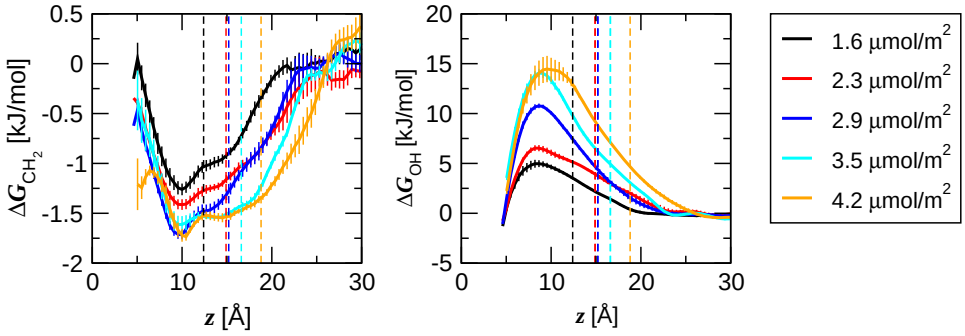

Figure 9.8: Incremental free energy profiles. Dashed vertical lines indicate the location of the GDS.

For the hydroxyl increment, the general shape of the free energy profile also shows little dependence on surface coverage. Moving from the mobile phase into the stationary phase the free energy of transfer increases and reaches a maximum at $z \approx 9$ Å (i.e., a free energy barrier) and then decreases as the silica surface is approached. The height of this barrier increases continuously from about 5 kJ/mol at the lowest density to about 15 kJ/mol at the highest density. The increased height of this barrier is the direct result of the depletion of water and methanol within the interior of the bonded phase.

9.3 Conclusions

Particle-based Monte Carlo simulations were carried out to examine the effects of grafting density on solute retention in RPLC. The simulated retention data shows excellent agreement with the thermodynamic data measured experimentally. The partition coefficients for both the polar and nonpolar solutes studied show a maximum as grafting density is increased. This maximum is found at lower densities for the polar solute. The molecular mechanism of solute retention does not appear do change drastically upon increasing grafting density. However, there are multiple modes of retention for both nonpolar and polar solutes and the relative importance of each of these modes does show dependence on bonding density.

Chapter 10

Effects of Polar Embedded Groups

10.1 Background

Alkyl-modified surfaces are extremely versatile materials, and among their most important applications is reversed-phase liquid chromatography (RPLC) where alkyl ligands grafted onto silica microspheres form the stationary phase. The separation of analytes in RPLC originates from the differing affinities of the analytes for the stationary and mobile phases. Octadecylsilane (C_{18}) ligands are most commonly used as bonded phase in RPLC, and through optimization of chromatographic parameters (mobile phase composition, temperature, and their gradients) an exceptionally wide range a separations can be achieved. However, in certain cases the chromatographer cannot find a set of parameters that allows for the necessary selectivity and/or reproducibility. In these cases one may desire to change the chemistry of the stationary phase itself. To this effect, a wide variety of RPLC phases containing polar functionality have become commercially available. One such class of phases, called polar-embedded phases, contain polar moieties within the alkyl chain. Most commonly this polar group is placed three methylene units up from the silica substrate and is followed by 8 to 18 more methylene

[†] This chapter describes the outcome of a collaborative research project carried out by Jake L. Rafferty and advised by J. Ilja Siepmann and Mark. R. Schure. A report on this research project has been published [71].

units. Common polar-embedded groups include amides, ethers, carbamates, and ureas.

Polar-embedded phases were originally developed to reduce peak tailing with basic analytes [186], but the molecular-level reasons for their improved performance are not yet fully understood. Peak tailing in RPLC is most often the result of strong interactions of the basic solute with the residual (acidic) silanols. It has been suggested that these interactions are reduced by polar-embedded phases through various mechanisms including a blocking of residual silanols on the silica substrate by the polar-embedded groups [187, 188, 189], a layer of solvent near the polar groups that shields the silanols [187, 190, 191], or protonization of the polar groups leading to ionic repulsion of basic solutes [192, 193, 194].

Polar-embedded RPLC phases can also be advantageous when highly aqueous phases are required [189, 190, 191] because of their improved wettability over the traditional alkyl phases. Furthermore, polar-embedded phases can offer unique separation selectivities [189, 194, 195, 196, 197, 198] and this opens up the door to wide variety of separations not possible on alkyl phases.

In order to more effectively use existing polar-embedded phases and to develop novel RPLC stationary phases with the desired characteristics, there is a need to better understand how these phases function at the molecular level. In particular, specific interactions of analytes with the polar-embedded groups may allow one to design chromatographic systems that enhance the importance of analyte functional groups for separation, rather that properties of entire molecules, such as lipophilicity, that dominate retention on the traditional alkyl phases. Thereby, one may achieve orthogonal retentive phases that better mimic the interactions of drug molecules or toxins with their natural targets [199]. Furthermore, the insight gained from this work on polar-embedded phases is relevant to numerous biological processes, for example, the transport of drugs across lipid bilayers.

To provide a molecular-level understanding of polar-embedded RPLC phases, the present study examines three different stationary phases using molecular simulation. The first phase contains an embedded amide functionality, the second possesses two ether groups, and the third is a traditional alkyl phase for comparison (see Figure 10.1). In particular, the effects of these polar-embedded groups on stationary-phase wetting,

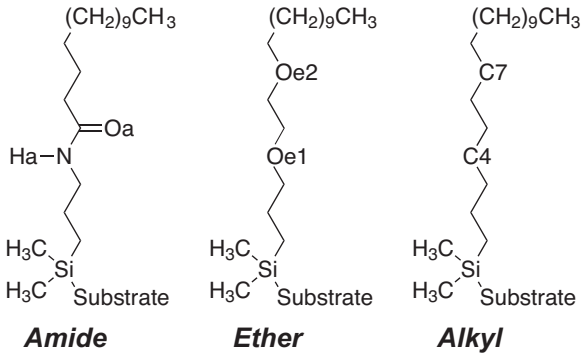

Figure 10.1: Bonded phase chemical structures.

chain conformation, and solute retention are examined. In addition, the possible mechanisms for reduced silanol activity with polar-embedded phases are discussed.

10.2 Simulation Details

Configurational-bias Monte Carlo simulations in the NpT version of the Gibbs ensemble were carried out to investigate the structural and retentive properties of three different reversed-phase packings in contact with methanol/water mobile phases ranging in composition from pure water to pure methanol. As described in Chapter 5, the Gibbs ensemble simulations utilize three separate simulation boxes that are in thermodynamic contact but do not share an explicit interface. The first simulation box contains the model stationary phase in contact with solvent while the second and third boxes contain a mobile phase solvent reservoir and a ideal vapor phase, respectively.

The three different stationary phases used in this study were a traditional alkyl phase, a phase with an amide functionality, and a phase with two ether groups. The chemical structures of the chains in each of the three phases are shown in Figure 10.1. For the polar-embedded phases, the polar group was placed three methylene groups up from the silicon link atom and the length of the terminal alkyl segment following the polar group was chosen such that polar embedded chains had the same number of backbone segments as the C_{18} alkyl phase chains. All simulations were carried out with the bonded phase chains at the exact same grafting sites on the silica substrate in

order to afford a direct comparison. In addition to different stationary phases, mobile phases with four different water-methanol compositions were used: 0, 0.33, 0.67, and 1.0 molfraction methanol (denoted as systems WAT, 33M, 67M, and MET, respectively). The total numbers of solvent molecules ranged from 1200 in system WAT to 800 in system MET. Also present was a set of solutes (2 each of 1 to 4 carbon n-alkanes and n-alcohols) that allowed for an examination of the retention mechanism.

The simulations were performed at a temperature of 323 K and a pressure of 1 atm. At each solvent/stationary phase composition four independent simulations were carried out. Each independent simulation was equilibrated for at least 2 x 10^5 Monte Carlo (MC) cycles followed by an additional 2 x 10^5 MC cycles for production. One MC cycle corresponds to N MC moves, where N is the number of molecules in the three-phase system. Statistical uncertainties in the reported quantities were estimated from the standard error of the mean of the results from four independent simulations.

10.3 Results and Discussion

Snapshots of equilibrated configurations for each of the three bonded phases in system 33M are shown at the top Figure 10.2. From these, it can be immediately observed that a large number of solvent molecules are located within the polar-embedded phases while the alkyl phase is nearly void of solvent except very near the substrate. However, other differences between the three phases are more subtle and require a full analysis of the simulation trajectory.

10.3.1 Solvent Penetration and Wetting

In addition to the snapshots, Figure 10.2 also depicts the ensemble averaged density profiles for the solvent molecules and the bonded-phase atoms as a function of z, the distance from the silica surface. Starting at the silica surface and increasing in magnitude of z, a variety of different structural features in the solvent density are seen. The first is a sharp peak at $z \approx 3$ Å and is present in all systems. This peak corresponds to solvent molecules H-bonded to the dangling silanol groups (see Chapter 6). Next, and also in all systems, comes a region near $z \approx 5$ Å where the solvent density shows a minimum. This is a result of the crowding caused by the dimethyl side chains on the

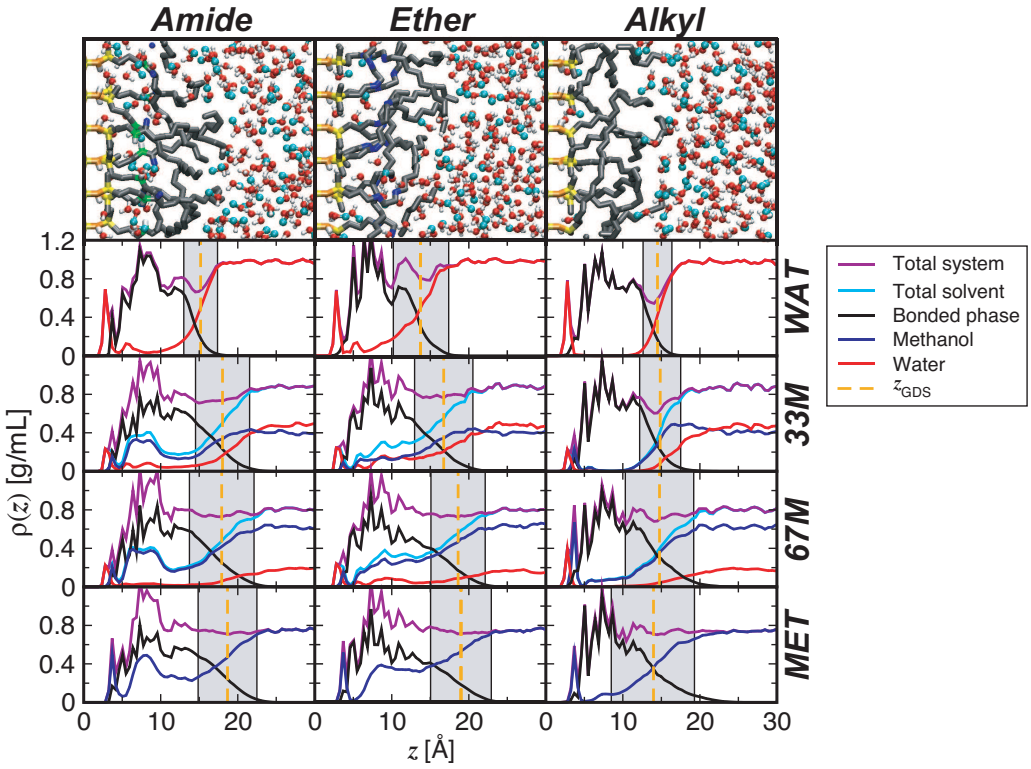

Figure 10.2: Snapshots of the three stationary phases with solvent 33M and density profiles for all 12 systems examined. The gray shaded area represents the interfacial region. The snapshots correspond to the same z-scale as the density profiles.

silane group (for clarity, these are not shown in the density profiles).

Moving further outward from the substrate, one begins to see distinct differences between the twelve stationary phase/solvent systems. For the polar-embedded phases, a significantly larger solvent density is found within the stationary phase for all mobile phase compositions. The amount of solvent penetration is smallest for the pure water systems, but it is noted that the water density extends all the way through the polar-embedded phases to the substrate while most of the alkyl phase is void of the solvent. The ether phase appears to be most wettable in pure water.

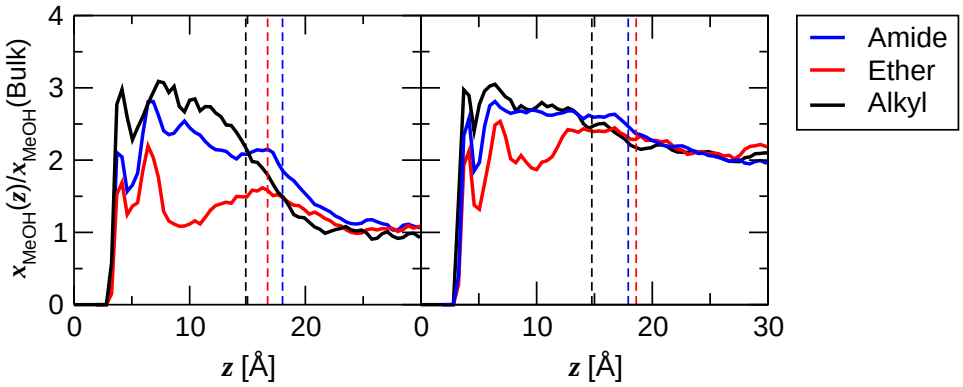

Figure 10.3: Local methanol molfraction enhancement profiles for systems 33M (left) and 67M (right).

For both the ether and the amide phase the overall solvent density within the stationary phase increases dramatically when moving from WAT to 33M, but then increases to a lesser extent with further increases in methanol content. This is also reflected by a corresponding shift of the Gibbs dividing surface (GDS) of the solvent to larger z-values for the two polar-embedded phases, while the location of the GDS does not depend strongly on the solvent composition for the alkyl phase.

The solvent density profiles show marked differences between the two polar phases. For the amide phase there is a maximum in the solvent density at $z \approx 9$ Å (corresponding to the position of the amide group) and a minimum around 12 Å. For the ether phase, the solvent density is less structured and shows a plateau for $8 < z < 14$ Å. Continuing on from the core of the bonded phase, the interfacial region is examined. Two key features are noted in this interfacial region, an enrichment in the methanol concentration for the mixed solvents and a minimum in the total density for solvents WAT and 33M. This minimum indicates a partial drying effect at the interface [133] and is most prevalent with pure water. The drying is less apparent for the polar embedded phases, especially the ether phase, and becomes insignificant with increasing methanol concentration. An analysis of the local mole fraction enhancements as a function of z (see Figure 10.3) shows that the alkyl phase has the highest affinity for methanol. The amide phase follows closely behind while the ether phase shows a much smaller methanol enrichment.

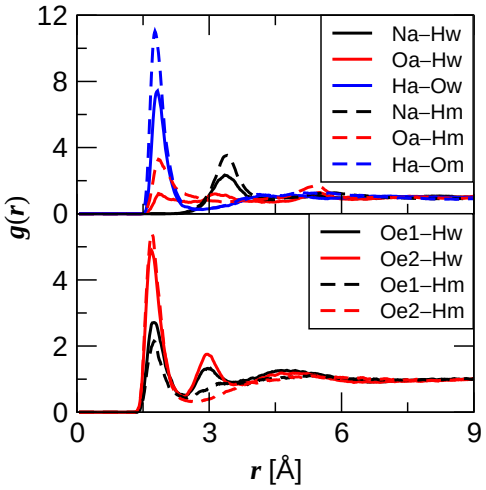

Figure 10.4: Bonded phase–solvent radial distribution functions for the amide (top) and ether (bottom) phases in solvent 33M. Definition for the atom labels in the legend is given in Table 10.1.

The maximum in methanol mole fraction enhancement occurs at $z \approx 8$ Å for all three stationary phases, but the peak is sharper for the polar embedded phases and is located near where the polar groups reside.

Information on the specific interactions between polar-embedded groups and solvent molecules can be gleaned from the radial distribution functions (RDFs) in Figure 10.4 and the analysis of the H-bonding presented in Table 10.1. For the amide phase, the RDFs indicate very strong H-bonding between the amide hydrogen and solvent oxygen (blue lines) and to a lesser degree between the carbonyl oxygen and the polar hydrogen of the solvent (red lines), whereas there is little indication for H-bonding to the amide nitrogen. For the ether phase, the RDFs show that the oxygen atom in position 7 of the chain is better solvated than the other oxygen atom. The relative peak heights indicate that the amide group is preferentially solvated by methanol, while in particular the ether oxygen in position 4 is preferentially solvated by water. The analysis of the number of H-bonds provides more quantitative information on these preferences. For example, opposite of what one would suspect based on the bulk solvent mole fractions, the amide phase forms twice as many H-bonds with methanol than with water in system

Table 10.1: Number of hydrogen bonds with solvent per stationary phase chain.[a,b]

Label	Definition			
Ow	water oxygen	Oa	amide oxygen	
Hw	water hydrogen	Ha	amide N-hydrogen	
Om	methanol oxygen	Oe1	bottom ether oxygen	
Hm	methanol hydrogen	Oe2	top ether oxygen	
		Amide Phase		
Solvent	Ha–Ow	Oa–Hw	Ha–Om	Oa–Hm	Total
WAT	0.36_3	0.35_2	–	–	0.71_5
33M	0.22_1	0.15_1	0.52_3	0.24_2	1.14_6
67M	0.08_1	0.09_1	0.71_2	0.30_3	1.19_7
MET	–	–	0.78_2	0.33_4	1.11_5
		Ether Phase		
Solvent	Oe1–Hw	Oe2–Hw	Oe1–Hm	Oe2–Hm	Total
WAT	0.45_1	1.00_1	–	–	1.44_2
33M	0.41_1	0.73_2	0.10_1	0.25_1	1.49_4
67M	0.28_2	0.46_3	0.16_1	0.44_3	1.34_9
MET	–	–	0.21_1	0.67_1	0.89_2

[a]Subscripts indicate the standard error of the mean in the final digit.
[b]The amide nitrogen accepts a H-bond for less than 1% of chains.

33M (i.e., an enrichment by a factor of 4), while the ether phase forms about 25% more H-bonds with water than with methanol in system 67M (i.e., an enrichment by a factor of 2.5). Interestingly, the ether phase forms more H-bonds than the amide phase for all but system MET and is well wetted even for system WAT (see also Figure 10.2). The amide phase's reduced affinity to H-bond with water is likely the reason for a lower solvent density within the stationary phase in system WAT (see Figure 10.2). However, it is noted that the amide phase's strong preference to H-bond with methanol may allow it to be well solvated even in low-methanol mobile phases, e.g. 5% methanol.

10.3.2 Interactions of Polar-embedded Groups with Silanols

One possible reason for the reduced silanol activity found for the polar-embedded phase is that these polar groups may interact directly with the silanol groups thereby competing with the solutes for these silanol adsorption sites [187, 188, 189]. The simulations indicate that this explanation is unlikely. That is, the polar-embedded group–silanol

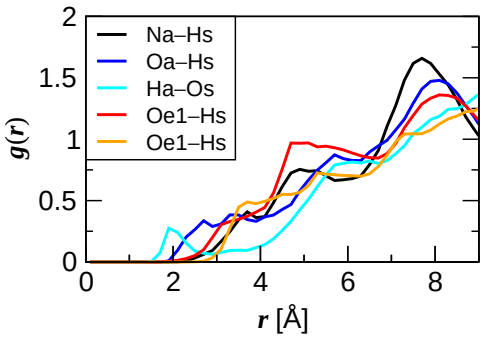

Figure 10.5: Polar-embedded group–silanol radial distribution functions in solvent system 33M. Labels Hs and Os correspond to the silanol hydrogen and oxygen, respectively.

RDFs in general do not exhibit any pronounced peaks at distances typical for a H-bond (see Figure 10.5 for system 33M) and only a small peak is found for the amide hydrogen–silanol oxygen. A H-bond analysis shows that, in all solvent systems, much less than 1% of polar-embedded groups form a H-bond with silanols. The reasons for this lack of H-bonding are likely geometric strain and steric limitations. There is only a three methylene group spacer between the polar group and the substrate and this small portion chain is simply not flexible enough to assume a conformation that brings the polar group in close enough contact with the silica surface. Furthermore, the two methyl side groups lead to steric crowding near the silica surface.

10.3.3 Bonded Phase Conformation

While the structure of various alkyl stationary phases in RPLC has been the topic of many experimental studies, little work has been done to characterize the structure of stationary phases with incorporated polar groups. Therefore, this section will focus on analyzing the structure of the polar embedded phases simulated in this work and comparing these results to the alkyl phase. A variety of measures describing chain conformation can be used to establish the structural similarities and differences between the different bonded phases studied here (see Table 10.2). These measures aim at discerning order and disorder in the stationary phase and can be used to explain the retentive characteristics of these phases, which it the topic of the following section.

Table 10.2: Averages of some conformational properties for stationary phases with and without polar embedded groups.[a,b]

	WAT			33M		
	Amide	Ether	Alkyl	Amide	Ether	Alkyl
r_{ete}/ [Å]	14.8_1	14.7_4	16.2_4	15.6_6	15.1_4	15.7_4
$z_{\mathrm{CH_3}}$/ [Å]	11.2_1	10.0_1	9.1_1	15.0_3	13.5_2	11.5_1
$\cos\theta_{\mathrm{ete}}$	0.48_3	0.39_2	0.37_2	0.69_9	0.59_7	0.43_3
S_{16}	-0.023_3	-0.05_1	-0.14_2	0.17_1	0.07_1	-0.10_1
f_{gauche}	0.30_2	0.28_1	0.25_1	0.29_1	0.31_1	0.27_1
	67M			MET		
	Amide	Ether	Alkyl	Amide	Ether	Alkyl
r_{ete}/ [Å]	16.1_3	15.7_2	16.1_3	16.4_5	16.0_3	16.4_3
$z_{\mathrm{CH_3}}$/ [Å]	15.4_2	15.5_3	11.9_2	16.1_2	15.6_2	12.0_2
$\cos\theta_{\mathrm{ete}}$	0.69_3	0.69_5	0.52_2	0.74_6	0.68_6	0.49_6
S_{16}	0.19_1	0.14_3	-0.08_2	0.21_1	0.17_1	-0.06_1
f_{gauche}	0.28_1	0.30_1	0.26_5	0.28_1	0.29_2	0.25_1

[a]Subscripts indicate the standard error of the mean in the final digit.
[b]These conformational properties are defined in Chapter 5.

The density profiles for the different stationary phases (see Figure 10.2) already give some indication of chain conformation. As methanol content in the mobile phase is increased, the bonded phase density extends further into the mobile phase, and this extension is greater for the polar-embedded phases. The extension of the chains can be quantified by the average height of the terminal methyl group, $z_{\mathrm{CH_3}}$, which increases significantly with increasing methanol concentration and is typically about 3–4 Å larger for the polar-embedded phases as compared to the alkyl phase.

Chain alignment can be quantified by $\cos\theta_{\mathrm{ete}}$, or the cosine of the angle between chain end-to-end vectors and the normal to the silica substrate. Values of unity for the cosine indicate a chain orientation perpendicular to the silica surface and values of zero indicate chains parallel to the surface. Table 10.2 gives the average value of $\cos\theta_{\mathrm{ete}}$ while Figure 10.6 depicts its distribution. These data indicate that the chains prefer a more erect conformation for all bonded phases when the methanol fraction is increased. Comparing the different stationary phases shows that (with the exception of system WAT where the distributions are similar) the polar-embedded phases have a stronger preference for vectors being perpendicular to the substrate. The average

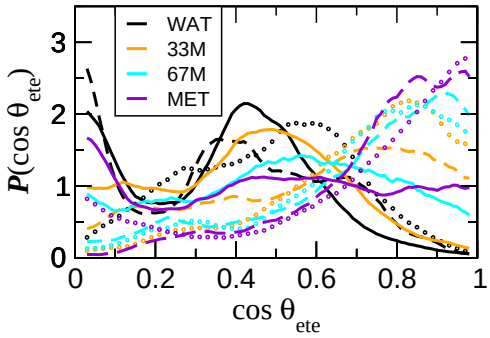

Figure 10.6: Probability distribution for the cosine of the angle between the chain end-to-end vector and the normal to the silica substrate. The amide, ether, and alkyl phases are represented by dotted, dashed, and solid lines, respectively.

values of $\cos\theta_{\text{ete}}$ are largest for the amide phase, closely followed by the ether phase, and smallest for the alkyl phase in all four solvents.

Complementary, but more localized, information on chain alignment can be gained from the orientational order parameter S_i along the chain backbone (defined in Chapter 5). As seen in Figure 10.7, the first 1–3 vector (S_1) prefers to be perpendicular to the substrate and the terminal 1–3 vector (S_{16}) shows a near random orientation for all three bonded phases in solvent 33M . However, what happens in between these two end vectors is different for the three bonded phases. For the amide phase, the S_3 to S_5 values are larger than for the other phases. These vectors correspond to the position of the amide group and the larger S values are likely due to its rigidity (and intermolecular H-bonding, see below). The remaining portion of the amide phase is very similar to the ether phase and the S_i values for both polar-embedded phases are shifted upward compared to the alkyl phase. Although not shown here, the order parameters for the other solvent compositions show very similar trends.

The fraction of gauche defects along the chain backbone in solvent 33M is also depicted in Figure 10.7. Interestingly, the total number of gauche defects are quite similar for all twelve systems (see Table 10.2). The polar-embedded chains have slightly more gauche defects (≈29%) than the alkyl phase (≈25%). However, an examination of the fraction of gauche defects along the chain backbone indicates striking patterns of

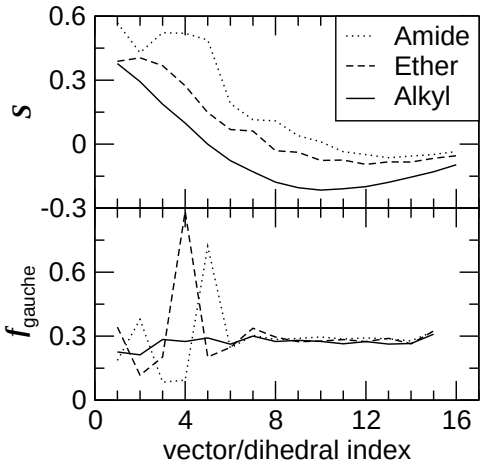

Figure 10.7: Order parameter (top) and fraction of gauche defects (bottom) along the chain backbone in solvent 33M.

conformational defects near the grafting point for the polar-embedded phases, while the the alkyl chains show a relatively flat profile. For example, the dihedral angle possessing the most defects involves O–C–C–O for the ether phase and the torsion with the least gauche defects involves C–NH–CO–C for the amide phase, i.e., the two ether groups introduce flexibility in the backbone while the amide group is relatively rigid.

The various measures of stationary phase chain order presented above mostly indicate that the polar-embedded phases are more ordered than the standard alkyl phase. This enhanced ordering may simply be due to the increased amount of solvent within the more wettable polar-embedded phases. However, this enhanced ordering may also be the result of specific H-bond interactions in which solvent molecules can tether the chains to each other or to the residual silanol groups. Furthermore, since the amide group possesses both H-bond donor and acceptor capabilities, these chains can directly H-bond with each other. Diagrams of these possible hydrogen bond tethers along with a simulation snapshot of a solvent mediated tether are shown in Figure 10.8. The numbers of such H-bonded tethers per stationary phase chain are listed in Table 10.3.

For the amide phase, there are ≈0.27 direct H-bonds between embedded groups for the WAT mobile phase, while the number is close to 0.08 for the methanol-containing phases. Overall, there are more solvent-mediated tethers and direct links for WAT

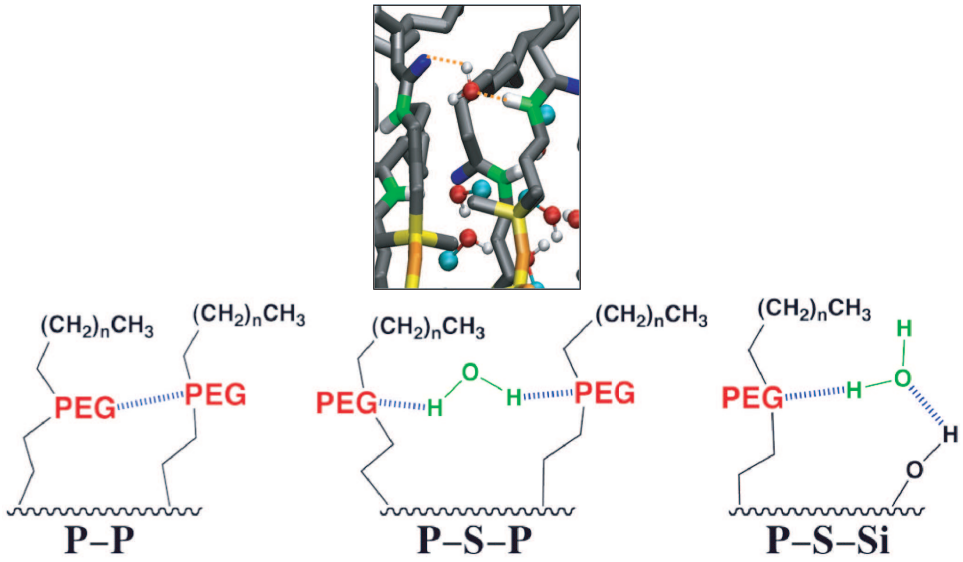

Figure 10.8: Definitions of the different types of hydrogen bonded tethers for polar embedded groups (PEG) and snapshot of a solvent mediated tether.

Table 10.3: Number of hydrogen-bonded tethers per stationary phase chain.[a,b]

	Amide Phase			Ether Phase	
	P–P[b]	P–S–P[c]	P–S–Si[d]	P–S–P	P–S–Si
WAT	0.27_8	0.16_2	0.38_9	0.20_3	0.16_2
33M	0.08_4	0.26_7	0.06_3	0.05_1	0.17_6
67M	0.05_3	0.24_7	0.06_4	0.08_2	0.17_9
MET	0.10_4	0.18_5	0.03_1	0.00_0	0.03_2

[a]Subscripts indicate the standard error of the mean in the final digit.
[b]The definitions of P–P, P–S–P, and P–S–Si are depicted in Figure 10.8

solvent (0.82 and 0.36 for the amide and ether phase, respectively) than for the other solvents, which makes sense since water has more H-bond donor sites than methanol. For the three methanol containing solvents, solvent tethers between amides are more prevalent, while tethers to silanols are more prevalent for the ether phase. The significant amount of direct interchain H-bonding and solvent tethers helps to explain why amide phase is slightly more ordered than the ether phase and both are significantly more ordered than the alkyl phase.

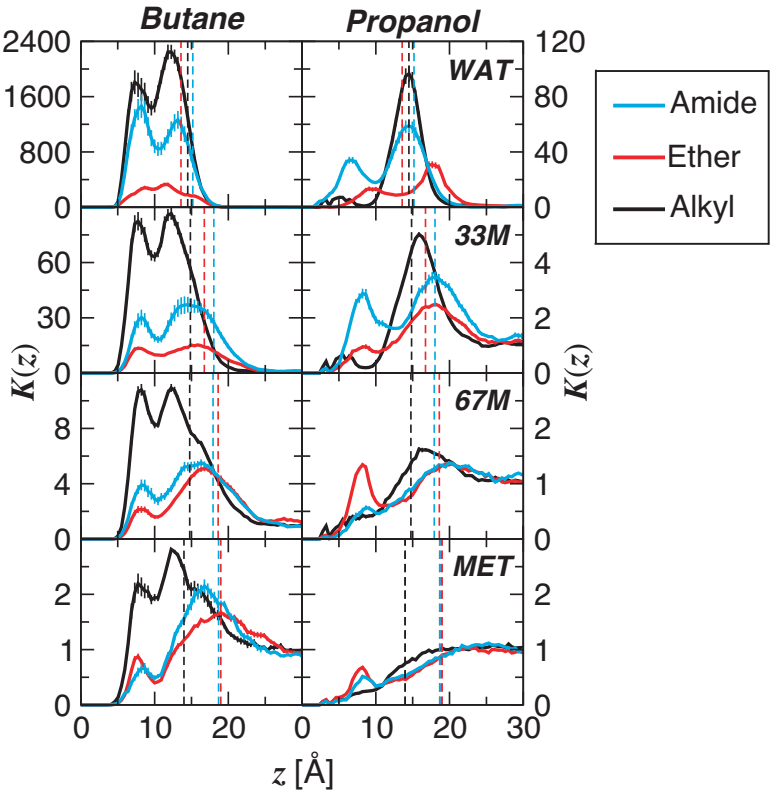

Figure 10.9: Distribution coefficient profiles for n-butane and 1-propanol on stationary phases with and without polar-embedded group. Dashed vertical lines denote the GDS.

10.3.4 Solute Retention

In order to understand the retention mechanism on polar-embedded phases, one needs to know where the solutes are preferentially retained and how the polar groups change the solute's H-bonding in comparison to traditional alkyl phases. Figure 10.9 depicts the the z-dependent distribution coefficients, or $K(z)$ profiles, for two of the probe solutes, n-butane and 1-propanol.

For n-butane, the shape of the $K(z)$ profiles is similar for the three different stationary phases and four solvents. The profiles are all bimodal with one peak near the center of the bonded phase ($z \approx 8$ Å) and another in the interfacial region, but inside of the GDS. However, as the methanol content is increased for the polar phases, the

peak in the center of the bonded phase becomes smaller relative to the interfacial peak. This is likely due to the large number of methanol molecules present in this region of the stationary phase (see Figure 10.2) as these can compete for space with the solute.

Regardless of bonded phase chemistry, the magnitude of $K(z)$ decreases dramatically with increasing methanol concentration. However, in all solvents the ether phase is the least retentive for n-butane while the alkyl phase is the most retentive. For system WAT, the retention of the nonpolar solute is similar on the alkyl and amide phases while the ether phase shows much less retention, especially in the interfacial zone. Again, this is likely due to solvent competition since the ether phase is most wettable in pure water and shows the largest overall density in the interfacial region. As the methanol concentration increases, the retentive properties of the polar-embedded phases begin to converge as both become saturated with solvent.

For 1-propanol in the alkyl phase, the strongest retention is observed in the interfacial region ($K(z)$ peak at $z \approx 15$ Å). There is very little retention in the center of the bonded phase, but small peaks around $z = 5$ Å indicate some retention near the silica substrate. 1-Propanol's interfacial affinity can be attributed to the favorable interaction of the hydrophobic tail with the stationary phase while its polar head remains in the solvent (see Chapter 7). For the polar-embedded phases, the $K(z)$ peak in the interfacial region is somewhat smaller and there is much more retention in the center of the bonded phase near the polar groups. This enhancement in retention in the center of the bonded phase results from the polar solute's ability to overcome the increased entropic cost of cavity formation through favorable H-bond interactions with the embedded group and the increased amount of sorbed solvent (see discussion below).

Free energy profiles for the retention of the methylene increment, $\Delta G_{\mathrm{CH_2}}(z)$, are presented in Figure 10.10. This quantity was chosen because it is frequently used to characterize RPLC columns and relates to the bonded phase's lipophilicity. The $\Delta G_{\mathrm{CH_2}}(z)$ profiles indicate that the methylene selectivity is lower for polar embedded phases in all solvent compositions studied, an observation also seen experimentally [189, 194, 195]. The ether phase shows the smallest affinity for the methylene group, probably the result of its preference to sorb water. As the methanol content of the mobile phase is increased, the three phases begin to converge in their methylene selectivity. This follows the trend of other the stationary phase properties reported here. All of the $\Delta G_{\mathrm{CH_2}}(z)$ profiles

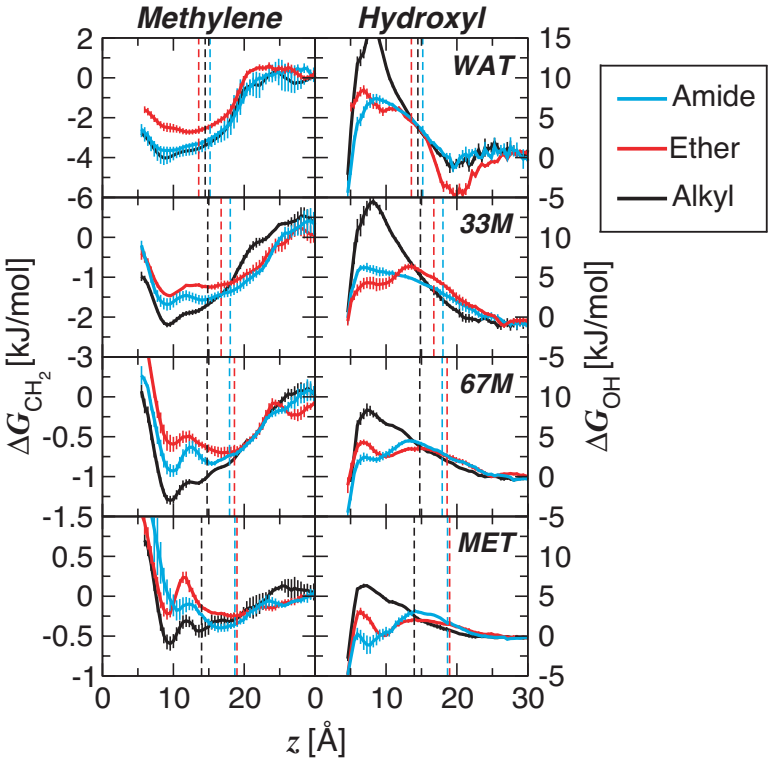

Figure 10.10: Incremental free energy profiles for methylene and hydroxyl groups on stationary phases with and without polar embedded groups.

have a minimum at $z \approx 9$ Å. At high methanol concentration (67M and MET), a second minimum appears for all phases just below their GDS. Nevertheless, for the alkyl phase the methylene selectivity is always greatest in the center of the bonded phase, i.e. partitioning is more important, but for the polar embedded phase adsorption at the bonded phase/solvent interface becomes more important at high methanol concentration. As explained for butane's $K(z)$ profile, this is most likely due to the increased amount of solvent within the polar-embedded phases that competes for space with the solutes near the polar-embedded groups.

To examine the affinity of the different stationary phases for polar groups, incremental free energy profiles for the hydroxyl group, $\Delta G_{\mathrm{OH}}(z)$, are presented in Figure 10.10. The $\Delta G_{\mathrm{OH}}(z)$ profiles show the opposite trend as observed for the methylene increment,

Table 10.4: Number of hydrogen bonds per alcohol solute molecule in stationary phases with and without polar-embedded group.[a,b]

	Amide Phase			Ether Phase			Alkyl Phase	
Solvent	N^{c}_{chain}	N_{SiOH}	N_{in}	N_{chain}	N_{SiOH}	N_{in}	N_{SiOH}	N_{in}
WAT	0.29_9	0.12_4	0.65_6	0.02_1	0.01_2	0.66_3	0.12_4	0.43_6
33M	0.12_2	0.03_1	0.93_3	0.07_1	0.05_2	0.80_2	0.08_2	0.41_3
67M	0.12_2	0.04_1	0.81_2	0.06_1	0.01_2	0.93_3	0.09_2	0.57_5
MET	0.10_2	0.04_1	0.81_3	0.09_1	0.05_2	0.83_2	0.07_1	0.41_1

[a]A solute is defined to be in the retentive phase when it is in the first solvation shell (6 Å) of any stationary phase segment.
[b]Subscripts indicate the standard error of the mean in the final digit.
[c]N_{chain}, N_{SiOH}, and N_{in} indicate the average H-bonds with polar-embedded groups, silanol groups, and sorbed solvent molecules (i.e., solvent inside the GDS).

i.e., selectivities for the hydroxyl group are higher in the polar embedded phases. For both the alkyl and polar phases, the free energy is lowest near the substrate and in the interfacial region. In between these two favorable locations there exists a free energy barrier. For the alkyl phase this free energy barrier is much higher, i.e., $\approx$ 10 kJ/mol higher as compared to either of the polar phases in systems WAT and 33M. The higher free energy barrier indicates that transfer of polar solutes from the mobile phase to the silica surface will be slower on the alkyl phase, a point that will become important later.

For alcohol solutes it is also of interest to understand how specific H-bond interactions contribute to the differences in retentive properties between the alkyl and polar-embedded phases (see Table 10.4). In all cases the alcohol solutes are able to form more H-bonds when inside the polar-embedded phases than when they are inside the alkyl phase. For example, in solvent 33M, the solutes form on average 1.09 H-bonds in the amide phase, 0.91 in the ether phase and 0.49 in the alkyl phase. Much of this increase in H-bonding is due to interactions with sorbed solvent, which is more prevalent in the more wettable polar-embedded phases. However, the solutes can directly H-bond with the polar-embedded groups, and it is found that the alcohols tend to form more H-bonds with the amide group than with the ether groups. Also of interest, the number of solute H-bonds with the silanol groups decreases significantly from a value of $\approx$0.09 for the alkyl phase (averaged over all four solvent compositions) to $\approx$0.06 for the amide phase and $\approx$0.03 for the ether phase.

Table 10.5: Incremental free energies of retention for methylene and hydroxyl groups.[a]

	ΔG_{CH_2}			ΔG_{OH}		
	Amide	Ether	Alkyl	Amide	Ether	Alkyl
WAT	-3.4_2	-2.4_2	-3.6_2	4.9_3	3.3_8	8.0_1
33M	-1.5_1	-1.24_2	-1.80_7	4.6_3	4.3_2	7.1_1
67M	-0.75_5	-0.61_8	-1.06_4	3.3_2	3.1_2	5.1_1
MET	-0.31_7	-0.16_4	-0.4_1	1.9_2	1.6_2	4.3_6

[a]Subscripts indicate the standard error of the mean in the final digit.

As discussed in Chapter 5, the incremental free energy profiles can be converted to net incremental free energies of retention. Use of the incremental free energies for the methylene and hydroxyl groups facilitates direct comparisons with experimental data based on retention measurements because these values are independent of the phase ratio. The free energies of retention for the methylene and hydroxyl increments are summarized in Table 10.5. It should be noted that, as discussed in Chapter 7, the methylene increment computed from simulation for a C_{18} alkyl phase in contact with water/methanol mobile phase shows excellent agreement with experimental data of Barman [171].

Recently, Euerby and Petersson studied a variety of stationary phases including three commercially available ones with embedded amide groups (and endcapped silanol groups) [189]. From their data for a 65/35 (v/v) methanol/water mobile phase, one obtains $\Delta G_{CH_2} = -0.82$ kJ/mol and ΔG_{OH} =4.1 kJ/mol. Data from similar work of Layne [194], but for a 65/35 (v/v) acetonitrile/water mobile phase, yields $\Delta G_{CH_2} = -0.83$ kJ/mol. The 33M and 67M solvent compositions used here correspond to ≈50% and ≈80% methanol by volume, and the corresponding free energies of retention for the methylene and hydroxyl groups bracket the experimental values by Euerby and Petersson. This validation from experimental thermodynamic measurements for the alkyl and amide phases suggest that one can indeed be confident in the microscopic information from the simulations.

10.3.5 Peak Tailing

As mentioned in the beginning of this chapter, three different explanations for the reduced peak tailing obtained with polar-embedded phases can be found in the literature [187, 188, 189, 190, 191, 192, 193, 194]. The first two explanations are related to a reduction in the accessibility of silanols either by direct H-bonding with the polar-embedded group or by an increased amount of solvent near the polar-embedded groups. The simulations show that the polar-embedded groups do not directly interact with the silanols, but that a significant amount of solvent tethers lead to a connection of polar-embedded groups with the silanols (see Table 10.3). The simulations also indicate that there is a great deal more solvent within the stationary phase for the polar-embedded phases, suggesting a greater saturation of the silanols by sorbed solvent. However, in Chapter 6 it shown that for a C_{18} phase in contact with water/methanol mixtures, the residual silanol sites are already saturated with solvent. Nevertheless, these two factors together yield to a significant reduction in the amount of H-bonding between alcohol solutes and residual silanols (see Table 10.4). The third possible explanation, that the polar-embedded group can become protonated and repel basic solutes, cannot be investigated with the current methodology because proton transfer is not allowed. Nevertheless, it is noted that the ether group is not basic and the amide group is only very slightly basic, thus protonation is not likely to play an important role for the polar-embedded phases studied here.

Based on the free energy profiles for the hydroxyl group (Figure 10.10), a new explanation for the reduction in peak tailing is proposed. For all stationary phases and all solvent compositions, there is a free energy barrier for the polar hydroxyl group to travel from the mobile phase to the silica substrate, but this barrier is greatly reduced (by as much as 10 kJ/mol) for the polar-embedded phases. This diminished free energy barrier should allow for relatively rapid transfer of polar solutes between the mobile phase and the silanol groups, and thus allow for a large number of adsorption/desorption events with the silanols during the retention process. Thus, peak tailing is reduced by a speed up in the kinetics, rather than by a reduction in silanophilic interactions.

10.4 Conclusions

The structural and retentive properties of three model RPLC systems, including a traditional alkyl phase and two polar-embedded phases, were studied by molecular simulation. The results show that specific H-bond interactions between solvent and the embedded polar groups makes the polar-embedded phases much more wettable than the alkyl phase. In addition, H-bond interactions directly between polar-embedded groups or through solvent tethers, lead to an enhanced ordering and more erect conformations for the polar-embedded phases.

The distribution coefficient profiles for alkanes and alkanols and the incremental free energy profiles for the methylene and hydroxyl groups indicate non-uniform affinities for the solutes within the bonded phases. These rugged free energy profiles bear similarities with those computed for phospholipid membranes [200]. The free energy profiles show that the polar-embedded phases are less selective for nonpolar species and this is likely a result of competition with solvent for space within the stationary phase. In contrast, the polar-embedded phases are more selective for polar groups, but the free energy for retention of the hydroxyl group is positive in all three phases. A larger number of H-bond sites within the polar-embedded phases, from both sorbed solvent and the polar-embedded groups themselves, are the reason for this enhanced affinity for polar solutes.

The simulations indicate that H-bonding between polar analytes and surface silanols is reduced by the polar-embedded phases and, more importantly, that these phases possess a diminished free energy barrier for the transfer of polar solutes from the mobile phase to the surface silanols. These two factors together are most likely responsible for the reduction in peak tailing with polar-embedded phases.

These results demonstrate that molecular-level insights gained from simulation can help to explain retention mechanisms in diverse RPLC systems. This may lead to the possibility of using simulation to explore and develop RPLC systems with enhanced selectivities for specific functional groups as found in drug molecules and toxins.

Chapter 11

The Effects of Chain Length, Pressure, and Pore Shape on Structure and Retention

There are a host of chromatographic parameters that can be adjusted when one seeks to achieve the most efficient separation. The chromatographer often spends a great deal of time optimizing these various chromatographic parameters each time a new separation problem is encountered. These method development tasks could be greatly facilitated by a more in depth, molecular-level understanding of how these different parameters effect structure and retention in RPLC. Previous chapters in this thesis have dealt with the effects of mobile phase composition, surface coverage, and polar embedded groups. In this chapter, simulations examining the effects of stationary phase chain length, pressure and pore shape are discussed. More background on each of these chromatographic parameters will be given in the Results and Discussion Section.

[†] This chapter describes the outcome of a collaborative research project carried out by Jake L. Rafferty and advised by J. Ilja Siepmann and Mark. R. Schure. A report on this research project has been published [74].

11.1 Simulation Details

In order to discern the effects of chain length, pressure, and pore shape, the configurational-bias Monte Carlo method was applied in the NpT Gibbs ensemble. As with the rest of the work described in this thesis, three simulations boxes were used; the first containing the stationary phase in contact with solvent, the second a bulk solvent reservoir, and the third a vapor phase. The simulations examining chain length make use of the planar slit pore setup described in Chapter 5. C_1, C_8, or C_{18} stationary phases were generated by grafting trimethyl, dimethyl octyl, or dimethyl octadecyl silanes to the two silica surfaces at a coverage of 2.9 μmol/m^2 (residual silanol density of 4.8 μmol/m^2). The chains were placed at the same random grafting locations on the silica surface (but avoiding chain overlap) to eliminate any effects due to chain/silanol arrangement. These simulations used a constant pressure of 1 atm. Pressure effects were examined by carrying out simulations of a C_{18} stationary phase, as described above, at multiple pressures (1, 400, and 1000 atm). Pore shape effects were examined by using an analogous three-box setup, but with a 60 Å cylindrical pore in place of a planar slit pore.

The cylindrical pore (Figure 11.1) was set up by first generating a slab of β-cristobalite with $L_x = 71.7$, $L_y = 21.5$, and $L_z = 71.7$ Å. A cylinder of diameter 60 Å was cut out of this slab by removing all atoms within 30 Å of the center of the slab's x-z plane. The resulting under-coordinated silicon and oxygen atoms at the cylinder's surface were capped with hydroxyl groups and hydrogen atoms, respectively. These new silanol sites were then randomly chosen as grafting sites for the C_{18} alkyl chains until a surface coverage of 2.9 μmol/m^2 was achieved (but avoiding chain overlap). The resulting density of residual silanol groups was 5.8 μmol/m^2. However, roughly a third of these were geminal and the total density of hydroxyl groups at the silica surface was 7.8 μmol/m^2, i.e., about 60% higher than for the slit pore setup. Simulations of the cylindrical pore were carried out at a pressure of 400 atm. This higher pressure was used, rather than the typical 1 atm, to avoid any possible issues with dewetting of the small pore at lower pressures [138].

Simulations for both the slit and cylindrical pore setups were carried at a temperature of 323 K and with a total of 800 water and 400 methanol (33% molfraction methanol). All systems also contained 14 solute molecules (two each for methane to

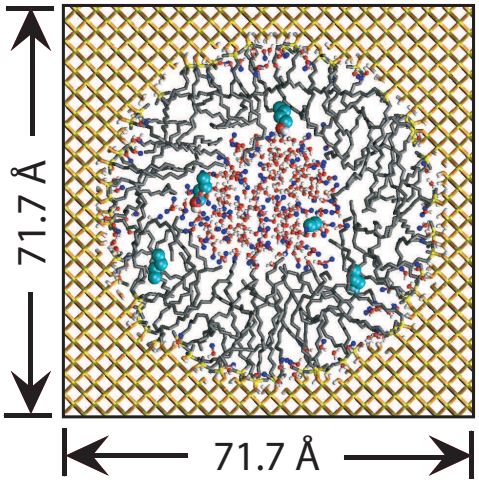

Figure 11.1: Simulation snapshot of the slitpore used for the examination of surface curvature effects. Water and methanol molecules are shown in the ball and stick representation with methyl groups, oxygens, and hydrogens in blue, white, and red, respectively. The stationary phase is depicted as tubes with CH_x groups in gray, silicon in yellow, oxygen in orange, and hydrogen in white. Solute molecules are represented by larger spheres with CH_x groups in cyan, oxygen in red, and hydrogen in white.

n-butane and ethanol to 1-butanol) and 20 helium atoms. The solute molecules allowed for an exploration of the retention mechanism and the helium was present to maintain a vapor box of adequate size. For the slit pore setup there were 18 stationary phase chains (9 on each side of the silica slab) and for the cylindrical pore there were 67 chains.

To generate equilibrated configurations for these systems, the alkyl chains were first allowed to relax in the absence of solvent (in vacuum) for a brief period via CBMC regrowths. After this, solvent molecules were randomly added to the box containing the stationary phase. After no further solvent could be added without overlap, the box containing the stationary phase was placed in thermodynamic contact with the mobile and vapor phase boxes. The simulations were then equilibrated for at least 2×10^5 Monte Carlo (MC) cycles. Following this was a production period of another 2×10^5 MC cycles during which average quantities were computed. For each system studied here, four independent simulations were run. Statistical uncertainties in all reported quantities were estimated from the standard error of the mean from these four independent simulations.

11.2 Analysis Details

Various properties used to characterize system structure and solvent distribution were defined in Chapter 5. However, some of these definitions need to be modified for discussion of the current systems. Chain alignment will again be quantified by the orientation of the chain end-to-end vector through $\cos\theta_{\mathrm{ete}}$. But here, the end-to-end vector originates at the silicon atom of the silane (instead of the carbon atom of the first methylene group to allow definition of the end-to-end vector for the C_1 chain) and ends at the terminal methyl position in the chain. The quantity θ_{ete} represents the angle between this vector and the normal to the silica surface. The cosine of this angle will be 1 for chains perpendicular to the substrate (aligned with the normal), 0 for parallel chains, and < 0 for chains whose terminal methyl group lies closer to the substrate than the silicon atom of the silane. For the C_1 phase (trimethyl silane), there are three possible terminal methyl groups. Only the outermost methyl group is considered when computing the average value for $\cos\theta_{\mathrm{ete}}$. This same convention is used when computing $z_{\mathrm{CH_3}}$, the height of the terminal methyl group above the silica surface.

Many quantities reported in this work involve angles measured with respect to the vector normal to the silica surface. In the slit pore setup, the silica surface is planar and lies in the x-y plane of the simulation box. Thus, there is no ambiguity in defining the surface normal. In the cylindrical pore setup (with the axis of the cylinder pointing along the y-direction) the surface normal is defined as the vector originating at the grafting position of the chain (i.e., the oxygen atom in –O-Si$(CH_3)_2$-CH_2–) and terminating at the center of the pore (at the same y-position as the grafting position). Other quantities are reported as a function of z, the distance from the silica surface. For both the slit pore and cylindrical pore simulations, the silica surface is defined by the surface's outermost silicon substrate atom. For the planar slit pore, all such silicon atoms lie in a plane at $z = 0$ Å. For the cylindrical pore there is a slight distribution of such silicon atoms. Thus, the average position of these silicon atoms is used, which turns out to be at a radius of 31.177 Å from the center of the pore, to define the cylindrical silica surface. The quantity z is then defined as the distance from this surface along the surface normal.

Table 11.1: Summary of the chromatographic parameters and average values of stationary phase and interfacial properties.[a,b,c]

Chain	Pore shape	Pressure	f_{gauche}	S_n	$\cos\theta_{\text{ete}}$	z_{CH_3}	z_{GDS}	δ_{int}
C_{18}	Planar slit	1 atm	0.27_1	-0.10_1	0.48_2	10.9_3	14.8_2	5.3_4
C_8	Planar slit	1 atm	0.34_1	0.06_2	0.68_1	9.4_1	10.3_1	7.4_3
C_1	Planar slit	1 atm	–	–	0.68_1	4.4_1	6.2_1	3.0_1
C_{18}	Planar slit	400 atm	0.28_1	-0.09_1	0.42_1	10.1_2	14.2_3	5.1_2
C_{18}	Planar slit	1000 atm	0.29_1	-0.08_2	0.40_1	9.5_1	13.7_1	5.1_4
C_{18}	Cylinder	400 atm	0.27_1	0.14_1	0.66_1	14.5_3	18.9_1	7.9_2

[a]A temperature of 323 K and mobile phase composition of 33% molfraction methanol were used for all systems.
[b]Subscripts indicate the standard error of the mean in the final digit.
[c]All lengths in units of Å.

11.3 Results and Discussion

11.3.1 Chain length effects

One parameter that is relatively straightforward to adjust in the synthesis of RPLC stationary phases is the length of the main alkyl chain of the grafted silanes. The effects on bonded phase structure and solute retention caused by adjusting the chain length have been intensely explored and linear chains with 8 or 18 carbons (octyl and octadecyl, respectively) have emerged as popular choices in RPLC [2, 201]. The length of the shorter side chains also influence grafted chain coverage and accessibility of residual silanols [137, 201, 202], but these effects are not investigated here. In many cases [173, 203, 204, 205], it has been observed that the separation selectivity is little changed by increasing the alkyl chain length for a given solute in RPLC when the solute is relatively small compared to the chain length [206]. Retention is almost always increased by an increase in the length of the grafted chains [3, 173, 203, 204, 205] and shape selectivity is greater for longer chains, in particular for C_{30} [207, 208, 209]. In this work, the effects of using the shortest member of the homologous series, C_1, and the two most popular lengths, C_8 and C_{18}, are examined for silanes with two methyl side chains, i.e., trimethyl, dimethyl octyl, and dimethyl octadecyl silane.

The chromatographic parameters used for the simulations of the C_1, C_8 and C_{18}

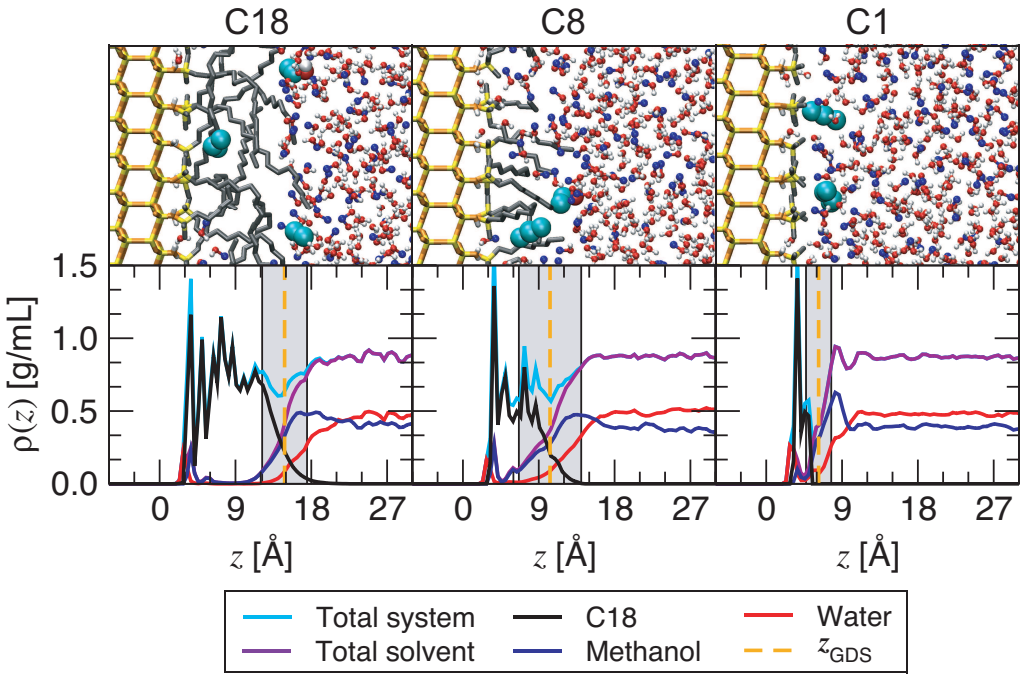

Figure 11.2: Top, simulation snapshots for stationary phases with different alkyl chain lengths (atom styles as in Figure 11.1). Bottom, density profiles for the corresponding systems. The shaded gray region depicts the 10–90 interfacial region as defined by the total solvent density.

systems are listed in Table 11.1. In particular, these simulations were carried out using the planar slit pore setup and the standard pressure of 1 atm. Snapshots of the three stationary phases with different alkyl chain lengths and the corresponding density profiles are shown in Figure 11.2. As one should expect, the thickness of the bonded-phase region (as indicated by the CH_x density profiles and the position of the GDS) decreases in a regular fashion with decreasing chain length. However, a more detailed analysis of the density profiles yields some remarkable differences. Whereas the C_{18} phase shows an extended region ($6\text{Å} < z < 12\text{Å}$) where the carbon density is close to the bulk density for liquid *n*-octadecane and the solvent density is close to zero, the carbon density in the middle part of the C_8 phase is closer to 0.5 g/mL, i.e. about 20% lower than bulk liquid *n*-octane at the same state point, and there is significant solvent penetration in this region. This leads to an increased interfacial width for the C_8 system compared to C_{18}. However, both phases show a similar extent of partial dewetting as

Table 11.2: Number of hydrogen bonds per surface silanol.[a]

System	N_{water}[b]	N_{MeOH}	N_{SiOH}[c]	N_{solute}	Total
C_{18}	0.46_2	0.24_1	–	0.005_1	0.71_3
C_8	0.38_2	0.28_2	–	0.007_1	0.67_3
C_1	0.57_1	0.17_1	–	0.004_1	0.74_1
C_{18} [400 atm]	0.46_1	0.23_1	–	0.005_1	0.70_1
C_{18} [1000 atm]	0.52_1	0.28_2	–	0.003_1	0.81_2
C_{18} [cylinder]	0.36_1	0.20_1	0.49_1	0.003_2	1.06_1

[a]Subscripts indicate the standard error of the mean in the final digit.
[b]N_{water}, N_{MeOH}, N_{SiOH}, and N_{solute} correspond to the average number of hydrogen bonds (per silanol) with water molecules, methanol molecules, other silanol groups, and solute molecules.
[c]Hydrogen bonds between two silanols are not possible on the planar surface.

indicated by the minimum in the total density near the GDS. The solvent structure at the interface between bonded and mobile phases for the C_1 system shows dramatic and, maybe, surprising differences from the other two systems. This interface is significantly sharper, there is a larger depletion in the total density, and the methanol density shows pronounced layering, i.e., behavior that is associated with "hard" walls [210].

For all systems, there is a peak in the solvent density near the substrate ($z \approx 3$ Å) that is indicative of solvent molecules that form direct hydrogen bonds to residual silanols (see Chapter 6). As can be inferred from the solvent density profiles, there does not appear to be more substrate bound solvent for the C_1 phase, and this is also born out by analyzing the number of hydrogen bonds per silanol (see Table 11.2), which shows no statistically significant difference in the total number of H-bonds for the C_1 and C_{18} phases. However, there are more H-bonds with water and fewer with methanol for the substrate with grafted C_1 chains as compared to the C_{18} system.

The methanol molfraction enhancements for the three systems with different chain lengths are depicted in Figure 11.3. As should be expected for hydrophobic surfaces, there is a significant enrichment of the methanol concentration in the interfacial region. For all three chain lengths, the value of the enrichment at the position of the (z_{GDS}) is close to 2, i.e., the surfaces have similar hydrophobic character, and the larger solvent depletion for the C_1 system is more an indication of the interfacial sharpness than of the hydrophobicity. Although the enrichment at z_{GDS} is similar for all three systems,

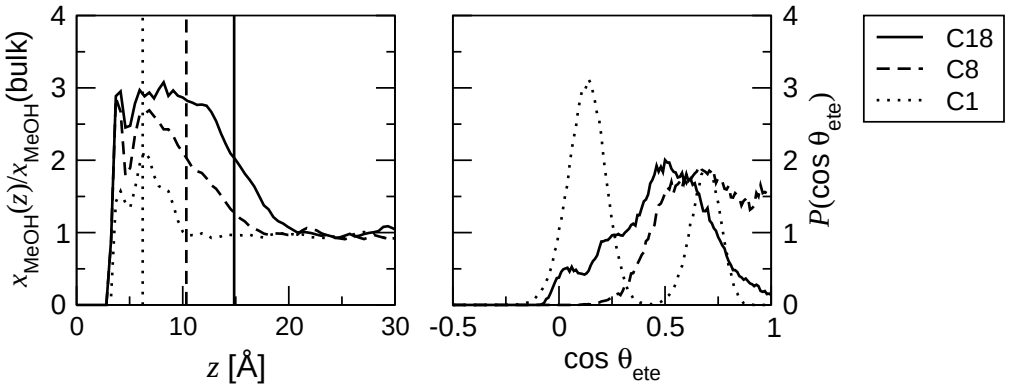

Figure 11.3: Methanol molfraction enhancement profiles (left) and end-to-end vector orientational distributions (right) for stationary phases with different alkyl chain lengths. Vertical lines denote the position of the GDS.

the behavior within the GDS shows stark differences. For the C_1 system, the maximum in the enrichment is at z_{GDS}, while the C_8 and C_{18} exhibit a broad peak inside the GDS and a sharp peak at $z \approx 4$ Å. The height of the sharp peak is nearly the same for C_8 and C_{18} phases and to some extent these enrichments reflect the similar ratios of the number of H-bonds formed by residual silanols with water and methanol molecules (see Table 11.2). The height of the broad peak for the C_{18} phase exceeds that for the C_8 phase and the peak for the former is more extended, i.e. the interior of the C_{18} phase is more hydrophobic than for C_8 and the hydrophobic region is much thicker for the former. This explains the lack of solvent penetration seen in the density profiles (see Figure 11.2).

Table 11.1 summarizes average values for properties pertaining to the chain conformation. The average fraction of gauche defects is slightly higher for the C_8 phase than for the C_{18} phase, but S_n and $\cos\theta_{\mathrm{ete}}$ are somewhat larger for C_8 than for C_{18} chains indicating a slightly more perpendicular alignment to the planar substrate for the C_8 chains. It is also noteworthy that the difference in the average z-location of the terminal methyl group ($z_{\mathrm{CH_3}}$) is relatively small between the C_8 and C_{18} systems and that $z_{\mathrm{CH_3}}$ is much closer to z_{GDS} for the C_8 chain. Both of these observations are related to the C_{18} chain's greater ability to fold back and have the terminal part of the chain pointing toward the substrate. The distribution of the orientation of the chain end-to-end vector with respect to the surface normal is shown in Figure 11.3. The distribution for the

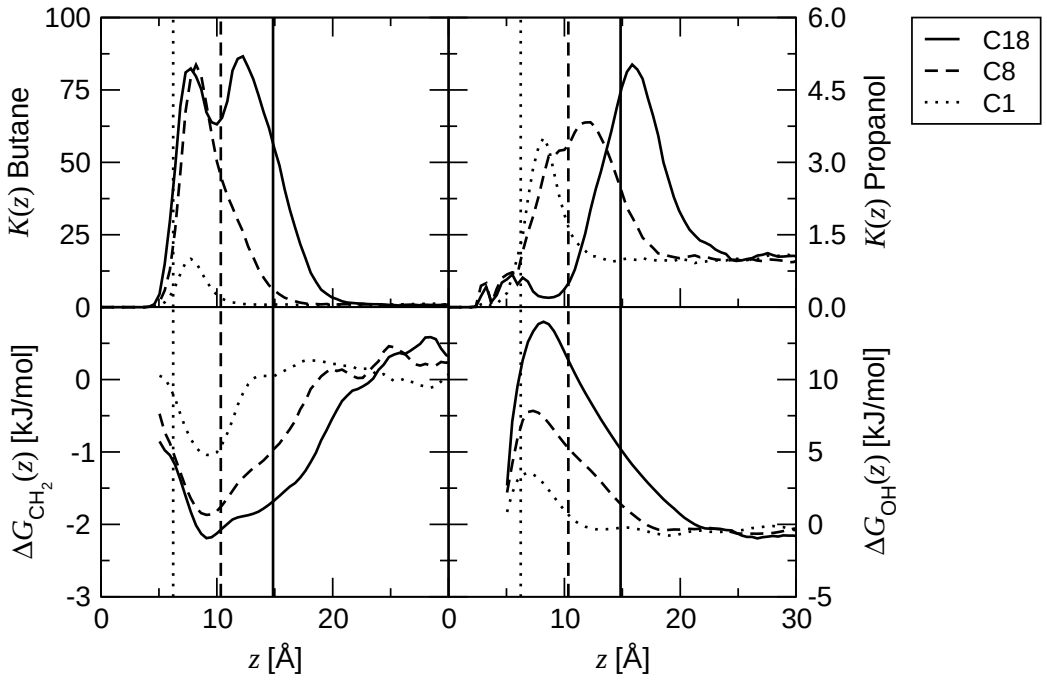

Figure 11.4: Solute distribution coefficient and incremental free energy profiles for stationary phases with different alkyl chain lengths. Vertical lines denote the position of the GDS.

C_8 system is shifted to larger values with a significant population for $\cos\theta_{\text{ete}} > 0.5$ compared to the C_{18} system, i.e. the C_8 chains are on average more erect but still far from a predominantly perpendicular orientation. The shoulder near $\cos\theta_{\text{ete}} \approx 0$ for the C_{18} chains is another indication of backfolding, i.e., terminal methyl groups that are at a similar height as the silane silicon atom. The distribution for the C_1 chains is bimodal and the peaks are relatively narrow due to the limited flexibility of the trimethyl silane group. The bimodal distribution is due to the two different angles with respect to the tetrahedral bonding arrangement – one methyl group points up (at an angle close to 55°) and the other two Si-C bonds are nearly parallel to the silica substrate.

The molecular-level retention thermodynamics on these three phases with different chain lengths are elucidated through plots of the solute distribution coefficient profiles for *n*-butane and 1-propanol and the incremental free energy profiles for the methylene and hydroxyl groups (see Figure 11.4). As discussed in detail in Chapter 7, *n*-butane solutes exhibit a bimodal distribution profile in the C_{18} phase. There is one peak

Table 11.3: Net distribution coefficients and incremental free energies of retention.[a,b]

System	K_{butane}	K_{propanol}	ΔG_{CH_2}	ΔG_{OH}
C_{18}	33_4	1.63_8	-1.80_7	7.13_{10}
C_8	20_1	1.82_9	-1.64_2	5.71_{16}
C_1	3.5_4	1.20_{10}	-0.90_7	3.14_{23}
C_{18} [400 atm]	33_4	1.63_9	-1.99_3	6.95_{11}
C_{18} [1000 atm]	32_2	1.68_{10}	-2.01_5	6.84_6
C_{18} [cylinder]	110_6	1.86_6	-2.46_3	8.79_5

[a]Subscripts indicate the standard error of the mean in the final digit(s).
[b]Energies in units of kJ/mol

buried deeply within the bonded chains ($z \approx 7$ Å) that is attributed to partitioning, and another peak just inside the GDS that is attributed to adsorption in the outer chain region. This bimodal character is absent for the C_8 and C_1 phases and there is only a single peak located at $z \approx 7$ Å. Whereas the peak height at $z \approx 7$ Å is similar for the C_{18} and C_8 phases, it is reduced by a factor of five for the C_1 phase. However, the absence of the bimodal character for the C_8 system and the fact that the single peak for C_8 nearly coincides with the partitioning peak found for the C_{18} phase do not imply that the adsorption contribution is negligible for *n*-butane on the C_8 phase. First, one should note that at the GDS, $K_{\text{butane}}(z) \approx 50$ for both the C_8 and C_{18} phases (and a similar observation can also be made for the incremental free energy of the methylene group, $\Delta G_{\text{CH}_2}(z_{\text{GDS}}) \approx -1.8$ kJ/mol). Secondly, the location of the single peak in $K_{\text{butane}}(z)$ with respect to z_{GDS} for the C_8 phase is quite similar to the relative location for the adsorption peak found for the C_{18} phase. Furthermore, this peak for the C_8 phase extends well beyond the GDS. Based on these observations it appears that both adsorption and partition contribute to the mechanism for retention of nonpolar analytes on the C_8 phase. However, due to the thinness of the C_8 phase the peaks due to these contributions are overlapped and difficult to resolve. However, it is clear that for C_1 phase that the peak at $z \approx 7$ Å is due to adsorption since this peak lies outside of the GDS for this system.

The net distribution coefficients for *n*-butane and the net incremental free energy for the methylene group are shown in Table 11.3. These data indicate that the stationary phase becomes slightly less retentive for nonpolar species when the chain length is decreased from C_{18} to C_8 and much less retentive when the chain length is decreased

to C_1. These retention energetics are consistent with the well-known observation that longer-chain RPLC systems are more retentive than shorter-chain RPLC systems [3, 173, 203, 204, 205]. The net retention thermodynamics for nonpolar solutes can be rationalized by the fact that, although the retention mechanism is similar on the C_{18} and C_8 phases, there is greater solvent penetration in the C_8 phase resulting in a less hydrophobic environment and thus less retention. The large decrease in retention for the C_1 phase occurs because the retention mechanism changes from a mix of partitioning and adsorption in the outer chain region to one dominated by adsorption in the methanol-enriched interfacial region.

A similar change in the retention mechanism is not observed for the 1-propanol solute and the hydroxyl increment. For all three stationary phases, the retention is clearly governed by an adsorption mechanism. The peak in $K_{\text{propanol}}(z)$ falls slightly outside z_{GDS} for all three systems and its height decreases as stationary phase chain length is decreased. For all three systems, there is also some adsorption near the silica substrate due to H-bonding of the solute directly to residual silanols and (more often) to solvent molecules near the substrate (see discussion below). The thickness of the C_{18} phase is sufficient to contain a central hydrophobic region that is avoided by the 1-propanol analytes (i.e., a minimum in $K_{\text{propanol}}(z)$). The incremental free energy profiles indicate that all three different phases are unretentive for the hydroxyl group. This leads to a free energy barrier of around 14 and 8 kJ/mol for the C_{18} and C_8 phases, respectively.

Table 11.4 summarizes the data of a H-bond analysis for the alcohol solutes. As can be seen, the number of H-bonds formed by the solutes with residual silanols are indeed very small irrespective of the chain length of the RPLC phase. For retained molecules, most of the H-bonds are formed with solvent molecules outside the GDS and this fraction is larger for the C_1 system. For all three systems, the total number of H-bonds for retained alcohol solutes is close to a value of 2. This is about 10% smaller than the total number of H-bonds found for alcohol solutes in the mobile phase (33% methanol). However, more instructive is a comparison to a bulk *n*-hexadecane phase saturated with 33:67 molfraction methanol:water where the total number of H-bonds is only 0.30, i.e., the adsorption of alcohols on common RPLC phases is quite different from the partitioning into a *n*-hexadecane phase.

Table 11.4: Hydrogen bond numbers for alcohol solute molecules in retentive and mobile phases.[a,b]

System	Pressure	N^{c}_{SiOH}	N^{d}_{in}	N^{e}_{out}	Total
C_{18}	1 atm	0.08_2	0.41_3	1.48_2	1.97_2
C_8	1 atm	0.13_2	0.45_3	1.43_1	2.02_2
C_1	1 atm	0.06_1	0.17_2	1.79_2	2.03_1
C_{18}	400 atm	0.10_3	0.40_1	1.51_3	2.01_1
C_{18}	1000 atm	0.06_1	0.42_2	1.55_3	2.03_1
C_{18} [cylinder]	400 atm	0.45_1	1.59_2	0.15_2	2.20_2
Solvent	Pressure		N_{H_2O}	N_{MeOH}	N_{Total}
33% methanol	1 atm		1.65_2	0.52_1	2.17_2
	400 atm		1.66_1	0.52_1	2.19_1
	1000 atm		1.69_2	0.53_1	2.22_1
n-hexadecane[f]	1 atm		0.03_1	0.27_5	0.30_6

[a]A solute is defined to be in the retentive phase when it is in the first solvation shell (6.0 Å) of any stationary phase segment.
[b]Subscripts indicate the standard error of the mean in the final digit.
[c]Average number (per alcohol solute) of hydrogen bonds with silanol groups.
[d]Average number of hydrogen bonds with solvent molecules inside the GDS.
[e]Average number of hydrogen bonds with solvent molecules outside the GDS.
[f]Saturated with 67/33 water/methanol.

11.3.2 Pressure Effects

One of the recent advances in liquid chromatography instrumentation is the utilization of very small particle diameter (< 2 μm) columns [211]. Because these columns exhibit very large backpressure, a large driving pressure, often exceeding 400 atm, is required to maintain a reasonable flow velocity. In these cases it has been observed [211, 212, 213, 214, 215, 216, 217, 218, 219] that there is a small pressure dependence of retention and that this arises from many sources which include the compressibilities of the mobile and stationary phases (where the latter is often estimated as the sum of a nearly incompressible silica matrix and a relatively compressible bulk octadecane region), the change in the partial molar volume of the solute, and changes in the structure of the bonded phase [215, 217]. In the case of the bonded phase, changes in the structure with respect to pressure are exceedingly difficult to measure experimentally. Here, the extent to which pressure (1, 400, and 1000 atm) can alter the structure

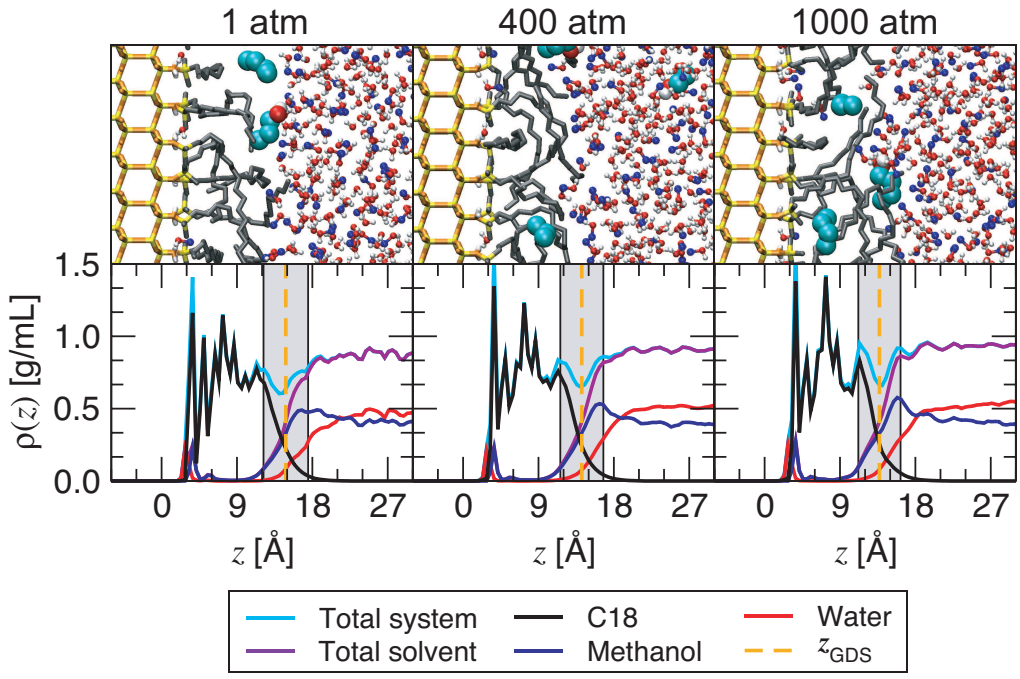

Figure 11.5: Top, simulation snapshots for stationary phases at different pressures (atom styles as in Figure 11.1). Bottom, density profiles for the corresponding systems. The shaded gray region depicts the 10–90 interfacial region as defined by the total solvent density.

of a C_{18} bonded phase and retention is examined.

Snapshots of the stationary phase and density profiles obtained at three different pressures are presented in Figure 11.5. The pressure-induced changes are rather small. With increasing pressure, the density depletion (partial dewetting) at z_{GDS} increases slightly, the peak in the methanol density at the outer range of the interface becomes more pronounced, and the values of z_{GDS} and z_{CH_3} decrease by about 1 Å (see Table 11.1). However, the interfacial width, the solvent depletion in the interior region of the C_{18} phase, and the molfraction enhancement (see Figure 11.6) are not appreciably affected by the pressure change. Similarly, the average fraction of gauche defects and the S_n order parameter show little change. The decrease in z_{CH_3} is reflected by a slight shift in the end-to-end vector orientational distribution to smaller $\cos\theta_{ete}$ values and the emergence of a peak at $\cos\theta_{ete} \approx 0$ indicates a larger fraction of backfolded chains at the higher pressures (see Figure 11.6).

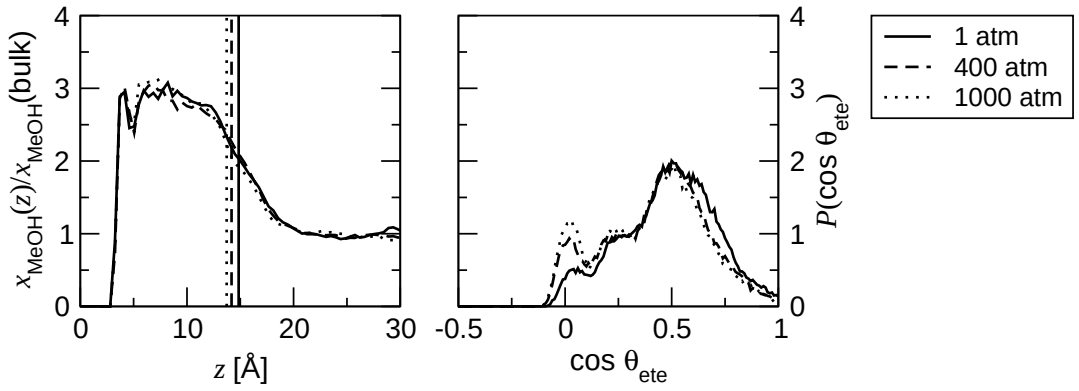

Figure 11.6: Methanol molfraction enhancement profiles (left) and end-to-end vector orientational distributions (right) for stationary phases at different pressures. Vertical lines denote the position of the GDS.

The effects of pressure on the retention thermodynamics are also quite small. At all three pressures, the distribution profiles for n-butane exhibit an adsorption and a partition contribution (see Figure 11.7) and the net distribution coefficient does not show any significant change. The incremental free energy profiles and the net free energy of transfer for the methylene group indicate a slightly more favorable interaction with the stationary phase at higher pressures, for example, ΔG_{CH_2} decreases from -1.8 kJ/mol at 1 atm to -2.0 kJ/mol at 1000 atm.

Unfortunately, experimental retention data under conditions very close to those used here is not available, but the trends in the simulation data do agree with other experimental work. McGuffin and Evans investigated the retention of fatty acid derivatives using a pure methanol mobile phase and found that the methylene increment decreased by about 6% upon increasing the pressure from 102 to 340 atm [218]. In another study, McGuffin and Chen report the change in molar volume for fatty acid derivatives upon increasing pressure from 57 to 340 atm [219]. Their data with a 2.7 μmol/m^2 monomeric C_{18} stationary phase, a pure methanol mobile phase, and at 303 K, indicates that the change in molar volume for the methylene group that is negative. Since a decrease in the methylene increment with pressure is observed, the simulation data indicate a trend similar to experiment.

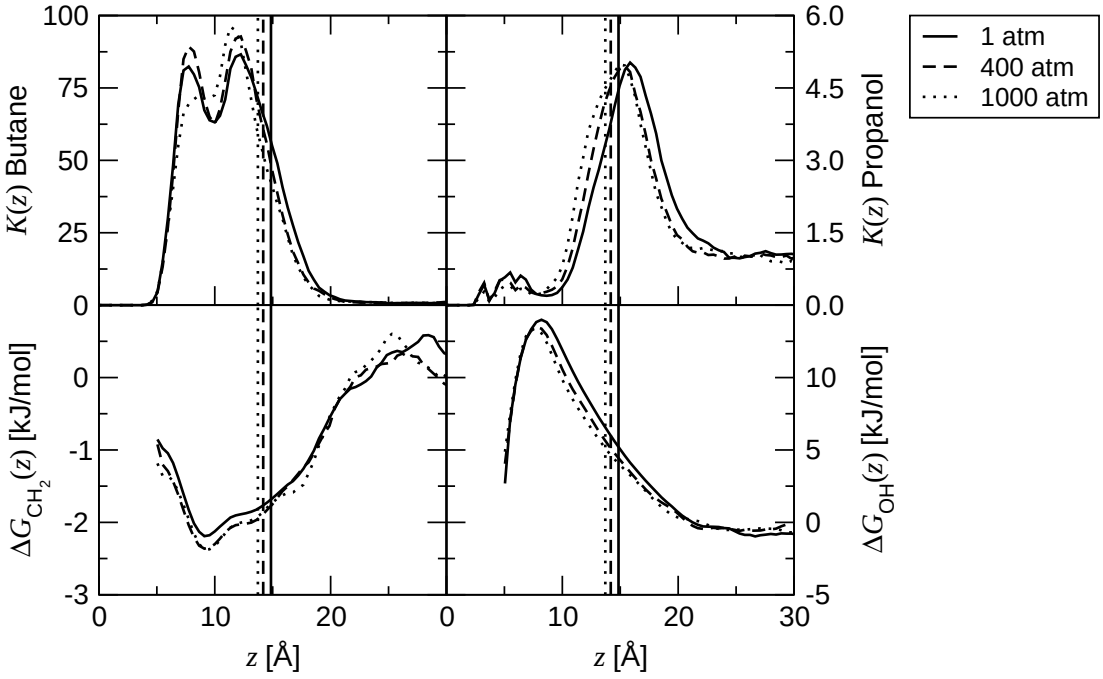

Figure 11.7: Solute distribution coefficient and incremental free energy profiles for stationary phases at different pressures. Vertical lines denote the position of the GDS.

11.3.3 Surface curvature

The mean pore diameter of the silica particles used in RPLC can range from around sixty to hundreds of angstoms. Clearly, as the pore size decreases the curvature of the surface in these pores must increase. The question here is if this curvature has any dramatic effects on structure and retention in RPLC. For example, at high surface curvature the distal ends of the alkyl chains may become more crowded and this could alter their conformation. Surface curvature has been investigated in a number of cases in surface chemistry, especially under the context of adsorption of polymers. Few investigations have dealt directly with the effect of surface curvature in RPLC because the atomic level characterization of the silica support is extremely difficult. Most spectroscopic methods that characterize chain conformation require the use of a flat silica surface and it is therefore difficult to probe the interior surfaces of the silica particles that are used in a chromatographic column. Because of this difficulty, indirect methods, such as retention or adsorption isotherm measurements, are typically used examine the effects of

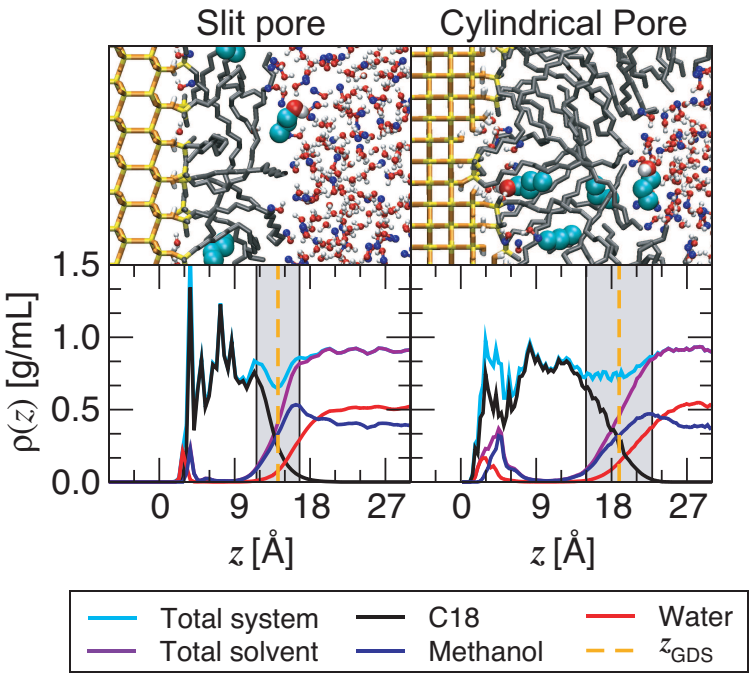

Figure 11.8: Top, simulation snapshots for stationary phases with different pore shapes (atom styles as in Figure 11.1). Bottom, density profiles for the corresponding systems. The shaded gray region depicts the 10–90 interfacial region as defined by the total solvent density.

curvature. However, molecular simulation affords one a very direct method to examine curvature effects. This section discusses simulations aimed at discerning these effects by examining two limiting cases, C_{18} chains grafted to a cylindrical pore with a 60 Å diameter and to a flat surface (zero curvature). It is assumed that at large diameters the curvature becomes small enough that it can be ignored and a slit pore model may be used. It should be noted that one well-known effect of pore curvature is a dewetting of smaller pores when mobile phases with a high concentration of water are used at lower pressures [138]. This is mainly a cappillary effect and will not be addressed here. Rather the goal of this work is to examine the effects of pore size on stationary phase structure and the retention mechanism.

As is immediately evident from the snapshots and density profiles for the C_{18} chains in the planar slit and cylindrical pores, the pore geometry has a rather substantial influence on the chain conformation and solvent penetration (see Figure 11.8). Most

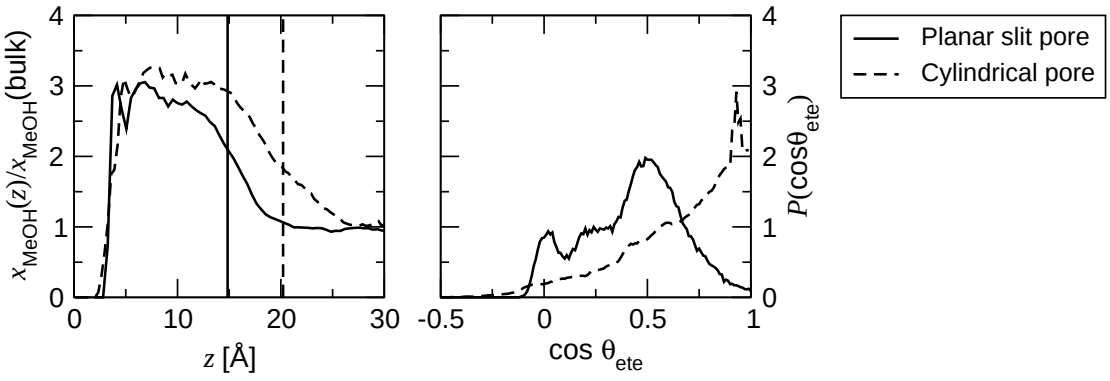

Figure 11.9: Methanol molfraction enhancement profiles (left) and end-to-end vector orientational distributions (right) for stationary phases at different pressures. Vertical lines denote the position of the GDS.

importantly, the width of the bonded phase region has increased by about 30% as measured by z_{GDS} and $z_{\mathrm{CH_3}}$ (see Table 11.1). The combination of the curvature of the silica substrate and the width of the C_{18} film leads to a highly curved C_{18}–mobile phase interface. It should be noted here that the mobile phase region does not necessarily need to be centered at the center of the cylindrical pore and the undulation along this curved interface is larger than for the planar slit pore. This contributes to some extent to the larger radially averaged interfacial width found for the cylindrical pore.

The carbon density for the cylindrical pore shows a depletion for 4 Å $< z <$ 7 Å where the chains are significantly more aligned with the substrate normal than for the planar slit pore and correspondingly the average S_n order parameter is increased. This depleted region is followed by an extended outer part of the C_{18} chains with a density close to that of bulk n-octadecane [220]. The depleted region and the extended outer part are associated with less backfolding of the C_{18} chains and an orientational distribution of end-to-end vectors that is shifted to significantly larger $\cos\theta_{\mathrm{ete}}$ values with a peak for orientations nearly perpendicular to the substrate. However, the fraction of gauche defects does not appear to be affected by the pore shape. Overall, the simulations suggest that adding curvature in a concave pore can actually cause the chains to extend even more than those on a flat surface in contrast to the suggestion by Rustamov and coworkers [45].

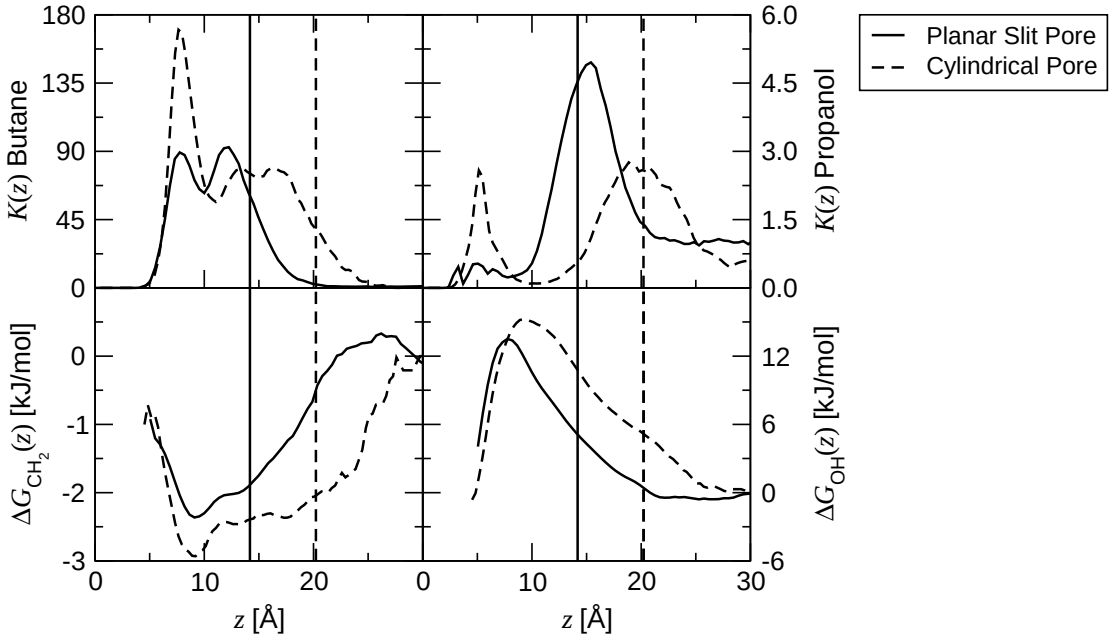

Figure 11.10: Solute distribution coefficient and incremental free energy profiles for stationary phases with different pore shapes. Vertical lines denote the position of the GDS.

As mentioned above, the curved substrate has a significantly higher density of dangling hydroxyl groups than the planar substrate (7.8 μmol/m^2 versus 4.8 μmol/m^2). The curvature and higher silanol density allow for direct H-bonds between silanols and each substrate hydroxyl forms on average about 0.5 H-bonds to other substrate hydroxyl groups (see Table 11.2). Furthermore, the higher density of silanols and the density depletion for the inner part of the C_{18} chains allow for a significantly higher density of solvent molecules near the substrate. However, the magnitude of the methanol molfraction enhancement is similar for the two pore geometries, but the enhancement extends further out for the cylindrical pore because of the larger width of the bonded phase (see Figure 11.9).

The changes in the chain conformation and solvent penetration induced by the substrate curvature lead to significant changes in the retention thermodynamics but not the retention mechanism, as will be shown below. The solute distribution profile for *n*-butane in the cylindrical pore still shows the characteristic bimodal shape as shown in

Figure 11.10. However, the density depletion and higher orientational order (e.g. larger S_n values) in the inner chain region of the cylindrical pore makes this partitioning region more favorable for n-butane and the height of the partition peak in the $K_{\text{butane}}(z)$ profile is nearly doubled compared to the planar slit pore. In contrast, the height of the peak in the adsorption region is somewhat lower but this region is more extended for the cylindrical pore than for the slit pore. The incremental free energy profile for the methylene increment (Figure 11.10) is shifted downward (more favorable) for the cylindrical pore and the net $\Delta G_{\text{CH}_2} = -2.5$ kJ/mol versus a value of -2.0 kJ/mol for the slit pore.

For the polar alcohol solutes, adsorption near z_{GDS} remains the predominant mode of retention for the cylindrical pore, but the changes in the inner region of the bonded phase (carbon density depletion, higher silanol and solvent densities) also allow for increased adsorption of 1-propanol near the substrate (see Figure 11.10). The enhanced availability of H-bonding sites near the substrate of the cylindrical pore is reflected in the four-fold increase in the numbers of H-bonds with both silanols and solvent molecules inside the GDS (Table 11.4). The ΔG_{OH} profile exhibits an increased barrier height with larger range (due to increased width of the alkyl phase), but also a more favorable region near the substrate for the cylindrical pore (due to increased silanol density).

11.4 Conclusions

Efficient Monte Carlo algorithms and accurate force fields are employed to carry out extensive simulations for model RPLC systems in order oto provide atomic-level information on the influence of some chromatographic parameters on chain conformation, solvent penetration, and the retention mechanism. The most important observations gleaned from these simulations are summarized here. Comparing C_{18} and C_8 bonded phases, it is found that the retention mechanism does not show significant changes for either nonpolar or polar analytes. However, the C_8 is less retentive for nonpolar groups and more retentive for polar groups due to increased solvent penetration into the bonded phase. Compared to a planar slit pore, the chains in a small cylindrical pore are more extended, the amount of solvent penetration is increased, and the curved bonded phase is more favorable for nonpolar methylene groups and less favorable for polar hydroxyl

groups. On the other hand, it is found that pressure leads only to relatively minor changes in structure and retention as long as the pore remains wetted.

Chapter 12

Molecular Origins of Shape Selectivity

12.1 Background

The chromatographic separation of the components in a chemical mixture is driven by the preferential distribution of each species between a mobile phase and a stationary phase. Of the various modes of chromatography, the most popular is reversed-phase liquid chromatography (RPLC). Here, the mobile phase is a polar hydro-organic solvent mixture and the stationary phase typically consists of non-polar dimethyl octadecyl silane (ODS) chains chemically grafted to a silica substrate. In most cases, the difference in retention times between two analyte molecules is governed by differences in their physical properties such as polarity or molecular weight. For example, a more polar analyte molecule will have a higher affinity to reside in the mobile phase and, therefore, have a shorter retention time. However, some RPLC systems also have the ability to separate analytes that have very similar chemical functionalities and physical properties, but differ mostly in molecular shape. This ability, termed "shape selectivity", is typically applied in the context of separating the geometric isomers of nearly rigid molecules, such as polycyclic aromatic hydrocarbons (PAHs), polychlorinated biphenyls, steroids, and

[†] This chapter describes the outcome of a collaborative research project carried out by Jake L. Rafferty and advised by J. Ilja Siepmann and Mark. R. Schure. A report on this research project has been submitted [77].

carotenoids.

PAHs are found naturally in oil and coal and are produced as byproducts in the combustion of carbon containing fuels. These organic molecules are an important class of environmental pollutants as a number of them are carcinogenic. The degree of carcinogenecity is highly dependent of the structure of the PAH, thus it is of great importance in the analysis of environmental samples to be able to separate the various structural isomers of a set of PAHs with the same molecular formula. Furthermore, understanding shape selectivity in RPLC may give some insight into biological processes like drug transport across lipid membranes. Like PAHs, many drugs molecules are rigid and the ordered alkyl chains in an RPLC stationary phase may have many similarities to the alkyl chains in biological membranes [40].

Due to the importance of the separation of PAH isomers, numerous chromatographic studies have been carried out to examine the analyte descriptors governing shape selectivity in RPLC and this topic has been discussed in detail multiple times by Sander, Wise and co-workers. [221, 222, 19, 178, 179, 223, 224] Because of the large amount of literature available, only a brief discussion of these descriptors will be given here. In general, it has been noted that for PAHs of the same molecular formula (i.e., geometric isomers), those with larger length to breadth (L/B) ratios and/or greater planarity are more retained. The L/B ratio is defined by drawing a 2D-box that completely encloses the molecule. The ratio of the length of the longer side of the box to the shorter side gives the L/B ratio. [221] It has also been observed that greater selectivity between different PAH isomers can be achieved by adjusting chromatographic parameters that lead to increased ordering of the stationary phase chains. These parameters include reduced temperature, increased grafting density, increased chain length, and the use of polymeric, as opposed to monomeric, bonded phases. [223, 224] Mobile phase composition has been shown to have little effect on shape selectivity.

To explain the retention behavior of PAHs, Wise and Sander proposed the "slot model". [222] This model envisions the bonded phase in RPLC as containing a number of narrow slots (like a kitchen toaster) into which the analyte molecules can penetrate. Each slot has a characteristic shape and size, i.e., it is a fixed and rigid cavity. Therefore, only analytes with appropriate dimensions can fit into a given slot. Molecules with larger L/B ratios are more narrow and should fit into a larger fraction of these slots

and, hence, these analytes are more retained. [222] Likewise, planar molecules will be more retained than non-planar molecules since they should also fit into more of the slots. The shape selectivity of a given column is often specified by its selectivity for a specific test mixture (such as the Standard Reference Material 869 Column Selectivity Test Mixture for Liquid Chromatograph [225]) with somewhat arbitrarily chosen values of selectivities delineating phases with low, intermediate, or high shape selectivity. These boundary values between low and high (or increased) shape selectivity usually involve relatively small changes in selectivity of about a factor of 1.5 to 2 (i.e., a difference in the transfer free energy of only 1.0 to 1.7 kJ/mol at room temperature). Such small changes in transfer free energies (or the retention factor) are unlikely to be related to significant changes in the retention mechanism or to be caused by the appearance of specific slots which rigid shape and size. Furthermore, the formation of these rigid slots in the bonded-phase region would presumably be associated with a significant entropic penalty for the chain conformations and a significant cost for the creation of a large surface area.

Most of the descriptions on the molecular mechanism behind shape selectivity are based on experimental retention data gathered under a variety of different chromatographic conditions. Retention data is thermodynamic by nature and cannot offer conclusive proof of a mechanism, rather it can only be used to infer a mechanism. A tool that can offer true microscopic details on the retention mechanism is molecular simulation. Recently, Lippa and coworkers have carried out molecular dynamics (MD) simulations to study the structure of alkylsilane chains grafted to a silica surface. [59, 60, 61] In these studies the effects of surface coverage, bonding chemistry (monomeric versus polymeric), temperature, and chain length were examined. It was found that those conditions leading to increased chain order correlated well with experimentally observed increases in shape selectivity. Additionally, the simulated stationary phases were analyzed for presence of slots which could serve as retention sites for PAH molecules. [61]. These authors concluded that higher density polymeric phases, which are known to be more shape selective, possess more highly ordered cavities of appropriate size for a specific PAH molecule.

While the MD simulations described above did give some molecular insights on shape selectivity, there are a several critical aspects missing from this work. [59, 60, 61]

First, the analysis of the various stationary phases for slots was carried out on a single configuration from the end of the MD trajectory, i.e., ignoring the statistical distribution of local environments present in a *liquid* phase. Second, the simulations were carried out in the absence of the mobile phase solvent. The presence of solvent can greatly influence the structure of the alkyl chains in the stationary phase. Second, no PAH analytes where present in the MD simulations. Lippa et al. simply inferred where the analytes may locate themselves based on an analysis of stationary phase structure. Finally, it was not verified whether the MD simulations can reach the same equilibrium structure distribution regardless of the initial configuration used for the simulations. This is a significant issue because the timescale limitations of MD simulations may not allow one to reach equilibrium structures or to sample chromatographic processes. For example, results from previous MD simulations have shown dramatically different results depending on whether the chains were started in the all-trans conformation [53, 58] or in collapsed states, [51, 52] and MD simulations including explicit solvent and analyte molecules were not able to sample multiple transfers of the analyte from the mobile to the stationary phase (and vice versa). [65]

The remainder of this chapter will discuss the application of Gibbs ensemble simulations using efficient Monte Carlo algorithms and realistic chromatographic models to examine shape selectivity in RPLC and its dependence on surface coverage. Included in the simulations are explicit solvent molecules and isomeric PAH solutes. The presence of these solute molecules allows for a very precise examination of the molecular mechanism of shape selectivity because during the simulation the atomic coordinates of all species in the model system are known exactly. It will be shown, by a detailed analysis of the entire simulation trajectory, that the stationary phase is a very heterogeneous environment for the various PAH solutes. There exist distinct retention retention sites for the different isomeric PAH solutes. However, these sites are not rigid cavities. Rather, the stationary phase structure in RPLC is dynamic and able to respond to the presence of the PAH solutes. The validity of the these molecular insights is supported the excellent agreement between the retention data calculated from simulation and that measured in experiment.

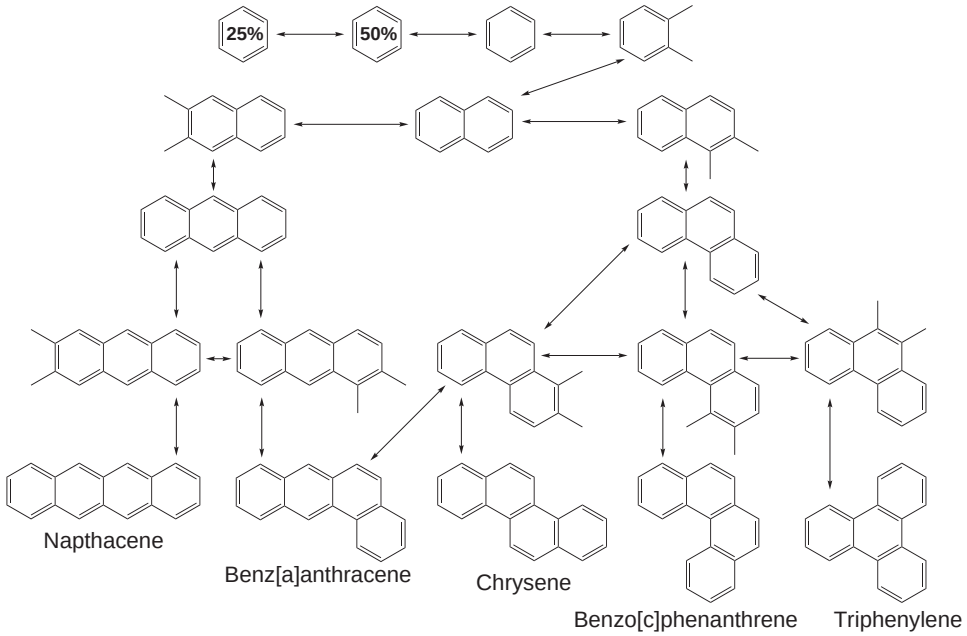

Figure 12.1: PAH solutes present in the simulations. The double headed arrows indicate the pairs involved in molecular identity interchange moves.

12.2 Simulation Details

To discern the molecular origins of shape selectivity in some traditional RPLC systems, coupled-decoupled configurational-bias Monte Carlo (CBMC) simulations in the NpT version Gibbs ensemble were used. The RPLC simulation setup and force field are described in detail in Chapter 5. Three different different surface coverages (1.60, 2.88, and 4.15 μmol/m^2) were examined in the simulations. These coverages were achieved by randomly grafting (5, 9, and 13) alkyl chains to each side of the silica substrate. The mobile phase consisted of 400 water and 800 acetonitrile molecules resulting in a mixture that was 67% molfraction (≈86% volume fraction) acetonitrile. In addition, a system with a water/methanol mobile phase (with the same concentration of the organic modifier as above) and the stationary phase at the intermediate coverage was also investigated. All simulations were carried out at a temperature of 308 K and pressure of 1 atm.

In addition to the stationary and mobile phase entities, one each of 19 different solute molecules were present in the simulations (see Figure 12.2). As described in previous chapters these solutes are allowed to transfer between the three boxes via CBMC particle exchange [91, 92] and identity interchange moves [93, 94], the latter between the pairs indicated by the double-headed arrows in Figure 12.2. One of the main objectives of this study was to examine the retention mechanism for the five different four-ring PAH isomers. This required a means in which to precisely sample the spatial distribution of these solutes. The traditional means of accomplishing this is through the CBMC particle exchange move. However, it is extremely inefficient to directly transfer these large solutes between boxes due to a high probability of inter-particle overlap during the move and thus a prohibitively low acceptance rate. To overcome this difficulty, only a partially interacting benzene molecule (25% of the interactions of a full benzene molecule) was directly exchanged between the three boxes. This partial molecule was then allowed to exchange its identity with a 50% interacting benzene, which could then exchange with a fully interacting benzene molecule. As indicated in Figure 12.2, this full benzene is then "grown" two segments at a time in order to generate the larger PAH solutes. This sampling scheme was rather efficient, a 10% acceptance rate was achieved for most of these identity interchange moves. This lead to relatively high precision in the calculated data, which will be presented later.

Because of the large number of solute molecules present in simulations, it was necessary to restrict their numbers in the stationary and mobile phase boxes in order to prevent an overloading of these phases. This was accomplished by applying a uniform bias potential for each solute in each of the three boxes. This bias potential was adjusted such that each solute spent 10% of its time in the stationary phase box, 10% in the mobile phase box, and 80% in the vapor phase box. Thus, on average, there were less two solutes in the stationary or mobile phases. The distribution coefficients, free energies of retention, and selectivity factors reported in this work are corrected for these bias potentials. During the equilibration period, it was observed that the larger PAH solutes had a tendency to cluster while in the vapor phase due to their extremely low vapor pressure. To eliminate this clustering, the PAH solutes were treated as ideal particles (no intermolecular interactions) while in the vapor phase. The solutes were fully interacting while in stationary and mobile phases. This is of no consequence to the

reported results as the vapor phase in these simulations is not involved in the retention process and is used here only as an intermediate transfer medium.

For each surface coverage studied, eight independent simulations were carried out. Each independent simulation was equilibrated for at least 2×10^5 Monte Carlo (MC) cycles followed by an additional 5×10^5 MC cycles for production. One MC cycle corresponds to N MC moves, where N is the number of molecules in the three-phase system. Statistical uncertainties in the reported quantities were estimated from the standard error of the mean of the results from the eight independent simulations.

12.3 Results and Discussion

An important aspect of simulation is validation against experimental results. If a simulation is able to reproduce the experimental data, then greater confidence may be given to molecular insights gleaned from the simulation. For validation of the current work, retention data was calculated from the simulations and compared to experiment. A detailed description of how retention data can be calculated from simulation was discussed in Chapter 5.

A comparison of simulated and experimental incremental free energies of retention for the phenyl group is presented in Table 12.1. This quantity is found by plotting the free energy of retention for linear PAHs (benzene, napthalene, anthracene, napthacene) versus the number of aromatic rings. The slope from a linear regression on this plot gives the incremental phenyl free energy. Table 12.1 shows that the free energies calculated from simulation are in good agreement with the experimental data [227, 226] over the range of grafting densities studied. There is a slight tendency for the TraPPE force field to overestimate the incremental transfer free energy. This overestimation of the phenyl increment is related to the fact that the PAH molecules are modeled by a united-atom force field [99] that does not explicitly treat the quadrupolar interactions of phenyl rings. Hence, the interactions with alkanes are somewhat overestimated [99, 228] and the interactions with polar species are underestimated. [229] However, one should note that the neglect of explicit quadrupolar interactions should influence the differences between geometric isomers to a much smaller extent because these isomers have similar out-of-plane charge distributions.

Table 12.1: Comparison of incremental free energies of retention for the phenyl group computed from simulation and obtained from experiment.

	Coverage μmol/m^2	$\Delta\Delta G_{\text{phenyl}}$
Simulation	1.60	-2.5 ± 0.2
	2.88	-2.9 ± 0.2
	4.15	-3.9 ± 0.5
Limsavarn and Dorsey [226],[a]	1.44	-2.1
	2.74	-2.3
	3.43	-2.4
	4.74	-2.7
Kawasaki and Jinno [227],[b]	N/A	-2.4

[a]Experimental data at 283 K using a 50/50 acetonitrile/water mobile phase
[b]Experimental data at 293 K using a 65/35 acetonitrile/water mobile phase

Next, the selectivities between the five isomeric PAHs of the molecular formula $C_{18}H_{12}$, i.e., the four-ring isomers napthacene (NAP), benz[a]anthracene (BaA), chrysene (CHR), BcP, and triphenylene (TrP), are compared to experimental data (see Table 12.2). The selectivity α is computed as the ratio of the capacity factor for a given four-ring PAH relative to TrP (or BcP), the least retained of the four-ring isomers, as follows

$$\alpha_x = k_x^{'}/k_{\text{TrP}}^{'} \tag{12.1}$$

The selectivities computed from simulation are in excellent agreement with experiment for different analytes, coverages, and mobile-phase modifiers. [8, 171, 230] The selectivities agree, within their respective uncertainties, for all but two of the 14 cases. The largest deviation is found for the NAP/TrP selectivity at 2.8 μmol/m^2, but even in this case the discrepancy is small corresponding to a difference in the free energy of retention of only 0.5 kJ/mol. This agreement is a testament to the precision of the simulation method and the accuracy of the force field. For example, the BaP/TrP selectivity at a coverage of 4.2 μmol/m^2 is slightly larger than 1.1. This represents a difference in free energy of retention of 0.2 kJ/mol, an extremely small quantity to measure in either experiment or simulation. In the following, we will focus on the systems containing

Table 12.2: Simulated selectivities of $C_{18}H_{12}$ PAH isomers relative to TrP compared to experiment at different surface coverages.

	Coverage (μmol/m^2)	Org. Mod.	NAP	CHR	BaA	BcP
Sim	4.15	ACN	1.56 ± 0.16	1.14 ± 0.08	1.16 ± 0.10	1.02 ± 0.04
Exp [8]	4.20	ACN	1.70	1.13	1.13	1.08
Sim	2.88	ACN	1.27 ± 0.14	1.12 ± 0.08	1.07 ± 0.09	1.06 ± 0.05
Exp [8]	2.84	ACN	1.58	1.08	1.12	1.06
Sim	1.60	ACN	1.11 ± 0.10	1.12 ± 0.09	1.01 ± 0.11	1.06 ± 0.10
Exp [8]	1.60	ACN	1.19	0.97	1.02	1.02
Sim	2.88	MeOH	1.46 ± 0.06	1.15 ± 0.08	1.04 ± 0.07	0.99 ± 0.11
Exp [171]	2.5	MeOH	1.42	1.13	1.14	–

acetonitrile as the organic modifier because, as indicated by the simulation and experimental data [8, 171, 230] shown in Table 12.2, there appears to be no significant difference in the shape selectivity between acetonitrile and methanol modifiers.

With the knowledge that the retention data for our model RPLC system are in very good agreement with experimental measurements, the remainder of this paper will be devoted to a detailed discussion of the molecular mechanism of retention and shape selectivity for PAHs. This discussion will begin with an examination of the differences in the retention mechanism for PAHs of different molecular weight and be followed by a description of the mechanism for the selectivity between PAHs with the same molecular weight, but with different molecular shape.

One important question regarding the retention mechanism is whether analytes are retained by adsorption at the stationary phase/mobile phase interface or whether they are fully embedded (i.e., partition) into the stationary phase. To examine this, Figure 12.2 shows the $K(z)$ profiles for PAHs ranging in size from one to four rings. In addition, a simulation snapshot at the top of Figure 12.2 is shown to give the reader a frame of reference for the z scale in the stationary phase box. From the $K(z)$ profiles, a number of clear trends emerge when the size of the analyte is increased. Due to the hydrophobic nature of aromatic hydrocarbons, the magnitude of the distribution coefficient increases with increasing number of rings and with increasing ODS surface

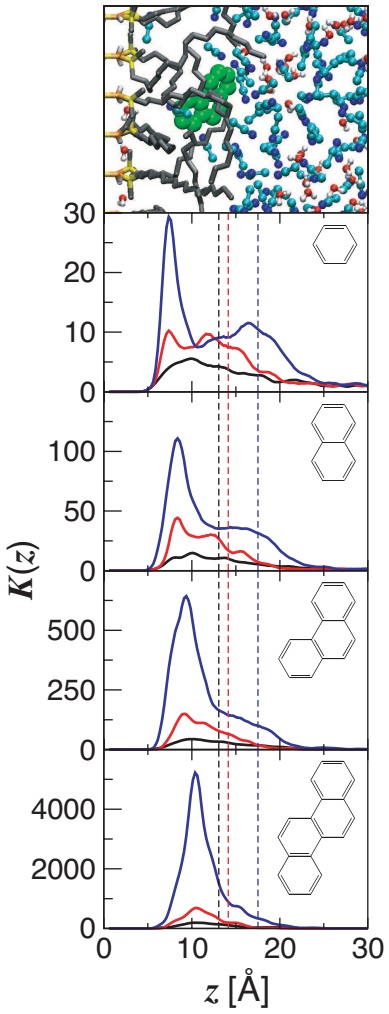

Figure 12.2: Distribution coefficient profiles for PAHs of increasing size. Data for surface coverages of 1.60, 2.88, and 4.15 μmol/m^2 are shown as black, red, and blue lines, respectively. Dashed vertical lines indicate the boundary containing 90% of the ODS carbon density. The simulation snapshot at the top shows the 3-ring phenanthrene analyte (green) in the 2.88 μmol/m^2 system. The z dimension of the snapshot corresponds to the z scale of the plots.

coverage. More interesting are the differences in the shapes of the $K(z)$ profiles. For the smallest analyte, benzene, there a two main peaks in the $K(z)$ profile. These peaks occur within the center of the bonded phase ($z \approx 8$ Å) and near the interface between

the stationary and mobile phases that is indicated here by the z value of the imaginary boundary that would contain 90% of the carbon density of the ODS chains. This bimodal behavior is similar to what has been observed from previous simulations with small alkane solutes and has been attributed to a mixed adsorption/partition mechanism of retention (see Chapters 7 and 9). With an increasing number of rings (molecular weight) of the PAHs, the peak at the interface begins to diminish and is only evident as a shoulder in the $K(z)$ profile for the large four-ring PAH. Thus, as the size of the PAH is increased the mechanism of retention shifts from a mix of partition and adsorption to a nearly pure partition mechanism. Another effect that is observed when the analyte size is increased is that the difference between the lowest and highest surface coverages becomes more pronounced. For benzene, the height of the main peak in the $K(z)$ profile decreases by roughly a factor of five when the surface coverage is changed from 4.2 to 1.6 μmol/m^2, whereas the peak height decreases by more than 20 for the four-ring CHR molecule. It appears that the low-density phase does not provide enough depth to fully accommodate the larger analytes.

Further information on the retention mechanism can be gained by examining the orientation of the analytes within the stationary phase. To accomplish this the alignment of the long axis of the analyte molecules (analogous to the length in the L/B ratio) with the vector normal to the silica surface was analyzed. The z-dependent order parameter, S, describing the angle θ_{I1} between these two vectors is defined as

$$S_{\theta_{\mathrm{I1}}}(z) = \frac{1}{2}\langle 3\cos^2\theta_{\mathrm{I1}}(z) - 1\rangle \tag{12.2}$$

Values approaching zero for this order parameter indicate a random orientation of the analyte (the magic angle can be ruled out in the simulation by evaluation of the distribution of θ_{I1}), values greater than zero indicate a preference for the analyte to be oriented perpendicular to the silica surface, and values less than zero indicate a parallel preference.

The order parameter profiles for PAH analytes of different size at a coverage of 4.15 μmol/m^2 are shown in Figure 12.3. The diagram to the right of the plot in this figure shows the definition of the angle θ_{I1} for napthalene. For the smallest solute benzene, there is a slight preference to be perpendicular when it is located in the center of the bonded phase and a preference to be parallel when very near the silica surface. In

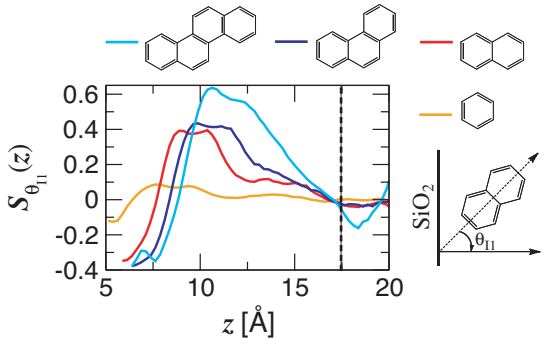

Figure 12.3: Order parameter profiles for PAHs of different size at a coverage of 4.15 μmol/m^2. The dashed vertical line indicates the boundary containing 90% of the ODS carbon density. The diagram to the right gives the definition of the angle θ_{I1}.

the interfacial region there is little orientational preference. As analyte size is increased, the same orientational preferences remain, but become highly amplified. For example, CHR is most retained at a position of about $z = 10$ Å and at this position the order parameter exceeds a value of 0.6 ($\theta_{I1} \approx 30°$). This orientational preference is much stronger than what has been previously observed for alkanes (see Chapters 7 and 9). This clearly suggests that although partitioning is the dominant mechanism for the larger PAH solute, it is much different than bulk liquid–liquid partitioning where one would expect no orientational preference.

Spatial heterogeneity is also present if one examines the distribution of the solutes in the plane containing the silica surface (the x-y plane). The lateral x-y distributions for the different sized PAH analytes when they are retained inside the stationary phase (as defined by the Gibbs dividing surface between mobile and stationary phases described in Chapter 5) are shown in Figure 12.4. It is evident that, regardless of size, the solutes are not distributed uniformly within the x-y plane. However, the lateral distributions become much more heterogeneous as analyte size is increased. The analytes tend to avoid the locations just above the grafting sites of the ODS chains and the larger solutes have fewer available spaces in which to accomplish this. Thus, it appears this non-uniform distribution is due to steric constraints within the stationary phase.

From the analysis of the vertical, lateral, and orientational distributions of the PAH

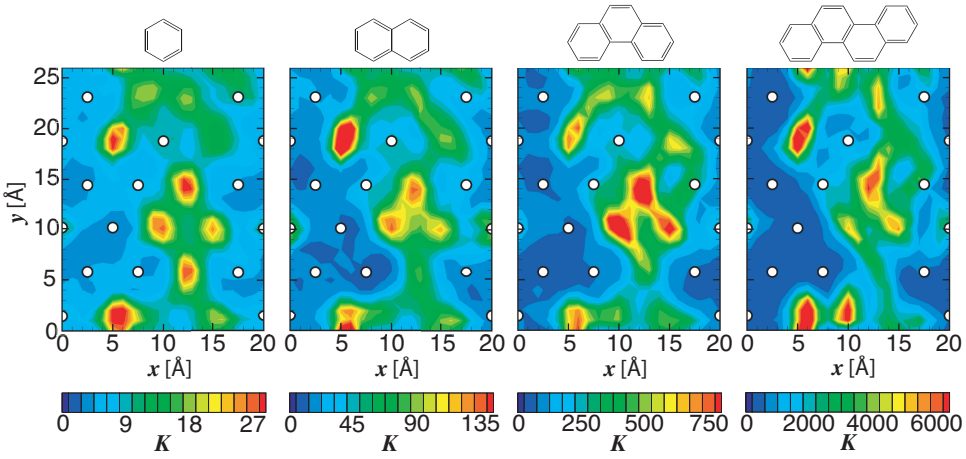

Figure 12.4: Lateral distribution of PAH solutes of different size in the x-y plane at a surface coverage of 4.15 μmol/m^2. The white circles indicate the grafting locations of the ODS chains.

analytes as a function of size, it becomes apparent that the stationary phase is a very heterogeneous environment, especially at higher grafting densities and for larger analytes. This points toward an explanation for the molecular origins of shape selectivity, but more detailed insight can be gained when two PAH analytes of the same size, but with different shapes are compared. For this purpose, the most retained solute (and one with the largest L/B ratio), napthacene (NAP), is compared to one of the least retained solutes, benzo[c]phenanthrene (BcP). In agreement with experimental data [227, 8, 230], our simulations show that the selectivity between these two solutes increases as the grafting density is increased.

The $K(z)$ profiles for NAP and BcP at the three different coverages are shown in Figure 12.5. At the two lower coverages, the BcP solute is slightly less retained, but the general shape of its $K(z)$ profile is similar to that for NAP. At the highest coverage, the BcP solute becomes less retained relative to NAP and the shape of the $K(z)$ profiles begin to show differences. For NAP, the profile is very sharp with a peak at $z = 11$ Å. For BcP, the profile is considerably broader and its peak is shifted to a smaller z value. It appears that BcP, the less elongated solute, is able to penetrate more deeply into the stationary phase, but that the free energy of transfer for NAP is more favorable.

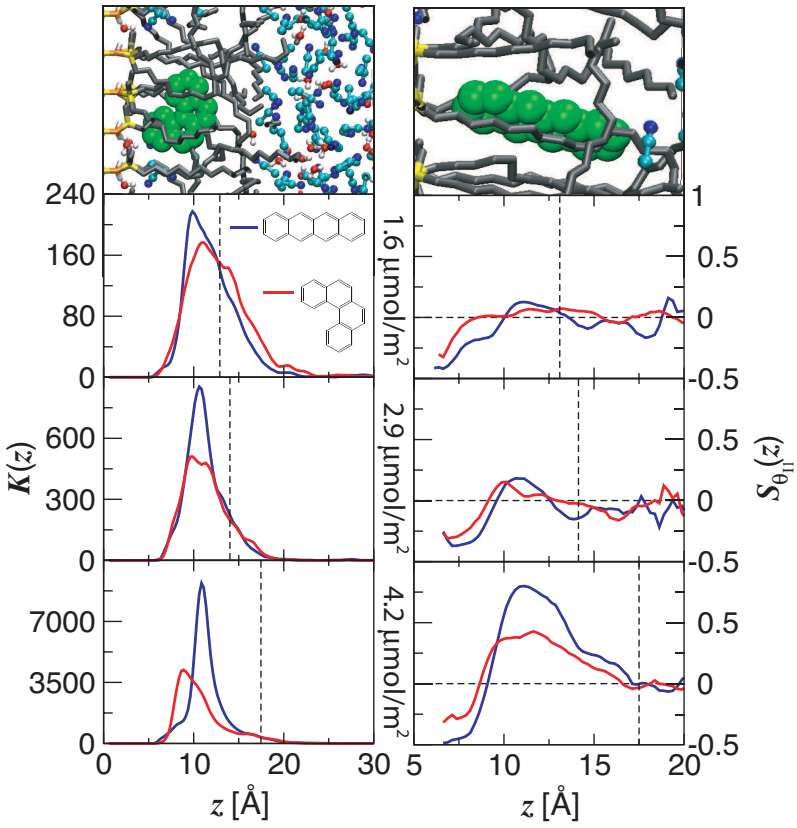

Figure 12.5: Distribution coefficient (left) and order parameter profiles (right) for the NAP and BcP PAH isomers. Dashed vertical lines indicate the boundary containing 90% of the ODS carbon density. The snapshots atop the profiles show BcP (left) and NAP (right) analytes. Both snapshots are for the 4.15 μmol/m^2 phase and the z dimension of the snapshots correspond to the z scale of the plots.

Figure 12.5 also depicts the $S(z)$ profiles for NAP and BcP at the three different coverages studied. At all surface coverages both solutes exhibit a preference to orient parallel to the silica surface when they are very close to it (center of mass at $z < 7$ Å). However, this is not of great consequence because the the $K(z)$ profiles indicate that there is very little retention in this region. The more interesting effects occur in the center of the bonded phase where the solutes are most retained ($z = 8$ to 14 Å). In this region, very little orientational preference is observed at the lowest coverage. However,

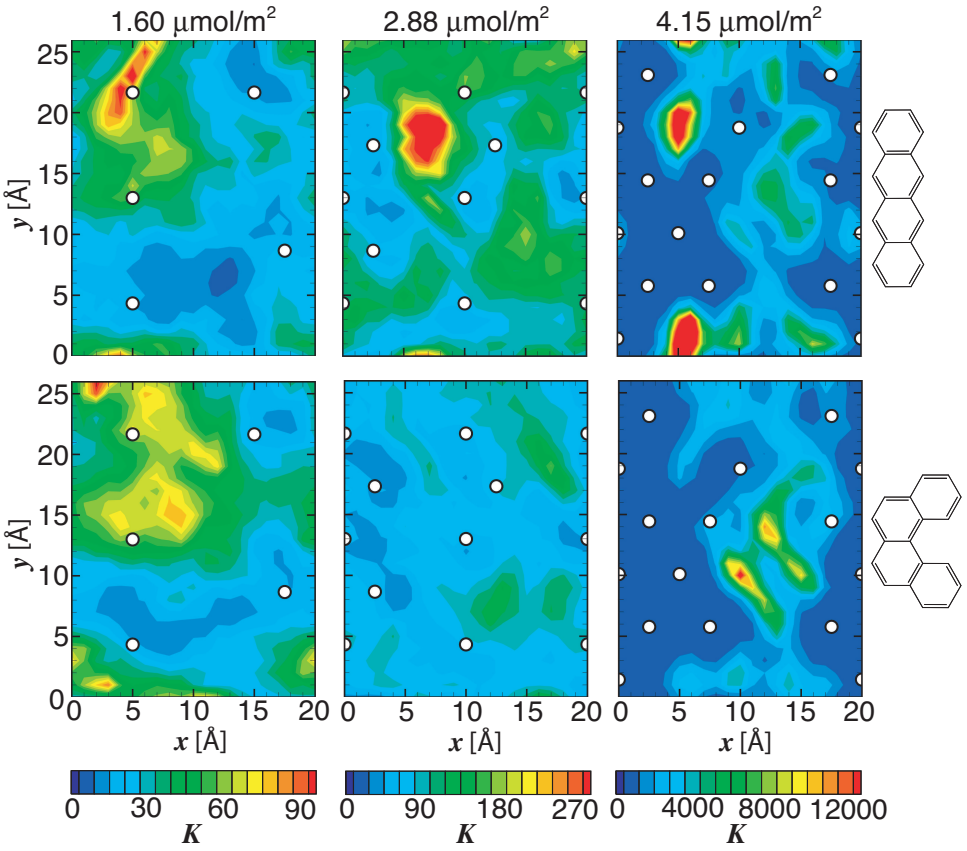

Figure 12.6: Lateral distribution of retained NAP (top) and BcP (bottom) analytes in the x-y plane at the three different surface coverages.

the $S(z)$ values become large and positive as the grafting density is increased showing that the solutes have an increasing preference to align perpendicular to the silica surface, i.e., with the alkyl chains. NAP, the more elongated and more retained solute, exhibits a greater preference for this perpendicular alignment, which explains why it does not penetrate as deeply into the stationary phase as BcP.

The lateral distributions of these two isomeric four-ring solutes in the x-y plane is shown in Figure 12.6. Here, one sees dramatic differences as the grafting density is increased. At the lowest coverage, both solutes exhibit a more uniform distribution (relative to the highest coverage) and the most probable locations for the two analytes

are in roughly the same regions. As the coverage is increased, the lateral distributions become much less uniform and, at the highest coverage, the most retentive regions for each analyte are at distinctively different x-y locations. It appears, based upon the grafting locations of the alkyl chains that the more elongated NAP molecule prefers more crowded chain regions and sits perpendicular to the surface while the more bulky BcP molecule prefers more open regions and has less of tendency to orient perpendicular. Hence, in the latter case, the lateral dimension of the retentive regions is considerably larger than what would be expected from a "slot" that would fit BcP like a glove.

From the heterogeneity of the lateral distributions, one can infer that there are indeed specific retentive regions and that the specificity of these regions becomes more pronounced at higher surface coverages where there is greater shape selectivity. At first hand, the existence of these retentive regions appears to be in agreement with the slot model. However, the slot model states that more elongated and, hence, narrower molecules "would fit into more of the available slots". [222] By this logic, the narrow NAP molecule should also be strongly retained in the same regions as the bulkier BcP molecule, but this is not observed. At the coverage of 4.15 μmol/m^2, BcP is most retained in the region around $x = 12$ Å, $y = 10$ Å, whereas NAP is less strongly retained in this region by a factor of about 2 compared to its most favored regions at $x = 6$ Å, $y = 2$ Å and at $x = 6$ Å, $y = 19$ Å. Furthermore, the logic of the slot model dictates that the bulkier BcP does not fit into the latter two retentive regions, but it is also found there albeit with K values that are about a factor of 3 to 4 smaller than for its own most favored region. Therefore, it is clear that the molecular origins of shape selectivity must be more complex and nuanced than envisioned by the slot model. Given the diffusiveness of the preferred retentive regions, one may speculate that the shape selectivity involves the ability of the ODS chains to provide favorable solvation environments by adapting to the presence of the analyte molecule, but that different local grafting environments play a role in determining how favorable the solvation environment can become for different analytes.

Analysis of the simulation trajectories allow us to distinguish whether the most favorable retentive regions are pre-existing, static slots or, on the contrary, slots are not naturally present and the stationary phase chains respond to the presence of the solutes in order to achieve these favorable regions. The two snapshots shown in Figure 12.7

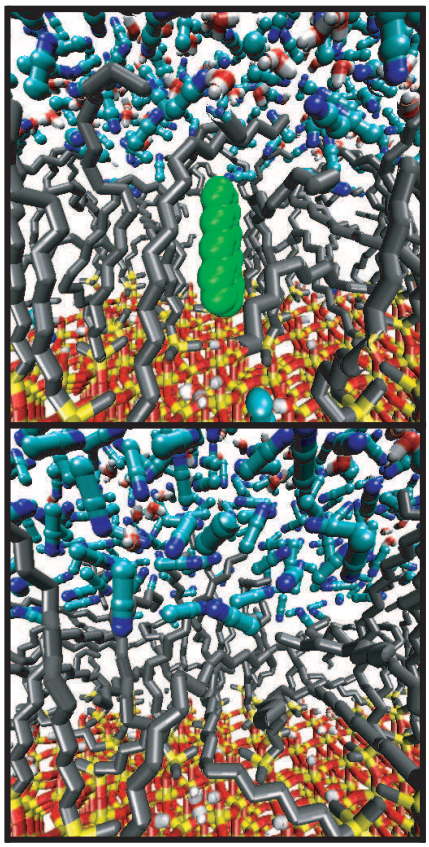

Figure 12.7: Snapshots of the stationary chain structure in the presence and absence of a solute. Both snapshots were taken from the same perspective, but at different periods during the simulation.

visually suggest that these retentive regions are neither static nor pre-existing. The top snapshot illustrates the 4.15 μmol/m^2 stationary phase in the presence of a retained napthacene solute. Around this solute, the chains are neatly aligned nearly perpendicular to the silica surface and form a well shaped cavity for the solute to reside in. The bottom snapshot depicts the exact same perspective, but for a configuration from the simulation when no solute is present. In this snapshot, the chains are less well aligned and the cavity is not present, rather the chains are able to relax and fill the space that was previously occupied by the solute. Thus, it appears that the chains respond to the presence of the solute and these retentive regions are not static. These snapshots,

Table 12.3: Structural properties of C_{18} stationary phase chains nearby a four-ring PAH molecule and in the absence of any analyte molecules.[a]

Coverage	Nearby Analyte			Without Analyte		
(μmol/m^2)	cos θ_{ete}	S_{16}	f_{gauche}	cos θ_{ete}	S_{16}	f_{gauche}
1.60	0.51_2	$+0.01_1$	0.24_1	0.37_6	-0.08_3	0.22_2
2.88	0.52_1	$+0.02_1$	0.24_1	0.45_2	-0.04_2	0.23_1
4.15	0.74_3	$+0.27_2$	0.24_1	0.67_1	$+0.17_1$	0.26_1

[a]Subscripts indicate the standard error of the mean in the final digit.

though intriguing, represent only two configurations from the entire simulation and it would be improper to draw any conclusions from these alone. However, a further analysis of the average chain properties throughout the entire simulation trajectories supports the dynamic view inferred from the snapshots.

To analyze the effect of retained solutes on ODS chain conformation, three structural properties are considered. The first is the cosine of the angle between the chain end-to-end vector and the normal to the silica substrate ($\cos\theta_{\text{ete}}$), the second is the order parameter for the angle between the 1–3 backbone vectors of the chain and silica substrate (S), and the third is the fraction of gauche defects (f_{gauche}). These quantities are defined in Chapter 5, however, for the present discussion these properties are computed separately for chains with no solute of any type present, and for chains with any four-ring PAH solute nearby. A solute is defined to be nearby the chain if r_{xy} is less than 7 Å. Here, r_{xy} is defined as

$$r_{xy} = \sqrt{(x_{\text{PAH}} - x_{\text{ODS}})^2 + (y_{\text{PAH}} - y_{\text{ODS}})^2} \tag{12.3}$$

where x_{PAH} and y_{PAH} correspond to the x and y center of mass coordinates of the PAH solute and x_{ODS} and y_{ODS} correspond to the grafting location of the stationary phase chain. This definition comes from the position of the first minimum in a two dimensional (x and y) radial distribution function between these sites.

Numerical data quantifying the effects of the analytes on the chain structure are summarized in Table 12.3. For all coverages, values of $\cos\theta_{\text{ete}}$ and S_{16} increase in the presence of a PAH analyte. This indicates an enhancement in the alignment and ordering when the chains are solvating a PAH molecule. The fraction of gauche defects

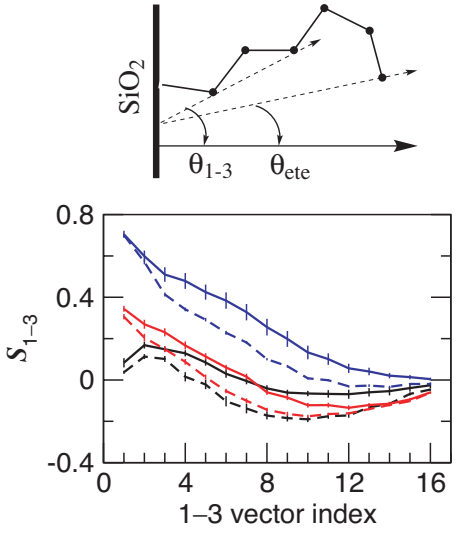

Figure 12.8: Top, definition of the 1–3 and end-to-end (ete) vectors used to characterize chain alignment. For clarity, the diagram is shown only for a C_6 chain. Bottom, order parameter along the chain backbone indicating chain alignment. Black, red, and blue lines correspond to surface coverages of 1.60, 2.88, and 4.15 μmol/m^2, respectively. Solid lines denote chains near a four-ring PAH molecule while dashed lines indicate chains in the absence of any analyte.

appears to be insensitive to the presence of analytes. More local information for the order parameter is shown in Figure 12.8, which gives the order parameter for each backbone position along the chain. The shift to larger values again indicates that the chains are more aligned when analyte molecules are present. However, these also show that this ordering effect is most pronounced in the central portions of the chains. The first and last backbone vectors seem to be influenced little by the analytes. This can be explained by the fact that the first backbone vector has less freedom of movement due to the grafting to the silica surface; since the analytes are most often fully embedded in the stationary phase, the terminal end of the chain may fold over the top of the solute and, thus, show less alignment. The latter effect is also evident in the snapshot (see top part of Figure 12.7).

The fact that the chain structure does respond to the PAH analytes does not rule out the possibility for pre-existing slots, however, it does indicate that these slots would

not be as rigid as has been implied by the MD simulations of Lippa and coworkers[61]. To examine whether these slots are pre-existing, the lateral density distributions of the carbon segments in the C_{18} chains in the absence of solute were computed. These density distributions were divided into two regions with respect to the surface normal. The inner region extends from the silica surface ($z = 0$ Å) to the z location where 50% of the total carbon density is contained and the outer region extends from this 50% location to the 90% location (see Figure 12.9). The x-y distributions of the carbon density in these two regions for the three different surface coverages are represented by the contour plots shown in Figure 12.9. Examination of these contour plots points to a non-uniform distribution of the carbon density in the inner region. There are definite regions of high and low carbon density. The regions of high carbon density occur, not surprisingly, near the grafting locations of the chains. Despite areas of lower density, extended regions of "empty space", or slots, large enough to accommodate any PAH analyte do not exist at the highest surface coverage. A comparison of the carbon density distribution for the highest surface coverage to the corresponding analyte distributions in Figure 12.6 indicates that the analytes are not retained in the regions where the lowest carbon density is found, but in regions where the carbon density exceeds values of 0.5 g/mL (when no analyte molecules are present), a significant density considering that the density of liquid n-hexadecane is 0.77 g/mL at this temperature. In order for the solutes to be retained in these locations the chains must respond and move out of the way. Therefore, these retentive regions are not pre-existing. Examination of the outer region yields further evidence that these retentive regions are not static slots. In particular for the highest coverage, again where the most shape selectivity is observed, the outer region is nearly homogeneous and has a density close to that of a liquid alkane. There are definitely no static slots, or regions of very low density, present in the outer region of the ODS chains at the highest coverage. Actually, only the low-grafting density phase possesses regions with rather low carbon density, but comparison to the analyte distributions shows rather convincingly that the analytes disfavor these regions.

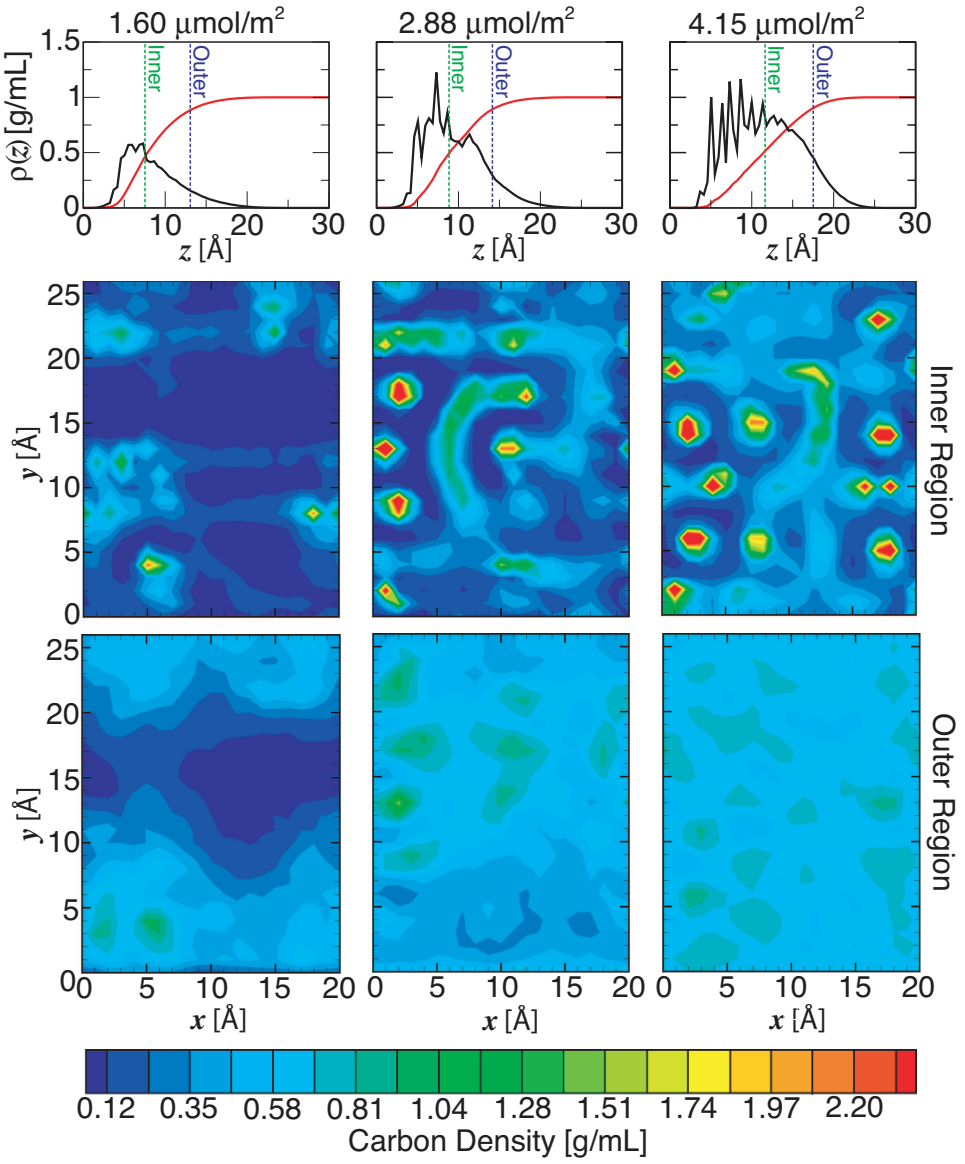

Figure 12.9: Top, definition of the inner and outer stationary phase regions. Black lines indicate the stationary phase carbon density as a function of z and red lines indicate the integral of the density fraction. Blue and green dashed vertical lines indicate where this integral reaches 50% and 90% of its limiting value (i.e., the boundaries of the inner and outer regions). Bottom, stationary phase carbon density in the x-y plane for these two regions obtained in the absence of any analyte molecules.

12.4 Conclusions

Efficient configurational-bias Monte Carlo simulations in the Gibbs ensemble using the accurate TraPPE force field have been carried out to examine shape selectivity of PAHs in RPLC systems with various ODS grafting densities. The simulations reproduce the experimental retention data for the phenyl increment and for the selectivities between the five isomeric PAHs of molecular formula $C_{18}H_{12}$. The dependence of these quantities on grafting density is also in agreement with experiment. Validation of the simulation results against experimental retention data allows for more confidence in the molecular details concerning the molecular retention mechanism gathered from the simulations.

The simulations indicate that the various PAH analytes exhibit a rather heterogeneous distribution when retained in the stationary phase. The PAH molecules prefer to be fully embedded in the stationary phase rather than adsorb at the stationary/mobile phase interface. When buried in the stationary phase the solutes prefer to align their long axes perpendicular to the silica surface and reside in regions where the ODS segment density in the absence of analytes would have intermediate values, i.e., neither on top of the grafting locations of the ODS chains nor too far away from these grafting locations. All of these effects become more pronounced at higher surface coverages and for larger PAH analytes.

In regards to shape selectivity, it is found here that there are different most favorable retentive regions for different isomeric four-ring PAHs and that these regions are found at different lateral locations within the stationary phase. However, other PAH isomers are not completely excluded from the most favorable retentive regions of another PAH isomer. For example, at a surface coverage of 4.15 μmol/m^2, the local distribution coefficient for BcP molecules in the regions most favorable for NAP differs only by a factor of less than 5 from the K value for NAP and a similar observation can be made for the region most favorable for BcP.

Finally, these favorable retentive regions are not pre-existing cavities or slots. When the analyte molecules are absent, these regions are occupied by the ODS chains. In the presence of analyte molecules, nearby ODS chains respond by becoming more aligned in order to create a solvation environment that can best accommodate the solute.

Chapter 13

Effects of Solute Chain Length

13.1 Background

Throughout most of this thesis relatively small solutes, like butane, were examined. However, larger PAH solutes were studied in the previous chapter. Here, it was shown that for small PAH solutes, like benzene, the retention mechanism is somewhat similar to butane (i.e., mixed adsorption/partition) but for large PAH solutes the retention mechanism is mainly partitioning. PAHs are conformationally rigid molecules, so it is now questioned whether this change in retention mechanism with increasing solute size occurs only for rigid solutes. In this chapter the retention mechanism of large, but flexible, solutes is examined by carrying out simulations of an RPLC system with linear alkane solutes up to 14 carbons in length.

In regards to solute chain length, it has been observed from retention measurements with various homologous series (for example, alkanes, alcohols, or carboxylic acids, with increasing chain length) that there is a discontinuity in plots of $\log k'$ vs. number of carbons [206, 231]. This discontinuity occurs about where the number of carbons in the solute exceeds the number of carbons in the stationary phase chains (the critical carbon number). Stated otherwise, the methylene increment ($\Delta G_{\mathrm{CH_2}}$) shows a small increase at this critical carbon number. For example, Tchapla and coworkers found, for a C_8 stationary phase and 10/90 (v/v) water/methanol mobile phase, that the methylene

† This chapter describes the outcome of a collaborative research project carried out by Jake L. Rafferty and advised by J. Ilja Siepmann and Mark. R. Schure.

increment increased (became less favorable) by 96 J/mol when the number of carbons in the solute was greater than ten [206]. From this it was suggested that the solutes fully embed themselves (partition) into the stationary phase until their length exceeds the length of the stationary phase and, after this, the remaining portion of the solute is forced to reside outside the stationary phase and adsorb at the surface [206, 231]. Indeed this is a very small change in free energy to suggest a change in the retention mechanism. However, given that simulation data from the present work have indicated $\Delta G_{\mathrm{CH_2}}(z)$ is only slightly smaller in the interfacial region as compared to in the center bonded phase (see Figures 7.3, 9.8 and 11.4), this explanation seems at least plausible.

13.2 Simulation Details

The simulations examining the effects of solute length made use of the configurational-bias Monte Carlo (CBMC) technique applied in the NpT Gibbs ensemble and the three-box slit pore set up as described in Chapter 5. The stationary phase consisted of a dimethyl octylsilane (C_8) chains grafted to a silica substrate at a coverage of 2.9 μmol/m^2. The mobile phase was a mixture of 33% water and 67% methanol. A total of 18 stationary phase chains and 400 water and 800 methanol molecules were present in the simulations. A similar C_8 stationary phase in contact with a water/methanol was examined in Chapter 11. Thus, an analysis of system structure will not be presented here. The main focus of this chapter is the examine the effects of solute chain length. For this purpose, 8 linear alkanes (methane, ethane, butane, hexane, octane, decane, dodecane, and tetradecane) were present in the simulations as probe solutes. 20 helium atoms were also present to maintain a vapor box of adequate size. Four independent simulations were carried out, each consisting of 2×10^5 Monte Carlo cycles of equilibration and 5×10^5 cycles of production.

Solvent and solute molecules were allowed to transfer between the three boxes via CBMC particle exchange [91, 92] and identity interchange moves [93, 94]. These identity interchange moves are absolutely necessary for sampling the spatial distribution of the large solutes. To avoid overloading the stationary and/or mobile phase with these large solutes it was necessary to apply a uniform bias potential in each simulation box such that each solute spent 20% of its time in the stationary phase box, 20% in the mobile

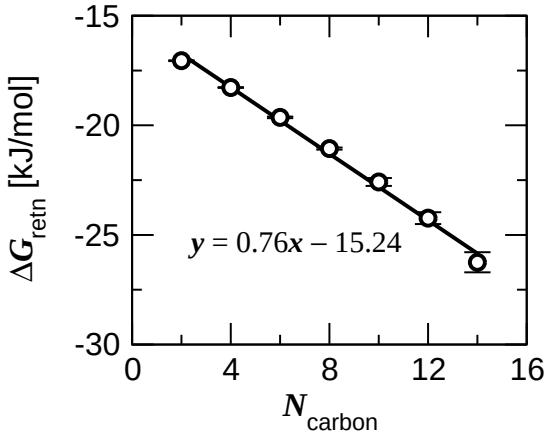

Figure 13.1: Free energy of retention versus solute carbon number for the homologous series of alkanes.

phase box, and 20% in the vapor phase box. Thus, on average, there were less than two solutes in the stationary or mobile phases. The distribution coefficients and free energies of retention reported in this work are corrected for these bias potentials. During the equilibration period, it was observed that the larger solutes had a tendency to cluster while in the vapor phase due to their low vapor pressure. To eliminate this clustering, the solutes were treated as ideal particles (no intermolecular interactions) while in the vapor phase. The solutes were fully interacting while in stationary and mobile phases. This is of no consequence to the reported results as the vapor phase in these simulations is not involved in the retentive process and is used here only as an intermediate transfer medium.

13.3 Results and Discussion

The computed free energy of retention for linear alkanes as a function of solute carbon number is shown in Figure 13.1. The slope of this plot corresponds to the methylene increment. It is evident from the plot that methylene increment does show an appreciable change when the solute carbon number is increased past the number of carbons in the stationary phase chains. However, it should be noted that the change in methylene

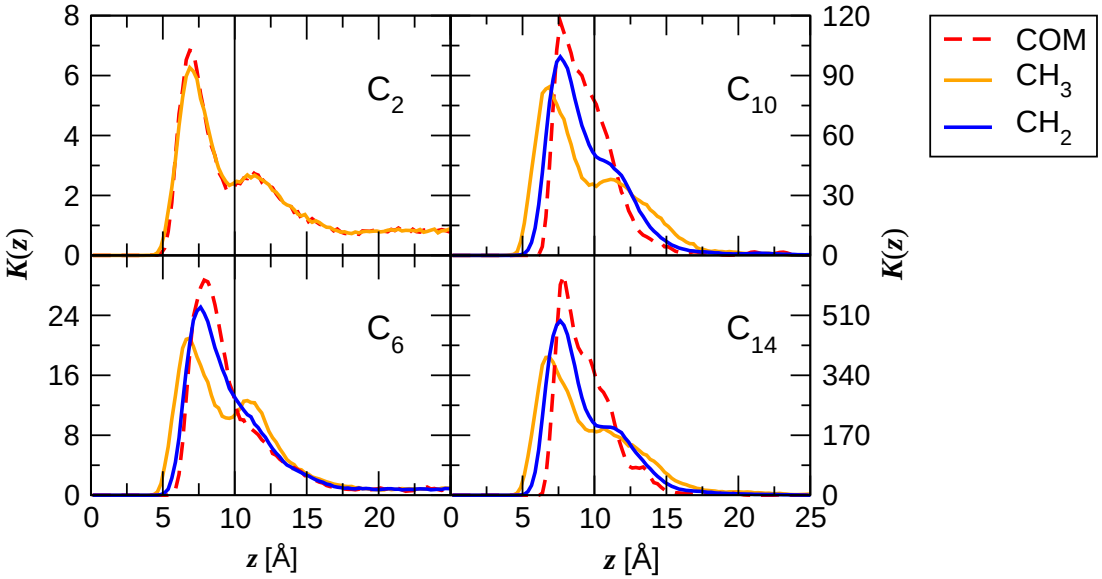

Figure 13.2: Distribution coefficient profiles for alkane solutes of different length. Vertical lines indicate the position of the GDS.

increment observed by Tchapla and coworkers is minute (0.096 J/mol), and although the uncertainties in free energies of retention computed from simulation are very small for smallest solutes examined (±20 J/mol for ethane), they become significant for the largest solutes (±400 J/mol for tetradecane). Thus, because of this inadequate precision, it difficult to judge whether the simulation results are inaccurate. By most standards these simulation results are extremely precise and it is just very difficult to observe such a small change in the methylene increment without prohibitively long simulations. Despite this, an analysis of the spatial and orientational distribution may still be useful for examining the retention mechanism of large, flexible solutes.

Distribution coefficients as a function of distance from the silica surface for solutes of varying length are presented in Figure 13.2. Throughout this thesis, these distribution coefficient profiles have been computed using the center of mass coordinates of the solutes. However, due to large size and flexibility of the solutes examined here these coordinates may not be the best descriptor of solute location. Therefore, in addition to center of mass (COM) position, profiles are also shown for the location of methyl

(CH_3) and methylene (CH_2) groups in the solutes. With the exception of ethane (C_2), the COM profiles for the solutes of different length appear somewhat similar. There is one peak inside the GDS and this peak has a shoulder the extends outside the GDS. The COM profile for C_2 shows a clear bimodal distribution with one peak inside the GDS and one peak outside. This bimodal behavior was observed for a C_4 alkane on a C_{18} stationary phase and attributed to a mixed adsorption/partition mechanism (see Chapter 7).

As mentioned above, the COM profile might not yield a full description of solute location. For example, the COM may be located inside the GDS (indicating a partition mechanism) while part of the solute is outside the GDS (partial adsorption). For this reason, CH_3 and CH_2 profiles were also examined. When viewing the CH_3 profiles, a bimodal behavior is observed in all systems and there is one peak inside the GDS and one peak outside. Furthermore, the CH_2 profiles indicate that there is a probability for methylene groups to be located well outside the GDS, however the most probable location for this group is inside the stationary phase. Thus, while the COM of the larger solutes is mainly located inside the GDS, the CH_3 group shows a fairly high probability to be located outside the GDS. These observations are consistent with the suggestion that large solutes are retained by embedding part of the chain inside of the stationary phase while the remainder of the chain adsorbs at the bonded phase surface [206, 231]. However, these observations are not consistent with the view that the small solutes fully embed themselves (partition) into the stationary phase. The bimodal COM distribution exhibited by the C_2 solute clearly demonstrates this.

Further information on the retention mechanism of these solutes can be seen in the order parameter profiles shown in Figure 13.3. The profiles show the order parameter for the 1–3 backbone vectors of the solute chain (S_i) plotted as a function of the z-location of the center of the backbone vector. Positive values for this order parameter indicate vectors aligned perpendicular to the silica surface, negative values indicate parallel vectors, and zero indicates vectors with no orientational preference. The order parameter profiles are fairly similar in shape regardless of solute size. However, they are shifted downward (more parallel preference) as solute size is increased. For values of $z < 7$ Å, the 1–3 backbone vectors show a preference to be parallel to the silica surface while at the GDS these vectors have a perpendicular preference. Just outside

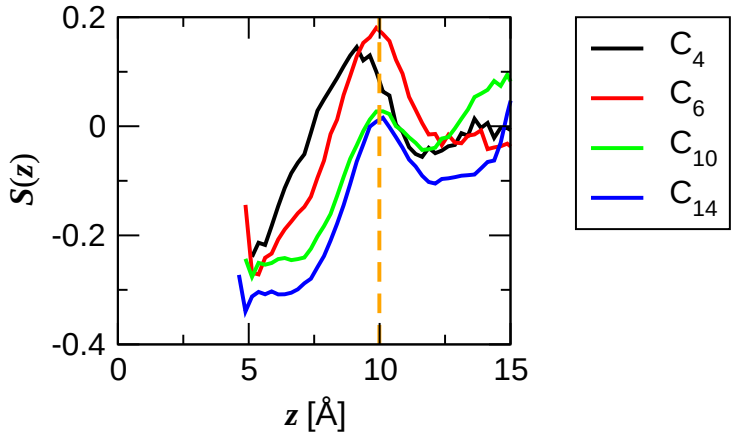

Figure 13.3: Order parameter profiles for linear alkane solutes of different length. The dashed lines indicate the position of the GDS.

the GDS, the vectors appear to have a slight parallel preference and moving further into the mobile they become randomly oriented. Thus, the portions of the alkyl chain that are buried deep inside the stationary phase are somewhat flat relative to the silica surface as they encounter the "wall" created by the dimethyl side chains of stationary phase. Near the ends of the stationary phase chains, solute segments are perpendicular and outside the stationary phase they lie flat against the alkyl surface. Again, these observation are consistent with suggested mechanism of retention for large solutes, but inconsistent with a pure partition mechanism for small solutes.

A representative snapshot for a retained C_{14} solute is shown in Figure 13.4. The location of this chain is consistent with the distribution coefficient profiles shown in Figure 13.2. I.e., the COM of the solute is at about $z = 8$ Å and the CH_3 groups are bimodally distributed with one inside the stationary phase and one at the surface. Consistent with the order parameter profiles, the portion of the chain nearest the silica substrate is flat as it encounters the dimethyl side chains and the remaining portion of the solute inside the stationary phase is perpendicular to the silica surface. The portion of the solute outside the stationary phase is lying flat atop the alkyl surface.

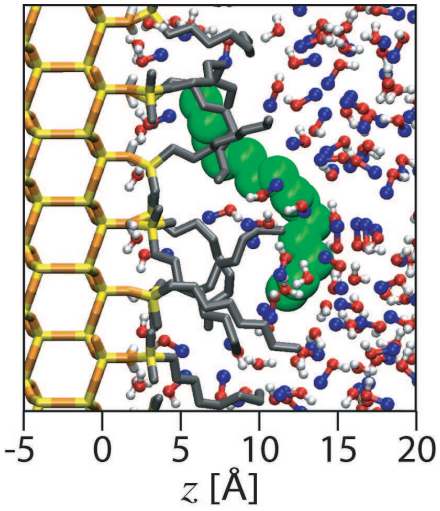

Figure 13.4: Snapshot of a C_{14} alkane solute retained on a C_8 stationary phase.

13.4 Conclusions

The proposed mechanism of retention for large flexible solutes based on experimental retention data [206, 231] appears to be correct. Larger alkanes partially embed themselves in the stationary phase while the remainder of the solute is adsorbed at the stationary phase surface. However, the proposed change in retention mechanism when going from small solutes to large solutes is not observed. Small solutes are not retained solely by a partition mechanism, rather they also show a mixed adsorption/partition mechanism. Thus, for flexible solutes, the retention mechanism does not change with solute size. The only difference is that, due to their length, large flexible solutes can exhibit both absorption and partition simultaneously. This is in contrast to rigid PAH solutes (see Chapter 12). In this case, smaller solutes show a mixed adsorption/partition mechanism while larger solutes are retained primarily by a partition mechanism.

References

[1] J. L. Humphrey, G. E. Keller II, Separation Process Technology, McGraw-Hill, New York, 1997.

[2] R. E. Majors, Current trends in HPLC column usage, LC GC North Amer. 25 (2007) 532–544.

[3] U. D. Neue, HPLC Columns: Theory, Technology and Practice, Wiley-VCH, New York, 1997.

[4] A. Braithwate, F. J. Smith, Chromatographic Methods, Chapman and Hall, 1985.

[5] P. W. Carr, D. E. Martire, L. R. Snyder, Preface, J. Chromatogr. A 656 (1993) 1.

[6] H. Colin, G. Guiochon, Comparison of some packings for reversed-phase high-performance liquid-solid chromatography: II. Some theoretical considerations, J. Chromatogr. 158 (1978) 183–205.

[7] K. B. Sentell, J. G. Dorsey, Retention mechanisms in reversed-phase liquid chromatography. Stationary-phase bonding density and partitioning, Anal. Chem 61 (1989) 930–934.

[8] K. Sentell, J. G. Dorsey, Retention mechanism in reversed-phase chromatography: Stationary phase bonding density and solute selectivity, J. Chromatogr. 461 (1989) 193–207.

[9] B. Buszewski, Z. Suprynowicz, P. Staszczuk, K. Albert, B. Pfleiderer, E. Bayer, Effect of coverage density on the retention mechanism in reversed-phase high-performance liquid chromatography, J. Chromatogr. 499 (1990) 305–316.

[10] A. Tchapla, S. Heron, E. Lesellier, H. Colin, General view of molecular interaction mechanisms in reversed-phase liquid chromatography, J. Chromatogr. A 656 (1993) 81–112.

[11] P. W. Carr, J. Li, A. J. Dallas, D. I. Eikens, L. T. Tan, Revisionist look as solvophobic driving forces in reversed-phase liquid chromatography, J. Chromatogr. A 656 (1993) 113–133.

[12] P. W. Carr, L. C. Tan, J. H. Park, Revisionist look at solvophobic driving forces in reversed-phase liquid chromatography III. Comparison of the behavior of nonpolar and polar solutes, J. Chromatogr. A 724 (1996) 1–12.

[13] J. H. Park, Y. K. Lee, Y. C. Weon, L. C. Tan, J. Li, L. Li, J. F. Evans, P. W. Carr, Revisionist look at solvophobic driving forces in reversed-phase liquid chromatography IV. Partitioning vs. adsorption mechanism on various types of polymeric bonded phases , J. Chromatogr. A 767 (1997) 1–10.

[14] L. C. Tan, P. W. Carr, Revisionist look at solvophobic driving forces in reversed-phase liquid chromatography II. Partitioning vs. adsorption in monomeric alkyl bonded phase supports, J. Chromatogr. A 775 (1997) 1–12.

[15] R. P. J. Ranatunga, P. W. Carr, A study of the enthalpy and entropy contributions of the stationary phase in reversed-phase liquid chromatography, Anal. Chem. 72 (2000) 5679–5692.

[16] C. Horváth, W. Melander, I. Molnár, Solvophobic interactions in liquid chromatography with nonpolar stationary phases, J. Chromatogr. 125 (1976) 129–156.

[17] A. Vailaya, C. Horváth, Solvophobic theory and normalized free energies of nonpolar substances in reversed phase chromatography, J. Phys. Chem. B 101 (1997) 5875–5888.

[18] A. Vailaya, C. Horváth, Retention in reversed-phase chromatography: partition or adsorption?, J. Chromatogr. A 829 (1998) 1–27.

[19] L. C. Sander, S. A. Wise, Shape selectivity in reversed-phase liquid chromatography for the separation of planar and non-planar solutes, J. Chromatogr. A 656 (1993) 335–351.

[20] D. R. Devido, J. G. Dorsey, H. S. Chan, K. A. Dill, Oil/water partitioning has a different thermodynamic signature when the oil solvent chains are aligned than when they are amorphous, J. Phys. Chem. B 102 (1998) 7272–7279.

[21] K. Kaczmarski, W. Prus, T. Kowalska, Adsorption/partition model of liquid chromatography for chemically bonded stationary phases of the aliphatic cyano, reversed-phase C_8 and reversed-phase C_4 types, J. Chromatogr. A 869 (2000) 57–64.

[22] P. Nikitas, A. Pappa-Louisi, P. Agrafiotou, New insights on the retention mechanism of non-polar solutes in reversed-phase liquid chromatographic columns, J. Chromorogr. A 1034 (2004) 41–54.

[23] F. Gritti, G. Guichon, Critical contribution of nonlinear chromatography to the understatnding of the retention mechanism in reversed-phase liquid chromatography, J. Chromatogr. A 1099 (2005) 1–42.

[24] Y. V. Kazakevich, R. LoBrutto, F. Chan, T. Patel, Interpretation of the excess adsorption isotherms of organic eluent on the surface of reversed-phase adsorbents: Effect on the analyte retention, J. Chromatogr. A 913 (2001) 75–87.

[25] F. Gritti, G. Guiochon, Adsorption mechanism in reversed-phase liquid chromatography: Effect of the surface coverage of a monomeric C18-silica stationary phase, J. Chromatogr. A 1115 (2006) 142–163.

[26] L. C. Sander, K. A. Lippa, S. A. Wise, Order and disorder in alkyl stationary phases, Anal. Bioanal. Chem. 382 (2008) 646–668.

[27] S. C. Rutan, J. M. Harris, Electronic spectroscopic investigations of the stationary phase in reversed-phase liquid chromatography, J. Chromatogr. A 656 (1993) 197–215.

[28] K. B. Sentell, Nuclear magnetic resonance and electron spin investigations of liquid chromatographic retention mechanisms: Stationary phase structure, J. Chromatogr. A 656 (1993) 231–263.

[29] R. C. Bogar, J. C. Thomas, J. B. Callis, Lateral diffusion of solutes bound to the alkyl surface of C_{18} reversed-phase liquid chromatographic packings, Anal. Chem. 56 (1984) 1080–1084.

[30] R. L. Hansen, J. M. Harris, Lateral diffusion of molecules partitioned into the silica-bound alkyl chains: Influence of chain length and bonding density, Anal. Chem. 68 (1996) 2879–2884.

[31] M. J. Wirth, J. D. Burbage, Adsorbate reorientation at a water/(octadecylsilyl)-silica interface, Anal. Chem. 63 (1991) 1311–1317.

[32] M. J. Wirth, D. J. Swinton, Single-molecule probing of mixed-mode adsorption at a chromatographic interface, Anal. Chem. 70 (1998) 5264–5271.

[33] M. D. Ludes, M. J. Wirth, Single-molecule resolution and fluorescence imaging of mixed-mode sorption of a dye at the interface of C_{18} and acetonitrile/water, Anal. Chem. 74 (2002) 386–393.

[34] M. J. Wirth, D. J. Swinton, M. D. Ludes, Adsorption and diffusion of single molecules at chromatographic interfaces, J. Phys. Chem. B 107 (2003) 6258–6268.

[35] Z. Elkoshi, E. Grushka, Hydrophobic interaction and chromatographic processes, J. Phys. Chem 85 (1981) 2980–2986.

[36] D. E. Martire, R. E. Boehm, Unified theory of retention and selectivity in liquid chromatography. 2. Reversed-phase liquid chromatography with chemically bonded phases, J. Phys. Chem. 87 (1983) 1045–1062.

[37] M. Jarionec, D. E. Martire, A general model of liquid–solid chromatography with mixed mobile phases involving concurrent adsorption and partition effects, J. Chromatogr. 351 (1986) 1–16.

[38] J. A. Marqusee, K. A. Dill, Solute partitioning into chain molecule interphases monolayers, bilayer membranes, and micelles, J. Chem. Phys 96 (1986) 434–444.

[39] K. A. Dill, The mechanism of solute retention in reversed-phase liquid chromatography, J. Phys. Chem. 91 (1987) 1980–1988.

[40] J. Dorsey, K. A. Dill, The molecular mechanism of retention in reversed-phase liquid chromatography, Chem. Rev. 89 (1989) 331–346.

[41] P. T. Ying, J. G. Dorsey, K. A. Dill, Retention mechanisms of reversed-phase liquid chromatography: determination of solute-solvent interaction free energies, Anal. Chem. 61 (1989) 2540–2546.

[42] M. Jaroniec, Partition and displacement models in reversed-phase liquid chromatography with mixed eluents, J. Chromatogr. A 656 (1993) 37–50.

[43] R. Tijssen, P. J. Shoenmakers, M. R. Böhmer, L. K. Koopal, H. A. H. Billiet, Lattice models for the description of partitioning/adsorption and retention in reversed-phase liquid chromatography, including surface and shape effects, J. Chromatogr. A 656 (1993) 135–196.

[44] R. E. Boehm, D. E. Martire, Theory of liquid chromatographic retention and solute-transfer thermodynamics using the Bethe-Guggenheim quasi-chemical approach, J. Phys. Chem 98 (1994) 1317–1327.

[45] I. Rustamov, T. Farcas, F. Chan, R. LoBrutto, H. M. McNair, Y. V. Kazakevich, Geometry of chemically modified silica, J. Chromatogr. A 913 (2001) 49–63.

[46] F. Gritti, Y. V. Kazakevich, G. Guiochon, Effect of surface coverage of end-capped C_{18}-silica on the excess adsorption isotherms of commonly used organic solvents from water in reversed phase liquid chromatography, J. Chromatogr. A 1169 (2007) 111–124.

[47] J. E. Pemberton, M. Ho, C. J. Orendorff, M. W. Ducey, Raman spectroscopy of octadecylsilane stationary phase conformational order: Effect of solvent, J. Chromatogr. A 913 (2001) 243–252.

[48] M. W. Ducey, C. J. Orendorff, J. E. Pemberton, L. C. Sander, Structure-function relationships in high-density octadecylsilane stationary phases by Raman spectroscopy. 2. Effect of common mobile phase solvents, Anal. Chem. 74 (2002) 5585–5592.

[49] S. J. Klatte, T. L. Beck, Molecular dynamics of tethered alkanes: Temperature-dependent behavior in a high density chromatographic system, J. Phys. Chem. 97 (1993) 5727–5734.

[50] S. J. Klatte, T. L. Beck, Molecular dynamics simulations of tethered alkane chromatographic stationary phases, J. Phys. Chem. 99 (1995) 16024–16032.

[51] S. J. Klatte, T. L. Beck, Microscopic simulation of solute transfer in reversed phase liquid chromatography, J. Phys. Chem. 100 (1996) 5931–5934.

[52] T. L. Beck, S. J. Klatte, Computer simulations of interphases and solute transfer in liquid and size exclusion chromatography, in: J. F. Parcher, T. L. Chester (Eds.), Unified Chromatography, ACS Symposium Series, Vol. 748, American Chemical Society, Washington, D.C., 2000, pp. 67–81.

[53] M. R. Schure, Molecular dynamics of liquid chromatography: Chain and solvent structure visualization, in: J. J. Pesek, I. E. Leigh (Eds.), Chemically Modified Surfaces, Royal Society of Chemistry, Cambridge, 1994, pp. 181–189.

[54] M. R. Schure, Particle simulation methods in separation science, in: P. R. Brown, E. Grushka (Eds.), Advances in Chromatography, Vol. 39, Marcel Dekker, New York, 1998, pp. 435–441.

[55] I. Yarovsky, I. Yu, M.-I. Aguilar, M. T. W. Hearn, High-performance liquid chromatography of amino acids, peptides and proteins. CXXV. Molecular dynamics simulation of n-butyl chains chemically bound to silica-based reversed phase high performance liquid chromatography sorbents, J. Chromatogr. A 660 (1994) 75–84.

[56] I. Yarovsky, M.-I. Aguilar, M. T. W. Hearn, Influence of the chain length and surface density on the conformation and mobility of n-alkyl ligands chemically immobilized onto a silica surface, Anal. Chem. 67 (1995) 2145–2153.

[57] I. Yarovsky, M. T. W. Hearn, M.-I. Aguilar, Molecular simulation of peptide interactions with an RP-HPLC sorbent, J. Phys. Chem. B 101 (1997) 10962–10970.

[58] J. T. Slusher, R. D. Mountain, A molecular dynamics study of a reversed-phase liquid chromatography model, J. Phys. Chem. B 103 (1999) 1354–1362.

[59] K. A. Lippa, L. C. Sander, R. D. Mountain, Molecular dynamics simulation of alkylsilane stationary-phase order and disorder. 1. Effects of surface coverage and bonding density, Anal. Chem. 77 (2005) 7852–7861.

[60] K. A. Lippa, L. C. Sander, R. D. Mountain, Molecular dynamics simulation of alkylsilane stationary-phase order and disorder. 2. Effects of temperature and chain length, Anal. Chem. 77 (2005) 7862–7871.

[61] K. A. Lippa, L. C. Sander, Identification of isolated cavity features within molecular dynamics simulated chromatographic surfaces, J. Chromatogr. A 1128 (2006) 79–89.

[62] K. Ban, Y. Saito, K. Jinno, Characterization of the microscopic surface structure of the octadecylsilica stationary phase using a molecular-dynamics simulation, Anal. Sci. 20 (2004) 1403–1408.

[63] K. Ban, Y. Saito, K. Jinno, Molecular-dynamics simulation for the characterization of liquid chromatography stationary phase: Effect of temperature, Anal. Sci. 21 (2005) 397–402.

[64] X. Dou, H. Wang, J. Han, Molecular dynamics simulation of the effects of mobile phase modification on interactions in reversed-phase liquid chromatography, J. Liq. Chromatogr. Relat. Technol. 29 (2006) 2559.

[65] A. Fouqueau, M. Meuwly, R. J. Bemish, Adsorption of acridine orange at a $C_{8,18}$/water/acetonitrile interface, J. Phys. Chem. B 111 (2007) 10208–10216.

[66] J. Braun, A. Fouqueau, R. J. Bemish, M. Meuwly, Solvent structures of mixed water/acetonitrile mixtures at chromatographic interfaces, Phys. Chem. Chem. Phys. 10 (2008) 4765–4777.

[67] S. M. Melnikov, A. Höltzel, A. Seidel-Morgenstern, U. Tallarek, Influence of residual silanol groups on solvent and ion distribution at a chemically modified silica surface, J. Phys. Chem. C 113 (2009) 9230–9238.

[68] L. Zhang, L. Sun, J. I. Siepmann, M. R. Schure, A molecular simulation study of the bonded-phase structure in reversed-phase liquid chromatography with neat aqueous solvent, J. Chromatogr. A 1079 (2005) 127–135.

[69] L. Zhang, J. L. Rafferty, J. I. Siepmann, B. Chen, M. R. Schure, Chain conformation and solvent partitioning in reversed-phase liquid chromatography: Monte carlo simulations for various water/methanol concentrations, J. Chromatogr. A 1126 (2006) 219–231.

[70] J. L. Rafferty, L. Zhang, J. I. Siepmann, M. R. Schure, Retention mechanism in reversed-phase liquid chromatography: A molecular prospective, Anal. Chem. 79 (2007) 6551–6558.

[71] J. L. Rafferty, J. I. Siepmann, M. R. Schure, Molecular-level comparison of alkylsilane and polar-embedded reversed-phase liquid chromatography systems, Anal. Chem. 80 (2008) 6214–6221.

[72] J. Rafferty, J. Siepmann, M. Schure, Influence of bonded-phase coverage in reversed-phase liquid chromatography via molecular simulation. I. Effects on chain conformation and interfacial properties, J. Chromatogr. A 1204 (2008) 11–19.

[73] J. Rafferty, J. Siepmann, M. Schure, Influence of bonded-phase coverage in reversed-phase liquid chromatography via molecular simulation. II. Effects on solute retention, J. Chromatogr. A 1204 (2008) 20–27.

[74] J. L. Rafferty, J. I. Siepmann, M. R. Schure, The effects of chain length, embedded polar groups, pressure, and pore shape on structure and retention in reversed-phase liquid-chromatography: Molecular-level insights from Monte Carlo simulations, J. Chromatogr. A 1216 (2008) 2320–2331.

[75] J. L. Rafferty, J. I. Siepmann, M. R. Schure, Understanding the retention mechanism in reversed-phase liquid chromatography: Insights from molecular simulation, in: P. R. Brown, E. Grushka (Eds.), Advances in Chromatography, Vol. 48, Marcel Dekker, New York, 2009, *In Press*.

[76] J. L. Rafferty, L. Sun, J. I. Siepmann, M. R. Schure, Investigation of the driving forces for retention in reversed-phase liquid chromatography: Monte carlo simulations of solute partitioning between n-hexadecane and various aqueous-organic mixtures, Fluid Phase Equilibr. (2009) *Submitted for publication*.

[77] J. L. Rafferty, L. Sun, J. I. Siepmann, M. R. Schure, Retention mechanism of polycyclic aromatic hydrocarbons in reversed-phase liquid chromatography and the molecular origins of shape selectivity, Anal. Chem. (2009) *Submitted for publication*.

[78] J. L. Rafferty, L. Sun, J. I. Siepmann, M. R. Schure, Monte Carlo simulation of reversed-phase liquid chromatographay: Effects of water/acetonitrile concentration on structure and retention, J. Chromatogr. A (2009) *Submitted for publication*.

[79] D. A. McQuarrie, Statistical Mechanics, University Science Books, 2000.

[80] M. P. Allen, D. J. Tildesley, Computer Simulation of Liquids, Oxford University Press, Oxford, 1987.

[81] N. Metropolis, A. Rosenbluth, M. Rosenbluth, A. Teller, E. Teller, Equation of state calculations by fast computing machines, J. Chem. Phys. 21 (1953) 1087–1092.

[82] A. Z. Panagiotopoulos, Direct determination of phase coexistence properties of fluids by monte carlo simulation in a new ensemble, Mol. Phys. 61 (1987) 813–826.

[83] A. Z. Panagiotopoulos, N. Quirke, M. Stapleton, D. J. Tildesley, Phase equilibria by simulation in the Gibbs ensemble. Alternative derivation, generalization and application to mixture and membrane equilibria, Mol. Phys. 63 (1988) 527–545.

[84] J. J. de Pablo, J. M. Prausnitz, Phase equilibria for fluid mixtures from Monte Carlo simulation, Fluid Phase Equilibr. 53 (1989) 177–189.

[85] A. Ben-Naim, Statistical Thermodynamics for Chemists and Biochemists, Plenum, 1992.

[86] M. G. Martin, J. I. Siepmann, Calculating Gibbs free energies of transfer from Gibbs ensemble Monte Carlo simulations, Theor. Chem. Acc. 99 (1998) 347–350.

[87] P. Kollman, Free energy calculations: Applications to chemical and biochemical phenomena, Chem. Rev. 93 (1993) 2395–2417.

[88] J. I. Siepmann, A method for the direct calculation of chemical potentials for dense chain systems, Mol. Phys. 70 (1990) 1145–1158.

[89] J. I. Siepmann, D. Frenkel, Configurational-bias Monte Carlo: A new sampling scheme for flexible chains, Mol. Phys. 75 (1992) 59–70.

[90] T. J. H. Vlugt, M. G. Martin, B. Smit, J. I. Siepmann, R. Krishna, Improving the efficiency of the configurational-bias Monte Carlo algorithm, Mol. Phys. 94 (1998) 727–733.

[91] G. C. A. M. Mooij, D. Frenkel, B. Smit, Direct simulation of phase equilibria of chain molecules, J. Phys.: Condens. Matter 4 (1992) L255–L259.

[92] M. Laso, J. J. de Pablo, U. W. Suter, Simulation of phase equilibria for chain molecules, J. Chem. Phys. 97 (1992) 2817–2819.

[93] J. I. Siepmann, I. R. McDonald, Monte Carlo simulations of mixed monolayers, Mol. Phys 75 (1992) 255–259.

[94] M. G. Martin, J. I. Siepmann, Predicting multicomponent phase equilibria and free energies of transfer for alkanes by molecular simulation, J. Am. Chem. Soc. 119 (1997) 8921–8924.

[95] C. D. Wick, J. I. Siepmann, Self-adapting fixed-end-point configurational-bias Monte Carlo method for the regrowth of interior segments of chain molecules with strong intramolecular interactions, Marcomolecules 33 (2000) 7207–7218.

[96] See http://www.chem.umn.edu/groups/siepmann/trappe/intro.php for more information.

[97] M. G. Martin, J. I. Siepmann, Transferable potentials for phase equilibria. 1. United-atom description of n-alkanes, J. Phys. Chem. B 102 (1998) 2569–2577.

[98] M. G. Martin, J. I. Siepmann, Novel configurational-bias Monte Carlo method for branched molecules. Transferable potentials for phase equilibria. 2. United-atom descriptsion of branched alkanes, J. Phys. Chem. B 103 (1999) 4508–4517.

[99] C. Wick, M. G. Martin, J. I. Siepmann, Transferable potentials for phase equilibria. 4. United-atom description of linear and branched alkenes and alkylbenzenes, J. Phys. Chem. B 104 (2000) 8008–8016.

[100] B. Chen, J. J. Potoff, J. I. Siepmann, Monte Carlo calculations for alcohols and their mixtures with alkanes. Transferable potentials for phase equilibria. 5. United-atom description of primary, secondary, and tertiary alcohols, J. Phys. Chem. B 105 (2001) 3093–3104.

[101] J. M. Stubbs, J. J. Pottoff, J. I. Siepmann, Transferable potentials for phase equilibria. 6. United-atom description for ethers, glycols, ketones and aldehydes, J. Phys. Chem. B 108 (2004) 17596–17605.

[102] C. D. Wick, J. M. Stubbs, N. Rai, J. I. Siepmann, Transferable potentials for phase equilibria. 7. United-atom description for nitrogen, amines, amides, nitriles, pyridine, and pyrimidine, J. Phys. Chem. B 109 (2005) 18974–18982.

[103] N. Lubna, G. Kamath, J. Potoff, N. Rai, J. I. Siepmann, Transferable potentials for phase equilibria. 8. United-atom description for thiols, sulfides, disulfides, and thiophen, J. Phys. Chem. B 109 (2005) 24100–24107.

[104] R. S. K. S. Vahvaselka, M. Torkkel, Determination of liquid structures of the primary alcohols methanol, ethanol, 1-propanol, 1-butanol and 1-octanol by X-ray scattering, J. Appl. Cryst. 28 (1995) 189–195.

[105] B. Smith, R. Srivastava, Thermodynamic Data for Pure Compounds: Part B Halogenated Hydrocarbons and Alcohols, Elsevier, Amsterdam, 1986.

[106] M. Kelkar, J. Rafferty, J. Siepmann, E. Maginn, Prediction of viscosities and vapor-liquid equilibria for five polyhydric alcohols by molecular simulation, Fluid Phase Equil 260 (2009) 218–231.

[107] C. D. Wick, J. I. Siepmann, M. R. Schure, Molecular simulation of concurrent gas-liquid interfacial adsorption and partitioning in gas-liquid chromatography, Anal. Chem. 74 (2002) 3518–3524.

[108] M. G. Martin, J. I. Siepmann, M. R. Schure, Simulating retention in gas-liquid chromatography, J. Phys. Chem. B. 103 (1999) 11191–11195.

[109] C. D. Wick, M. G. Martin, J. I. Siepmann, M. R. Schure, Simulating retention in gas-liquid chromatography: Benzene, toluene, and xylene solutes, International Journal of Thermophysics 22 (2001) 111–122.

[110] C. D. Wick, J. I. Siepmann, M. R. Schure, Influence of analyte overloading on retention in gas-liquid chromatography: A molecular simulation view, Anal. Chem. 74 (2002) 37–44.

[111] C. D. Wick, J. I. Siepmann, W. L. Klotz, M. R. Schure, Temperature effects on the retention of n-alkanes and arenes in helium-squalane gas-liquid chromatography: Experiment and molecular simulation, J. Chromatogr. A 954 (2002) 181–190.

[112] L. Sun, J. I. Siepmann, W. L. Klotz, M. R. Schure, Retention in gas-liquid chromatography with a polyethylene oxide stationary phase: Molecular simulation and experiment, J. Chromatogr. A 1126 (2006) 373–380.

[113] L. Sun, C. D. Wick, J. I. Siepmann, M. R. Schure, Temperature dependence of hydrogen bonding: An investigation of the retention of primary and secondary alcohols in gas-liquid chromatography, J. Phys. Chem. B 109 (2005) 15118–15125.

[114] B. Chen, J. I. Siepmann, Microscopic structure and solvation in dry and wet octanol, J. Phys. Chem. B 110 (2006) 3555–3563.

[115] L. Zhang, J. Siepmann, Direct calculation of Henry's law constants from Gibbs ensemble Monte Carlo simulations: Nitrogen, oxygen, carbon dioxide, and methane in ethanol, Theor. Chem. Acc. 115 (2006) 391–397.

[116] K. Anderson, J. Siepmann, Solubility in supercritical carbon dioxide: Importance of the Poynting correction and entrainer effects, J. Phys. Chem. B 112 (2008) 11374–11380.

[117] J. Stubbs, J. Siepmann, Binary phase behavior and aggregation of dilute methanol in supercritical carbon dioxide: A Monte Carlo simulation study, J. Chem. Phys 121 (2004) 1525–1534.

[118] L. Zhang, J. Siepmann, Pressure dependence of the vapor-liquid-liquid phase behavior of ternary mixtures consisting of n-alkanes, n-perfluoroalkanes and carbon dioxide, J. Phys. Chem. B 109 (2005) 2911–2919.

[119] N. Rai, J. Rafferty, A. Maiti, J. Siepmann, Prediction of the bubble point pressure for the binary mixture of ethanol and 1,1,1,2,3,3,3-heptafluoropropane from Gibbs ensemble Monte Carlo simulations using the TraPPE force field, Fluid Phase Equil. 260 (2007) 199–211.

[120] J. Potoff, J. Siepmann, Vapor-liquid equilibria of mixtures containing alkanes, carbon dioxide and nitrogen, AIChE J. 47 (2001) 1676–1682.

[121] N. Rai, A. Wagner, R. Ross, J. Siepmann, Application of the TraPPE force field to predicting the hildebrand solubility parameters of organic solvents and monomer units, J. Chem. Theor. Comp. 4 (2008) 136–144.

[122] R. Nellas, B. Chen, J. Siepmann, Dumbbells and onions in ternary nucleation, Phys. Chem. Chem. Phys 9 (2007) 2779–2781.

[123] B. Chen, J. Siepmann, M. Klein, Simulating the nucleation of water/ethanol and water/n-nonane mixtures: Mutual enhancement and two-pathway mechanism, J. Am. Chem. Soc. 125 (2003) 3113–3118.

[124] J. Stubbs, J. Siepmann, Aggregation in dilute solutions of 1-hexanol in n-hexane: A Monte Carlo simulation study, J. Phys. Chem. B 106 (2002) 3968–3978.

[125] P. W. Carr, R. M. Doherty, M. J. Kamlet, R. W. Taft, W. Melander, C. Horváth, Study of the temperature and mobile phase effects in reversed-phase liquid chromatography by the use of the solvatochromic comparison method, Anal. Chem. 58 (1986) 2674–2680.

[126] A. M. Stalcup, D. E. Martire, S. A. Wise, Thermodynamic comparison of monomeric and polymeric C_{18} bonded phases using aqueous methanol and acetonitrile mobile phases, J. Chromatogr. 442 (1988) 1–14.

[127] A. Alvarez-Zepeda, B. N. Barman, D. E. Martire, Thermodynamic study of the marked differences between acetonitrile/water and methanol/water mobile-phase systems in reversed-phase liquid chromatography, Anal. Chem. 64 (1992) 1978–1984.

[128] W. L. Jorgensen, J. Chandrasekhar, J. D. Madura, R. W. Impey, M. L. Klein, Comparison of simple potential functions for simulating liquid water, J. Chem. Phys 79 (1983) 926–935.

[129] J. Rafferty, L. Zhang, N. Zhuravlev, K. Anderson, B. Eggimann, M. McGrath, J. Siepmann, Large-scale Monte Carlo simulations for aggregation, self-assembly and phase equilibria, in: R. Ross, S. Mohanty (Eds.), Large Scale Molecular Dynamics, Nanoscale and Mesoscale Modeling and Simulation, Wiley Publishing, New Jersey, 2008, pp. 189–200.

[130] A. J. P. Martin, R. L. M. Synge, A new form of chromatograhy employing two liquid phases I. A theory of chromatography 2. Application to the microdetermination of the higher monoamino-acids in proteins, Biochem. J. 35 (1941) 1358–1368.

[131] R. D. Mountain, Molecular dynamics study of water-acetonitrile mixtures, J. Phys. Chem. A 103 (1999) 10744–10748.

[132] J. M. Stubbs, J. I. Siepmann, Elucidating the vibrational spectra of hydrogen-bonded aggregates in solution: Electronic structure calculations with implicit solvent and first principles molecular dynamics simulations with explicit solvent for 1-hexanol in n-hexane, J. Am. Chem. Soc. 127 (2005) 4722–4729.

[133] K. Lum, D. Chandler, J. D. Weeks, Hydrophobicity at small and large length scales, J. Phys. Chem. B 103 (1999) 4570–4577.

[134] Y. Arai, H. Higashiuchi, Y. Sakuragi, Correlation of LLE in 1-alkanol + n-alkane binary mixtures using the modified Wilson equation, Fluid Phase Equilibr. 89 (1993) 187–196.

[135] T. Furuya, T. Ishikawa, T. Funazukuri, Y. Takebayashi, S. Yoda, K. Otake, T. Saito, Measurement and correlation of liquid–liquid equilibria for acetonitrile + n-alkane systems, Fluid Phase Equilibr. 257 (2007) 147–150.

[136] C. D. Wick, J. I. Siepmann, M. R. Schure, Simulation studies on the effects of mobile phase modification in liquid chromatography, Anal. Chem. 76 (2004) 2886–2892.

[137] N. D. Zhuravlev, J. I. Siepmann, M. R. Schure, Surface coverages of bonded-phase ligands on silica: A computational study, Anal. Chem. (2001) 4006–4011.

[138] T. H. Walter, P. Iraneta, M. Capparella, Mechanism of retention loss when C_8 and C_{18} HPLC columns are used with highly aqueous mobile phases, J. Chromatogr. A 1075 (2005) 177–183.

[139] R. M. McCormick, B. L. Karger, Distribution phenomena of mobile-phase components and determination of dead volume in reversed-phase liquid chromatography, Anal. Chem. 52 (1980) 2249–2257.

[140] A. G. Bezus, A. V. Kiselev, A. A. Lopatkin, P. Q. Du, Molecular statistical calculation of thermodynamic adsorption characteristics of zeolites using atom-atom approximation. 1. Adsorption of methane by zeolite NaX, J. Chem. Soc., Faraday Trans. 74 (1978) 367–379.

[141] T. J. H. Vlugt, W. Zhu, F. Kapteijn, J. A. Moulijn, B. Smit, R. Krishna, Adsorption of linear and branched alkanes in the silicalite-1, J. Am. Chem. Soc. 120 (1998) 5599–5600.

[142] E. Demiralp, T. Çağin, W. A. Goddard, Morse stretch potential charge equilibrium force field for ceramics: Application to the quartz-stishovite phase transition and to silica glass, Phys. Rev. Lett. 82 (1999) 1708–1711.

[143] A. Seelig, J. Seelig, The dynamic structure of fatty acyl chains in a phospholipid bilayer measured by deuterium magnetic resonance, Biochemistry 13 (1974) 4839–4845.

[144] P. van der Ploeg, H. J. C. Berendsen, Molecular dynamics simulation of a bilayer membrane, J. Chem. Phys. 76 (1982) 3271–3276.

[145] A. Zangwill, Physics at Surfaces, Cambridge University Press, Cambridge, UK, 1988.

[146] A. W. Adamson, A. P. Gast, Physical Chemistry of Surfaces, 6th Edition, Wiley-Interscience, New York, 1997.

[147] J. W. Cahn, J. E. Hilliard, Free energy of a nonuniform system. I. Interfacial free energy, J. Chem. Phys. 28 (1958) 258–267.

[148] T. L. Hill, Thermodynamics of Small Systems, Parts I and II, Dover, New York, 1994.

[149] M. Pursch, L. C. Sander, H. J. Egelhaaf, M. Raitza, S. A. Wise, D. Oelkrug, K. Albert, Architecture and dynamics of C_{22} bonded interphases, J. Am. Chem. Soc. 121 (1999) 3201–3213.

[150] D. W. Sindorf, G. E. Maciel, Si-20 CP-MAS NMR-studies of methylchlorosilane reactions on silica gel, J. Am. Chem. Soc. 103 (1981) 4263–4265.

[151] G. E. Maciel, D. W. Sindorf, V. J. Bartuska, Characterization of silica-attached systems by Si-29 and C-13 cross-polarization and magic-angle spinning nuclear magnetic resonance, J. Chromatogr. 205 (1981) 438–443.

[152] K. Albert, E. Bayer, Charaterization of bonded phases by solid-state NMR-spectroscopy, J. Chromatogr. 544 (1991) 345–370.

[153] L. C. Sander, J. B. Callis, L. R. Field, Fourier transform infrared spectrometric determination of alkyl chain conformation on chemically bonded reversed-phase liquid chromatography packings, Anal. Chem. 55 (1983) 1068–1075.

[154] S. Singh, J. Wegmann, K. Albert, K. Müller, Variable temperature FT-IR studies of n-alkyl modified silica gels, J. Phys. Chem. B 106 (2002) 878–888.

[155] J. M. W. Ducey, C. J. Orendorff, J. E. Pemberton, L. C. Sander, Structure–function relationships in high-density octadecylsilane stationary phases by Raman spectroscopy. 1. Effects of temperature, surface coverage, and preparation procedure, Anal. Chem. 74 (2002) 5576–5584.

[156] C. J. Orendorff, J. M. W. Ducey, J. E. Pemberton, L. C. Sander, Structurefunction relationships in high-density octadecylsilane stationary phases by Raman spectroscopy. 3. Effects of self-associating solvents, Anal. Chem. 75 (2003) 3360–3368.

[157] C. A. Doyle, T. J. Vickers, C. K. Mann, J. G. Dorsey, Characterization of C_{18} bonded liquid chromatographic stationary phases by Raman spectroscopy: The effect of mobile phase composition, J. Chromatogr. A 877 (2000) 25–39.

[158] C. A. Doyle, T. J. Vickers, C. K. Mann, J. G. Dorsey, Characterization of C_{18} bonded liquid chromatographic stationary phases by Raman spectroscopy: The effect of temperature, J. Chromatogr. A 877 (2000) 41–59.

[159] M. C. Henry, L. K. Wolf, M. C. Messmer, In situ examination of the structure of model reversed-phase chromatographic interfaces by sum-frequency generation spectroscopy, J. Phys. Chem. B 107 (2003) 2765–2770.

[160] M. C. Henry, E. A. Piagessi, J. C. Zesotarski, M. C. Messmer, Sum-frequency observation of solvent structure at model chromatographic interfaces: Acetonitrile-water and methanol-water systems, Langmuir 21 (2005) 6521–6526.

[161] C. H. Lochmuller, A. S. Colborn, M. L. Hunnicutt, J. M. Harris, Organization and distribution of molecules chemically bound to silica, Anal. Chem. 55 (1983) 1344–1348.

[162] C. H. Lochmuller, M. L. Hunnicutt, Solvent-induced conformational changes on chemically modified silica surfaces, J. Phys. Chem. 90 (1986) 4318–4322.

[163] M. E. Montgomery, M. A. Green, M. J. Wirth, Orientational dynamics of a hydrophobic guest in a chromatographic stationary phase: effect of wetting by alcohol, Anal. Chem. 64 (1992) 1170–1175.

[164] L. C. Sander, C. J. Glinka, S. A. Wise, Determination of bonded phase thickness in liquid chromatography by small angle neutron scattering, Anal. Chem. 62 (1990) 1099–1101.

[165] Z. Li, S. C. Rutan, S. Dong, Wetting of octadecylsilylated silica in methanol-water eluents, Anal. Chem. 68 (1996) 124–129.

[166] R. K. Gilpin, M. E. Gangoda, A. E. Krishen, Effect of conditioning solvent on the orientation of bonded hydrocarbon moieties in totally aqueous mobile phases, J. Chromatogr. Sci. 20 (1982) 345–348.

[167] S. S. Yang, R. K. Gilpin, Reordering resolvation of silica immobilized non-hydrogen bonding ligands used as stationary phases in high-performance liquid-chromatography, J. Chromatogr. 394 (1987) 295–303.

[168] L. Sun, J. I. Siepmann, M. R. Schure, Monte Carlo simulations of an isolated n-octadecane chain solvated in water-acetonitrile mixtures, J. Chem. Theory Comput. 3 (2007) 350–357.

[169] B. P. Johnson, M. G. Khaledi, J. G. Dorsey, Solvatochromic solvent polarity measurements and retention in reversed-phase liquid chromatography, Anal. Chem. 58 (1986) 2354–2365.

[170] A. Alvarez-Zepeda, Part I. A thermodynamic study of acetonitrile + water mixtures in reversed-phase liquid chromatography. Part II. A gas chromatographic study of the effect of temperature and column pressure on solute retention on a bonded phase using helium and carbon dioxide as mobile phases, Ph.D. thesis, Georgetown University, Washington DC (1991).

[171] B. N. Barman, A thermodynamic investigation of retention and selectivity in reversed-phase liquid chromatographic systems, Ph.D. thesis, Georgetown University, Washington DC (1986).

[172] J. J. Kirkland, J. W. Henderson, Reversed-phase HPLC selectivity and retention characteristics of conformationally different bonded alkyl stationary phases, J. Chromatogr. Sci. 32 (1994) 473–480.

[173] J. E. J. Kikta, E. Grushka, Retention behavior on alkyl bonded stationary phases in liquid chromatography, Anal. Chem. 48 (1976) 1098–1104.

[174] M. C. Hennion, C. Picard, M. Caude, Influence of the number and length of alkyl chains on the chromatographic properties of hydrocarbonaceous bonded phases, J. Chromatogr. 166 (1978) 21–35.

[175] N. Tanaka, H. Goodell, B. L. Karger, The role of organic modifiers on polar group selectivity in reversed-phase liquid chromatography, J. Chromatogr. 158 (1978) 233–248.

[176] M. L. Miller, R. W. Linton, S. G. Bush, J. W. Jorgenson, Correlation of retention behavior with quantitative analysis of octadecyl bonded chromatographic supports, Anal. Chem. 56 (1984) 2204–2210.

[177] K. Miyabe, G. Guiochon, Influence of the modifications conditions of alkyl bonded ligands on the characteristics of reversed-phase liquid chromatography, J. Chromatogr. A 903 (2000) 1–12.

[178] L. C. Sander, S. A. Wise, Influence of stationary phase chemistry on shape recognition in liquid chromatography, Anal. Chem. 67 (1995) 3284–3292.

[179] L. C. Sander, M. Pursch, S. A. Wise, Shape selectivity for constrained solutes in reversed-phase liquid chromatography, Anal. Chem. 71 (1999) 4821–4830.

[180] K. Jinno, Chromatographic Seperations Based on Molecular Recognition, Wiley, New York, 1997.

[181] P. B. Wright, E. Lamb., J. G. Dorsey, R. G. Kooser, Microscopic order as a function of surface coverage in alkyl-modified silicas: Spin probe studies, Anal. Chem. 64 (1992) 785–789.

[182] L. Sun, J. I. Siepmann, M. R. Schure, Conformation and solvation structure for an isolated *n*-octadecane chain in water, methanol, and their mixtures., J. Phys. Chem. B 110 (2006) 10519–10519.

[183] R. G. Nuzzo, E. M. Korenic, L. H. Dubois, Studies of the temperature-dependent phase behavior of long-chain normal-alkyl thiol monolayers on gold, J. Chem. Phys. 93 (1990) 767–773.

[184] J. I. Siepmann, I. R. McDonald, Monte Carlo study of the properties of self-assembled monolayers formed by adsorption of $CH_3(CH_2)_{15}SH$ on the (111) surface of gold, Mol. Phys. 79 (1993) 457–473.

[185] K. Miyabe, G. Guiochon, Influence of the modification conditions of alkyl bonded ligands on the characteristics of reversed-phase liquid chromatography, J. Chromatogr. A 903 (2000) 1–12.

[186] T. L. Ascah, B. Feibush, Novel, highly deactivated reversed-phase for basic compounds, J. Chromatogr. 506 (1990) 357–369.

[187] T. L. Ascah, K. M. Kallury, C. A. Szafranski, S. D. Corman, F. Liu, Characterization and high performance liquid chromatographic evaluation of a new amide-functionalized reversed phase column, J. Liq. Chrom. Rel. Tech. 19 (1996) 3049–3073.

[188] C. R. Silva, I. C. S. F. Jardim, C. Airoldi, Development of new urea-functionalized silica stationary phases. Characterization and chromatographic performance, J. Chromatogr. A 913 (2001) 65–73.

[189] M. R. Euerby, P. Petersson, Chromatographic classification and comparison of commercially available reversed-phase liquid chromatographic columns containing polar embedded group/amino endcappings using principal component analysis, J. Chromatogr. A 1088 (2005) 1–15.

[190] U. D. Neue, Y. F. Cheng, Z. Lu, B. A. Alden, P. C. Iraneta, C. H. Khoebe, K. Van Tran, Properties of reversed phase packings with an embedded polar group, Chromatographia 54 (2001) 169–177.

[191] R. E. Majors, M. Pryzbyciel, Columns for reversed-phase LC seperations in highly aqueous mobile phases, LCGC North Am. 20 (2002) 584–593.

[192] E. Cruz, M. Euerby, C. Johnson, C. Hackett, Chromatographic classification of commercially available reversed-phase HPLC columns, Chromatographia 44 (1997) 151–161.

[193] J. E. O'Gara, D. P. Walsh, C. H. Phoebe, B. A. Alden, E. S. P. Bouvier, P. C. Iraneta, M. Capparella, T. H. Walter, Embedded-polar-group bonded phases for high performance liquid chromatography, LC-GC North Am 19 (2001) 632–642.

[194] J. Layne, Chracterization and comparisom of the chromatographic performance of conventional, polar-embedded, and polar-endcapped reversed-phase liquid chromatography stationary phases, J. Chromatogr. A 957 (2002) 149–164.

[195] D. V. McCalley, Comparison of the performance of conventional C_{18} phases with others of alternative functionality for the analysis of basic compounds by reversed-phase liquid chromatography, J. Chromatogr. A 844 (1999) 23–28.

[196] U. D. Neue, B. A. Alden, T. H. Walter, Universal procedure for the assessment of the reproducibility and the classification of silica-based reversed-phase packings II. Classification of reversed-phase packings, J. Chromatogr. A 849 (1999) 101–116.

[197] N. S. Wilson, J. Gilroy, J. W. Dolan, L. R. Snyder, Column selectivity in reversed-phase liquid chromatography VI. Columns with embedded of end-capping polar groups, J. Chromatogr. A 1026 (2004) 91–100.

[198] T. Czajkowski, I. Hrabovsky, B. Buszewski, R. K. Gilpin, M. Jarionec, Comparison of the retention or organic acids on alkyl and alkylamide chemically bonded phases, J. Chromatogr. A 691 (1995) 217–224.

[199] J. Clardy, C. Walsh, Lessons from natural molecules, Nature 432 (2004) 829–837.

[200] J. L. MacCallum, D. P. Tieleman, Computer simulation of the distribution of hexane in a lipid bilayer: Spatially resolved free energy, entropy, and enthalpy profiles, J. Am. Chem. Soc. 128 (2006) 125–130.

[201] J. J. Kirkland, Development of some stationary phases for reversed-phase high-performance liquid chromatography, J. Chromatogr. A 1060 (2004) 9–21.

[202] J. J. Kirkland, J. L. Glajch, R. D. Farlee, Synthesis and characterization of highly stable bonded phases for high-performance liquid chromatography column packings, Anal. Chem. 61 (1989) 2–11.

[203] K. K. Unger, N. Becker, P. Roumeliotis, Recent developments in the evaluation of chemically bonded silica packings for liquid chromatography, J. Chromatogr. 125 (1976) 115–127.

[204] P. Roumeliotis, K. K. Unger, Structure and properties of n-alkyldimethylsilyl bonded silica reversed-phase packings, J. Chromatogr. 149 (1978) 211–224.

[205] K. Karch, I. Sebestian, I. Halász, Preparation and properties of reversed phases, J. Chromatogr. 122 (1976) 3–16.

[206] A. Tchapla, H. Colin, G. Guiochon, Linearity of homologous series retention plots in reversed-phase liquid chromatography, Anal. Chem. 56 (1984) 621–625.

[207] L. C. Sander, S. A. Wise, Effect of phase length on column selectivity for the separation of polycyclic aromatic hydrocarbons by reversed-phase liquid chromatography, Anal. Chem. 59 (1987) 2309–2313.

[208] L. C. Sander, K. E. Sharpless, N. E. Craft, S. A. Wise, Development of stationary phases for the separation of cartenoid isomers, Anal. Chem. 66 (1994) 1667–1674.

[209] S. Strohschein, M. Pursch, D. Lubda, K. Albert, Shape selectivity of C_{30} phases for RP-HPLC separation of tocopherol isomers and correlation with MAS NMR data from suspended stationary phases, Anal. Chem. 70 (1998) 13–18.

[210] J. Mittal, J. R. Errington, T. M. Truskett, Does confining the hard-sphere fluid between hard walls change the average properties?, J. Chem. Phys, 126 (2007) 244708.

[211] F. Gritti, G. Guiochon, Ultra high pressure liquid chromatography: Column permeability and changes of the eluent properties, J. Chromatogr. A 1187 (2008) 165–179.

[212] B. A. Bidlingmeyer, L. B. Rogers, Investigation of pressure-induced changes in the chromatographic selectivity of methyl and ethyl orange on silica gel, Sep. Sci. 7 (1972) 131–158.

[213] B. A. Bidlingmeyer, R. P. Hooker, C. H. Lochmuller, L. B. Rogers, Improved chromatographic rsolution from pressure-induced changes in liquid-solid distribution ratios, Sep. Sci. 4 (1969) 439–446.

[214] G. Guiochon, M. J. Sepaniak, Influence of pressure on solute retention in liquid chromatography, J, Chromatogr. A 606 (1992) 248–250.

[215] M. Martin, G. Guiochon, Effects of high pressure in lqiuid chromatography, J. Chromatogr. A 1090 (2005) 16–38.

[216] F. Gritti, G. Guiochon, Influence of the pressure on the properties of chromatographic columns II. The column hold-up volume, J. Chromatogr. A 1070 (2005) 13–22.

[217] F. Gritti, G. Guiochon, Influence of the pressure on the properties of chromatographic columns III. Retention volume of thiourea, hold-up volume, and compressibility of the C_{18} layer, J. Chromatogr. A 1075 (2005) 117–126.

[218] V. L. McGuffin, C. E. Evans, Influence of pressure on solute retention in liquid-chromatography, J. Microcol. Sep. 3 (1991) 513–520.

[219] V. L. McGuffin, S. Chen, Molar enthalpy and molar volume of methylene and benzene homologues in reversed-phase liquid chromatography, J. Chromatogr. A 762 (1997) 35–46.

[220] D. R. Caudwell, J. P. M. Trusler, V. Vesovic, W. A. Wakeham, The viscosity and density of n-dodecane and n-octadecane at pressures up to 200 MPa and temperatures up to 473 K, Intl. J. Thermophys. 25 (2004) 1339–1352.

[221] S. A. Wise, W. J. Bonnett, F. R. Guenther, W. E. May, A relationship between reversed-phase C18 liquid-chromatographic retention and the shape of polycyclic aromatic-hydrocarbons, J. Chromatogr. Sci. 19 (1981) 457–465.

[222] S. A. Wise, L. C. Sander, Factors affecting the reversed-phase liquid chromatographic seperation of polycyclic aromatic hydrocarbons, J. High Resol. Chromatogr. 8 (1985) 248–255.

[223] K. A. Lippa, L. C. Sander, S. A. Wise, Chemometric studies of polycyclic aromatic hydrocarbon shape selectivity in reversed-phase liquid chromatography, Anal. Bioanal. Chem. 378 (2004) 365–377.

[224] C. A. Rimmer, K. A. Lippa, L. C. Sander, Shape selectivity in reversed-phase liquid chromatography, LC GC N. Am. 26 (2008) 984–998.

[225] L. C. Sander, S. A. Wise, Certificate of analysis, standard reference material 869a, column selectivity test mixture, nIST, Gaithersburg, MD, 1998.

[226] L. Limsavarn, J. G. Dorsey, Influence of stationary phase solvation on shape selectivity and retention in reversed-phase liquid chromatography, J. Chromatogr. A 1102 (2006) 143–153.

[227] K. Jinno, K. Kawasaki, Correlation between the retention data of polycyclic aromatic hydrocarbons and several descriptors in reversed-phase HPLC, Chromatographia 17 (1983) 445–449.

[228] C. D. Wick, M. G. Martin, J. I. Siepmann, M. R. Schure, Simulating retention in gas-liquid chromatography: Benzene, toluene, and xylene solutes, Intl. J. Thermophys. 22 (2001) 111–122.

[229] N. Rai, J. I. Siepmann, Transferable potentials for phase equilibria. 9. Explicit-hydrogen description of benzene and 5-membered and 6-membered heterocyclic aromatic compounds, J. Phys. Chem. B 111 (2007) 10790–10799.

[230] S. R. Cole, J. G. Dorsey, Effect of stationary phase solvation on shape selectivity in reversed-phase high-performance liquid chromatography, J. Chromatogr. 635 (1993) 177–186.

[231] G. E. Berendsen, L. D. Galan, Role of chain length of chemically bonded phases and the retention mechanism in reversed-phase liquid chromatography, J. Chromatogr. 196 (1980) 21–37.